UNIVERSITAT RAMON LLULL

DOCTORAL THESIS

Title	Novel protocols in restoration of corroded Pb metals from Cultural Heritage artifacts
Presented by	Patrícia Giménez Barrera
Centre	IQS School of Engineering
Department	Chemical Engineering and Material Sciences
Directed by	Dr. Salvador Borrós Gómez Dr. Sergi Colominas Fuster

Sé que tiene usted sueños de los que nada me dice. No los quiero conocer. Pero le digo una cosa: ¡Vívalos todos, viva esos sueños, eríjales altares! No es lo perfecto, pero es un camino. Ya se verá si nosotros, usted y yo y algunos más, somos capaces de renovar el mundo. Pero debemos renovarlo en nosotros mismos, día a día; si no, nada valemos.

Demian (1919), Hermann Hesse.

Acknowledgements

En primer lloc, vull expressar els meus agraïments al meu director de tesi, en Dr. Salvador Borrós. Gràcies per la seva ajuda i suport durant el meu temps com a membre del teu grup d'investigació GEMAT. Estic sincerament agraïda per donar-me l'oportunitat de formar part d'aquest equip, recolzant-me en la meva trajectòria de pur aprenentatge en tants sentits. Les seves lliçons sobre la investigació i la vida m'han ajudat a créixer i a superar els desafiaments que he trobat en el meu camí. Vull destacar la gran sort que he tingut de conèixer un referent científic com ell, amb molt d'amor i renom en tantes branques de la ciència. Tot i les dificultats que puguin haver suposat aquest camí, estic segura que ha valgut la pena i que els aprenentatges que he adquirit seran un gran valor afegit en la meva vida professional i personal.

Per altra banda vull agrair també enormement al meu codirector Dr. Sergi Colominas. Agraeixo haver-me obert les portes al seu grup d'investigació a electromètrics. Gràcies per la seva paciència i sobretot per la part humana que m'han impulsat en molts moments, i que tanmateix el fan ser un gran investigador i docent científic. He tingut la gran fortuna de treballar sota el seu suport, ajudant-me a posar ordre en les meves idees i assolir els meus objectius.

Expresso també el meu agraïment al Dr. Jordi Abellà, tanmateix per donar-me l'oportunitat de formar part del seu grup d'investigació d'electromètrics i per permetre'm realitzar una gran quantitat d'experiments en el laboratori. La confiança depositada en mi dins del seu grup de recerca, m'ha ajudat molt durant una gran part de l'experimental i he après molt dels seus coneixements com a gran referent de l'electroquímica.

També vull destacar l'ajuda que he rebut del Dr. Carles Colominas durant els experiments de XRD. El seu coneixement en el camp de la cristal·lografia ha estat clau per al desenvolupament d'aquesta investigació. Estic agraïda per les seves explicacions clares que han estat de gran valor en aquest tesi. Tanmateix, agraeixo molt l'ajuda de la seva doctoranda, Neus Sala per tot el seu temps invertit en mi i els seus consells per la present tesi.

Agrair també als membres del MNAC, especialment al restaurador i conservador Àlex Masalles, especialista en materials inorgànics. Estic molt agraïda per donar-me l'oportunitat de formar part del seu projecte del Violinista de Pau Gargallo i per obrir-me les portes del seu laboratori. He après molt de la seva experiència i coneixement en el camp de la restauració i conservació d'art.

Vull mencionar també a les persones que han col·laborat d'alguna manera en experiments o plantejaments essencials dins d'aquesta tesi. Moltes gràcies al Dr. Robert Texidó per tot el que ha aportat a la meva tesi, no tan sols d'experimental, sinó també per la teva part humana amb tant de carisma que el fa ser qui és. Gràcies per la seva col·laboració essencial en diversos experiments i plantejaments.

Gràcies també a la Núria i la Marina (de Mats Vells) per donar-me un cop de mà especialment als primers moments de la meva tesi. També agrair a la Dra. Ana Ramos, per ajudar-me amb moltes de les caracteritzacions, així com també aconsellar-me en diversos moments. Menciono tanmateix al cap de taller Cèsar Alquézar, a qui tantes vegades he acudit i m'ha ajudat a tirar endavant els meus experiments. Finalment, no m'oblido tampoc de les converses amb la senyora Pilar, amb la que he compartit petits moments a IQS i molts trajectes cap a casa quan tornava de les auxiliaries a la nit.

I parlant de suport incondicional, moltes gràcies a tot el grup de GEMAT, qui em va acollir amb els braços oberts quan encara sortia del niu des d'una branca diferent. Sense dubte els portaré dins del meu record, no només per haver compartit tants moments durant aquests anys, sinó per ser qui sou. Als més veterans, dono les gràcies novament Robert i també a en Joan per totes les ajudes que m'han aportat al llarg d'aquesta etapa i haver compartit amb la seva personalitat tan única. Gràcies a tota la resta del gran equip que va compartir amb mi aquesta etapa a GEMAT; Ana Mas, Peri, Cris, Núria, Laura, Alba, Mire, Pol, Germán, Tito i Tony. No oblidaré pas les birres, sopars i fires que m'he fet amb tots ells. A en Toni, li dedico unes línies especials, perquè ha estat molt important en molts moments d'aquesta etapa. Per les nostres bogeries i la facilitat per fer-me riure en tants moments, gràcies amic. També agrair a Coral, Xavi i Elena de Tractivus, que van aparèixer en la meva darrera etapa i amb els que també m'enduc bons moments.

També vull mencionar a tot el grup d'electromètrics, amb els que m'enduc bons records durant la última etapa de la meva tesi. Als aleshores doctorands, Marc i Marga, agraeixo molt la seva ajuda en els meus experiments, per ser tant propers i fer-me recolzament personal i laboral. També agrair especialment als TFM, Enric, Toni, Òscar, Aniol, José i Iván. Moltes gràcies a tots per fer del grup un ambient de treball afable i proper, amb molts moments divertits que mai oblidaré. Agrair especialment a l'Iván, que ha passat de ser un company de laboratori a un company molt important de vida. Agraeixo tenir aquesta ment al meu costat, tan creativa i sensible que el caracteritza, i que fan d'ell una persona amb un món interior molt especial. Gràcies per fer camí junts.

Vull mencionar de fora d'IQS, que no han participat de forma directa en el meu doctorat, però han estat presents a la meva vida durant tots aquests anys. Als meus amics de la carrera, per la seva autenticitat que han fet que avui dia els meus anys de carrera siguin inoblidables. Especialment, Àlex i Vivi, per la seva personalitat divertida i sensible, pel seu recolzament i preocupació, sempre al peu del canó. També a les meves amigues de tota la vida, Patricia y Cristina, per recolzar-me en tot moment i compartir de primera mà gairebé tots els bons i mals moments de tots els meus reptes personals des de molt joves. Menciono també a la Laia, Tania i Sandra per compartir aquesta darrera trajectòria amb mi. A en Luis, que m'ha acompanyat sempre, animant-me i recolzant-me en les meves decisions, estic molt orgullosa de tenir-lo com a amic. Miquel, gràcies a ell també per tot el suport, per les nostres bogeries i per regalar-me tantes anècdotes divertides. Marc, per estar indirectament recolzant-me en molts moments, gràcies. I finalment, a les persones més recents, Cris, Ivana i Pili, que m'han estat acompanyant especialment en aquesta última trajectòria, preocupant-se i compartir les seves vivències amb mi amb tanta vitalitat i afecte. Finalment, dedico unes línies per agrair a tot l'equip de Momentum el suport que m'ha donat durant aquesta última trajectòria.

Per últim, vull dedicar unes línies molt importants per als meus pares, que han estat els pilars fonamentals de tota la meva vida i gràcies a ells he arribat aquí. Els agraeixo tot l'amor i perseverança que han implicat en mi. M'han ensenyat a estimar l'art i la ciència com a dos mons convergents que han format part de tot aquest camí. Mama, papa, moltes gràcies a vosaltres. Tots els meus esforços us els dedico a vosaltres.

A tots els mencionats, i que de ben segur que em deixo moltes persones més, però doneu-vos per al·ludides. Celebro tots els vostres assoliments i propòsits que heu compartit també amb mi.

Summary

In cultural heritage, numerous artifacts made from ductile metals can be found, posing significant challenges when it comes to their proper conservation. Despite the studies dedicated to understanding the degradation process of this type of material, there is still a lack of consolidated protocols for its restoration. It should be noted that corrosion resistance depends not only on the chemical environment but also on the type of metal, mechanical forces, and physical parameters involved, which increases the need to develop specific restoration alternatives. Thus, the objective of this study was to provide an approach to the conservation and restoration of ductile metals that protects the integrity of cultural heritage artifacts. In this sense, some of the problems associated with traditional techniques are described, and basic information about the properties of ductile metals regarding their possible forms of deterioration is provided. A corrosion study was first carried out on lead samples exposed to different aggressive solutions at varying concentrations. Traditional corrosion treatments such as chemical cleaning and electrochemical reduction were then performed, followed by a cleaning methodology based on the use of cold plasma, which has been used in the conservation field of metals. Since plasma generates reactive species, its interaction with the metal surface is highly efficient and has a very fast kinetics that allows for optimization of the restoration time. Furthermore, it is important to highlight that this is a controlled process in terms of parameters such as gas composition and flow, intensity, and reaction time. In this context, the study provides a useful discussion of the process and the results obtained on real-scale lead samples. Since this technique reduces the risk of creating by-products, it is a non-invasive application that allows for a substantial improvement over the more traditional techniques used in the field of science conservation.

Resum

En el patrimoni cultural, es poden trobar nombrosos artefactes fabricats amb metalls dúctils, la qual cosa planteja importants reptes quan es tracta de la seva adequada conservació. Malgrat els estudis dedicats a comprendre el procés de degradació d'aquest tipus de material, encara hi ha una manca de protocols consolidats per a la seva restauració. Cal assenyalar que la resistència a la corrosió no només depèn de l'entorn químic, sinó també del tipus de metall, les forces mecàniques i els paràmetres físics involucrats, la qual cosa augmenta la necessitat de desenvolupar alternatives específiques de restauració. Per tant, l'objectiu d'aquest estudi va ser proporcionar un enfocament per a la conservació i restauració de metalls dúctils que protegeixi la integritat dels artefactes del patrimoni cultural. En aquest sentit, es descriuen alguns dels problemes associats amb les tècniques tradicionals i es proporciona informació bàsica sobre les propietats dels metalls dúctils en relació amb les seves possibles formes de deteriorament. Es va realitzar primer un estudi de corrosió en mostres de plom exposades a diferents solucions agressives amb concentracions variables. A continuació, es van dur a terme tractaments tradicionals de corrosió, com ara neteja química i reducció electroquímica, seguits d'una metodologia de neteja basada en l'ús de plasma fred, que s'ha utilitzat en el camp de la conservació de metalls. Atès que el plasma genera espècies reactives, la seva interacció amb la superfície del metall és altament eficient i té una cinètica molt ràpida que permet optimitzar el temps de restauració. A més, és important destacar que aquest és un procés controlat en termes de paràmetres com ara la composició i el flux de gas, la intensitat i el temps de reacció. En aquest context, l'estudi proporciona una discussió útil sobre el procés i els resultats obtinguts en mostres de plom a escala real. Donat que aquesta tècnica redueix el risc de crear subproductes, és una aplicació no invasiva que permet una millora substancial en comparació amb les tècniques més tradicionals utilitzades en el camp de la ciència de la conservació.

Resumen

En el patrimonio cultural, se pueden encontrar numerosos artefactos fabricados con metales dúctiles, lo que plantea importantes desafíos cuando se trata de su adecuada conservación. A pesar de los estudios dedicados a comprender el proceso de degradación de este tipo de material, todavía existe una falta de protocolos consolidados para su restauración. Cabe señalar que la resistencia a la corrosión no solo depende del entorno químico, sino también del tipo de metal, las fuerzas mecánicas y los parámetros físicos involucrados, lo que aumenta la necesidad de desarrollar alternativas específicas de restauración. Por lo tanto, el objetivo de este estudio fue proporcionar un enfoque para la conservación y restauración de metales dúctiles que proteja la integridad de los artefactos del patrimonio cultural. En este sentido, se describen algunos de los problemas asociados con las técnicas tradicionales y se proporciona información básica sobre las propiedades de los metales dúctiles en relación con sus posibles formas de deterioro. Se realizó primero un estudio de corrosión en muestras de plomo expuestas a diferentes soluciones agresivas con concentraciones variables. Luego, se llevaron a cabo tratamientos tradicionales de corrosión, como limpieza química y reducción electroquímica, seguidos de una metodología de limpieza basada en el uso de plasma frío, que se ha utilizado en el campo de la conservación de metales. Dado que el plasma genera especies reactivas, su interacción con la superficie del metal es altamente eficiente y tiene una cinética muy rápida que permite optimizar el tiempo de restauración. Además, es importante destacar que este es un proceso controlado en términos de parámetros como la composición y el flujo de gas, la intensidad y el tiempo de reacción. En este contexto, el estudio proporciona una discusión útil sobre el proceso y los resultados obtenidos en muestras de plomo a escala real. Dado que esta técnica reduce el riesgo de crear subproductos, es una aplicación no invasiva que permite una mejora sustancial en comparación con las técnicas más tradicionales utilizadas en el campo de la ciencia de la conservación.

List of abbreviations

AC	Alternating current
AcOH	Acetic acid
ASTM	American Society for Testing and Materials
Cdl	Double-layer Capacitance
CIP	Confocal Image Profiling
EC	Equivalent Circuit
CPE	Constant Phase Element
CV	Cyclic Voltammetry
EDS	Energy Dispersive X-Ray Spectroscopy
EDTA	Ethylenediaminetetraacetic acid
EIS	Electrochemical Impedance Spectroscopy
EN	European Norm
GEMAT	Grup d'Enginyeria de Materials
ICCROM	International Centre for the Study of the Preservation and Restoration of Cultural Property
ICDD	International Centre for Diffraction Data
JEOL	Japan Electron Optics Laboratory
mm/yr	Millimeters Per Year
MNAC	Museu Nacional d'Art de Catalunya
NTP	Non-thermal plasma
OMS	3D Optical Measuring System
PGSTAT	Potentiostat/Galvanostat
PTFE	Polytetrafluoroethylene
RDE	Rotating Disk Electrode
Rp	Polarization resistance
SCE	Saturated Calomel reference Electrode

SEM	Scanning Electron Microscopy, Scanning Electron Microscopy
SiC	Silicon Carbide
TP	Thermal Plasma
TW	Tap water
WS	Working solution
UNESCO	Educational, Scientific and Cultural Organization
VOCs	Volatile Organic Compounds
XPS	X-ray Photoelectron Spectroscop
TP/NTP	Thermal Plasma/Non Thermal Plasma
XRD	X-ray Diffraction

Table of contents

1. Motivation and aims

Creativity and its transmission of ideas give society a purely human identity that surrounds and determines it. In Kant's theory of beauty, empirical and intellectual concepts are emphasized: "*Yet in all beautiful art what is essential consists in the form, which is purposive for observation and judging, where pleasure is at the same time culture, and disposes the spirit to ideas, hence makes it receptive to several sorts of pleasures and entertainment"* [1]. The voice of art is the protagonist of multiple contexts rooted in our daily life and social construction. This is a concept in which society participates in its creation, as a natural impulse of humanity due to the need to have its own heritage.

The significance of it is closely tied to the essential components that shape its identity and its inherent association to the culture. [2,3]. Under this concept, it is of utmost importance to preserve Cultural Heritage artifacts because they provide us with valuable information about history and its value. To achieve this, it is essential to study the materials used in these artefacts, which provides contextual information and helps to evaluate their state of conservation, leading to the development of appropriate treatment procedures. [4,5].

On November 16 in 1972, the "Convention for the Protection of the World Cultural and Natural Heritage" was adopted by UNESCO [6], and in 1978 a meeting was organized by the ICCROM Standards and Training Committee in which the main activities of the conservator-restorer were defined [7]. Modern conservation ethics generally do not aim to restore the original state of historical artifacts. Instead, the focus is on preserving and stabilising the artifacts in their current state, while also respecting their cultural and historical significance. This approach recognizes that the passage of time and the effects of aging and decay are a natural part of an artifact's history, and attempts to strike a balance between preserving the object's physical integrity and maintaining its authenticity and cultural value. In some cases, conservation efforts may involve minimal interventions to repair damage or stabilise deteriorating materials, but the goal is generally to avoid altering the original character or appearance of the object as much as possible [8–10].

In this context, one of the most complex challenges faced is the conservation of metals which have a multitude of artistic, architectural, and technical applications in the Cultural Heritage field. Among them, ductile metals constitute a significant part of this heritage as they are highly malleable and easy to shape into various forms. However, as is well known, the instability of collections and their long-term conservation is threatened by the corrosion phenomenon, which is a global problem that has been increasing for over a decade. Thus, the intervention of the conservator-restorer in safeguarding these collections is increasingly necessary. The selection of the proper treatment is mainly determined by the state of conservation and the type of metal. In the case of ductile and malleable metals like lead, conservation poses particular challenges due to their physical and chemical conditions.

Metallic lead is documented as one of the first metal castings of whom many artworks were made [11]. Its main issue is the degradation suffered by organic acid environments, such as acetic acid vapours, which are usually produced by wooden boxes or objects that can be found near the metallic lead artefacts [12–15]. Acetic acid vapours are the most dangerous compounds for metallic lead due to the resulting corrosion products formed on the metallic surface with a porous and heterogeneous layer structure. This promotes the dissolution by the acidic environment of the protective lead oxide layer formed by the oxygen in contact with the metallic surface [13,16–18].

For this reason, this kind of attack comprises several problems, in which a continuous corrosion process is observed without the ability to be passivated, losing the integrity of its structure. The corrosion process can be classified as active corrosion, which typically begins in localized areas called pits. This type of corrosion is formed in lead by volatile organic compounds (VOCs), which produce initial compounds such as lead acetate and lead formate [19–21]. These products are unstable, so in the long term, more stable phases of lead carbonate are formed when they come into contact with CO_2 of the environment. Lead carbonate layers are often very porous with small cracks that allow the re-entry of aggressive species. According to Turgoose [21], one of the first authors to describe lead corrosion, acetic acid that condenses on a corroded lead object, can dissolve some of the carbonate corrosion products leaving acetate ions to carry some of the corrosion current and

allowing Pb^{2+} to migrate away from the metal surface, allowing further corrosion. The lead carbonate layer can vary depending on the environment surrounding the artefact. For example, when the artefact is buried in alkaline carbonate soil with a high atmospheric pressure of carbon dioxide, the main lead carbonate phase formed is cerussite ($PbCO_3$) [21]. Conversely, when the artifact is exposed to the open atmosphere for a long period of time with a low atmospheric pressure of carbon dioxide, the main lead carbonate phase formed is hydrocerussite ($Pb_3(CO_3)_2(OH)$) [21,22]. These compounds are formed in the metal surface and in some areas their big volume can displace the initial corrosion layer. This can lead to difficulties in reading superficial inscriptions, and in some cases, the complete disintegration of the artifact [23].

Mechanical and chemical cleanings, such as the *Caley method* [24], were used during the fifties to extract corrosion products of lead metals, but results were not too favourable, due to the hard methodology and heterogeneity resulting. In 1956, the electrolytic reduction was promoted by Plenderleith [25]**.** *The Conservation of Antiquities and Works of Art* summarizes the practices he did and which also were used at the British Museum Laboratory. In the following years, works by A. France-Lanord, R.M Organ and T. Stambolow [26] were published on historical reviews of electrochemical techniques applied to conservation, which contributed to the dissemination of these techniques within scientific conservation. In 1994, Carradice and Campbell [27] proposed potentiostatic reduction in which the potential was controlled instead of the current, and this technique was used not only for lead but also for silver and copper [28–30]. At a later time, researchers from conservation science worked quite successfully on the potentiostatic reduction [23,31,32]. However, nowadays, electrolytic methods are not commonly used in the treatment of corroded historical artifacts due to several factors related to their effectiveness and potential risks. One issue is the limited ability of electrolytic reduction to penetrate thick corrosion layers, as it relies on the movement of ions through the aqueous solution. Additionally, the process can result in the loss of surface details, such as engravings, and can cause damage to the metal itself if not carefully monitored.

A more recent approach on the use of electrolytic treatments is based on the development of an electrolytic pencil called PLECO. This was made possible through

a close collaboration between the Haute Ecole Arc (UR-Arc CR), EDANA team (Ergonomics, Design and Applied Anthropology) of the Haute Ecole Arc Ingénierie and FabLab Neuchâtel [33,34]. It was developed to address some of the limitations of conventional treatments such as chemical, mechanical or electrolytic cleaning. It can be locally used on surfaces that cannot be submerged due to size, non-uniform corrosion, or inseparable composition, which is a common issue with some heritage objects. One of the most significant advantages of the PLECO is that it prevents the degradation of non-metallic elements, which can be an issue with traditional electrolytic processes in which the entire artefact is immersed. The PLECO has been successful in cleaning metals such as tarnished silver and lead with active corrosion, marking a significant step forward in the conservation of metallic artefacts from Cultural Heritage [35–37].

Over the past few years, there has been growing interest in the use of non-thermal plasma in the field of Cultural Heritage [38–43]. For example, Christian Degrigny made several significant contributions to the cleaning and stabilisation of corroded lead samples using plasma techniques. One of his major contributions is the development of a plasma system capable of producing a stable and dense hydrogen plasma, which can effectively reduce corrosion layers on lead objects [23]. Additionally, Degrigny conducted extensive research on the effects of plasma treatment on the microstructure and mechanical properties of lead objects. It was found that the plasma treatment does not significantly alter the microstructure or mechanical properties of lead [23], making it a safe and effective method for cleaning the corroded surface. The reported issue was that hydrogen plasma only caused a slight reduction in the thickness of the corrosion layer on the surface of the lead, and prolonged exposure of three hours did not result in further reduction. This lack of further reduction was attributed to the resulting metallic lead once reduced the corrosion products on the top of the corrosion layer, which acted as a barrier to hydrogen ions [23].

The main goal of this thesis is the study of conservation of the sculpture the Violinist (1920) made by Pau Gargallo. This sculpture is a portrait of the musician Francesc Costa (1891-1959) and actually is in the *Museu d'Art de Catalunya* (MNAC) in Barcelona, Spain. Its fragility and delicate state of conservation was the cause of

the need for intervention by using a particular treatment. Then, non-thermal plasma was suggested as a possible treatment for that purpose. To achieve that, this thesis was structured in the following work plan:

1. Different solutions of aggressive compounds were used to induce lead corrosion in the gas phase. The concentration of these compounds was also varied. Then, the resulting surfaces were characterized and compared with existing information in the literature to see if the behaviour of the obtained layers imitates that of real objects (**chapter 2**).

2. Different electrolytic reduction treatments were applied to lead samples previously corroded by AcOH vapours. The characterization of the surfaces, before and after treatment, was compared to evaluate the effectiveness of each method in reducing the corrosion products on the lead surfaces (**chapter 3**).

3. A non-thermal plasma of argon and hydrogen was used to stabilise corroded lead surfaces affected by AcOH vapours. Different parameters were varied to determine its effectiveness on the treatment. After cleaning, the surfaces were characterized focusing on the use of XPS analysis (**chapter 4**).

4. Electrochemical Impedance Spectroscopy (EIS) was used to evaluate the corroded lead surfaces before and after treatment by non-thermal plasma and consolidative reduction (**chapter 5**).

5. non-thermal plasma was used under appropriate conditions to clean areas affected by the emission of volatile organic compounds (VOCs) in the sculpture "*El Violinista*" created by Pau Gargallo in 1920.

A brief description of the tasks performed in each chapter is provided in the following paragraphs.

Chapter 2 describes an investigation into the corrosion behaviour of metallic lead when exposed to various gas phases of corrosive solutions, including NaCl, H_2SO_4, HCOOH, and AcOH. The purpose was to develop models that simulate the

corrosion layers of real historical objects. These models are important for analysis, experimentation, testing and practical restoration purposes, and are crucial for evaluating and establishing conservation protocols before treating real historical objects [20,44].

Characterization techniques such as X-ray Diffraction (XRD), Scanning Electron Microscopy (SEM), and Confocal Image Profiling (CIP) were used to investigate the corrosion behaviour of lead samples that were degraded due to exposure of the corrosive environments. Additionally, the corrosion rate was calculated using gravimetric experiments and the Tafel Extrapolation method in both alkaline and acidic solutions.

In **chapter 3**, galvanostatic and potentiostatic methods were compared. The purpose of this comparison was to identify any issues related to their use. The primary goal of using these methods was to stabilise lead surfaces affected by active corrosion. This could be achieved by electrolytic reduction of the corrosion products that had been formed on the surface of the metal [27]. By doing this, it is possible to stop the progression of corrosion that can cause irreversible damage to the metal. Different characterization techniques were also used to analyse and compare the resulting surfaces of each electrolytic method.

It has been demonstrated by different authors, for example Christian Degrigny, that the use of non-thermal plasma can reduce corrosion layers on lead objects [23]. However, it was also reported on his studies that hydrogen plasma may not penetrate deep enough to reach the corroded metal underneath only. Then, **Chapter 4** aimed to clean and stabilise lead with active corrosion through a reduction treatment involving hydrogen plasma, as well as an etchant process using argon plasma. The plasma reactor was designed and constructed by the *Grup d'Enginyeria de Materials* (GEMAT) at Institut Químic de Sarrià - Universitat Ramon Llull (IQS-URL) and has been described in previous publications by the group. The non-thermal plasma treatment involved a mixture of hydrogen and argon gases, with a high electron temperature (<10,000 K) and low density compared to the atoms, allowing for the creation of a room-temperature plasma. This generated many reactive species, resulting in chemical reactions that could effectively treat the corroded lead surfaces.

Hydrogen was selected to generate a reductive plasma that would cause chemical reactions on the corroded surface. Meanwhile, argon plasma was used to remove a portion of the surface products accelerating the process through an "etching effect" [45–47]. In this context, the cleaning process would be based mainly between the plasma and atoms or molecules from the corroded surface, converting them into decomposition by-products that are subsequently removed by the vacuum pump. Plasma generates highly reactive species and its interaction with the surface is very efficient. This fact would allow for optimizing the time of treatment of ductile metals in front of the electrolytic treatments.

Chapter 5 explores the application of Electrochemical Impedance Spectroscopy (EIS) in evaluating the effectiveness of conservation treatments for corroded lead specimens. These treatments are essential to slow down the corrosion process and preserve the artifact. However, determining the effectiveness of these treatments can be a challenge. EIS is a powerful technique that characterizes corrosion and can provide valuable information on the effectiveness of surface cleaning/stabilisation treatments. We will discuss the application of EIS to corroded lead samples, and showcase case studies that demonstrate its effectiveness in evaluating the success of different surface treatments.

Finally, **Chapter 6** described the application of non-thermal plasma treatment in a sculpture with a poor state of conservation. In cooperation with the *Museu Nacional d'Art de Catalunya (MNAC)* and with the *Institut Químic de Sarrià - Universitat Ramon Llull* (IQS-URL), a project to stabilise the corroded surface of the sculpture "El Violinista" by Pau Gargallo (1881-1934) was performed. The problem with its initial state of conservation occurred from the incompatibility between the materials comprising its structure (metallic lead and pine wood). The corrosion of lead was primarily caused by the release of acetic acid, along with small amounts of formic, propionic, and butyric acid from the wooden core onto the lead metal. The outcome was a significant structural deformation with notable metal loss in some parts of the sculpture [48]. Furthermore, the results obtained after the treatment were analysed using different characterization techniques.

1.1 References

[1] P. Guyer, Kant's Conception of Fine Art, The Journal of Aesthetics and Art Criticism. 52 (1994) 275–285. https://doi.org/10.2307/431427.

[2] E.Z. Acosta, Sobre patrimonio y desarrollo. Aproximación al concepto de patrimonio cultural y su utilización en procesos de desarrollo territorial, PASOS. Revista de Turismo y Patrimonio Cultural. 9 (2011) 101–113.

[3] G. Weiss, A Scientific Concept of Culture, Am Anthropol. 75 (1973) 1376–1413. https://doi.org/10.1525/aa.1973.75.5.02a00130.

[4] M. Vecco, A definition of cultural heritage: From the tangible to the intangible, J Cult Herit. 11 (2010) 321–324. https://doi.org/10.1016/j.culher.2010.01.006.

[5] H. Hirsenberger, J. Ranogajec, S. Vucetic, B. Lalic, D. Gracanin, Collaborative projects in cultural heritage conservation – management challenges and risks, J Cult Herit. 37 (2019) 215–224. https://doi.org/10.1016/j.culher.2018.10.006.

[6] Unesco Convention for the Protection of the World Cultural and Natural Heritage, International Legal Materials. 11 (1972) 1358–1366. https://doi.org/10.1017/S0020782900055674.

[7] The conservator-restorer: a definition of the profession, Museum International. 39 (1987) 231–233. https://doi.org/10.1111/j.1468-0033.1987.tb00699.x.

[8] M.D.L. de Castro, A. Jurado-López, The role of analytical chemists in the research on the cultural heritage, Talanta. 205 (2019) 120106–120116. https://doi.org/10.1016/j.talanta.2019.07.001.

[9] D. Anglos, A.G. Karydas, Non-destructive and microanalytical techniques in art and cultural heritage (Technart 2009), Anal Bioanal Chem. 395 (2009) 1947–1948. https://doi.org/10.1007/s00216-009-3194-x.

[10] V. Ferretti, M. Bottero, G. Mondini, Decision making and cultural heritage: An application of the Multi-Attribute Value Theory for the reuse of historical buildings, J Cult Herit. 15 (2014) 644–655. https://doi.org/10.1016/j.culher.2013.12.007.

[11] M. Boldyrev, Lead: properties, history, and applications, WikiJournal of Science. 1 (2018) 7. https://doi.org/10.15347/wjs/2018.007.

[12] M.K. Budd, Corrosion of metals in association with wood, Applied Materials Research. (1965) 124–125.

[13] J. Tétreault, E. Stamatopoulou, Determination of concentrations of acetic acid emitted from wood coatings in enclosures, Studies in Conservation. 42 (1997) 141–156. https://doi.org/10.1179/sic.1997.42.3.141.

[14] P.C., C.G.C. and G.J.D. Arni, The emission of corrosive vapours by wood, I. Survey of the acid-release properties of certain freshly felled hardwoods and softwoods, Journal of Applied Chemistry. 15 (1965) 305–313.

[15] L.T. Gibson, C.M. Watt, Acetic and formic acids emitted from wood samples and their effect on selected materials in museum environments, Corros Sci. 52 (2010) 172–178. https://doi.org/10.1016/j.corsci.2009.08.054.

[16] J. Tétreault, J. Sirois, E. Stamatopoulou, Studies of lead corrosion in acetic acid environments, Studies in Conservation. 43 (1998) 17–32. https://doi.org/10.1179/sic.1998.43.1.17.

[17] A. Niklasson, L.-G. Johansson, J.-E. Svensson, Influence of Acetic Acid Vapor on the Atmospheric Corrosion of Lead, J Electrochem Soc. 152 (2005) B519. https://doi.org/10.1149/1.2084348.

[18] J. Tétreault, E. Cano, M. van Bommel, D. Scott, M. Dennis, M.-G. Barthés-Labrousse, L. Minel, L. Robbiola, Corrosion of Copper and Lead by Formaldehyde, Formic and Acetic Acid Vapours, Studies in Conservation. 48 (2003) 237–250. https://doi.org/https://doi.org/10.1179/sic.2003.48.4.237.

[19] S.B. Lyon, Corrosion of Lead and its Alloys, in: Shreir's Corrosion, Elsevier, 2010: pp. 2053–2067. https://doi.org/10.1016/B978-044452787-5.00098-6.

[20] A. Niklasson, L.-G. Johansson, J.-E. Svensson, The influence of relative humidity and temperature on the acetic acid vapour-induced atmospheric corrosion of lead, Corros Sci. 50 (2008) 3031–3037. https://doi.org/10.1016/j.corsci.2008.08.009.

[21] S. Turgoose, The corrosion of lead and tin before and after excavation, in: C.E. Miles and S.C. Pollard (Eds.), Lead and Tin: Studies in Conservation and Technology. 3 (1985) 15–26.

[22] A.N. Abu Baker, The corrosion characteristics and electrochemical conservation treatment for an archaeological lead ossuary from Jordan, Ge-Conservacion. 22 (2022) 154–161. https://doi.org/10.37558/gec.v22i1.1093.

[23] C. Degrigny, R. le Gall, Conservation of ancient lead artifacts corroded in organic acid environments: electrolytic stabilisation/consolidation, Studies in Conservation. 44 (1999) 157–169. https://doi.org/10.1179/sic.1999.44.3.157.

[24] E.R. Caley, Coatings and Incrustations on Lead Objects from the Agora and the Method Used for Their Removal, Studies in Conservation. 2 (1955) 49. https://doi.org/10.2307/1504917.

[25] A.E.A.W. Harold James Plenderleith, The Conservation of Antiquities and Works of Art: Treatment, Repair and Restoration, (1966) 1–373. https://doi.org/0-7141-0227-X.

[26] A.I.P. and M.A. Joaquín Barrio, Jorge Chamón, Electrochemical techniques applied to the conservation of archaeological metals from Spain: a historical review, Journal of Solid State Electrochemistry. 13 (2009) 1767–1776. https://doi.org/10.1007/s10008-009-0876-4.

[27] I.A. Carradice, S.A. Campbell, The Conservation of Lead Communion Tokens by Potentiostatic Reduction, Studies in Conservation. 39 (1994) 100–106. https://doi.org/10.2307/1506559.

[28] M.C. Bernard, E. Dauvergne, M. Evesque, M. Keddam, H. Takenouti, Reduction of silver tarnishing and protection against subsequent corrosion, Corros Sci. 47 (2005) 663–679. https://doi.org/10.1016/j.corsci.2004.07.015.

[29] J.M. Cronyn, Elements of Archaeological Conservation, Routledge, 2003. https://doi.org/10.4324/9780203169223.

[30] A.B. Paterakis, The Influence of Conservation Treatments and Environmental Storage Factors on Corrosion of Copper Alloys in the Ancient Athenian Agora, Journal of the American Institute for Conservation. 42 (2003) 313–339. https://doi.org/10.1179/019713603806112787.

[31] E. Cano, D.M. Bastidas, V. Argyropoulos, S. Fajardo, A. Siatou, J.M. Bastidas, C. Degrigny, Electrochemical characterization of organic coatings for protection of

historic steel artefacts, Journal of Solid State Electrochemistry. 14 (2010) 453–463. https://doi.org/10.1007/s10008-009-0907-1.

[32] C. Degrigny, Use of electrochemical techniques for the conservation of metal artefacts: a review, Journal of Solid State Electrochemistry. 14 (2010) 353–361. https://doi.org/10.1007/s10008-009-0896-0.

[33] G.B.C.D.C.B.H.C. Romain Jeanneret, When rapid prototyping meets electrochemistry: the Pleco, an electrolytic pencil for the localized cleaning of tarnished silver and gilded silver, WAAC Newsletter . 36 (2014) 37–40.

[34] G. Bussy, FabLabs, Product Design and Anthropotechnology, in: Inside Anthropotechnology, John Wiley & Sons, Inc., Hoboken, NJ, USA, 2017: pp. 129–145. https://doi.org/10.1002/9781119452775.ch6.

[35] R.D.C.F.C.W.D.T.A. JEANNERET, Using the Pleco for electrolytic treatments of inseparable metal components on artefacts comprising organics, in: C.C. and A.P. R. Menon (Ed.), Proceedings of the ICOM-CC Metal WG Interim Meeting, METAL 2016, New Dehli, India, 2016: pp. 228–234.

[36] C.J.R.W.D. Degrigny, Local cleaning with the Pleco electrolytic pencil of the tarnished Saint Candide reliquary head at the Treasury of Saint-Maurice Abbey, Valais (Switzerland), E-Preservation Science. 12 (2015) 20–27.

[37] A.C.C.D. Nicola Ricotta, Analysis of Heterogeneous Tarnish on Silver-based Alloys Using the Pleco for Local, Controlled Electrolytic Cleaning, in: Metal 2022, Proceedings of the Interim Meeting of the ICOM-CC Metals Working Group, Helsinki, ICOM-CC ; The National Museum of Finland, Helsinki, Finland, 2022: pp. 248–252.

[38] A. Patelli, E. Verga, L. Nodari, S.M. Petrillo, A. Delva, P. Ugo, P. Scopece, A customised atmospheric pressure plasma jet for conservation requirements, IOP Conf Ser Mater Sci Eng. 364 (2018) 012079. https://doi.org/10.1088/1757-899X/364/1/012079.

[39] R. Tiňo, K. Vizárová, F. Krčma, Plasma Surface Cleaning of Cultural Heritage Objects, in: Nanotechnologies and Nanomaterials for Diagnostic, Conservation and Restoration of Cultural Heritage, Elsevier, 2019: pp. 239–275. https://doi.org/10.1016/B978-0-12-813910-3.00011-2.

[40] E. Grieten, O. Schalm, P. Tack, S. Bauters, P. Storme, N. Gauquelin, J. Caen, A. Patelli, L. Vincze, D. Schryvers, Reclaiming the image of daguerreotypes: Characterization of the corroded surface before and after atmospheric plasma treatment, J Cult Herit. 28 (2017) 56–64. https://doi.org/10.1016/j.culher.2017.05.008.

[41] O. Schalm, P. Storme, A. Gambirasi, M. Favaro, A. Patelli, How effective are reducing plasma afterglows at atmospheric pressure in removing sulphide layers: Application on tarnished silver, sterling silver and copper, Surface and Interface Analysis. 50 (2018) 32–42. https://doi.org/10.1002/sia.6329.

[42] V.M. Donnelly, A. Kornblit, Plasma etching: Yesterday, today, and tomorrow, Journal of Vacuum Science & Technology A: Vacuum, Surfaces, and Films. 31 (2013) 0508251–05082548. https://doi.org/10.1116/1.4819316.

[43] P. Fojtíková, V. Sázavská, F. Mika, F. Krčma, Effect of Hydrogen Plasma on Model Corrosion Layers of Bronze, J Phys Conf Ser. 715 (2016) 012006. https://doi.org/10.1088/1742-6596/715/1/012006.

[44] F. Deflorian, M. Fedel, Electrochemical analysis of the degradation of lead alloy organ-pipes due to acetic acid, J Cult Herit. 14 (2013) 254–260. https://doi.org/10.1016/j.culher.2012.06.002.

[45] J.W. Coburn, H.F. Winters, Plasma etching—A discussion of mechanisms, Journal of Vacuum Science and Technology. 16 (1979) 391–403. https://doi.org/10.1116/1.569958.

[46] Abdul Wasy Zia, YI-QI Wang, Seunghun Lee, Effect of Physical and Chemical Plasma Etching on Surface Wettability of Carbon Fiber-Reinforced Polymer Composites for Bone Plate Applications, Advances in Polymer Technology. 34 (2015) 21480–21484. https://doi.org/10.1002/adv.21480.

[47] R.A. Gottscho, Microscopic uniformity in plasma etching, Journal of Vacuum Science & Technology B: Microelectronics and Nanometer Structures. 10 (1992) 2133–2147. https://doi.org/10.1116/1.586180.

[48] A. Masalles, E. Lehmann, D. Mannes, Non-destructive Investigation of "The Violinist" a Lead Sculpture by Pablo Gargallo, Using the Neutron Imaging Facility NEUTRA in the Paul Scherrer Institute, Phys Procedia. 69 (2015) 636–645. https://doi.org/10.1016/j.phpro.2015.07.090.

2. Morphological and structural characterization of corroded lead samples

A wide variety of corrosion products can be formed on metallic lead surfaces, in both acidic and alkaline mediums. Despite that lead is not a noble metal, its corrosion resistance is usually high, due to the resulting compounds formed on the surface. This means that corrosion is mainly controlled by the physicochemical properties of the formed corrosion layers. To study and compare the morphology of these structures and their resistance in aggressive mediums, corrosion was induced by vapour tests using different working solutions on metallic lead samples. The resulting corrosion layers will be characterized and compared in the present chapter.

2.1. Introduction

Lead has been used for various purposes since ancient times, including the creation of utensils, coins, medals, and sheets with engraved inscriptions. The Egyptians utilized lead in the making of statues, sarcophagi, and pipelines, while the Ancient Greeks and Romans used significant amounts of lead for water distribution systems and household items, as well as artistic objects. From the 15th to the 19th centuries, lead was widely used in construction, including architectural elements, and pewter organ pipes were also made with lead for their excellent sound quality [1]. However, by 1970, the health risks associated with daily contact with lead led to its replacement with alternative materials and reduced its use in items such as pipelines and household objects [2]. Currently, lead and lead alloys are primarily used for industrial applications due to their physical and chemical properties [3–6].

Lead is not considered a noble metal because of its negative standard reduction potential of -0.126 V. That means that when it is exposed to moisture and air it can

be oxidized forming different compounds on its surface. The product composition and morphology of this layer can vary depending on the specific corrosive environment, as well as the exposure time and temperature. The formation of that layer can reduce the corrosion rate of the underlying metal by forming a barrier that inhibits the diffusion of corrosive agents to the metal surface. However, the effectiveness of this barrier depends on the porosity, solubility, thickness and adherence of the layer [7–10]. Therefore, the corrosion resistance of lead is not solely dependent on its standard reduction potential but rather on the ability of the corrosion layer to form and maintain an effective barrier against further corrosion.

In this context, the corrosion rate of metallic lead depends primarily on the physical and chemical properties of these resulting layers. Hence, atmospheric corrosion can follow two scenarios, as shown in Figure 2-1.

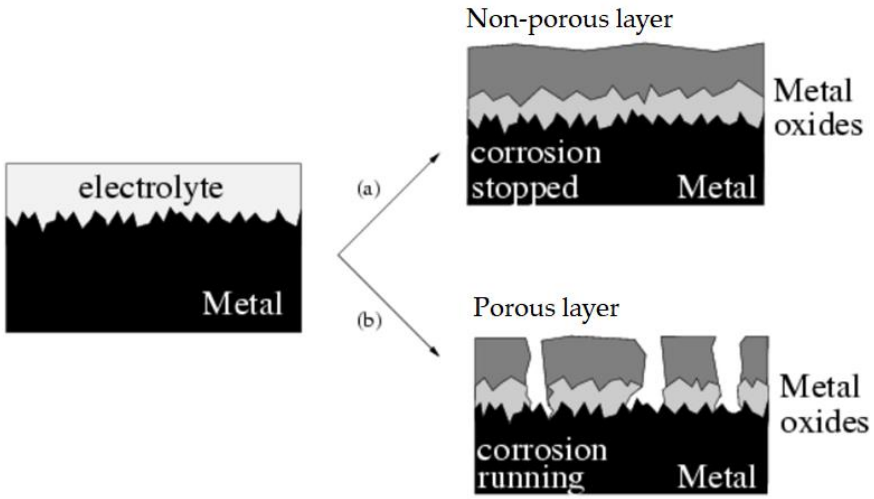

Figure 2-1. Schematic atmospheric corrosion principle, *a;* protective compact passive layer, *b;* non-protective porous layer [11].

The passivation process occurs when the resulting corrosion layer is compact and formed by poorly soluble compounds, which favours the protection against

further corrosion. As shown in Figure 2-1 *a*, the resulting film is adherent and non-porous. This means that the corrosion reaction becomes very slow or even stops over time. In contrast, corrosion processes cannot be stopped when the resulting layer is very porous and with low adherence to the metallic surface (see Figure 2-1 *b*, or if the corrosion compounds formed are soluble in the environment. In this case, the porosity of such layer allows the access of water and oxygen to the underlying metal, favouring new corrosion processes. The solubility of these corrosion compounds can also lead to their dissolution and loss of protection. As it happens in all metals, it should be noted that the corrosion rate depends not only on the electrochemical reactivity of the metal but also on the morphology and composition of the formed corrosion layers.

When metallic lead is exposed to atmospheric oxygen, it spontaneously forms lead oxide layer. This layer covers the surface of the metal and forms a protective film that helps to prevent further corrosion of the metal. This process is called natural passivation because the metal is passivated or protected without the need for any additional treatment or coating. In Figure 2-2, two types of lead oxide are presented in corroded Pb surfaces.

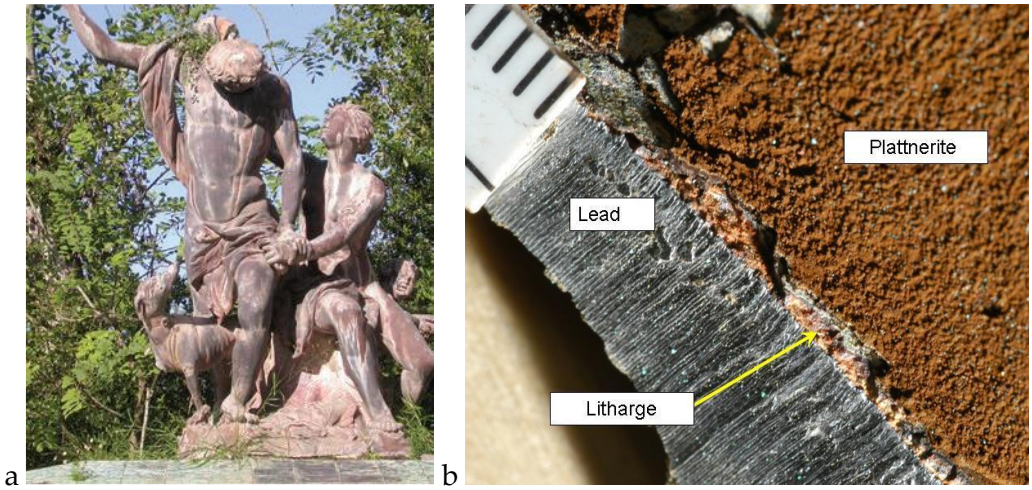

Figure 2-2. *a;* Sculpture representation of *Venus and Adonis* from the Garden of the National Palace of Queluz (Portugal), exhibiting significant distortion of the head position before being intervened. The reddish surface was related to the lead oxide (litharge and plattnerite) [12]. *b;* Lead service line with litharge, corresponded to Pb(II) oxide layer closest to the pipe wall

overlain by a thin layer of calcite (calcium carbonate) and then by the plattnerite corresponded to Pb(IV) oxide [13].

An example of lead natural passivation in a rural environment, where air pollution is not a serious problem, is shown in the sculpture of Venus and Adonis from the Garden of the National Palace of Queluz in Portugal. According to the bibliography [12], in its low-polluted environment, the metallic sculpture (see Figure 2-2 a was oxidized to litharge, red lead oxide (PbO) that grows in slightly alkaline conditions. Additionally, some dark brown layers were also found on the sculpture, related to plattnerite (lead dioxide, PbO_2). The formation of plattnerite was faster in areas exposed to full sunlight and where water or moisture was likely to run over the surface [12]. Figure 2-2 *b* shows the cross-section of a lead service line, where litharge grew as a compact film between the bare metal and plattnerite. Note that lead oxide (PbO) is nearly insoluble in water at 25°C, with a solubility of less than 10^{-4} g/dm^3 [14]. This promotes the stability of the corrosion layer and also of the metallic core.

Litharge is the alpha form of lead oxide, while massicot is the beta form of lead oxide. Their crystal structures are shown in Figure 2-3.

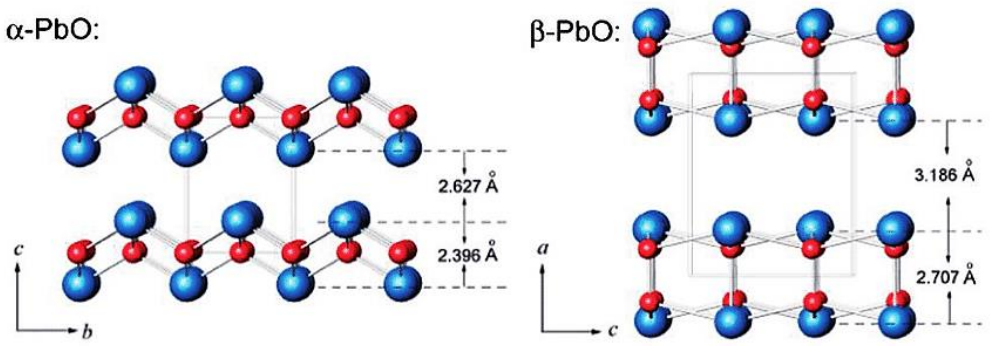

Figure 2-3. Crystal structures of α-PbO (litharge) and β-PbO (massicot) [15]. Pb atoms are represented as the blue spheres and O atoms are represented as the red spheres.

The tetragonal crystalline structure of litharge (α-PbO) is red with a bandgap of 1.9-2.2 eV and it is stable at room temperature. On the other hand, the orthorhombic crystalline structure of massicot (β-PbO) is yellow with a bandgap of 2.7 eV and it is only stable at high temperatures, above 488°C [15]. Due to this, the most common oxide passivation structure found on metallic Pb surfaces is litharge. In certain cases, dark brown lead dioxide (PbO_2), informally known as puce oxide, can also form as an orthorhombic structure (scrutinyite, α-PbO_2) or a tetragonal structure (plattnerite, β-PbO_2) [16]. In these cases, the stable phase is plattnerite (β-PbO_2), which can recrystallize on the surface layers of metastable scrutinyite crystals (α-PbO_2) [16]. Lead dioxide is typically mixed with lead oxide in contaminated atmospheres under specific conditions, such as intense light and high humidity [12].

A different situation is observed when lead artefacts are exposed to atmospheric conditions in polluted areas. Acid rain is formed when pollutants such as sulphur dioxide (SO_2) and nitrogen oxide (NO_x) are released into the atmosphere from sources like industrial and transportation emissions. These pollutants react with water, oxygen, and other chemicals to form acidic compounds, such as sulphuric acid and nitric acid. When lead artefacts are exposed to that environment, anglesite ($PbSO_4$) is commonly formed. It is usually found with lead oxide, lead chloride, lead carbonate or other lead compounds as shown in Figure 2-4.

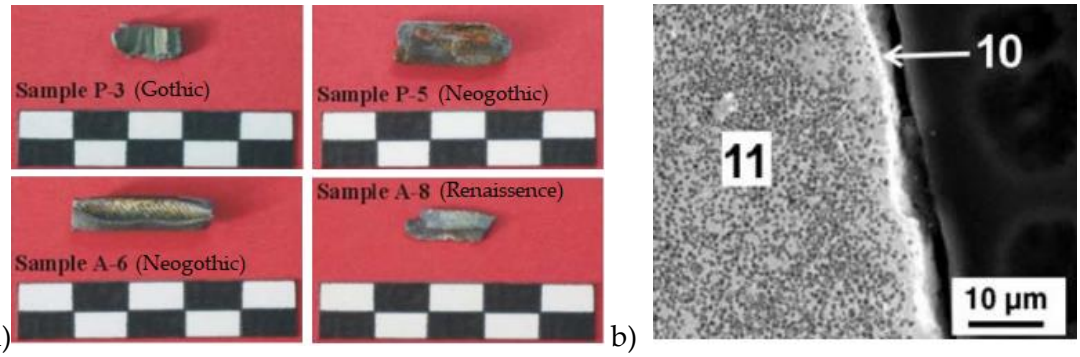

Figure 2-4. *a*; Lead came samples analysed by M. García-Heras et al. [17]. Sample P-3 is from Royal Windows, Cathedral of Köln (Germany), P -5 from St. Laurentius Church (Warendorf, Germany), A-6 from St. John Church (Antwerpen, Belgium) and A-8 from St. Lenaarts Church

(province of Antwerpen, Belgium), *b*; SEM micrograph of a polished cross-section of the same lead came sample of the 16th century (Renaissance) from St. Lenaarts Church (province of Antwerpen, Belgium) [17].

Figure 2-4 shows an example of lead corrosion layer in historical lead fragments. These fragments are "lead cames" which are lead strips or bars used to join together pieces of coloured glass in the construction of stained-glass windows. Lead, like other materials forming stained glass windows, is subjected to weathering phenomena, and a film is rapidly formed on its surface when exposed to the atmosphere. As shown in Figure 2-4 *a*, different fragments of lead cames are shown from a bibliographic report prepared by M. García-Heras et al. [17]. It showed a high concentration of anglesite on the surface, especially in the Renaissance sample A-8. The study found that there were no differences between the light line on the surface and the micro-granulated lead body. Both were found to have only lead and a high concentration of sulphur. The high sulphur content suggested was attributed to the presence of lead sulphate and it was formed due to regional pollution originating from the heavily contaminated city of Antwerpen [17].

The formation of a lead sulphate layer results in a passive protective layer of anglesite. Lead sulphate has a low solubility of 4×10^{-4} g/cm^3 at 25 °C [14] and the morphology is compact with strong adherence, which easily passivates the metal core as it grows. It is described in the bibliography that $PbSO_4$ forms a dense layer with very small pores that are impermeable to HSO_4^- and SO_4^{2-} ions. This results in a controlled corrosion rate due to the physicochemical properties of the surface products [18]. Because of its characteristics, anglesite is a very stable compound and has been used as a pigment or in combination with other materials for aesthetic purposes in Cultural Heritage artefacts [19–21].

In marine environments, the presence of chloride promotes the formation of halogenated lead compounds with very different corrosion behaviour. For example, the metallic surface can undergo oxidation through the reaction of lead oxide with humidity and Cl^-, forming the basic lead chloride laurionite [Pb(OH)Cl]. In the presence of CO_2 and Cl^-, the phase formed is phosgenite ($Pb_2CO_3Cl_2$). Other insoluble

lead mixed compounds and non-stoichiometric lead oxide (PbO_x) can also be formed [17]. Although laurionite layers are quite porous, they have low solubility and are usually found in the presence of other more compact and low-solubility compounds, such as anglesite and/or lead oxide [22,23]. Therefore, the lead matrix tends to become passivated. An example of a historical lead sculpture (Saint Catherine Church of Vasilyevsky Island, Saint Petersburg) with a high content of laurionite is shown in Figure 2-5.

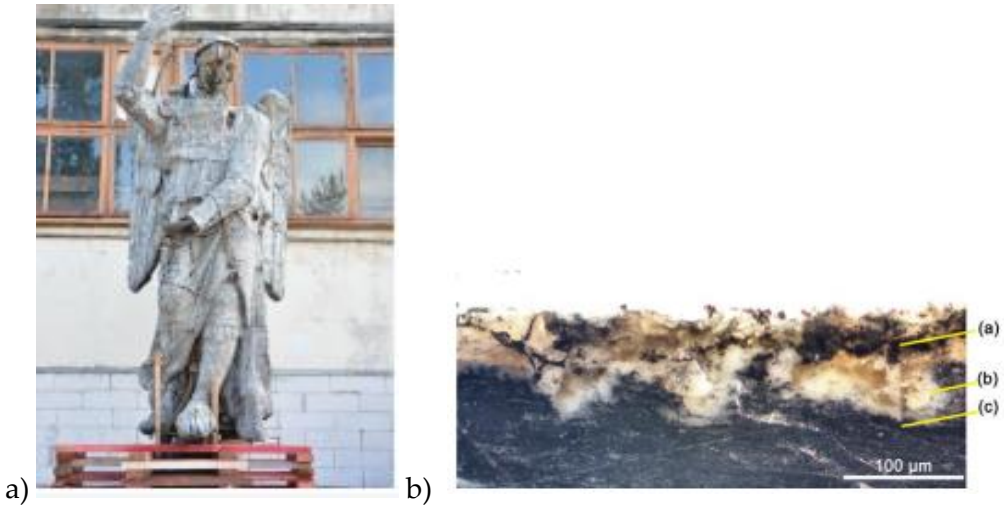

Figure 2-5. *a;* Outdoor statue of an angel by sculptor I. P. Prokofiev, dated 1823, from the dome of Saint Catherine Church of Vasilyevsky Island in Saint Petersburg, *b*; Macro-photo of the cross-section of a lead sample from the sculpture [24].

It was observed on the sculpture that the corrosion layer contained different phases (see Figure 2-5 b. The brown areas of part *(a)* were related to anglesite. The white areas of part *(b)* presented a significantly high content of laurionite (Pb(OH)Cl) and small amounts of anglesite. Additionally, hydrocerussite was also present in the white areas. The dark layer adjacent to the metal of part *(c)*, was related to litharge. These findings suggest that different corrosion mechanisms may be occurring in different areas of the samples. The marine air of Saint Petersburg led to the appearance of laurionite, as a result of the reaction of sodium chloride with lead

oxide. Taking into account that lead chloride has a low solubility in water (7×10^{-2} g/cm^3 at 25 °C [14]), it is quite stable and rarely dissolved when in contact with water.

Lead degradation when exposed to organic acid atmospheres is considered the most challenging situation. It is known that certain species of wood are very aggressive to lead because of the breakdown of cellulose in the timber and it produces volatile organic compounds (VOCs), especially acetic acid. The effect of VOCs on lead corrosion is significant in the context not only of buildings but also in museums for the display of historic artefacts. The main compound formed when the lead is exposed to acetic acid vapours is in the short-term lead acetate, also known as the "salt of Saturn" or "lead sugar" [25]. Lead acetate is very unstable due to its irregular morphology and high solubility (4.5×10^{-1} g/cm^3 at 25 °C [14]). Another compound produced by VOCs is lead formate, which is formed when exposed to formic acid vapours and presents high solubility (1.6×10^{-1} g/cm^3 at 25 °C [14]). Note that both compounds, lead acetate and lead formate are much more soluble than lead chloride and lead sulphate (7×10^{-2} g/cm^3 and 4×10^{-4} g/cm^3 respectively both at 25 °C [14]). Lead acetate and lead formate commonly originate in conjunction with wooden materials.

Due to the instability of these compounds, this type of corrosion usually begins as a localized process and eventually leads to the formation of a more stable and uniform corrosion layer of carbonate over the long term, due to the presence of atmospheric CO_2. The source of these pollutants (acetic and formic acids) is linked to the building materials used in the enclosure. Hardwoods, such as oak, are known to emit high concentrations of acetic acid, with as much as 7% of the wood's weight being released as acetic acid vapour over two years at 48°C [26–28]. This is due to the hydrolysis of acetyl group esters in the hemicellulose, which is one-third of the total carbohydrate in the wood. Softwoods contain less hemicellulose and therefore emit less acetic acid. The production of formic acid from wood is generally lower and less well understood [29]. An example of this type of corrosion is shown in Figure 2-6 [30]. In this figure different corroded lead organ pipes by VOCs are shown.

a)  b) 

Figure 2-6. *a;* Organ completed by F. Stellwagen in 1637 in Lübeck, Germany. Severely corrosion-damaged organ pipe made by lead can be observed [30], *b;* Corroded lead-tin organ pipe after 15 years on the wooden support in the organ of Madonna delle Laste Sanctuary (Trento, Italy) [31].

Figure 2-6 *a* shows the lead pipes of the organ from St Jakobi church in Lübeck, Germany. Pipes were mainly corroded at the feet, where the air is blown into them at low pressure. Different causes of the corrosion were considered, including VOCs released from wood over time, and the combined effects of temperature, humidity and pollutants [30]. Another example is the lead-tin alloy organ pipe shown in Figure 2-6 *b*. The degradation of the lead structure was mainly due to the formation of highly soluble corrosion products such as lead formate or lead acetate, which prevent the passivation of the metal surface and, therefore, cause continuous corrosion of the metal [31].

If lead formate is produced, it tends to stabilise into a passivating crystalline layer over time [10]. However, lead acetate films are very unstable and not commonly found isolated on metallic lead surfaces. Over long periods and in the presence of atmospheric CO_2 and O_2, lead acetate and lead formate are converted into more

stable phases of lead carbonate and lead oxide. This often results in a mixed corrosion layer of litharge (α-PbO), lead acetate ($Pb(C_2H_3O_2)_2$) and lead carbonate, such as, from the less to the most insoluble, hydrocerussite ($Pb_3(CO_3)_2(OH)$), cerussite ($PbCO_3$) and plumbonacrite ($Pb_{10}O(CO_3)_6(OH)_6$). These carbonates can originate from each other and undergo phase changes under specific environmental conditions. This carbonatation process tends to form a more stable corrosion layer over the long term, which can help to slow down the corrosion rate and increase the overall durability of the surface material [32].

The specific form of lead carbonate that is generated depends on the pH of the environment and the presence of other ions or compounds. As described in the bibliography [33], hydrocerussite ($Pb_3(CO_3)_2(OH)$) and plumbonacrite ($Pb_{10}O(CO_3)_6(OH)_6$) are typically found in neutral to slightly alkaline environments, while cerussite ($PbCO_3$) is more commonly found in more neutral environments. An example of the resulting appearance when the surface is carbonated is shown in Figure 2-7.

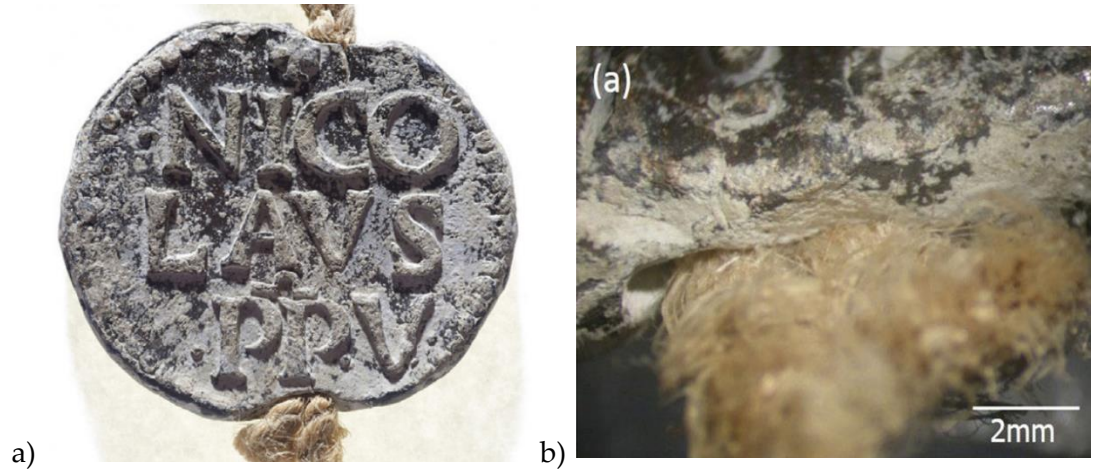

Figure 2-7. *a;* Lead seal (Pope Nicolas V) dating from 1451 (©Aubert Arc'Antique) with lead carbonate corrosion as described by C. Fontaine, et al [34], *b;* Interface between lead seal and cord before reduction with the electrolytic pencil, the Pleco (©HE-Arc/Arc'Antique) [34].

The lead seal of Pope Nicolas V shown in Figure 2-7 has a surface covered by a thin and tightly packed layer of lead carbonate. It affected the relief decorations as reported by C. Fontaine, et al [34]. The corrosion products can be observed in image *b*, which was taken before the surface reduction by the electrolytic pencil Pleco [34]. These white compounds shown in image *b* were a mixture of lead carbonate and other compounds such as lead acetate hydroxide. It was formed on the surface of the object that was exposed to VOCs from an oak storage box. The corrosion was particularly active in this case.

In a humid environment and the presence of CO_2, lead is first oxidized forming a protective layer of lead oxide, and subsequently, on its surface, lead carbonate is also formed, typically plumbonacrite ($Pb_{10}O(CO_3)_6(OH)_6$). However, in the presence of VOCs, lead corrosion is started by the dissolution of the oxide film to form lead acetate. [10,31,35]. The acidification of the surface electrolyte leads to the formation of lead ions and hydroxide ions that combine with OH^- anions and CO_3^{2-} from the dissolution of existing carbonates to form voluminous lead carbonate. These displace the existing corrosion compounds causing surface loss [7–10]. This process was first proposed by Turgoose [36] and confirmed by Degrigny and Le Gall [37].

Lead carbonate has very low solubility in water at (3.3×10^{-14} g/dm^3 at 25°C [14]) and the corrosion layer's morphology is porous and rough due to the voluminous lead carbonate, which is formed by crystalline agglomerations [18]. As mentioned, this porous structure allows the entry of corrosive species from the environment, making the corrosion layer unstable in different atmospheres.

Understanding the main differences of the corrosion layers morphology produced within specific environments such as museum interiors, enclosed storage boxes or outdoor atmospheres, it is important to develop treatments and to identify realistic conservation goals. For this reason, induced corrosion models with specific experimental conditions are useful to study the morphology of the resulting layers and predict their behaviour under different scenarios. It should be considered that a corrosion process takes years under real conditions, while laboratory experiments are always limited in time. Moreover, this long-term period generally causes multiples electrochemical reactions that cannot be quantified. This is because chemical species are not usually isolated from the environment. However, analysing

the properties of corrosion models allows us to identify their origin and predict some corrosion behaviours under corrosive environments.

Inherently, studies of the velocity at which the surface is corroded help to obtain an approximation of the real long-term corrosion rate. A typical methodology to evaluate the corrosion rate is gravimetric analysis. It is derived, usually, from dividing an observed uniform corrosion loss by the length of time of exposure [38]. Therefore, the corrosion rate can be determined gravimetrically or using electrochemical tools such as the Tafel extrapolation [39,40]. By extrapolating the slopes from two branches (anodic and cathodic), the current exchange density i_0 (A/cm^2) can be calculated. With this value, the corrosion rate in mm/yr can be estimated [41].

In this chapter, the corrosion behaviour of metallic lead was studied through laboratory tests using distinct corrosive environments: NaCl, H_2SO_4, HCOOH and AcOH. For that porpoise, a set of different lead coupons was exposed to vapours of solutions of the before mentioned compounds. Its selection criteria were:

- Sodium chloride is commonly found in marine environments where saline fogs are produced by the evaporation of seawater.
- Sulphuric acid is usually produced in atmospheres containing sulphur dioxide from industrial zones or polluted areas. SO_2 reacts with water, oxygen, and other chemicals to form acidic compounds such as sulphuric acid which is carried with rain (acid rain) [14]. Then, when lead is exposed to acid rain it tends to form a lead sulphate layer.
- Acetic acid and formic acid are volatile organic compounds commonly found in wood materials [42].

The resulting Pb surfaces were analysed using optical microscopy, scanning electron microscopy (SEM), and X-ray diffraction to study the morphology and composition of the corrosion layers.

It is worth mentioning that a high concentration of each corrosive compound (3 M, 8 M and 13 M) and a temperature higher than room temperature (40 °C) were selected to accelerate the corrosion processes of the lead samples.

Moreover, the corrosion rate of the exposed samples was measured using two techniques: gravimetric measurements and Tafel extrapolation. Gravimetric analyses were performed on corroded samples after the first 7 days of exposure to aggressive media. For Tafel extrapolation, the samples were first corroded for 28 days in the vapour tests mentioned earlier. Afterwards, the corroded lead samples were analysed using the Tafel extrapolation in 0.1 M nitric acid and synthetic tap water, to compare the corrosion resistance of the resulting layers.

Note that gravimetric analysis was used to obtain the corrosion rate, which involves measuring the mass loss of a metal sample over an extended period of time. In contrast, Tafel extrapolation, was used to measure the instantaneous corrosion rate of the already formed layer under specific electrochemical conditions in alkaline and acid solutions. Since each method provides different information, these will be discussed in different sections.

2.2. Experimental set-up

2.2.1. Sample preparation and induced corrosion in the gas phase

A set of 12 samples (2 cm x 2.5 cm) of lead sheet (99.99%), composed almost exclusively from metallic lead, and traces of aluminium and steel according to the European Standard EN12588, from AMAT METALPLAST SA and supplied by the *Museu d'Art de Catalunya, MNAC*) with a thickness of 2 mm were subjected to corrosion in various environments. The dimensions of the lead samples and the test set-up are shown in Figure 2-8.

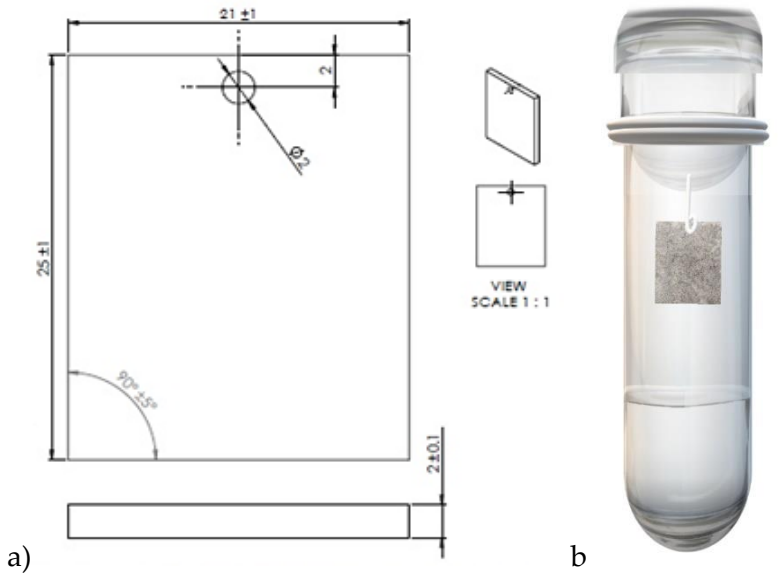

Figure 2-8. *a;* Dimensions of the used samples, *b;* Pb samples suspended on test tubes with different liquid corrosive environments.

The corrosive environments were created in frosted glass test tubes with a diameter of 29/32 mm and a length of 130 mm. The test tubes were filled with 30 ml of different working solutions (equivalent to 1/3 of the available volume of the test tube) consisting of two inorganic compounds, NaCl and H_2SO_4, and two organic compounds, HCOOH and AcOH, in water (all from PanReac Applichem®) at concentrations of 3 M, 8 M, and 13 M. In that way, the gas phase (equivalent to 2/3 of the available volume of the test tube) can rapidly achieve the liquid-gas equilibrium conditions. The proportions of 1/3 corrosive liquid and 2/3 gas phase were selected to ensure that the sample was exposed to enough corrosive environment while also allowing for the formation of a gas phase above the solution. The samples were hung with a nylon thread, suspended in the test tubes, and exposed to vapours for one month (28 days) in an oven at 40 °C. Note that, high concentrations of the corrosive compounds and a temperature slightly higher than room temperature (40 °C) were selected to accelerate the corrosion processes of the lead samples.

2.2.2. Surface characterization of corroded samples

2.2.2.1. *Cross-section preparation*

To perform the stratigraphic analysis of the formed corrosion layers, a cross-section of the samples was done and then fixed with PhenoCure black thermoplastic resin from Buehler® using a *SimpliMet XPS1 Automatic Mounting Press* instrument. Although malleable and ductile metals are sensitive to heat and pressure, according to the Buehler® SumMet™ Guide [43]. In this case, the parameters for the corroded lead samples were selected at a temperature of 135 °C with a pressure of 17-20 MPa, slightly less than the standards. The encapsulation process is brief (less than 2 minutes) and unlikely to significantly impact the microstructure at this temperature. Also, only optical microscopy was used to analyse the thickness and penetration of the layers in these sections. After that, to reduce the formation of shrinkage gaps, the samples were cooled under pressure to at least 50 °C.

The final step was polishing to give a mirror-like appearance, which was done using an EcoMet 300 grinder/polisher and AutoMet 300 power head with p600-p800-p1200 SiC papers (5 minutes each in rotatory mode and water-cooled). Finally, 6 μm of Buehler's MetaDi polycrystalline diamond suspension in a VelTex diamond cloth was used for 10 minutes to complete the metallographic preparation.

2.2.2.2. *SEM-EDS analysis*

Samples were characterized by JEOL JSM-5310 scanning electronic microscope (SEM) coupled with an Oxford Inca Energy (20 kV) 200 EDS system.

2.2.2.3. *X-ray diffraction analysis*

X-ray diffraction (XRD) analysis was performed using an X'Pert PANalytical Diffractometer and a CuKα radiation source in a Bragg-Brentano configuration on the surface of the treated lead samples. The data was collected in continuous scan mode, with 2θ data ranging from 10° to 80° and a 0.013° sampling pitch, at a scan

rate of 3° per minute. The crystalline phases were identified using the X'Pert Highscore software and the intensities of the standard sample were retrieved from the PDF-2 database of the International Centre for Diffraction Data® (PDF4+).

2.2.2.4. *Optical microscope*

Images of the corroded samples were obtained using a Nikon Microscope Cover Type 104-Lab SMZ MXA22061 and a Photonic Optics PL 3000B cold light illuminator. The images were analysed using Nikon Imaging Software NIS-Elements F Ver. 4.00.06. A zoom of 3x was used for the general surface and 6.3x for the stratigraphy.

2.2.3. Corrosion rate determination by mass loss tests.

Gravimetric analysis was performed following the Standard Procedure for Preparing, Cleaning, and Evaluating Corrosion Test Specimens (ASTM G31) [41].

To perform the measurements, samples were prepared as described in section 4.2.1 and were measured and weighed. Then, the lead samples were exposed to the corrosive environments for 7 days (as described in section 2.2.1). After that, the corrosion products were removed from the surfaces by scrubbing with a non-metallic bristle brush, sonication and rinsed several times with deionized water. Since no heavily incrusted corrosion products were obtained, chemical and electrochemical cleaning methods were not used [41] in order to avoid the removal of metal.

The samples were rinsed with deionized water and degreased with isopropanol. Finally, they were weighed again. The obtained results were used to calculate the corrosion rate using the following equation [41]:

Equation 2-1 $$CR\ (mm/yr) = \frac{\Delta W \cdot K}{A \cdot T \cdot D}$$

Where ΔW is the weight loss (g), in this case after 7 days of exposure, the K constant has a value of 87.6 to convert in the corrosion rate units desired (mm/yr), A

is the surface area in (cm^2), D is the density of metal (11.34 g/cm^{-3} [18]), and T is the time (h).

2.2.4. Tafel extrapolation measurements

Tafel extrapolation was performed using an Autolab PGSTAT 302N potentiostat/galvanostat. An AMETEK Scientific Instruments (K0235) Flat Cell Kit was used in a three-electrode experimental set-up. Measurements were taken on lead samples previously corroded by vapour tests using different working solutions (NaCl, H_2SO_4, HCOOH and AcOH at 3 M, 8 M and 13 M concentrations). A platinum mesh (Pt 99.99%) was used as a counter electrode, and an Ag/AgCl/KCl (3 M) was used as a reference electrode. Tafel extrapolation measurements were performed with a polarization of ±150 mV vs. Eoc and a sweep rate of 10 mV/s. Data modelling was done using Nova 2.1 Software.

Two different electrolytes were used for the measurements: 0.1 M nitric acid and simulated tap water (3.04 mM $CaCl_2$ and 0.54 mM $MgSO_4$ in deionized water with 50 mM sodium borate added to maintain an alkaline pH of 9.4 [44]).

2.3. Results and discussion of the morphological characterization of the formed corrosion layers

The following chapter will describe the morphology of the corrosion layers formed on lead samples exposed to the selected environments: NaCl, H_2SO_4, HCOOH and AcOH. Sodium chloride is mainly found in marine environments, sulphuric acid in areas with high pollution levels or acid rains and acetic acid as also formic acid are mainly present in wooden materials. To determine how representative the resulting layers are, they will be compared to real objects in the conclusions of this chapter.

It is worth mentioning that while laboratory experiments can provide valuable insights into corrosion behaviour, they may not always be fully representative of the corrosion processes that occur in historical lead artifacts exposed to outdoor

environments. Corrosion in real samples can be influenced by a range of factors such as temperature, humidity, and exposure to pollutants among others. Therefore, it is important to consider the limitations of laboratory experiments and to validate the results obtained in real-world conditions. However, the experiments performed can provide a valuable starting point for developing corrosion models and for understanding the fundamental processes that underlie corrosion of lead historical artifacts. Note that the four selected chemicals (NaCl, H_2SO_4, HCOOH and AcOH) represents the most common environments that induces corrosion layers in lead artifacts. In this chapter it will be discussed whether the models obtained in the laboratory are comparable to those formed in real samples.

The morphological study will be carried out by optical and scanning electron microscopy, while its crystallographic structure and composition will be determined by X-ray diffraction (XRD) analysis.

2.3.1. Lead corrosion in the gas phase of sodium chloride solutions

In marine environments, saline fogs from seawater are formed by small droplets carrying different salts such as sodium chloride. In contact with metallic lead, these atmospheres commonly produce lead chloride compounds in the corrosion layer like laurionite and hydrocerussite [24]. In the present work, samples were exposed for 28 days to NaCl vapour tests to recreate a corrosion layer formed by marine fogs on lead.

The characterization results of the corroded samples are shown in Figure 2-9, presented as a 3x3 matrix. The resulting surfaces are displayed in three rows, differentiated by the concentration of the working solutions during the experiment, from top to bottom: 3 M, 8 M, and 13 M, respectively. Close-up images of corroded surfaces taken by an optical microscope are displayed in the first column (Figures *a*, *d*, and *g*). Cross-sections of the corroded samples, also analysed by an optical microscope, are displayed in the second column (Figures *b*, *e*, and h. Finally, SEM micrographs of the corroded surfaces are shown in the third column (Figures *c*, *f*, and *i*).

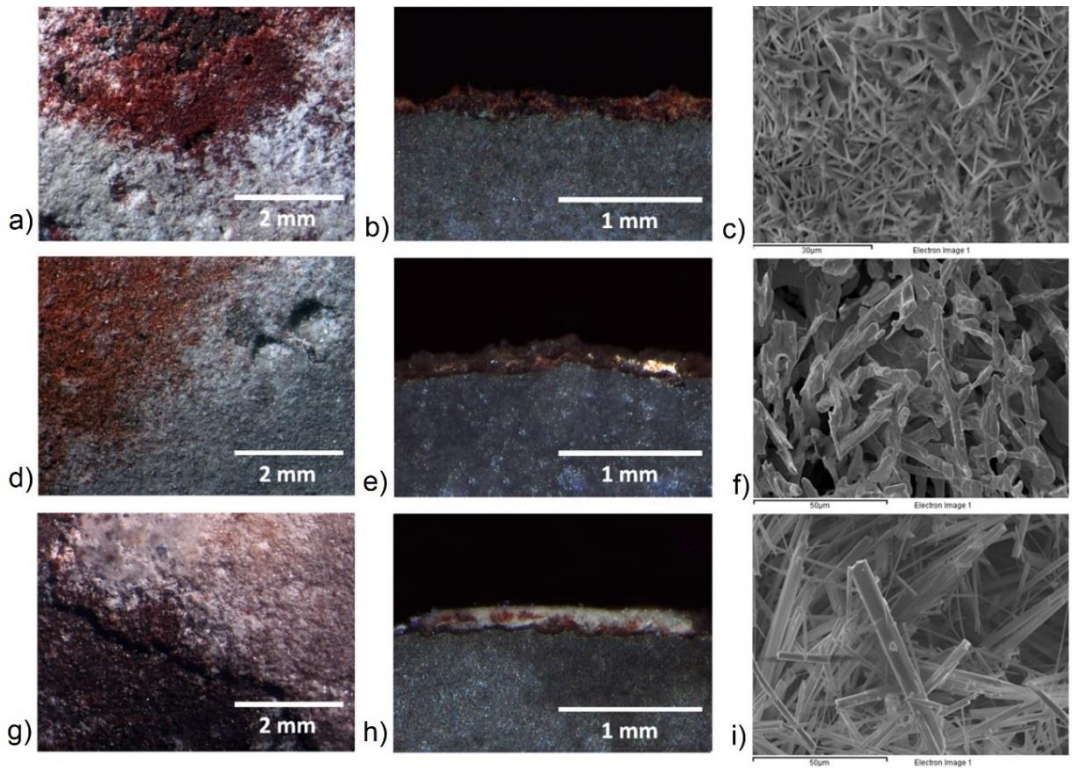

Figure 2-9. Gas-phase corroded Pb samples under sodium chloride dissolutions at different concentrations (from top to bottom: 3 M, 8 M and 13 M respectively) – *a, d* and *g;* close-up images of corroded surfaces recorded with optical microscope – *b, e* and *h;* cross-sections recorded with an optical microscope – c, *f* and *i*; corroded surfaces recorded with Scanning Electrode Microscope (3 M scaled at 30 μm, 8 M and 13 M scaled at 50 μm).

As shown in Figure 2-9 *a, d,* and *g,* the corroded samples exposed to different NaCl concentrations presented localized reddish and white products. Concerning the images *b, e,* and *h,* corresponding to the cross-sections, a corrosion layer of ~200 μm in thickness was observed on all surfaces, with white compounds predominating at 13 M. The main difference was observed in the SEM micrographs of images *c, f,* and *i*. The resulting corrosion layer formed when Pb was exposed to NaCl consists of orthorhombic structures with tabular, prismatic, or acicular crystals [22]. Using 3 M NaCl, as shown in *c,* small sheetlets were obtained on the sample surface, mostly from the lateral side and ~7 μm in length. In contrast, at 8 M and 13 M, elongated and tabular crystals were observed on the corrosion structures, resulting in ~30 μm in

length and ~2 μm in width on the corroded sample using 8 M, and ~80 μm in length and ~4 μm in width on the corroded sample using 13 M.

The crystal structure observed on the corroded sample exposed to 3 M NaCl is typically found in lead hydroxide [45], where the sheetlets are oriented parallel to the growth direction and are distributed homogeneously on the surface. As the NaCl concentration increased, needle-shaped crystals were also formed and grew to a larger size. The database patterns, corresponding to metallic lead, litharge (PbO, red colour), and lead oxide hydroxide chloride (Pb(OH)Cl, white), are displayed in Figure 2-10.

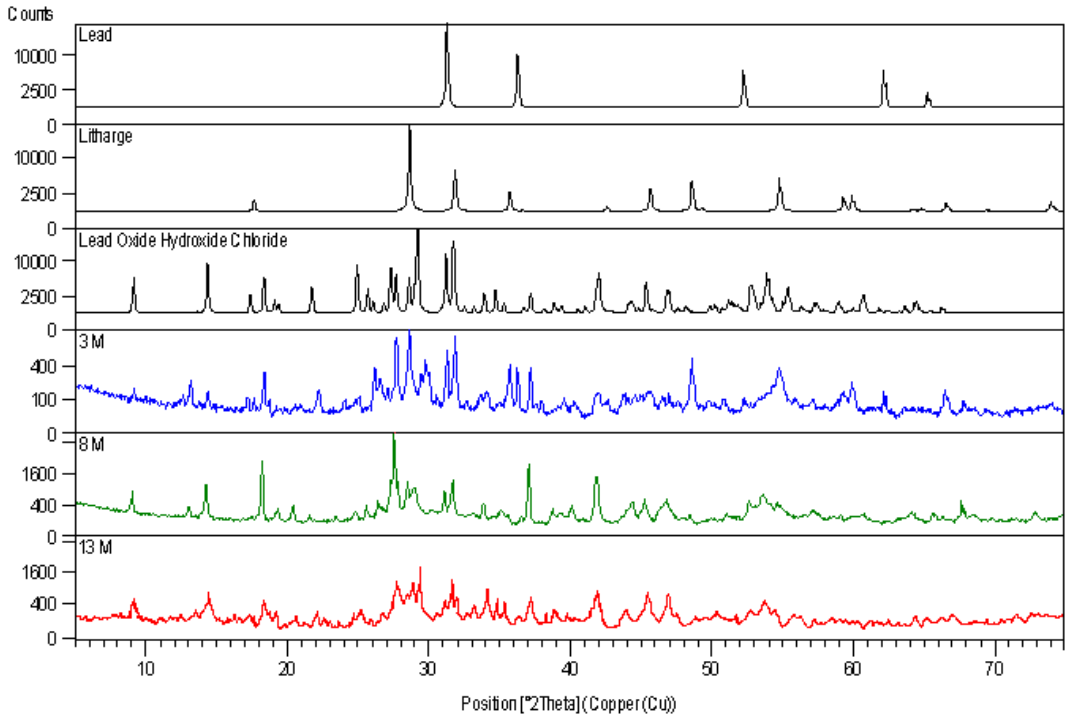

Figure 2-10. Database patterns (black) from International Centre for Diffraction Data® (PDF4+); lead, litharge and lead oxide hydroxide chloride spectra. Corroded samples in the laboratory spectra (blue, green and red); 3 M, 8 M and 13 M.

As shown in Figure 2-10, lead oxide hydroxide chloride and litharge (lead oxide) were present in the three samples. The formation of lead oxide and lead chloride can be described by the following reactions;

Reaction 2-1 $$O_2\ (g) + Pb\ (s) \rightarrow PbO\ (s)$$

Reaction 2-2 $$PbO\ (s) + NaCl\ (s) + H_2O\ (l) \rightarrow Pb(OH)Cl\ (s) + NaOH\ (aq)$$

In the pH range greater than 7, the corrosion mechanism is initiated by oxygen producing a PbO layer. When droplets from the saline solution carrying NaCl evaporate and condense on the surface, they precipitate in the form of lead chloride due to its high insolubility. Lead chloride has a low solubility value in water (7 x 10-2 g/cm^{-3} at 25 °C [14]), resulting in a mixed layer of litharge and lead chloride.

2.3.2. Lead corrosion in the gas phase of sulphuric acid solutions

The production of sulphuric acid is mainly due to the oxidation of gaseous sulphur dioxide, which is a common component in polluted environments. Corrosion caused by pollution factors is quite prevalent. The characterization results of Pb samples exposed to H_2SO_4 are displayed in Figure 2-11, presented in the same 3x3 matrix format as described in the previous section 2.3.1.

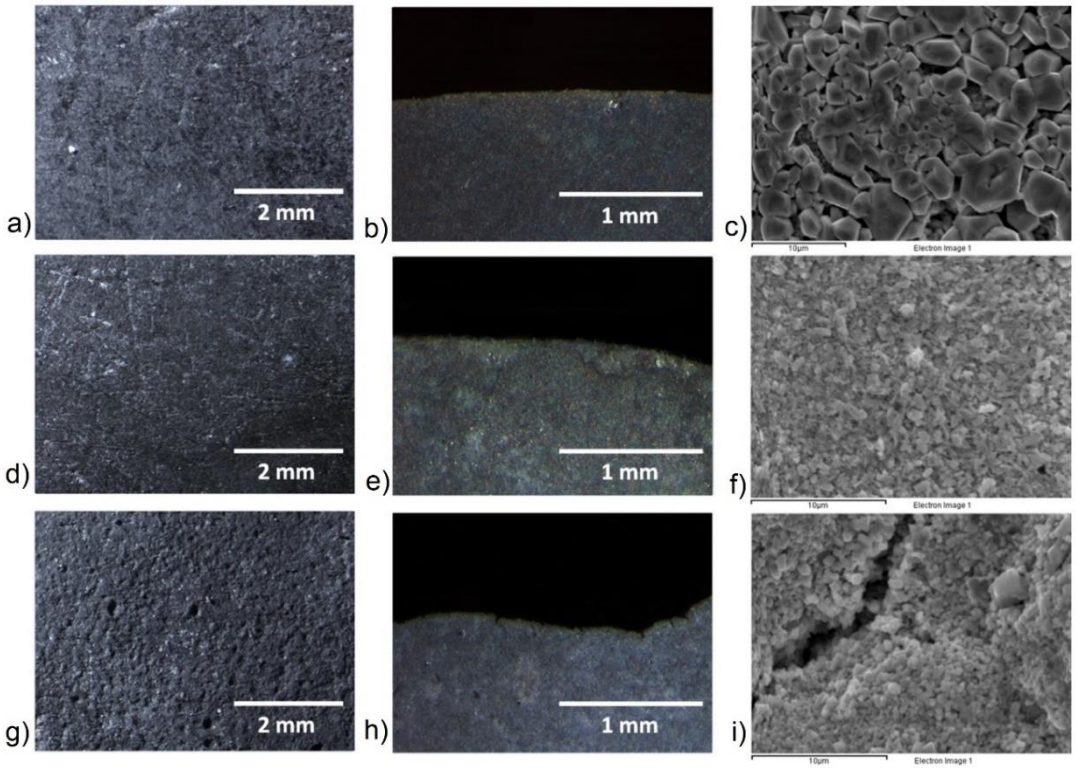

Figure 2-11. Gas phase corroded Pb samples under sulphuric acid dissolutions at different concentrations (from top to bottom: 3 M, 8 M and 13 M respectively) – *a, d* and g*:* close-up images of corroded surfaces recorded with an optical microscope – *b, e* and h*:* cross-sections recorded with an optical microscope; *c, f* and i: corroded surfaces recorded with Scanning Electrode Microscope (all scaled at 10 μm).

As shown in Figures 2-11 *a, d,* and *g*, the corroded samples exposed to different H_2SO_4 concentrations presented a smooth appearance with very tiny dimples, especially when using a concentration of 13 M. In the cross-section images shown in Figures b, *e,* and *h*, a very thin corrosion layer was obtained, which was almost imperceptible, indicating a very thin formed layer. The main difference was observed in the SEM micrographs shown in Figures c, *f,* and *i*. At a concentration of 3 M H_2SO_4, roundish crystals of approximately 3 μm and 5 μm in size were observed, and small aggregates of crystal-shaped particles less than 1 μm in size were also seen in the interstitial spaces. At a concentration of 8 M H_2SO_4, small crystals of approximately 1 μm with different shapes were observed on the entire surface. Finally, at a

concentration of 13 M H_2SO_4, crystals less than 1 μm in size were also formed, but smaller than those formed at a concentration of 8 M. In addition, small cracks were present on this last surface.

Differences in crystal size were related to the nucleation kinetics and crystal growth. When the solution contained a higher concentration of sulphuric acid, more crystal nuclei formed, which could actually limit crystal size. Therefore, the growth of the crystals depended on the concentration of sulphuric acid present in the solution [46,47].

XRD measurements of the corroded samples using the three concentrations of H_2SO_4 are shown in Figure 2-12, along with database patterns of lead and lead sulphate ($PbSO_4$, which are colourless to white but often tinted yellow or green).

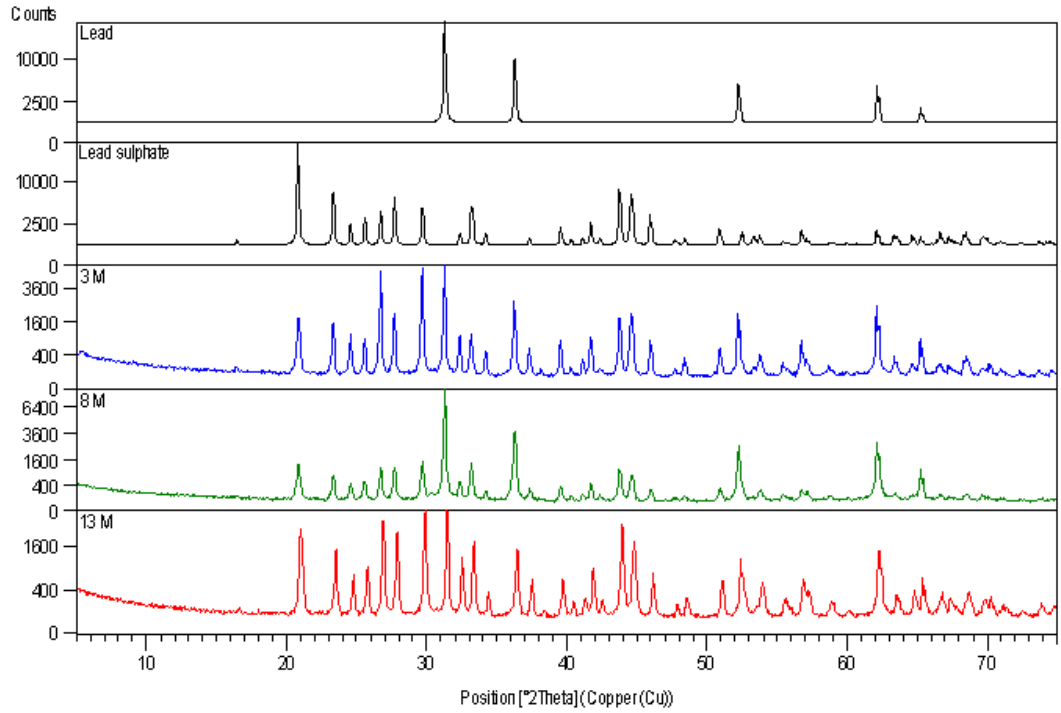

Figure 2-12. Database patterns (black) from International Centre for Diffraction Data® (PDF4+); lead and lead sulphate spectra. Corroded samples in the laboratory spectra (blue, green and red); 3 M, 8 M and 13 M.

As shown in Figure 2-12, the diffractograms show peaks for metallic lead and lead sulphate. The formation of this layer was produced by the condensation of droplets from sulphuric acid solutions. Due to the acidic pH range, the corrosion process in this case is initiated by proton activity rather than oxygen, as demonstrated by the use of NaCl vapours (see section 1.3.1). The lead surface reacts quickly with sulphuric acid, forming lead sulphate;

Reaction 2-3 $$Pb\ (s) + H_2SO_4\ (aq) \rightarrow PbSO_4\ (s) + H_2\ (g)$$

When lead is in contact with droplets containing sulphuric acid, a very low-solubility compound of lead sulphate ($PbSO_4$) is formed on the surface (4×10^{-4} g/cm^3 at 25 °C [14]). The resulting crystals grow in a compact structure with very small pores. The crystals are smaller when the concentration of sulphuric acid is increased, due to a higher number of crystal nuclei. In this context, the resulting layers are very compact, protecting the metal from further corrosion [48].

2.3.3. Lead corrosion in the gas phase of formic acid solutions

Formic acid (HCOOH) was selected as a volatile organic compound found in many Cultural Heritage environments. Formic acid is present in oil-based paints and as an atmospheric pollutant originating from wooden displays or storage. This acid has a vapour pressure of >80 mmHg at 40 °C [49] and easily become into the gas phase. The characterization results of corroded Pb samples by HCOOH vapours are shown in Figure 2-13, as a 3x3 matrix with the same structure as the previous section 2.3.2.

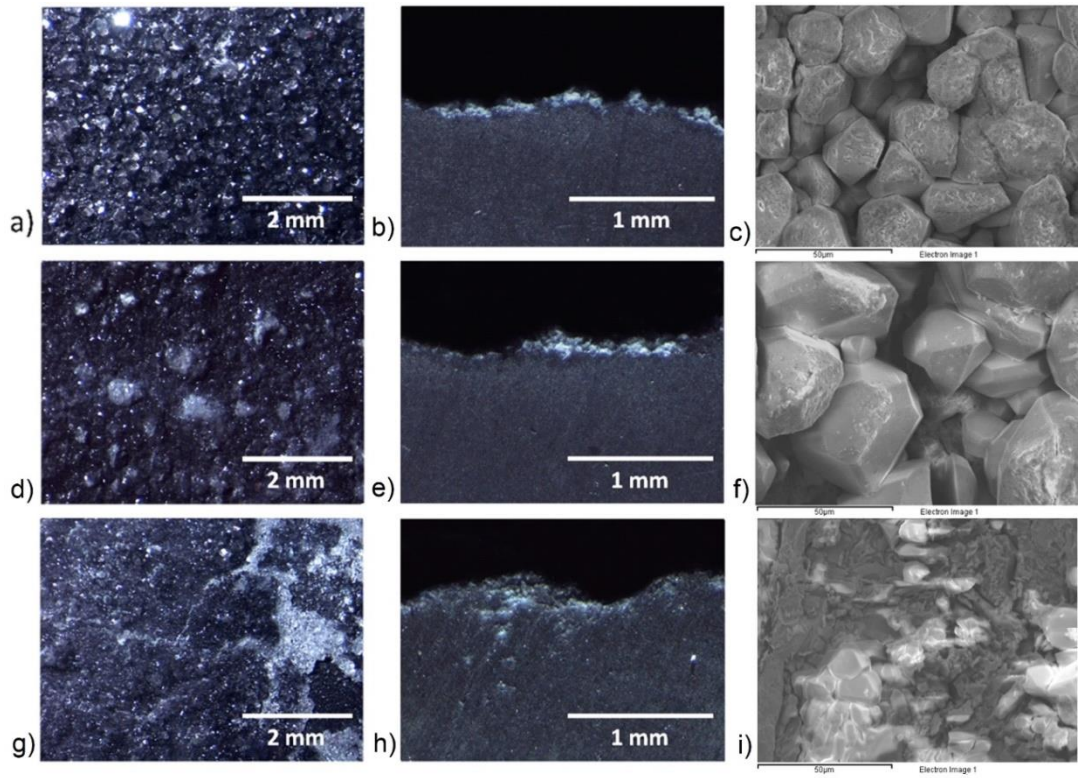

Figure 2-13. Gas phase corroded Pb samples under formic acid solutions at different concentrations (from top to bottom: 3 M, 8 M and 13 M respectively) – *a, d* and *g;* close-up images of corroded surfaces recorded with an optical microscope – b, e and h: cross-sections recorded with an optical microscope – *c, f* and *i;* corroded surfaces recorded with Scanning Electrode Microscope (all scaled at 50 μm).

As shown in Figure 2-13, in environment 3 M (a), a homogeneous corroded surface is observed. As the concentration increased to 8 M and 13 M (*d* and *g*, the corrosion layer became heterogeneous. This was formed mainly by crystalline agglomerations in localized areas. The cross-section shown in Figure 2-13 *b* (3 M) shows a corrosion layer of approximately 120 μm thick, formed by clustered surface crystals. As the concentration increased to 8 M and 13 M, the layer became more irregular. In the SEM micrograph shown in Figure 2-13 *c* (3 M), rounded crystals with a size ranging from approximately 30 μm to 50 μm in diameter were observed. In the case of 8 M, the crystal size increased (from approximately 50 μm to 100 μm) as

shown in Figure 2-13 *f*. However, a decrease in crystal size was obtained at 13 M (from approximately 30 μm to 50 μm), with a very heterogeneous distribution as observed in Figure 2-13 *i*.

These types of morphological differences, which resulted from the three formic acid vapour test concentrations, were also described in the sulphuric acid vapour tests from the previous section 2.3.2. The number of crystal nuclei increased as the concentration increased, due to the high kinetic energy. As a result, the crystal size formation was smaller. The corroded surface showed an irregular layer with small embedded crystals. Smaller roundish particles less than 10 μm were also observed, possibly related to lead oxide crystals.

The XRD patterns of the corroded samples exposed to different formic acid concentrations are presented in Figure 2-14. For comparison, the database pattern of lead formate ($Pb(HCO_2)_2$, which is colourless to white) is included.

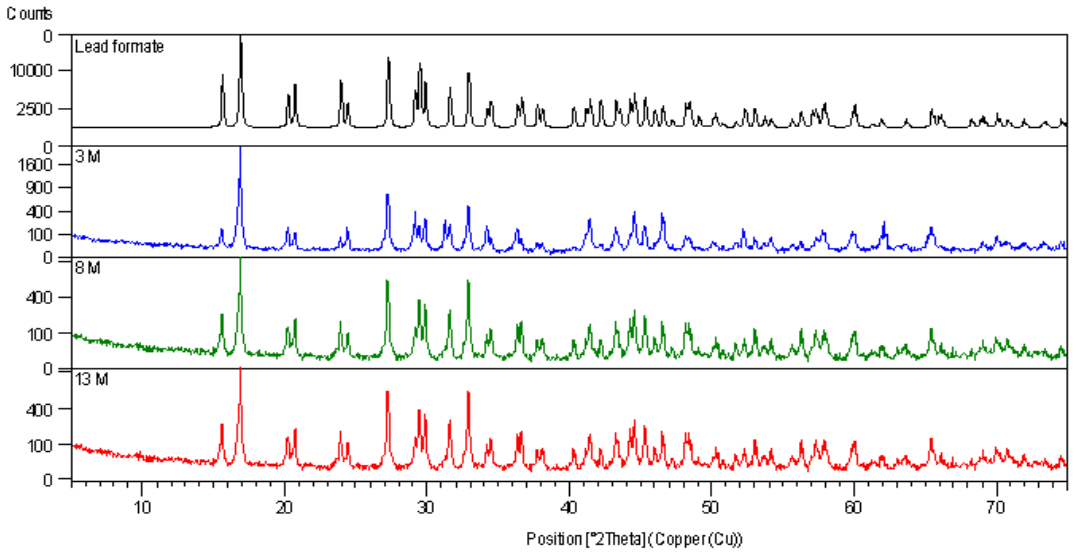

Figure 2-14. Database patterns (black) from Database patterns from International Centre for Diffraction Data® (PDF4+); lead and formate spectra. Corroded samples in the laboratory spectra (blue, green and red); 3 M, 8 M and 13 M.

Peaks of lead formate were observed in all the diffractograms (see Figure 2-14). Lead formate consists of a three-dimensional polymeric structure with Pb^{2+} nodes connected by bridging formate anions and has high solubility (1.6×10^{-1} g/cm^3 at 25 °C [14]). Compared to the previous corroded samples exposed to NaCl and H_2SO_4, HCOOH has a very high vapour pressure and more acidic species can be present in the condensed droplets. The corrosion process was formed according to the following reaction:

Reaction 2-4 $$2HCOOH + Pb \rightarrow Pb(HCOO)_2 + H_2$$

Compared to sodium chloride and sulphuric acid solutions, formic acid has high vapour pressure and therefore a higher concentration of acid is in contact with the lead surface. The reaction is initiated by proton activity and the reaction rate increases at higher acid concentrations. In this context, the growth of crystals is hindered due to the fast formation of new nuclei. The resulting compounds of lead formate and lead formate hydroxide are in good agreement with bibliographic data [10].

2.3.4. Lead corrosion in the gas phase of acetic acid solutions

Finally, acetic acid was selected as the working solution for corroding metallic lead samples by vapour tests. Acetic acid is also classified as a volatile organic compound (VOC) with a high vapour pressure of over 30 mmHg at 40°C [50] This can be produced in a variety of cultural heritage contexts, such as silicone sealants, deteriorating cellulose acetate, paints, linoleum, or cleaning solutions. Acetic acid vapours are especially emitted by wooden objects at high concentrations. The results are shown in Figure 2-15 as a 3x3 matrix, following the same structure as described in the previous section 2.3.3.

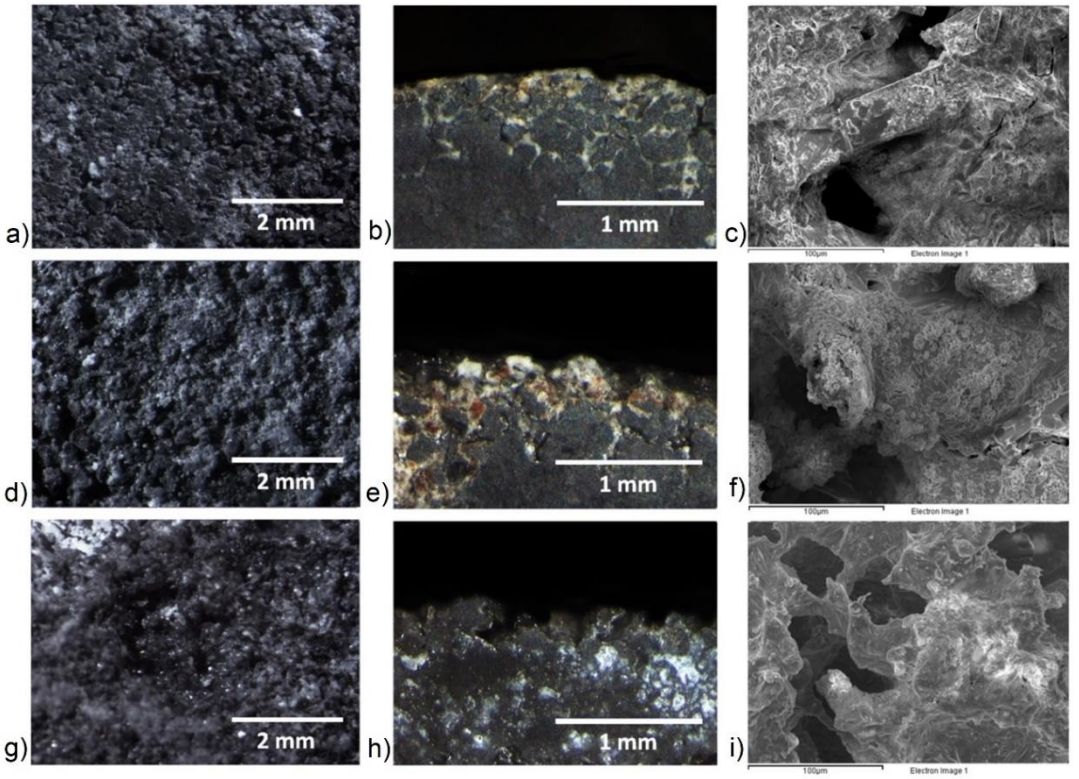

Figure 2-15. Gas phase corroded Pb samples under acetic acid solutions at different concentrations (from top to bottom: 3 M, 8 M and 13 M respectively) – *a*, *d* and *g;* close-up images of corroded surfaces recorded with an optical microscope – *b*, *e* and *h;* cross-sections recorded with an optical microscope – c, *f* and *i*: corroded surfaces recorded with Scanning Electrode Microscope (all scaled at 100 μm).

The corroded sample exposed to a 3 M solution of acetic acid (AcOH) showed a severe degradation, with small, distributed holes on the surface, as shown in Figure 2-15 *a*, *b* and *c.* As observed in b, the sample presented white, yellowish products that covered the entire surface, forming a very irregular corrosion layer of approximately 70 μm in thickness. In Figure 2-15 *e*, new reddish and white heterogeneous crystals were observed on the corroded sample using an 8 M solution and were related to lead acetate. At 13 M, as shown in *h*, severe degradation was observed on the metallic surface due to its dissolution as the acetic acid concentration increased. Finally, very porous surfaces were observed in the SEM micrographs c, *f* and *i*, and as the

concentration increased, the degradation of the metallic matrix became more severe. As reported in numerous studies [7,8,51], the corrosion of metallic lead by acetic acid is usually initiated by pitting corrosion, which breaks the oxide layer's passivation. This localized form produces agglomerated compounds that increase and eventually cover the entire surface, forming a rough and porous corrosion layer. As a result, the surface is not passivated, leading to further corrosion products.

XRD measurements on the corroded samples using different concentrations of AcOH are shown in Figure 2-16. To be compared, data base pattern of lead acetate oxide hydrate (colourless to white or white-yellowish $Pb(CH_3COO)_2{\cdot}2Pb(OH)_2$) is included.

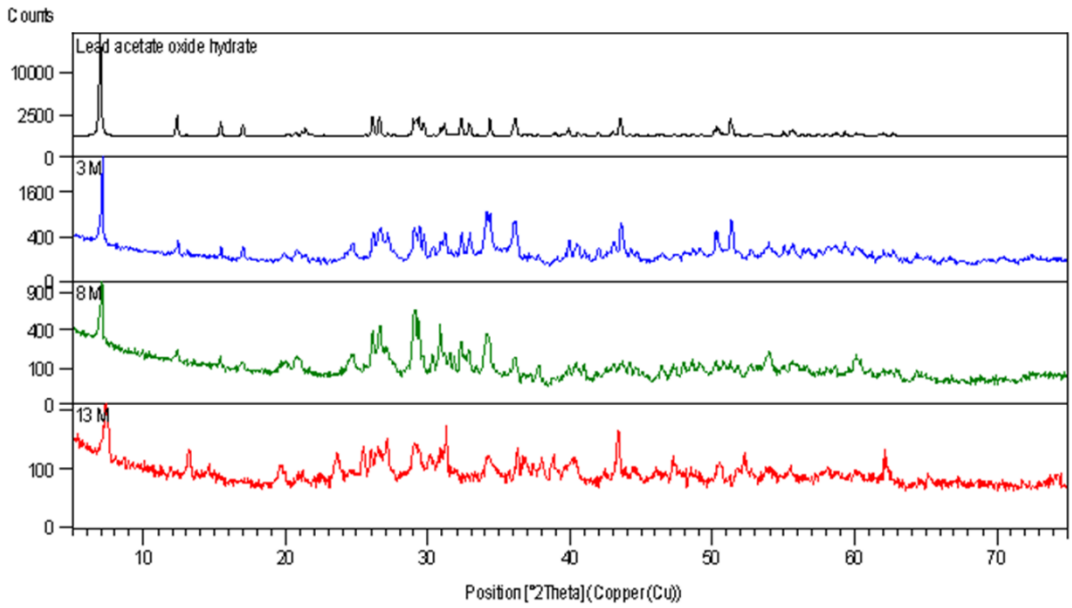

Figure 2-16. Database patterns (black) from Database patterns from International Centre for Diffraction Data® (PDF4+); lead and lead acetate oxide hydrate spectra. Corroded samples in the laboratory spectra (blue, green and red); 3 M, 8 M and 13 M.

Lead corrosion by AcOH vapours is an electrochemical process that triggers an acid-base reaction, generating soluble corrosion products of lead acetate [52] (4.5 x 10-1 g/cm3 [14]). The main resulting corrosion compound for all samples shown in Figure 2-16 was lead hydroxide acetate, as expressed in the following global reaction:

Reaction 2-5 $$Pb\ (s) + \ 2CH_3COOH\ (aq) \rightarrow H2\ (g) + Pb(CH_3COO)_2\ (s)$$

Reaction 2-6 $$2Pb(CH_3CO_2)_2\ (s) + 2H_2O\ (l) \rightarrow Pb(OH)_2\ (s) + 2CH_3COOH(s)$$

Acetic acid has a high vapour pressure, which promotes an increase in the corrosion rate. This occurs due to a potential difference in the system between the condensed droplets and the metallic surface. The corrosion process is initiated by proton activity, resulting from the acidic pH range. This produces lead acetate and/or lead acetate hydroxide, which are highly soluble and unstable compounds. These form an irregular and highly porous film, allowing the introduction of acidic species into the metallic matrix, and initiating a new corrosion process. The surface is not passivated, leading to severe degradation.

2.4. Corrosion rate determination of lead samples

To analyse the corrosion rate values of Pb surfaces exposed to different vapour tests, gravimetric and Tafel extrapolation analyses were performed. Corrosion rates were obtained through gravimetric analysis after 7 days of exposure to the different vapours (as described in section 2.2.3). This time frame was sufficient to analyse the results obtained from gravimetric measurements on Pb samples exposed to the different vapour tests presented in this chapter.

In addition, to examine the passivation effect of these layers, the exposure was extended to 28 days to achieve a higher layer thickness, and Tafel extrapolation analysis was performed. For this methodology, an alkaline medium (simulated tap water) and an acidic medium (as outlined in section 2.2.4) were used to compare the protective behaviour of the resulting layers in different media.

2.4.1. Determination of corrosion rate by gravimetric analysis

Corrosion rate values of the corroded Pb samples by the vapour exposition using NaCl and H_2SO_4 at different concentrations are presented in Figure 2-17.

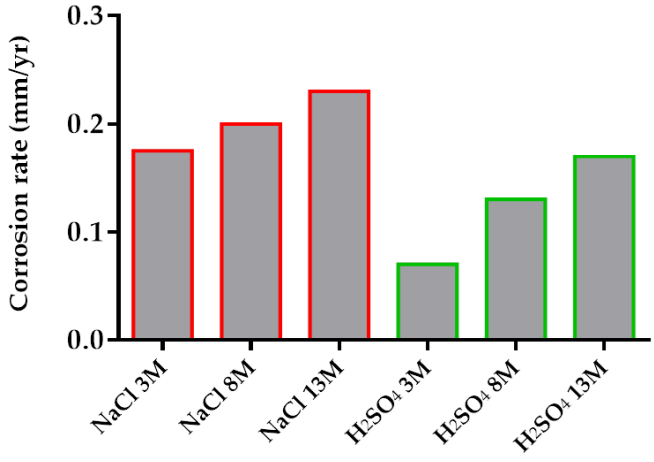

Figure 2-17. Corrosion rate values (mm/yr) of the corroded Pb samples by vapour tests using inorganic working solutions (NaCl 3 M, 8 M and 13 M, and H_2SO_4 3 M, 8 M and 13 M).

In Figure 2-17, Pb samples exposed to NaCl showed corrosion rates of 0.17 mm/yr (3 M), 0.20 mm/yr (8 M), and 0.23 mm/yr (13 M). The samples exposed to H_2SO_4 showed corrosion rates of 0.07 mm/yr (3 M), 0.13 mm/yr (8 M), and 0.17 mm/yr (13 M). As observed, all values in both environments were at a low level, which is related to the morphological characteristics of the formed surface layers. The corrosion rate values were slightly higher for NaCl-corroded surfaces compared to H_2SO_4. corroded surfaces. This was due to the higher degree of porosity and lower compactness of lead chloride and hydrochloride layers compared to lead sulphate layers. In addition, this difference could also be influenced by the solubility values of the resulting surface products, which was 1.0×10^{-4} g/dm^3 for lead chloride and 1.0×10^{-8} g/dm^3 for lead sulphate.

The corrosion rate values resulting from the Pb samples exposed to vapour using HCOOH and AcOH at different concentrations are presented in Figure 2-18.

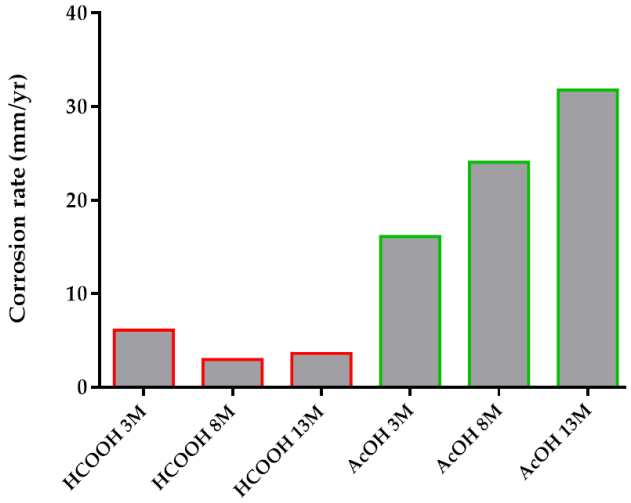

Figure 2-18. Corrosion rate values (mm/yr) of the corroded Pb samples by vapour tests using organic volatile compounds working solutions (HCOOH 3 M, 8 M and 13 M, and AcOH 3 M, 8 M and 13 M).

In this case, all corrosion rates were higher than those obtained with NaCl and H_2SO_4 due to the soluble and porous layers formed on the surfaces. As shown in Figure 2-18, samples exposed to acetic acid presented corrosion rate values of around 5 mm/yr (6.10 mm/yr for 3 M, 2.96 mm/yr for 8 M, and 3.62 mm/yr for 13 M). Corrosion rates obtained with acetic acid exposure were much higher than those exposed to formic acid. In addition, the calculated corrosion rates increased as the concentration of acetic acid increased (16.11 mm/yr for 3 M, 24.06 mm/yr for 8 M, and 31.76 mm/yr for 13 M). The surface layer was much more irregular after acetic acid exposure, resulting in high porosity and low compactness, in comparison with those exposed to formic acid (see section 2.3.1). In addition, lead acetate is more soluble (solubility at 25 °C is 4.5 x 10^{-1} g/cm^3 [14]) than lead formate (solubility at 25 °C is 1.6 x 10^{-1} g/cm^3 [14]), producing a faster dissolution of the metal due to its exposure to the medium.

2.4.2. Determination of corrosion rate by Tafel extrapolation

Tafel extrapolation was performed on corroded lead samples without removing the corrosion products from the metal surface. The experiments were performed using simulated tap water with a pH of 9.4 and 0.1 M nitric acid as working electrolytes.

Tap water was selected due to its frequent presence in humid environments where historical artefacts and their metallic surfaces may be exposed. However, as its chemical composition is challenging to reproduce, synthetic tap water (TW) was prepared as described in the reference [44]. Additionally, 0.1 M nitric acid was selected for its high reactivity with lead. Rathgen [53] first described a procedure for restoring corroded metals, in which diluted nitric acid was used for chemical cleaning. This can disrupt the corrosion layers, but it can also dissolve the oxide protective films and the metallic matrix. The use of nitric acid was also intended to study the different protective mechanisms of the resulting corrosion layers in an aggressive acidic medium compared to the slightly alkaline tap water.

As an example, Tafel plots on corroded samples exposed to vapours of solutions containing sulphuric acid at the three concentrations (3M, 8M and 13M) were obtained in simulated Tap Water (pH=9.4). Data is shown in Figure 2-19.

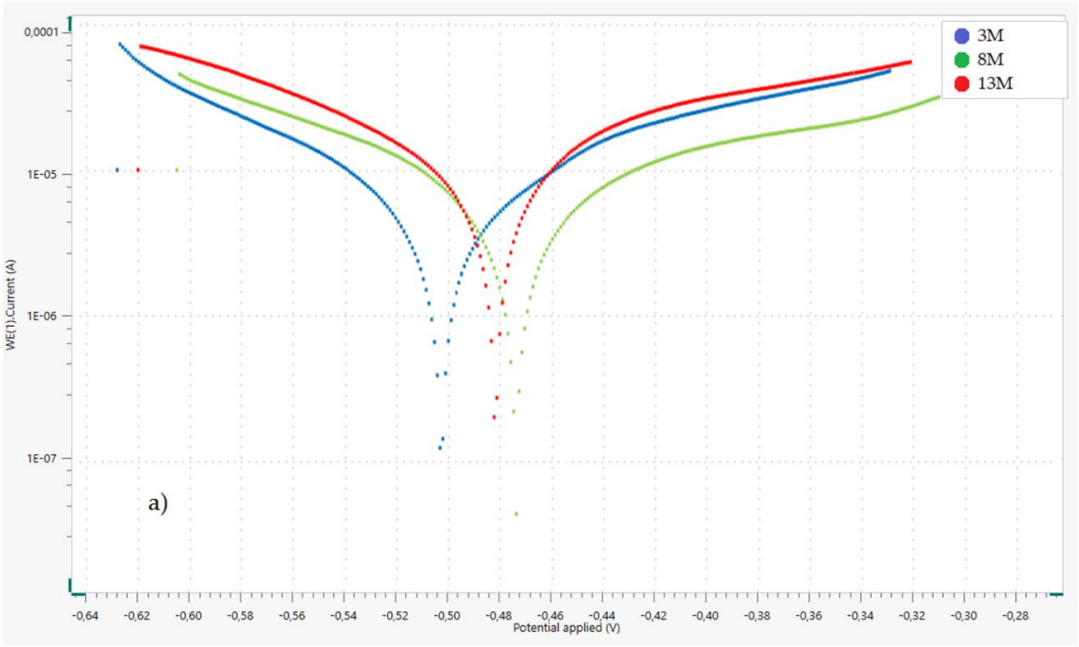

Figure 2-19. Tafel extrapolation in Tap Water solution at 9.4 pH, for Pb samples corroded by sulphuric acid gas phase at different concentrations.

Tafel analysis was performed in the above shown curves using the software Nova 2.1 and the obtained values are shown in Table 2-1:

Table 2-1. Comparison of the products obtained in historical lead objects and laboratory-induced corrosion in metallic lead samples.

Tap water 9.4 pH						
Sample	**I_{corr} (A/cm^{-2})**	**R_p(Ω)**	**Corr. Rate (mm/yr)**	**Ecorr (V)**	**|ba| (V/dec)**	**|bc| (V/dec)**
H_2SO_4 3 M	5.03*10^{-6}	5204	0.15	-0.50	0.12	0.11
H_2SO_4 8 M	4.84*10^{-6}	5906	0.14	-0.47	0.15	0.11
H_2SO_4 13 M	7.33*10^{-6}	3351	0.23	-0.48	0.11	0.11

Thus, corrosion rate values obtained by Tafel extrapolation (using simulated TW and nitric acid electrolyte) on Pb samples exposed to NaCl and H_2SO_4 are shown in Figure 2-20. Raw data and Tafel analysis are shown in the supplementary information of this chapter.

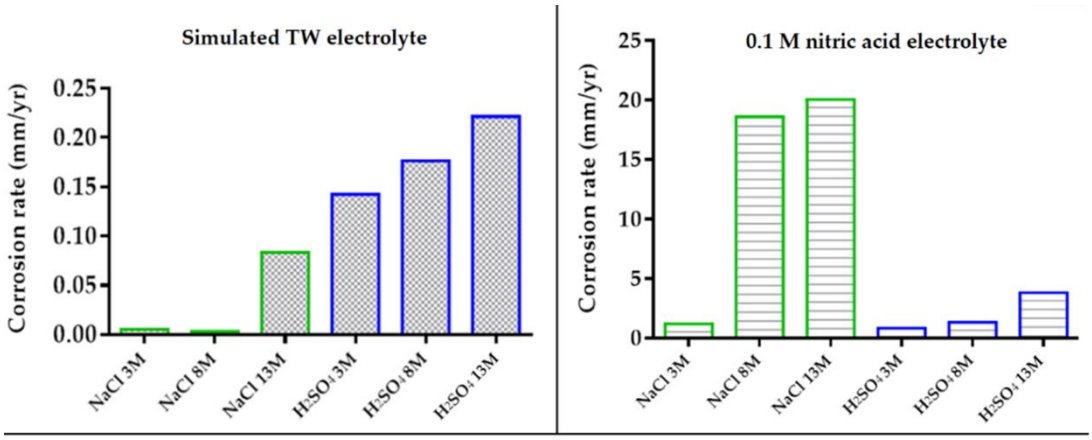

Figure 2-20. Tafel Extrapolation values using simulated tap water 9.4 pH (left) and 0.1 M nitric acid (right) on corroded Pb samples by NaCl and H_2SO_4 vapours.

In the case of using TW as an electrolyte (as shown in Figure 2-20, on the left), the samples exposed to the gas phase of solutions containing NaCl presented very low corrosion rates, with values smaller than 0.01 mm/yr (at 3 M and 8 M) and 0.07 mm/yr (at 13 M). It is possible that channels were produced in the elongated and tabular crystals formed (see Figure 2-9), allowing the corrosive solution to access the metal and leading to higher corrosion rates compared to the other concentrations. The formation of such channels can be due to differences in the crystal structure or the growth rate of the corrosion products. Moreover, all three values were lower than those obtained for the samples exposed to H_2SO_4 (0.15 mm/yr for 3 M, 0.18 mm/yr for 8 M, and 0.23 mm/yr for 13 M). Lead chloride has a slightly higher solubility (7 x 10-2 g/cm^{-3} at 25°C) compared to lead sulphate (4 x 10-4 g/cm^{-3} at 25°C) [14]. This solubility difference allows for hydrolysis to take place in the basic TW medium. This hydrolysis process promotes the precipitation of lead hydroxide. The pores of the surface layer were covered by this precipitate, resulting in a more compact structure.

In contrast, lead sulphate is very insoluble, which limits the formation of lead hydroxide. Additionally, the thin layers of lead sulphate that were formed presented small cracks, which could increase the corrosion rates when the metal was exposed to the simulated TW (as discussed in section 1.3.1). In general, all values were very low and note that, 0.15 mm/yr is considered a good corrosion resistance value [54].

The Tafel extrapolation results using 0.1 M nitric acid indicated that samples exposed to the gas phase of NaCl solutions (1.55 mm/yr for 3 M, 18.78 mm/yr for 8 M, and 20.34 mm/yr for 13 M) had in general higher corrosion rates compared to those exposed to the gas phase of H_2SO_4 solutions (1.24 mm/yr for 3 M, 2.54 mm/yr for 8 M, and 4.34 mm/yr for 13 M). This was attributed to the higher solubility of lead chloride, which led to the breakdown of the protective layer and corrosion of the metal. Furthermore, lead oxide and hydroxide layers could not form in this acidic environment, and hence no additional protection was provided. On the other hand, lead sulphate layers had a more stable and compact morphology with lower solubility, providing better protection to the metallic surface in the acidic medium.

Corrosion rate values obtained by Tafel extrapolation (using simulated TW and nitric acid electrolyte) on Pb samples exposed to AcOH and HCOOH are shown in Figure 2-22. Raw data and Tafel analysis are shown in the supplementary information of this chapter.

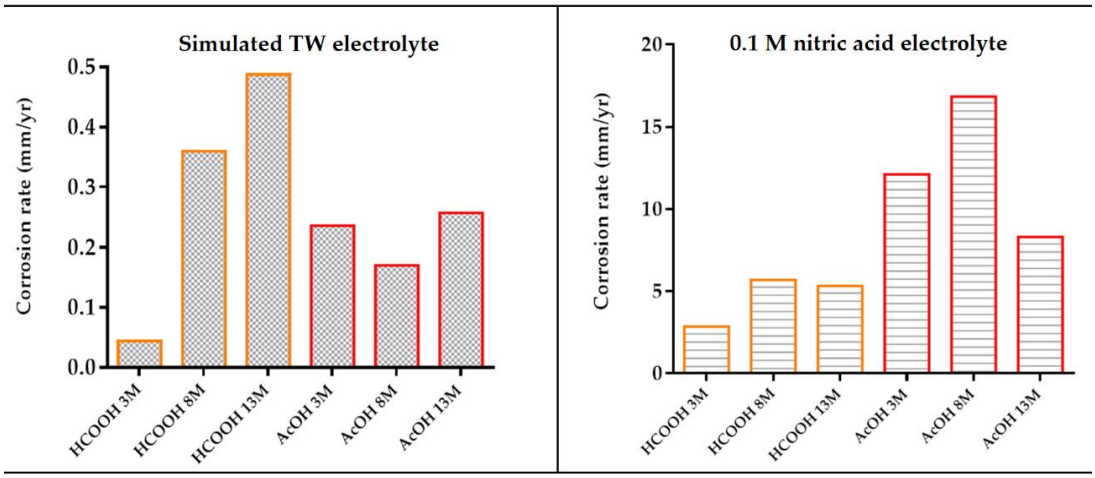

Figure 2-21. Tafel Extrapolation values using simulated tap water 9.4 pH (left) and 0.1 M nitric acid (right) on corroded Pb samples by AcOH and HCOOH vapours.

As shown in Figure 2-22 (left), the corrosion rate values were low for the corroded Pb exposed to the gas phase of solutions containing HCOOH (0.04 mm/yr for 3 M, 0.35 mm/yr for 8 M, and 0.48 mm/yr for 13 M) and AcOH (0.24 mm/yr for 3 M, 0.18 mm/yr for 8 M, and 0.16 mm/yr for 13 M) when using the simulated tap water-electrolyte. Similar to the samples exposed to NaCl, due to the solubility of both compounds (lead formate and lead acetate), the released lead ions produced lead hydroxide due to the alkaline environment. It filled the pores of the corrosion layer, promoting an increase in protection. It is worth mentioning that due to the passivation effect observed the values obtained for both media (AcOH and HCOOH) are relatively small, less than 0.5 mm/yr which is considered satisfactory for most metals [54].

This effect was not observed when using 0.1 M nitric acid as an electrolyte. The corrosion rate values were much higher for the corroded samples exposed to HCOOH vapour (2.57 mm/yr for 3 M, 5.82 mm/yr for 8 M, and 4.89 mm/yr for 13 M) and AcOH vapour (13.88 mm/yr for 3 M, 18.43 mm/yr for 8 M, and 8.67 mm/yr for 13 M). In this case, lead hydroxide could not be formed due to the acidic pH of the medium. The dissolution of lead formate and lead acetate is initiated by proton activity due to the high solubility of these compounds [55]. As a result, the sample

became unprotected, yielding a high corrosion rate. The corrosion layers are also very porous and irregular, allowing the interaction between the electrolyte and the metallic Pb surface.

2.5. Concluding remarks

Chapter 2 discusses the importance of generating corrosion models in the laboratory before establishing conservation/restoration protocols. Several characterization techniques involve the use of destructive methods, necessitating the preparation of corroded samples in the laboratory for analysing the surface behavior in different contexts. Physical parameters of corrosion layers, such as solubility, porosity, and adhesion, help to understand how degradation evolves under certain conditions. In this context, metallic lead samples were exposed to vapours of different environments: sodium chloride, sulphuric acid, formic acid, and acetic acid. The goal was to recreate in the laboratory the most common environments in which lead artefacts can suffer when exposed to atmospheric conditions. To accelerate the corrosion phenomenon in the metal surface high electrolyte concentrations (3M, 8M and 13M) and a working temperature (40°C) higher than room temperature were used.

In general, the corrosion rates obtained for the samples exposed to vapours of solutions containing NaCl and H_2SO_4 yielded a low level of corrosion, that is, both environments generated protective corrosion layers. This phenomenon can be explained by the morphology of these layers. On the one hand, samples exposed to vapours of solutions containing NaCl formed layers composed of a mixture of lead chloride and lead oxide. Its morphology varies from tabular, prismatic, or acicular crystals at 13M NaCl to small sheetlets at 3M NaCl. In all cases a, certain grade of porosity was obtained. Nevertheless, due to the thickness of the layers and the low solubility of the formed products the base metal remained protected. On the other hand, samples exposed to vapours of solutions containing H_2SO_4 formed roundish crystals of different sizes, from ~5μm at 3M H_2SO_4 to <1μm at 13M H_2SO_4. Due to the low porosity and its compacity the metal remained protected.

A different scenario was obtained when Pb was exposed to vapours of solutions containing formic (HCOOH) and acetic acid (AcOH). In both cases, high corrosion rates were obtained. In the case of metallic Pb exposed to HCOOH vapours, small crystals were obtained, decreasing in size as the concentration of formic acid increased in the working solutions. The resulting corrosion layers were thin, porous and irregular, especially at a high concentration (13 M) formed by agglomerated rounded crystals. When samples were exposed to vapours of AcOH solutions, the corrosion layers formed on the surface were very heterogeneous and porous. Note that in both environments (HCOOH and AcOH) the obtained morphology promoted a continuous degradation of the metallic matrix because the bare metal was continuously exposed to the environment. The cause is the formation of pores in the corrosion layer and also the solubility of both surface compounds (lead formate and lead acetate).

In a different set of experiments, the behaviour of the corroded coupons was evaluated in different media (0.1 M nitric acid and simulated tap water at pH=9) by determining the corrosion rate using the Tafel method. Note that when simulated Tap Water was used the formed lead salts can be partially hydrolyzed to form lead hydroxide, which precipitates due to the slightly alkaline medium. This promoted a plus of protection by covering the pores from the surface layers. However, when 0.1 M nitric acid was used, this alkaline effect was not possible, and the obtained corrosion rates were higher. A similar tendency was obtained for the samples exposed to formic (HCOOH) and acetic acid (AcOH). However, in all cases, the obtained corrosion rates were higher than those obtained with the samples exposed to NaCl and H_2SO_4. It was due to the high solubility and porosity of the corrosion layer (lead formate and acetate).

It is important to mention that corrosion was induced in the laboratory by exposing the samples to vapours of solutions containing different chemicals (NaCl, H_2SO_4, HCOOH and AcOH) that promote corrosion. In a natural context, these chemicals are rarely isolated, so corrosion products can widely vary. Furthermore, the time of exposition is very different in real contexts, in which metals can be corroded over hundreds or thousands of years, but in a laboratory, these can be reproduced after days. To compare the compounds formed in natural processes

when the lead is exposed to atmospheric conditions and those obtained in the laboratory, Table 2-1 is presented. In this table, the first and second column show the environment in which the archaeological object has been exposed, the third column shows its main constituents, the fourth column indicates the environment created in the laboratory to simulate the natural environment, and finally, the last column shows the products formed on the laboratory samples.

Table 2-2. Comparison of the products obtained in historical lead objects and laboratory-induced corrosion in metallic lead samples.

Real environment	**Real-case artefact**	**Compounds on real artefact**	**Induced environment**	**Compounds on Pb laboratory samples**
Urban pollution, acid rains	Fragment of lead came (A-8) (16th century) from St. Lenaarts Church in the province of Antwerpen, Belgium [17]	Mainly anglesite and traces of lead sulphide, calcite, hydrocerussite, laurionite and other lead carbonates.	Sulphuric acid (3 M, 8 M and 13 M solutions)	Lead sulphate in all concentrations
Marine	Lead angel sculpture (1823) by I. P. Prokofiev, of Vasilyevsky Island in Saint Petersburg [24]	Major amount of laurionite, mixed with anglesite, hydrocerussite and litharge.	Sodium chloride (3 M, 8 M and 13 M solutions)	A mixture of lead oxide and lead oxide hydroxide chloride. This last increases at 13 M
VOCs from nearby wood materials	Lead pipes of the organ (1637) from St Jakobi church in Lübeck, Germany [30,56]	Major amounts of hydrocerussite, mixed with plumbonacrite, lead oxide formate and lead oxide acetate.	Formic acid (3 M, 8 M and 13 M solutions)	Lead formate in all concentrations
			Acetic acid (3 M, 8 M and 13 M solutions)	Lead acetate oxide hydrate in all concentrations

The first case of Table 2-2 corresponds to a historical lead sample from St. Lenaarts Church in the province of Antwerpen, Belgium, that was exposed to high pollution levels [17]. The sample was from a village near Antwerpen and showed a corrosion layer due to the presence of lead sulphate from environmental pollution. In addition, a small amount of lead chloride was also detected. Its microstructure was analysed with SEM, presenting a thin and compact layer formed by small crystals mainly of lead sulphate. This agrees with the samples prepared in the laboratory, whose surface resulted in a thin layer formed by rounded lead sulphate crystals that protect the surface from further corrosion. [17].

Anglesite is a mineral with the chemical formula $PbSO_4$, which is a lead sulphate. It typically occurs as secondary mineral deposits in the oxidized zones of lead ore deposits and is usually found in association with galena, cerussite, and other lead minerals. While lead sulphate and anglesite are not exactly the same product, they are very similar and assumed to exhibit the same behaviour [57]. Given that the morphology and corrosion behaviour of the samples prepared in the laboratory were very similar to those found in real-case examples, it is possible to assume that the tests performed in the laboratory can mimic environments where anglesite is formed on historical lead objects.

The second example shown in Table 2-2 is the lead angel sculpture located on Vasilyevsky Island, Saint Petersburg [24], which was exposed to a marine environment. The cross-section of the sculpture exhibited a mixture of different phases with varying colours. Raman spectroscopy revealed that each layer contained mainly laurionite combined with anglesite, lead oxide, and small amounts of hydrocerussite. The lead chloride product was described as an orthorhombic crystal and bigger than the other described compounds. This causes the surface to be non-uniform, with uneven density and adhesion due to the presence of different phases in different areas.

In the case of the lead samples prepared in the laboratory (exposed to NaCl), voluminous white crystals of lead chloride mixed with lead oxide were formed resulting in a thick corrosion layer. The metal surface was protected despite the formation of a porous and non-uniform layer of lead chloride, thanks to its thickness and mixture with lead oxide. This mixture of different phases with different

structures was also observed on the surface of the sculpture described in Figure 2.5, where lead chloride crystals form a thick layer of laurionite mixed with lead oxide and anglesite.

Acetic acid and formic acid released from wooden materials like oak can cause severe corrosion in lead structures, as shown in the third corrosion example of the lead pipes in the St. Jakobi Church in Lübeck, Germany [56]. After being analysed with X-Ray Diffraction, the corrosion compounds produced were mainly hydrocerussite, plumbonacrite, lead oxide formate, and lead oxide acetate. Corrosion occurred gradually in pipes, resulting in the development of cracks and holes which eventually lead to collapse. The corrosion layers were analysed by SEM [30,56] and it was concluded that the surface was covered by globular structures of different shapes producing a very porous surface [31].

In the case of the resulting samples after being exposed to formic acid vapours, rounded crystals of lead formate were uniformly distributed on the surface producing a non-severe degradation. However, lead samples exposed to acetic acid vapours showed a close similarity in the microstructure to that observed in the lead pipes example. The corrosion behaviour in the example of the historic lead exposed to wood VOCs indicates that the amount of acetic acid and its effect on the surface was greater than that of other organic acids. Therefore, this suggests that very similar atmospheres can be created by obtaining representative samples. This type of active corrosion was also measured in the corrosion rate of samples exposed to AcOH vapours, which are shown in section 2.4. Lead carbonate, such as hydrocerussite, is quite difficult to obtain in a short time. For this reason, lead samples corroded in the laboratory by VOCs (formic acid and acetic acid vapours) only presented lead formate and lead acetate oxide hydrate. However, it was assumed that the obtained results were in good agreement with those obtained in real samples.

To summarize the chapter, the corrosion rate of lead depends on the physical and chemical properties of the resulting corrosion layers. The passivation process occurs when the corrosion layer is compact and formed by poorly soluble compounds. In contrast, corrosion processes cannot be stopped when the resulting layer is very porous, with low adherence to the metallic surface and/or soluble in the environment. Thus, the resulting morphology and chemical properties of the

corrosion layer plays an important role when predicting the long-term stability of the artefact. The results of the experiments shown in this chapter demonstrate that we can simulate in the laboratory corrosion layers like those on historical lead artefacts exposed to atmospheric conditions. Note that the exposition time of these artefacts to atmospheric environments can vary from hundreds to thousands of years and usually very complex corrosion layers are obtained. The fact of being able to reproduce it in a short term in the laboratory is considered an important goal in this thesis.

2.6. References

[1] B. Schotte, The consolidation of fragile metallic objects, (2007) 1–199. https://biblio.ugent.be/publication/470013.

[2] S. Caito, M. Aschner, Developmental Neurotoxicity of Lead, in: 2017: pp. 3–12. https://doi.org/10.1007/978-3-319-60189-2_1.

[3] P. Gao, Y. Liu, W. Lv, R. Zhang, W. Liu, X. Bu, G. Li, L. Lei, Methanothermal reduction of mixtures of PbSO4 and PbO2 to synthesize ultrafine α-PbO powders for lead acid batteries, J Power Sources. 265 (2014) 192–200. https://doi.org/10.1016/j.jpowsour.2014.04.045.

[4] S. Hua, Y. Guo, Z. Wang, A study of the corrosion of negative-plate lead-antimony lugs in lead/acid batteries, J Power Sources. 45 (1993) 131–138. https://doi.org/10.1016/0378-7753(93)87002-K.

[5] D. Pavlov, G. Petkova, T. Rogachev, Influence of H2SO4 concentration on the performance of lead-acid battery negative plates, J Power Sources. 175 (2008) 586–594. https://doi.org/10.1016/j.jpowsour.2007.09.015.

[6] M. Boldyrev, Lead: properties, history, and applications, WikiJournal of Science. 1 (2018) 7. https://doi.org/10.15347/wjs/2018.007.

[7] J. Tétreault, J. Sirois, E. Stamatopoulou, Studies of lead corrosion in acetic acid environments, Studies in Conservation. 43 (1998) 17–32. https://doi.org/10.1179/sic.1998.43.1.17.

[8] A. Niklasson, L.-G. Johansson, J.-E. Svensson, Atmospheric Corrosion of Lead; The Influence of Formic Acid and Acetic Acid Vapors, J Electrochem Soc. 154 (2007) C618. https://doi.org/10.1149/1.2775173.

[9] A. Niklasson, L.-G. Johansson, J.-E. Svensson, The influence of relative humidity and temperature on the acetic acid vapour-induced atmospheric corrosion of lead, Corros Sci. 50 (2008) 3031–3037. https://doi.org/10.1016/j.corsci.2008.08.009.

[10] J. Tétreault, E. Cano, M. van Bommel, D. Scott, M. Dennis, M.-G. Barthés-Labrousse, L. Minel, L. Robbiola, Corrosion of Copper and Lead by Formaldehyde, Formic and Acetic Acid Vapours, Studies in Conservation. 48 (2003) 237–250. https://doi.org/https://doi.org/10.1179/sic.2003.48.4.237.

[11] D. Mérillou, S., Dischler, J., & Ghazanfarpour, Corrosion: Simulating and Rendering., in: Graphics Interface., 2001.

[12] L.A. Barros, M.J.B. Neto, A.E. Charola, C. Coelho, I. Cordeiro, V. Costa, J.D. Rodrigues, F. Grilo, R. Harris, F.M.A. Henriques, J.I. Nogueira, N. Proença, M. Raposo, S. Santa-Rita, M.L.S. Vieira, M.A.V. Anjos, V. Vieira, The Gardens of the National Palace of Queluz. Conservation Intervention, in: A.E. Charola, J.D. Rodrigues (Eds.), World Monuments Fund, Associação World Monuments Fund Portugal World Monuments Fund, Portugal, 2012: p. 150.

[13] Www.sedimentaryores.net, Some common Pb minerals and their chemical formulas, (n.d.). https://www.sedimentaryores.net/Pipe Scales/Minerals/Litharge.html.

[14] V. Costa, F. Urban, Lead and its alloys: metallurgy, deterioration and conservation, Studies in Conservation. 50 (2005) 48–62. https://doi.org/10.1179/sic.2005.50.Supplement-1.48.

[15] A. Bratovcic, Synthesis, Characterization, Applications, and Toxicity of Lead Oxide Nanoparticles, in: Lead Chemistry, IntechOpen, 2020: pp. 1–17. https://doi.org/10.5772/intechopen.91362.

[16] H.M. Zeyada, M.M. Makhlouf, Role of annealing temperatures on structure polymorphism, linear and nonlinear optical properties of nanostructure lead dioxide thin films, Opt Mater (Amst). 54 (2016) 181–189. https://doi.org/10.1016/j.optmat.2016.02.031.

[17] M. García-Heras, M.A. Villegas, J.M.A. Caen, C. Domingo, J.V. García-Ramos, Patination of historical stained windows lead cames from different European locations, Microchemical Journal. 83 (2006) 81–90. https://doi.org/10.1016/j.microc.2006.03.001.

[18] S.B. Lyon, Corrosion of Lead and its Alloys, in: Shreir's Corrosion, Elsevier, 2010: pp. 2053–2067. https://doi.org/10.1016/B978-044452787-5.00098-6.

[19] A. van Loon, P. Noble, D. de Man, M. Alfeld, T. Callewaert, G. van der Snickt, K. Janssens, J. Dik, The role of smalt in complex pigment mixtures in Rembrandt's Homer 1663: combining MA-XRF imaging, microanalysis, paint reconstructions and OCT, Herit Sci. 8 (2020) 1–19. https://doi.org/10.1186/s40494-020-00429-5.

[20] R. Siddall, Mineral Pigments in Archaeology: Their Analysis and the Range of Available Materials, Minerals. 8 (2018) 201–236. https://doi.org/10.3390/min8050201.

[21] R. Warchulski, M. Szczuka, K. Kupczak, Reconstruction of 16th–17th Century Lead Smelting Processes on the Basis of Slag Properties: A Case Study from Sławków, Poland, Minerals. 10 (2020) 1039–1058. https://doi.org/10.3390/min10111039.

[22] C.CH. Venetopoulos, P.J. Rentzeperis, The crystal structure of laurionite, Pb(OH)Cl, Z Kristallogr Cryst Mater. 141 (1975) 246–259. https://doi.org/10.1524/zkri.1975.141.16.246.

[23] S. Regenspurg, D.L. Driba, C. Zorn, Formation and significance of laurionite in geothermal brine, Environ Earth Sci. 75 (2016) 865–875. https://doi.org/10.1007/s12665-016-5668-4.

[24] D. Prokuratov, A. Samokhvalov, D. Pankin, O. Vereshchagin, N. Kurganov, A. Povolotckaia, A. Shimko, A. Mikhailova, R. Balmashnov, A. Reveguk, O. Smolyanskaya, D. Redka, V. Bobrovs, Investigation towards Laser Cleaning of Corrosion Products from Lead Objects, Heritage. 6 (2023) 1293–1307. https://doi.org/10.3390/heritage6020071.

[25] H. Pasco, L. Carlyle, M. Faustini, H. Glanville, C. Sanchez, P. Walter, L. de Viguerie, Investigating Nineteenth Century Gel Mediums: From Historical Recipes to Model Systems, Studies in Conservation. (2022) 1–8. https://doi.org/10.1080/00393630.2022.2031530.

[26] J. Tétreault, E. Stamatopoulou, Determination of concentrations of acetic acid emitted from wood coatings in enclosures, Studies in Conservation. 42 (1997) 141–156. https://doi.org/10.1179/sic.1997.42.3.141.

[27] M.K. Budd, Corrosion of metals in association with wood, Applied Materials Research. (1965) 124–125.

[28] P.C., C.G.C. and G.J.D. Arni, The emission of corrosive vapours by wood, I. Survey of the acid-release properties of certain freshly felled hardwoods and softwoods, Journal of Applied Chemistry. 15 (1965) 305–313.

[29] L.T. Gibson, C.M. Watt, Acetic and formic acids emitted from wood samples and their effect on selected materials in museum environments, Corros Sci. 52 (2010) 172–178. https://doi.org/10.1016/j.corsci.2009.08.054.

[30] C.M. Oertel, A. Richards, Music and materials: Art and science of organ pipe metal, MRS Bull. 42 (2017) 55–61. https://doi.org/10.1557/mrs.2016.294.

[31] F. Deflorian, M. Fedel, Electrochemical analysis of the degradation of lead alloy organ-pipes due to acetic acid, J Cult Herit. 14 (2013) 254–260. https://doi.org/10.1016/j.culher.2012.06.002.

[32] M. Mohammadzadeh, O.D. Basu, J.E. Herrera, Impact of Water Chemistry on Lead Carbonate Dissolution in Drinking Water Distribution Systems, J Water Resour Prot. 07 (2015) 389–397. https://doi.org/10.4236/jwarp.2015.75031.

[33] H.-H. Huang, The Eh-pH Diagram and Its Advances, Metals (Basel). 6 (2016) 23. https://doi.org/10.3390/met6010023.

[34] C. Fontaine, E. Guilminot, R. Jeanneret, L. Rossetti, Determination of parameters for local electrolytic treatment of corroded lead and lead-tin alloys, J Cult Herit. 20 (2016) 607–614. https://doi.org/10.1016/j.culher.2016.02.002.

[35] A. Niklasson, L.-G. Johansson, J.-E. Svensson, Influence of Acetic Acid Vapor on the Atmospheric Corrosion of Lead, J Electrochem Soc. 152 (2005) B519. https://doi.org/10.1149/1.2084348.

[36] S. Turgoose, The corrosion of lead and tin before and after excavation, in: C.E. Miles and S.C. Pollard (Eds.), Lead and Tin: Studies in Conservation and Technology. 3 (1985) 15–26.

[37] R.L.G. C. Degrigny, Conservation of ancientlead artifacts corroded in organic acid environments: electrolytic stabilisation/consolidation, Studies in Conservation. 44 (1999) 157–169.

[38] R.E. Melchers, Progress in developing realistic corrosion models, Structure and Infrastructure Engineering. 14 (2018) 843–853. https://doi.org/10.1080/15732479.2018.1436570.

[39] E. McCafferty, Validation of corrosion rates measured by the Tafel extrapolation method, Corros Sci. 47 (2005) 3202–3215. https://doi.org/10.1016/j.corsci.2005.05.046.

[40] D.A. Fischer, I.T. Vargas, G.E. Pizarro, F. Armijo, M. Walczak, The effect of scan rate on the precision of determining corrosion current by Tafel extrapolation: A numerical study on the example of pure Cu in chloride containing medium, Electrochim Acta. 313 (2019) 457–467. https://doi.org/10.1016/j.electacta.2019.04.064.

[41] American Society for Testing and Materials, ASTM G31- 72 Standard Practice for Laboratory Immersion Corrosion Testing of Metals, 1999.

[42] A.V. Echavarria, F.E. Echeverria, C. Arroyave, E. Cano,, J.M. Bastidas, Carboxilic Acids in the Atmosphere and Their Effect on the Degradation of IMetals, Corrosion Reviews. 21 (2003) 395–414. https://doi.org/10.1515/CORRREV.2003.21.5-6.395.

[43] Buehler - an ITW Company, The Sum of our Experience, A Guide to Materials Preparation & Analysis, 4th edition, Lake Bluff, USA, 2007.

[44] K. Saurbier, J.W. Schultze, J. Geke, Temporary inhibitors of corrosion in wet atmosphere: electrochemical investigations of the mechanism and efficiency, Electrochim Acta. 39 (1994) 1171–1178. https://doi.org/10.1016/0013-4686(94)E0033-V.

[45] M. Simon, R.A. Ford, A.R. Franklin, S.P. Grabowski, B. Menser, G. Much, A. Nascetti, M. Overdick, M.J. Powell, D.U. Wiechert, PbO as direct conversion x-ray detector material, in: M.J. Yaffe, M.J. Flynn (Eds.), 2004: pp. 188–199. https://doi.org/10.1117/12.533010.

[46] P. Gao, Y. Liu, W. Lv, R. Zhang, W. Liu, X. Bu, G. Li, L. Lei, Methanothermal reduction of mixtures of PbSO4 and PbO2 to synthesize ultrafine α-PbO powders for lead acid batteries, Journal of Power Sources. 265 (2014) 192–200. https://doi.org/10.1016/j.jpowsour.2014.04.045.

[47] S.A.A. Sajadi, A Comparative Investigation of Lead Sulfate and Lead Oxide Sulfate Study of Morphology and Thermal Decomposition, American Journal of Analytical Chemistry. 02 (2011) 206–211. https://doi.org/10.4236/ajac.2011.22024.

[48] R. Brinic, S., Metkos-Hukovic, M., & Babic, Impedance spectroscopy as a tool for characterization of surface films on lead and lead alloys., Journal of New Materials for Electrochemical Systems. 8(4) (2005) 273.

[49] K.J. Zeitsch, ed., I. Properties of formic acid, in: 2000: p. 247. https://doi.org/10.1016/S0167-7675(00)80042-1.

[50] K.J. Zeitsch, ed., H. Properties of acetic acid, in: 2000: p. 246. https://doi.org/10.1016/S0167-7675(00)80041-X.

[51] J. Garche, Corrosion of lead and lead alloys: influence of the active mass and of the polarization conditions, J Power Sources. 53 (1995) 85–92. https://doi.org/10.1016/0378-7753(94)01978-5.

[52] M.D. and M.Adriaens. Michel De Keersmaecker, How to preserve lead artifacts for future generations, in: S.B. and I.R. Mieke Adriaens (Ed.), Chemical Interactions between Cultural Artefacts and Indoor Environment, ACCO, Leuven, Belgium ; The Hague, The Netherlands, 2018: pp. 215–244.

[53] P.D. R., The Preservation of Antiquities, Nature. 134 (1934) 516–516. https://doi.org/10.1038/134516a0.

[54] N.D.G. Mars Guy Fontana, Corrosion Engineering, 3rd edition, Dallas, 1986.

[55] M.R. Schock, Response of lead solubility to dissolved carbonate in drinking water, J Am Water Works Assoc. 72 (1980) 695–704. https://doi.org/10.1002/j.1551-8833.1980.tb04616.x.

[56] S.L.K.A.L.R.C.J.B.L.-G.J. and J.-E.S. Annika Niklasson, Air Pollutant Concentrations and Atmospheric Corrosion of Organ Pipes in European Church Environments, Studies in Conservation. 53 (2008) 24–40.

[57] M. Monneron-Gyurits, E. Joussein, A. Courtin-Nomade, O. Grauby, E. Paineau, S. Reguer, M. Soubrand, A fast one-pot synthesize of crystalline anglesite by hydrothermal synthesis for environmental assessment on pure phase, Environmental Science and Pollution Research. 29 (2022) 17373–17381. https://doi.org/10.1007/s11356-021-17011-6.

Supplementary information

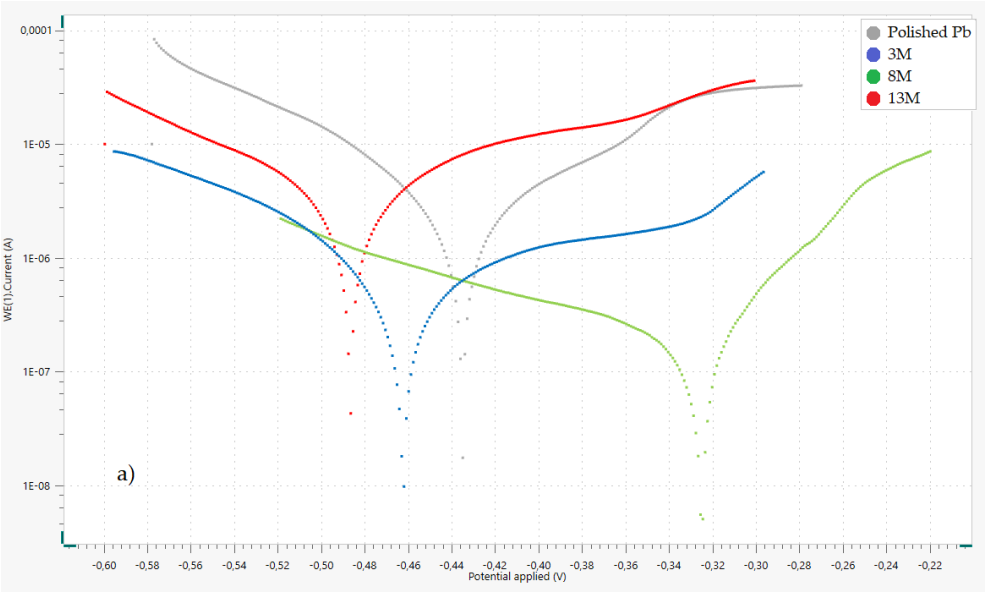

Figure 2-S1. Tafel extrapolation in Tap Water solution at 9.4 pH, for Pb samples corroded by NaCl gas phase at different concentrations.

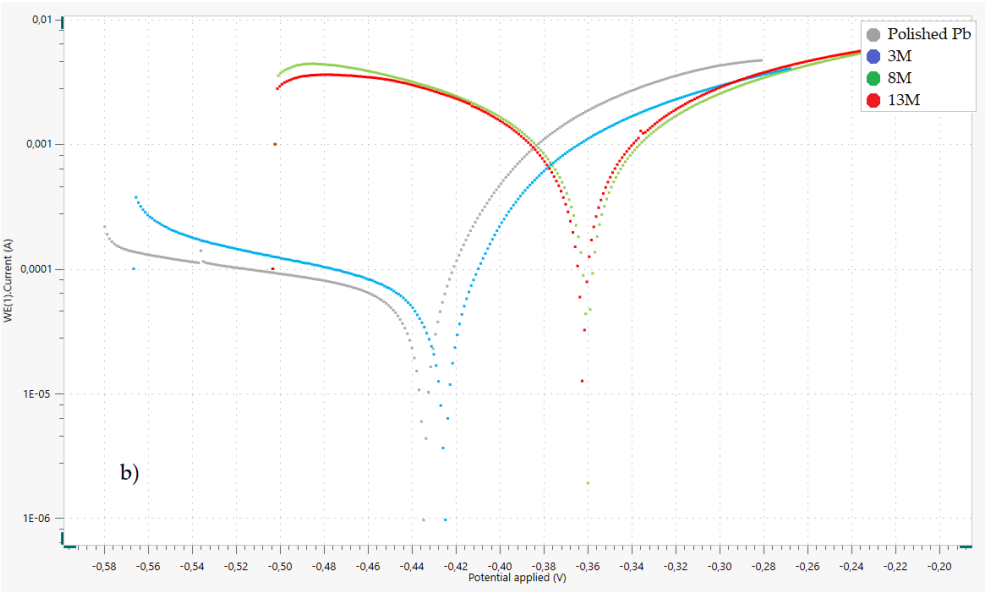

Figure 2-S2. Tafel extrapolation in nitric acid 0.1 M for Pb samples corroded by NaCl gas phase at different concentrations.

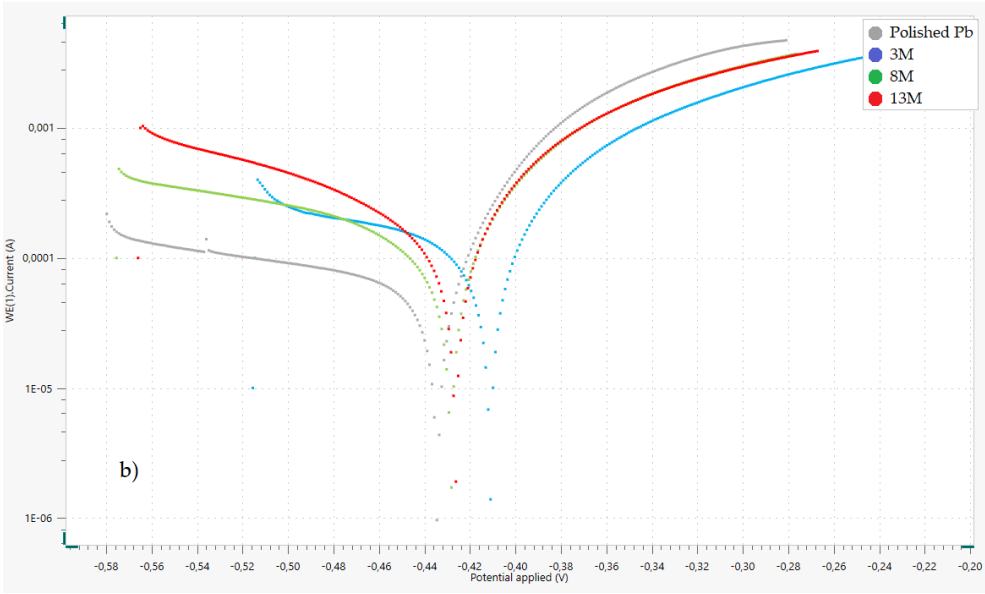

Figure 2-S3. Tafel extrapolation in nitric acid 0.1 M for Pb samples corroded by H_2SO_4 gas phase at different concentrations.

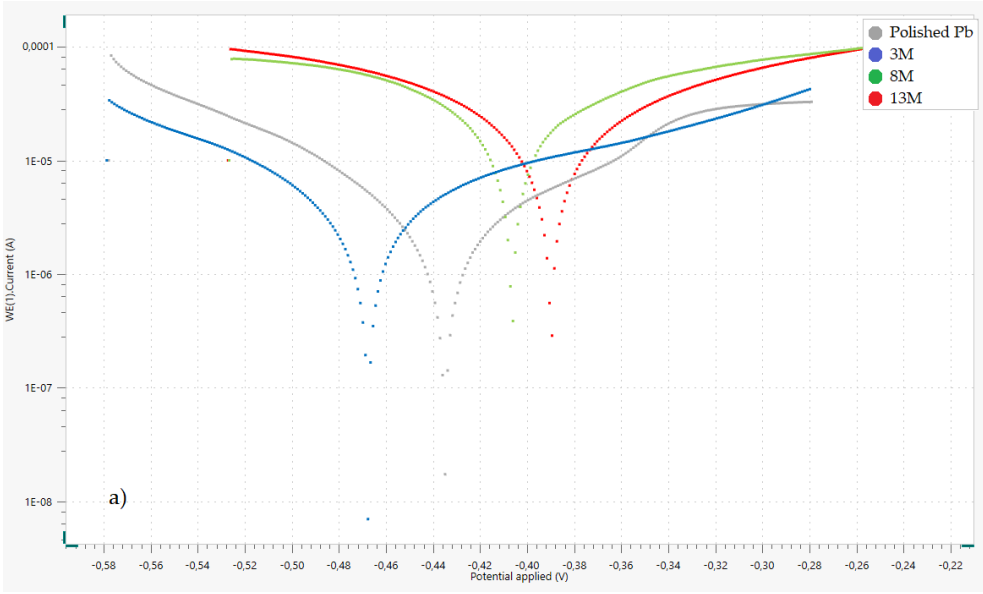

Figure 2-S4. Tafel extrapolation in Tap Water solution at 9.4 pH, for Pb samples corroded by HCOOH gas phase at different concentrations.

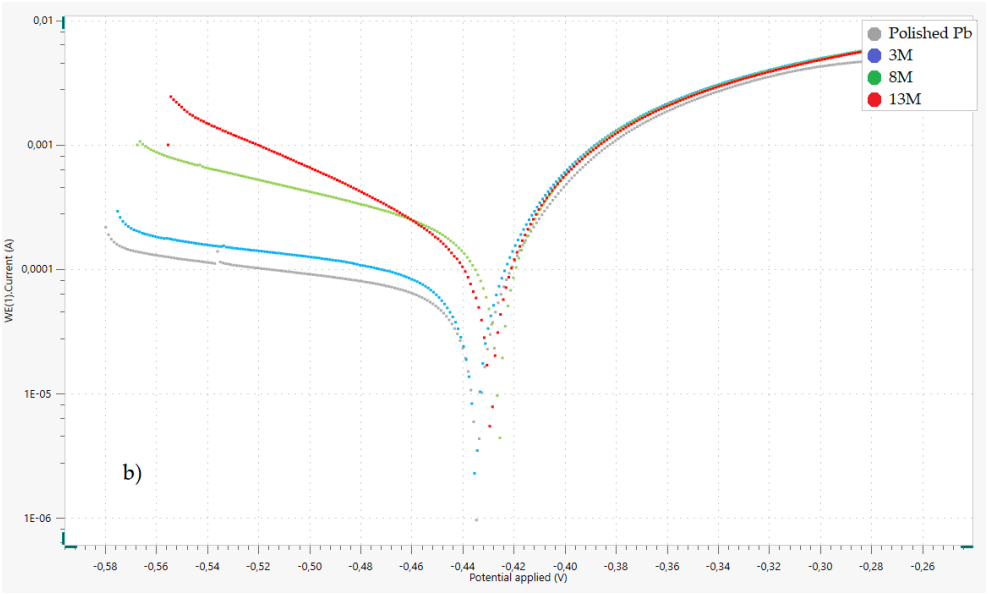

Figure 2-S5. Tafel extrapolation in nitric acid 0.1 M for Pb samples corroded by HCOOH gas phase at different concentrations.

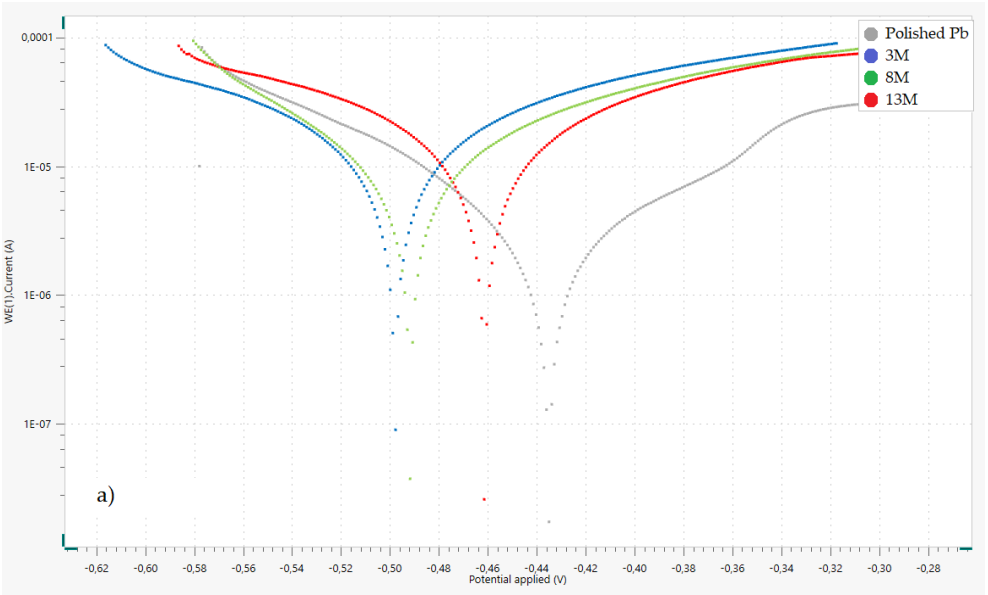

Figure 2-S6. Tafel extrapolation in Tap Water solution at 9.4 pH, for Pb samples corroded by AcOH gas phase at different concentrations.

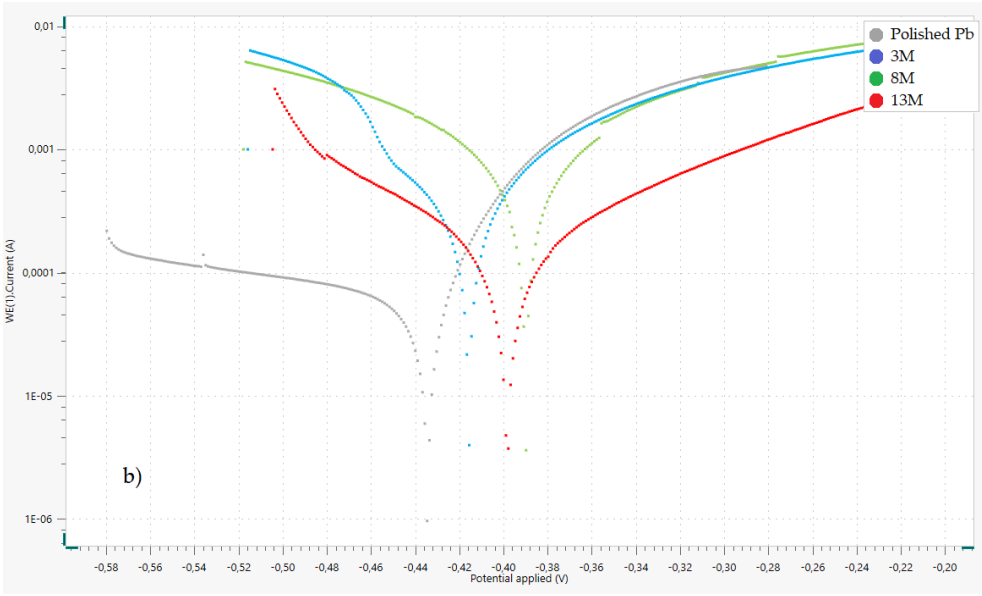

Figure 2-S7. Tafel extrapolation in nitric acid 0.1 M for Pb samples corroded by AcOH gas phase at different concentrations.

Table 2-S1. Tafel Extrapolation with Tap Water 9.4 pH analysis of corroded samples in NaCl gas phase.

Tap water 9.4 pH						
Sample	I_{corr} *(A/cm^{-2})*	R_p*(Ω)*	*Corr. Rate (mm/yr)*	*Ecorr (V)*	**|ba| (V/dec)**	**|*bc*| (V/dec)**
NaCl 3 M	1.86*10^{-7}	48300	0.01	-0.45	0.13	0.08
NaCl 8 M	1.81*10^{-7}	10789	0.00	-0.32	0.59	0.18
NaCl 13 M	2.46*10^{-6}	8552,3	0.07	-0.48	0.10	0.09

Table 2-S2. Tafel Extrapolation with nitric acid 0.1 M analysis of corroded samples in NaCl.

Nitric acid 0.1 M						
Sample	I_{corr} **(A/cm^{-2})**	R_p**(Ω)**	***Corr. Rate (mm/yr)***	***Ecorr (V)***	**|ba| (V/dec)**	**|*bc*| (V/dec)**
NaCl 3 M	6.87*10^{-5}	312	1.55	-0.43	0.00	0.26
NaCl 8 M	52.86*10^{-5}	34	18.78	-0.35	0.08	0.08
NaCl 13 M	81.53*10^{-6}	33	20.01	-0.36	0.11	0.12

Table 2-S3. Tafel Extrapolation with nitric acid 0.1 M analysis of corroded samples in H_2SO_4 gas phase.

Nitric acid 0.1 M						
Sample	**I_{corr} (A/cm^{-2})**	**R_p(Ω)**	**Corr. Rate (mm/yr)**	**Ecorr (V)**	**|ba| (V/dec)**	**|bc| (V/dec)**
H_2SO_4 3 M	1.0710^{-4}	184	1.24	-0.40	0.05	0.23
H_2SO_4 8 M	4.84*10^{-5}	188	2.54	-0.43	0.05	0.11
H_2SO_4 13 M	1.45*10^{-4}	135	4.34	-0.42	0.06	0.14

Table 2-S4. Tafel Extrapolation Tap Water 9.4 pH analysis of corroded samples in HCOOH gas phase.

Tap water 9.4 pH						
Sample	**I_{corr} (A/cm^{-2})**	**R_p(Ω)**	**Corr. Rate (mm/yr)**	**Ecorr (V)**	**|ba| (V/dec)**	**|bc| (V/dec)**
HCOOH 3M	2.57*10^{-6}	8111	0.04	-0.46	0.11	0.08
HCOOH 8 M	1.63*10^{-5}	1514	0.35	-0.40	0.11	0.10
HCOOH 13 M	1.52*10^{-5}	1803	0.48	-0.39	0.45	0.30

Table 2-S5. Tafel Extrapolation nitric acid 0.1 M analysis of corroded samples in HCOOH gas phase.

Nitric acid 0.1 M						
Sample	**I_{corr} (A/cm^{-2})**	**R_P(Ω)**	**Corr. Rate (mm/yr)**	**Ecorr (V)**	**|ba| (V/dec)**	**|bc| (V/dec)**
HCOOH 3 M	8.63*10^{-5}	229	2.57	-0.44	0.05	0.35
HCOOH 8 M	1.9*10^{-4}	108	5.82	-0.42	0.06	0.21
HCOOH 13 M	1.6*10^{-4}	104	4.89	-0.43	0.06	0.11

Table 2-S6. Tafel Extrapolation Tap Water 9.4 pH analysis of corroded samples in AcOH gas phase.

Tap water 0.1 M						
Sample	***I_{corr} (A/cm^{-2})***	***R_p(Ω)***	***Corr. Rate (mm/yr)***	**Ecorr (V)**	**|ba| (V/dec)**	**|*bc*| (V/dec)**
AcOH 3 M	9.96*10^{-6}	255	0.29	-0.49	0.12	0.11
AcOH 8 M	6.31*10^{-6}	2943	0.18	-0.49	0.09	0.07
AcOH 13 M	9.74*10^{-6}	2464	0.29	-0.46	0.11	0.10

Table 2-S7. Tafel Extrapolation nitric acid 0.1 M analysis of corroded samples in AcOH gas phase.

Nitric acid 0.1 M						
Sample	***I_{corr} (A/cm^{-2})***	***R_p(Ω)***	***Corr. Rate (mm/yr)***	**Ecorr (V)**	**|ba| (V/dec)**	**|*bc*| (V/dec)**
AcOH 3 M	4.6*10^{-4}	39	13.88	-0.41	0.11	0.06
AcOH 8 M	6.1*10^{-4}	35.35	18.43	-0.38	0.09	0.10
AcOH 13 M	1.2*10^{-4}	177.6	8.67	-0.39	0.10	0.09

3. Stabilisation by electrolytic reduction of Pb surfaces affected by active corrosion

Nowadays, electrolytic treatments are still in use to clean corroded metal surfaces. However, different limitations were observed when restoring metallic surfaces in a poor state of conservation. Since Cultural Heritage artefacts are complex objects, it is necessary to establish specific treatments. Conservation treatments are necessary to preserve artifacts, but they can also be somewhat invasive as they may involve making changes to it. Therefore, it is crucial to find the gentlest and less invasive approach to minimize any alterations to its surface that may promote further deterioration. In this chapter, galvanostatic and potentiostatic electrolytic reduction methods were performed to identify and verify any issues or differences in the effectiveness of the two methods. In addition, the objective of this chapter is to determine whether the potentiostatic polarisation represents a clear improvement versus galvanostatic methods.

3.1. Introduction

Metallic Pb artefacts from Cultural Heritage are usually covered with corrosion products. Then, it is necessary to find specific methodologies to preserve the metallic artefacts for future generations. Given the nature of metals as reactive material with the environment, their conservation is a challenge. Due to the malleable and ductile properties of Pb artefacts, these are vulnerable to being scratched, eroded, to suffer disintegration, deformation or other physical changes. For this reason, some surface cleaning treatments increase the risk of damage, especially for artefacts in a poor state of conservation.

As described in chapter 2, chemical baths were the first methodologies used during the 50s to clean the metallic surface [1]. The most common chemical cleaning treatment used for corroded lead samples was called the *Caley* method [2]. However, this treatment implied the use of HCl, which was very aggressive for the metallic surfaces. In 1953 a different method was proposed based on ion exchange between a synthetic resin (Amberlite IR 120 or Zeo-Karb 225) and hydrocerussite ($2PbCO_3 \cdot Pb(OH)_2$) [3], in which no solvent was needed. This method was used to remove lead carbonate, but it has never been proved to be useful for other lead corrosion compounds. In other cases, the most reported metal-chelating agent was ethylenediaminetetraacetic acid (EDTA 10 % w/v) or one of its salts [1], used for the complexation of Pb^{2+} ions. However, these chemical species can create new corrosion processes once again over time. In addition, in most cases, these treatments were not effective at all.

The use of electrochemical methods was introduced to clean corroded metal surfaces, improving the diffusion of the species through the interstitial spaces by applying an external current, which allows them to reach into the deepest areas. Note that when an artefact is placed in a chemical bath, chemicals react with the corrosion products on the surface of the metal, and over time, the corrosion dissolves away. This process can be slow, and it may be difficult for the chemicals to reach deep into the crevices and cavities of the artefact. In contrast, the electrical current causes an electrochemical reaction to occur on the surface of the metal, and this reaction is able to penetrate deep into the crevices and cavities of the artefact, effectively removing the corrosion from even the most hard-to-reach areas.

The use of electrochemical treatments was more efficient when cleaning corroded surfaces because a major quantity of reactive species can interact with the corroded surface with faster kinetics. From the end of the nineteenth century to the beginning of the 1980s, electrolytic techniques were used without any control of the applied potential to the metallic artefact. In 1926, Rathgen [4] described a procedure to clean corroded lead artefacts, where the source of energy was the formation of a galvanic cell between the object acting as a cathode and a less noble metal, usually zinc or aluminium, acting as an anode [5]. The lack of control over the electrochemical reactions was a strong disadvantage of the method, and also because the object was not visible during treatment. Therefore, the reactions that evolved on

the metal surface were not monitored, and often, some transformations of the corrosion layer were observed but not entirely understood.

Electrochemical techniques used to clean Pb samples from Cultural Heritage artefacts were especially promoted in 1956 by Plenderleith [6]. In the following years, different studies were published on historical reviews of electrochemical techniques applied to conservation, which contributed to the dissemination of these techniques within the scientific conservation field. In the early sixties, galvanostatic methods, which involve constant current polarisation, were described [5,7].

The first application of an electrolytic reduction treatment on lead objects was described by Organ in the early 1960s [5] and a schematic representation of the experimental set-up is shown in Figure 3-1.

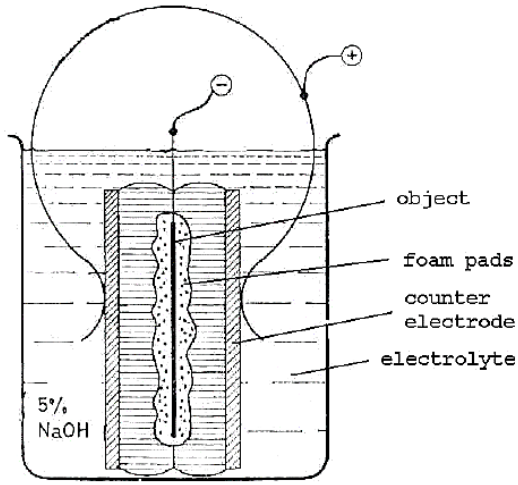

Figure 3-1. Experimental set-up of the electrolytic reduction proposed for corroded Pb [5].

The treatment described by Organ involved a constant current density of 100 $mA \cdot dm^{-2}$ to the corroded lead bullae in a 10% w/v sodium hydroxide solution for three days, followed by successive baths in 1 mM sulphuric acid until the pH of the acid remained unchanged for 30 minutes, and then with distilled water. After, the object was dried, brightened, and impregnated with hot paraffin wax. However, it was observed that corrosion reappeared after a certain period of time [5,7].

Note that during galvanostatic reduction, a constant electric current is passed through the corroded metal. The current provides electrons to the metal ions, causing them to be reduced to the metallic state. However, the reaction can also produce hydrogen gas bubbles, which can accumulate on the surface of the corroded metal and hinder the reduction process. It can be particularly problematic with samples that have intricate surface features such as drawings or engravings. The hydrogen gas produced during the reduction can accumulate in these features, leading to bubbles that can damage or even detach delicate surface features. The gas bubbles can also block the electrolyte flow around the sample, leading to uneven reduction and potential damage to the sample.

The Valectra division of Electricité de France played a significant role in the advancement of electrochemistry in conservation science by introducing the use of a constant potential polarisation in the late 1980s to monitor their behaviour in a solution or to determine the appropriate treatment conditions. This contribution marked a significant milestone in the development of conservation science to stabilise active corroded surfaces [8]. By fixing the applied electrochemical potential in the working electrode, it was possible to monitor the behaviour of metallic surfaces in a solution defining the proper treatment conditions and also prevent the formation of hydrogen bubbles. Later, other researchers from conservation science such as Carradice and Campbell [9] used this method for lead objects affected by VOCs.

In 1999, Degrigny and Le Gall [10] investigated the electrolytic consolidation/stabilisation of corroded metals used for different treatments, especially on iron, bronze, silver and lead. The electrolytic set-up is described in Figure 3-2.

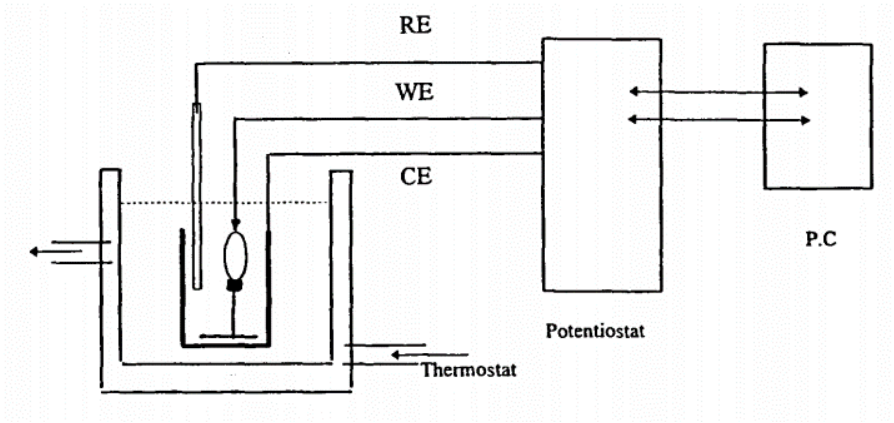

Figure 3-2. Electrolytic set-up with three electrodes. RE: saturated calomel reference electrode, CE: platinum counter-electrode, WE: working electrode.

As shown in Figure 3-2, the treatment was done with a potentiostatic system (constant applied electrochemical potential) using a platinum needle inserted in the metallic lead sample positioned vertically to ensure good electrical contact with the potentiostat [10]. They studied the effect of various electrolytes (NaOH, Na_2CO_3, H_2SO_4 and Na_2SO_4) upon the treatment result and concluded that Na_2SO_4 is a relatively inactive solution, implying that it is therefore a safe and efficient electrolyte.

In order to determine the proper applied electrochemical potential for the cathodic reduction, they compared the behaviour of artificially carbonated and naturally carbonated lead coupons in 0.5 M sodium sulphate solution by using a linear sweep polarization from 0.2 V versus SCE to -2.0 V versus SCE. The artificially carbonated lead coupon showed a reduction behaviour with one peak visible at -0.9 V versus SCE. A very similar reduction behaviour was observed when reducing the tick hydrocerussite layer from the naturally carbonated samples, showing a peak also around -0.9 V. Thus, this potential was selected by the authors for the cathodic reduction. The treatment lasted about five days. Figure 3-3 shows an example of the potentiostatic curve [8].

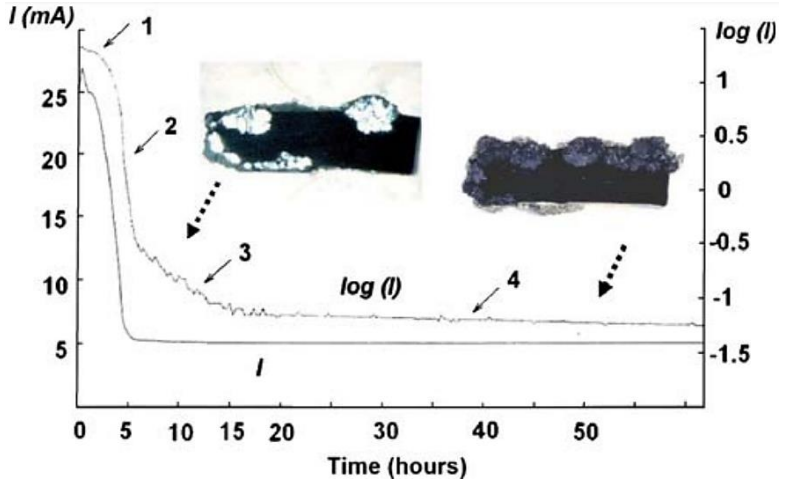

Figure 3-3. Chronoamperometry plot showing the progressive reduction of lead carbonate (mainly hydrocerussite) on cross sections of lead weights polarised at −0.65 V/Ag/AgCl/KCl in 0.5 M sodium sulphate (credit Arc'Antique) [8].

Log $|I_{red}|$ versus time was plotted in Figure 3-3 due to its particular benefits towards the end of the treatment when the current is minimal. Note that small variations in the current can be easily observed in these plots. This, in turn, helps in determining the effectiveness of the treatment, and for this reason, it was included in the chart [8]. The heterogeneous current distribution on the object, which may otherwise promote hydrogen evolution, was prevented depending on the applied potential. Using current versus time plots, $I_{red} = f(t)$, the reduction process was monitored and described in the bibliography [8,11]. The current first increases (1) but decreases abruptly afterwards (2) before reaching quite low values. In this region, the corrosion layer was progressively electrochemically reduced over its whole thickness. In the next step (3) the surface of the artefact seems to be metallic but corrosion products are still present underneath. These corrosion compounds are fully reduced at step 4. The final step 4 was observed after five days. Here, the current was stable, and the cathodic reduction was considered to be finished [10,11]. When the current flow was constant, the reduction of water is promoted, generating molecular hydrogen [11]. Thus, the end of the treatment was usually determined by the presence of small bubbles.

In this chapter, galvanostatic and potentiostatic electrolytic methods were compared. The purpose of this comparison was to identify any issues related to their use. The primary aim of using these methods was to stabilise lead surfaces affected by active corrosion. This could be achieved by electrolytic reduction of the corrosion products that had been formed on the surface of the metal. By doing this, it is possible to stop the progression of corrosion that can cause irreversible damage to the metal. Different characterization techniques were also used to analyse and compare the resulting surfaces of each electrolytic method.

3.2. Experimental set-up

3.2.1. Accelerated corrosion in metallic lead samples

A lead sheet sample (99.99%) supplied by the *MNAC,* of 12 x 15 cm and 1.5 mm of thickness was corroded in the laboratory by AcOH vapours for three months. The sample was suspended using a Teflon thread in a glass cell at room temperature and exposed to the gas phase of a 3 M AcOH solution. Then, the sample was exposed to the air for approximately one week.

3.2.2. Voltammetric measurements

A three-electrode set-up was used to perform voltammetric measurements: cyclic votammetries and linear sweep voltammetries. The system consisted of a platinum counter electrode (Pt 99.99%), an Ag/AgCl/KCl (3 M) reference electrode and a Pb working electrode of 2 mm of thickness were corroded in different environments (the same Pb sheet described in chapter 2). Na_2SO_4 0.5M was used as an electrolyte. All measurements were performed using a Metrohm Autolab PGSTAT 302N. To perform the cyclic voltammetry experiments, the scan rate was fixed at 10 mV/s^{-1}, starting at -2.0 V versus Ag/AgCl/KCl (3 M). and the applied potential at 1.8 V versus Ag/AgCl/KCl (3 M).

3.2.3. Electrolytic reduction

The system assembly for galvanostatic and potentiostatic reduction was performed in the laboratory with 0.5 M Na_2SO_4 as the electrolyte solution. The galvanostatic reduction was performed in a two-electrode system, in which the Pt counter electrode as an anode and Pb working electrode was used. The experiment was performed in disk areas (5.5 cm diameter) from the corroded Pb sample by AcOH vapours. The galvanostatic reduction was done at a current density of 10 $mA \cdot dm^{-2}$ (0.0238 mA absolute current in a sample area of 23.7 cm^2). It was found in bibliography [3,5] that a current of 100 $mA \cdot dm^{-2}$ was applied to a corroded lead object. However, authors mentioned that during electrolysis hydrogen bubbles were observed. To prevent this issue, a lower current density of 10 $mA \cdot dm^{-2}$ was assumed avoid this problem while reducing the corrosion layer.

In the case of potentiostatic reduction, a fixed potential of -0.9 V versus a reference electrode of Ag/AgCl/KCl (3 M) was applied. All measurements were performed using a potentiostat/galvanostat Metrohm Autolab PGSTAT 302N.

The cell system used for galvanostatic and potentiostatic reduction is presented in Figure 3-4. A three-electrode set-up for the potentiostatic reduction is also shown.

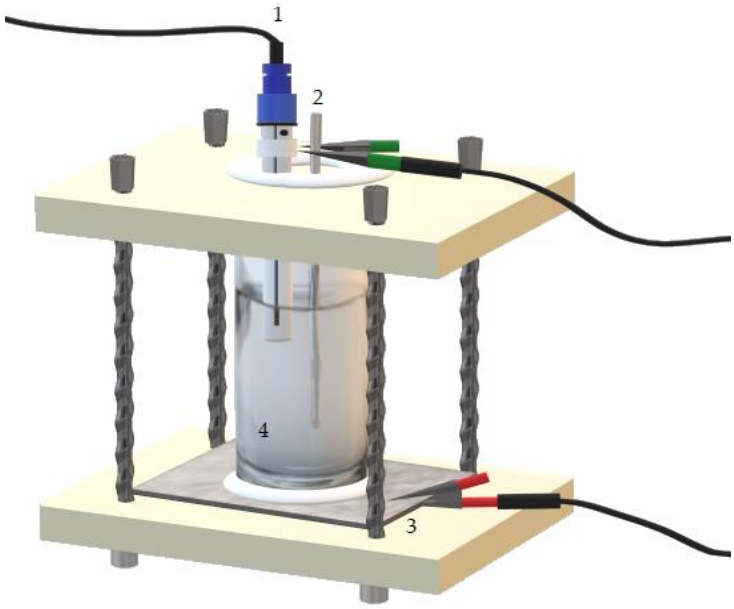

Figure 3-4. Three electrode systems for a potentiostatic reduction: 1 – Ag/AgCl/KCl 3 M Reference electrode; 2 – Pt Counter electrode; 3 – Pb Working electrode; 4 – 0.5 M Na_2SO_4 Electrolyte.

The system assembly was done by a tubular glass cell, supported between two methacrylate sheets on each edge. The Pb working electrode was used as a cathode and hold as described in Figure 3-4, using an O-ring to seal the glass tube in contact with the corroded surface area (5.5 cm diameter). After both electrolytic reductions, the surface was soaked in four or five successive washes of less than one minute with deionized water. After that, the surface was dried using a stream of air.

3.2.4. Confocal image profiling

A confocal microscope (Leica DCM 3D dual core 3D) was used to compare the different roughness between samples [12]. The analysis was performed using the average of four planes to consider a larger area. The main roughness indexes are Ra and Rq values. *Ra* is represented as the arithmetic roughness average of the surface and *Rq* is the standard deviation of the height distribution.

3.3. Results and discussion

3.3.1. Characterization of the corroded lead sample in the laboratory

A corroded lead surface was prepared in the laboratory following the conditions described in the experimental set-up (see section 3.2.1.). The obtained corrosion surface was uniform with a powdery and grey appearance, as can be seen in Figure 3-5.

Figure 3-5. Corroded surface after being exposed to the AcOH gas phase for three months, and into the air for approximately one week.

The surface of the corroded sample was analysed by X-ray diffraction to identify the resulting compounds. Database patterns of lead carbonate (plumbonacrite, $Pb_5(CO_3)_3O(OH)_2$) and lead acetate oxide hydrate were also included in Figure 3-6.

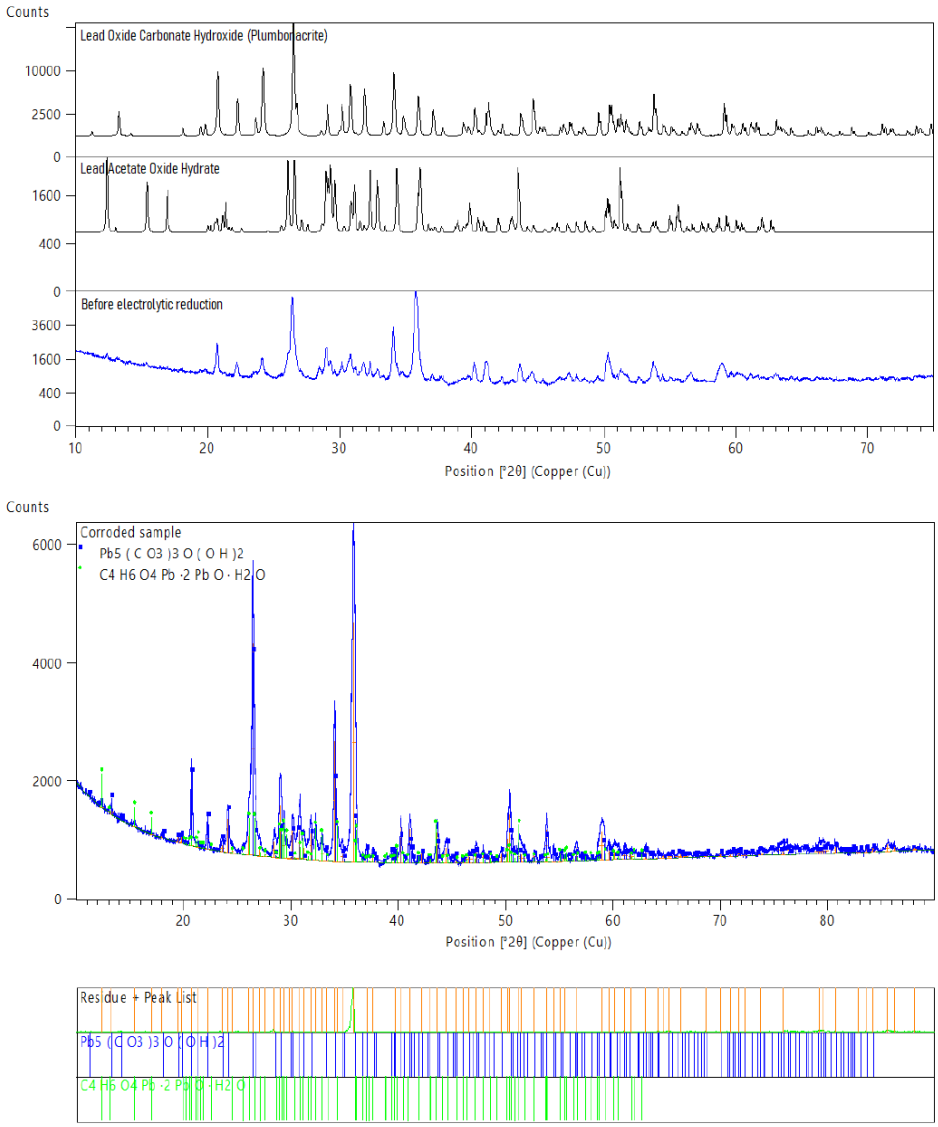

Figure 3-6. Database patterns from International Centre for Diffraction Data® (PDF4+) of lead oxide carbonate hydroxide (plumbonacrite) and lead acetate oxide hydrate. The blue diffractogram correspond to the corroded lead sample after exposure in AcOH vapours.

The resulting surface was formed by a complex corrosion layer consisting of various compounds. The peaks observed in the diffraction pattern matched with lead carbonate, specifically plumbonacrite as the predominant compound, and a secondary phase of lead acetate hydroxide. The diffraction pattern also indicated the complexity of the corrosion sample. However, the major peaks detected in the

diffraction pattern corresponded to plumbonacrite (observed at 27, 34, 36, 42, and 44 peak positions) and lead acetate (observed at 26, 29, 34, 16, 44, and 52 peak positions). When plumbonacrite is the primary type of basic lead carbonate on the lead surface, corrosion is typically uniform, but some local corrosion (pitting) may also occur [13], as observed in Figure 3-7. Plumbonacrite forms in the atmosphere, and the resulting layer is not very compact. The porous nature of the corrosion products allows aggressive compounds to reach the lead surface, leading to further corrosion [13].

Compared to the samples corroded in previous chapter, the conditions were varied in the present chapter 3. In this case, the formation of the corrosion layer was induced by reducing the levels of AcOH at room temperature, allowing for an increase in the activity of CO_2. Additionally, the sample was exposed under these conditions for a longer period (three months). However, since the experiment was performed in a closed glass chamber, the CO_2 acted as a limiting reactant and the capacity to generate lead carbonate was insufficient. Therefore, the sample was subsequently exposed to the open air for approximately one week to transform unstable lead acetate products generated by AcOH into more stable lead carbonate compounds.

3.3.2. Galvanostatic reduction measurements

Galvanostatic reduction can be used in corroded lead samples to remove the corrosion products from the surface of the lead. This process involves the use of an electrical current to reduce the corrosion products and convert them back into their original metallic form. In the restoration and conservation field, potentiostatic methods are often preferred over galvanostatic methods because they offer greater control and precision in the cleaning process. Actually, galvanostatic methods can be harmful in situations where the corrosion damage is extensive and complex, and where the artefact has irregular shapes or difficult-to-reach areas that require a very precise control over the cleaning process [8]. In these cases, potentiostatic methods may provide a better way to remove the corrosion products from the surface of the artefact minimizing the damage of the underlying metal. In addition, it may be used due to possible limitations in equipment or expertise. However, the purpose of the comparison of both methods in the present chapter, was to identify and verify any

issues or differences in the effectiveness of the two methods when used to stabilise lead surfaces affected by active corrosion. Using both techniques, it will be possible to observe whether significant changes are obtained after cathodic reduction of surfaces affected by active corrosion, which are formed by very porous and poorly adherent layers. In addition, the objective of this chapter is to determine whether the potentiostatic polarisation represents an improvement versus galvanostatic methods.

As described in section 3.2.3, the Pb working electrode was used as a cathode and held using an O-ring to seal the glass tube in contact with the corroded surface area (5.5 cm diameter). The experiment was performed at a constant current of -10 mA/dm^2 for 11 hours (-2.37 mA absolute current in a sample area of 23.7 cm^2) using 0.5 M Na_2SO_4 as electrolyte. The obtained ΔV versus t curve is presented in Figure 3-7. From here, in this section all electrochemical potentials were referred to Ag/AgCl/KCl (3M) reference electrode.

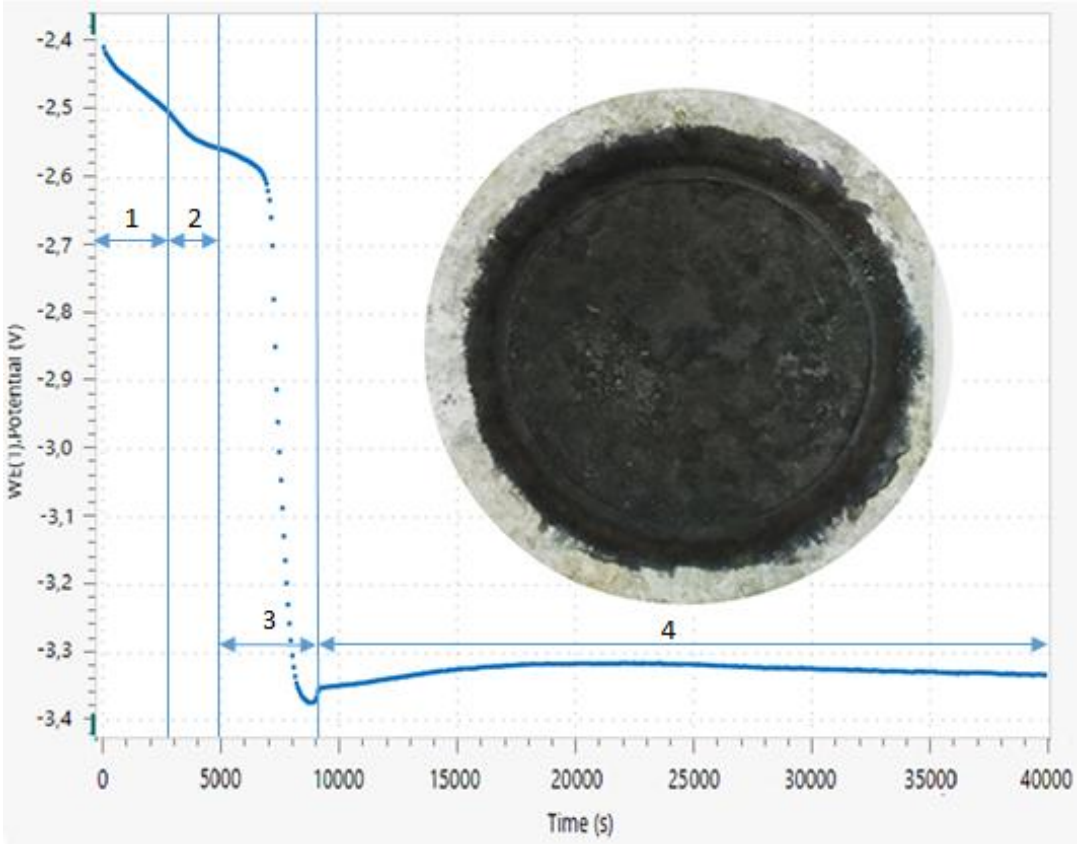

Figure 3-7. Reduction of lead samples in a galvanostatic system in 0.5 M Na_2SO_4 electrolyte.

As it is shown in Figure 3-7, a first reduction is observed in the first ~50 minutes (1) with a small potential decrease (from -2.40 V to -2.56 V). Next (2), from ~50 to ~83 minutes (-2.56 V to -2.58 V), another small decrease in current change was observed. After this (3), a slope change occurred from ~83 to ~150 minutes (-2.58 V to -3.36 V), probably because of the reduction of the corroded layer on the metal surface [11]. Finally, (4) from ~150 to the end of the experiment (-3.36 V to 3.37 V), the potential was nearly stabilised. The galvanostatic treatment is difficult to understand in identifying the chemical entities involved in the reactions taking place during the cathodic processes. Measurements are often complex given multiple reactions that can occur simultaneously during the process, and no bibliography of the present reduction was found.

As can be seen, the electrochemical potential of the working electrode was very negative, which implies that hydrogen bubbles were formed on the surface from the beginning of the treatment. The excessive amount of hydrogen bubbles can cause the detachment of corrosion products from the surface, and therefore, the corrosion layer is removed from the metallic sample by mechanical processes [14]. Thus, the idea of effective electrolytic treatment is to achieve the reduction of surface corrosion products while avoiding the production of hydrogen bubbles in the medium. At that point, it is worth mentioning that because of the limitations of this method (galvanostatic polarization), it is not commonly used and considered as a not appropriate approach for corroded lead [8–10,15]. In contrast, to prevent the production of hydrogen, consolidative reduction using potentiostatic methods is used in the conservation field [7,8,10,15] and it was explored in section 3.3.3.

3.3.2.1. Sample characterization after galvanostatic reduction

3.3.2.1.1. Scanning Electron Microscopy - Energy Dispersive X-Ray Spectroscopy analyses (SEM-EDS) surface analysis

In order to characterize the resulting surface after galvanostatic reduction, SEM micrographs are shown in Figure 3-8. SEM and XRD conditions were the same as previously described in chapter 2.

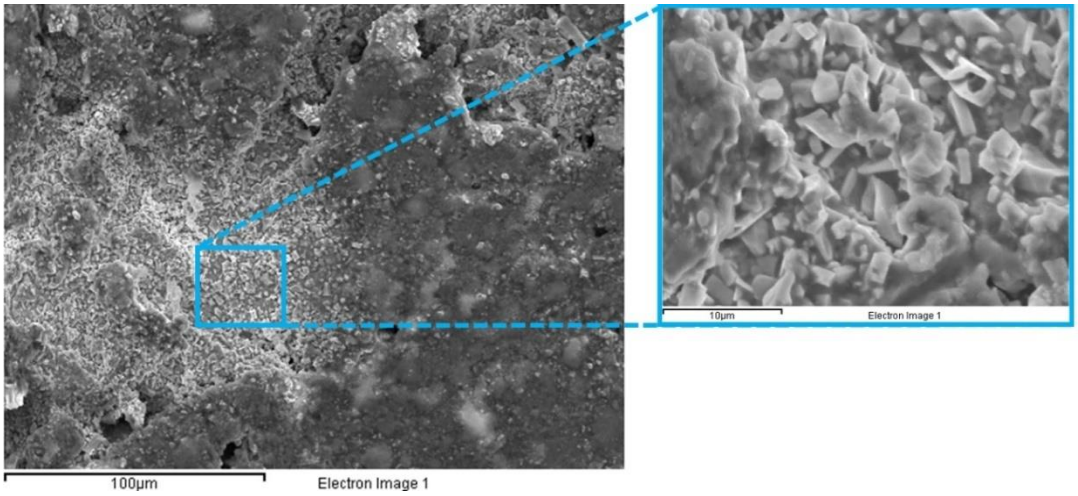

Figure 3-8. SEM micrograph scaled at 100 µm (left) after galvanostatic reduction and also amplification scaled at 10 µm (right) of crystal deposits on the analysed surface.

In the SEM micrograph shown in Figure 3-8 the presence of small cracks and different morphology compounds agglomerated in the narrow cavities were observed. The amplified region of the SEM micrograph of Figure 3-8, presented crystals of around 3 µm diameter. To identify the elementary composition of these compounds EDS analyses were performed and are presented in Figure 3-9.

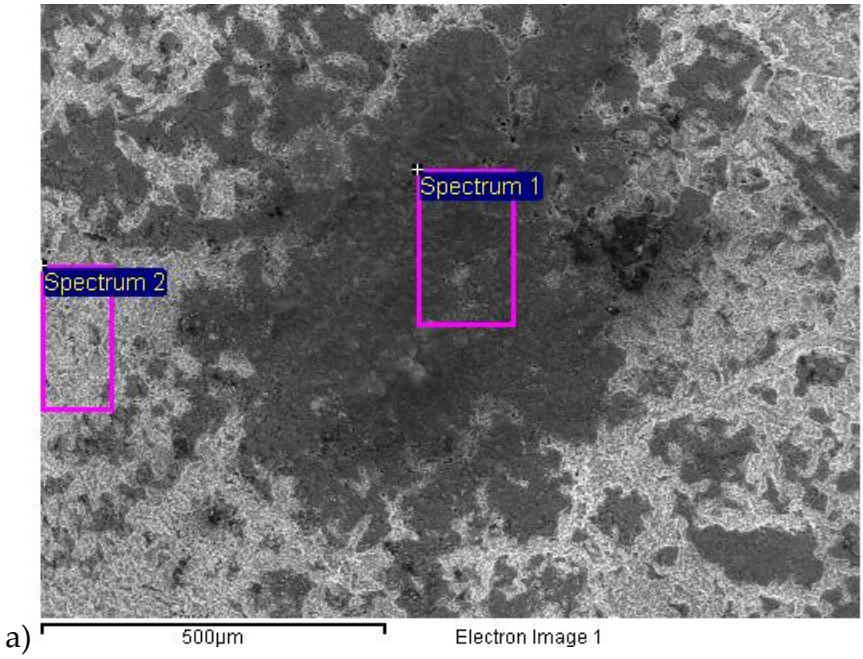

a)

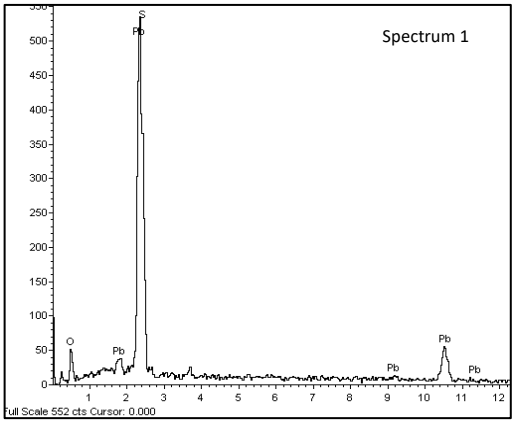

b)

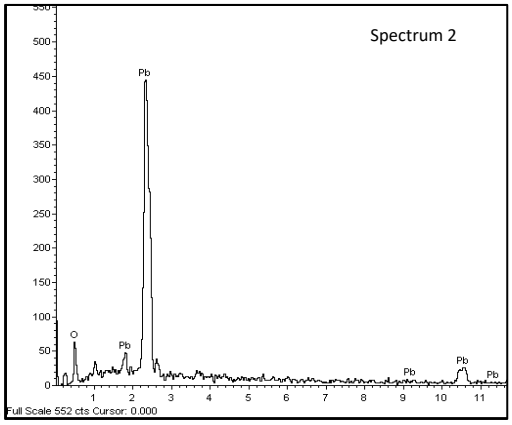

c)

Figure 3-9. *a*; SEM micrograph at 500 µm after the electrolytic reduction, *b*; Spectrum 1 resulting in Pb and O elements; c) Spectrum 2 resulting in Pb, O and S elements.

As shown in Figure 3-9 *a*, the SEM micrograph presented surface heterogeneities because of the different resulting structures. In the first EDS analysis shown in spectrum 1 in Figure 3-9 *b*, only lead and oxygen were present. In spectrum 2 in Figure 3-9 *c*, sulphur (Pb Kα 2.307 eV) and lead (Pb M 2.342 eV) [16] were detected by the software. X-ray energies emitted by lead and sulfur are very similar, then both

can undergo to overlapping and difficult its detection. XRD analyses were performed after electrolytic reduction (galvanostatic) and are shown in Figure 3-10.

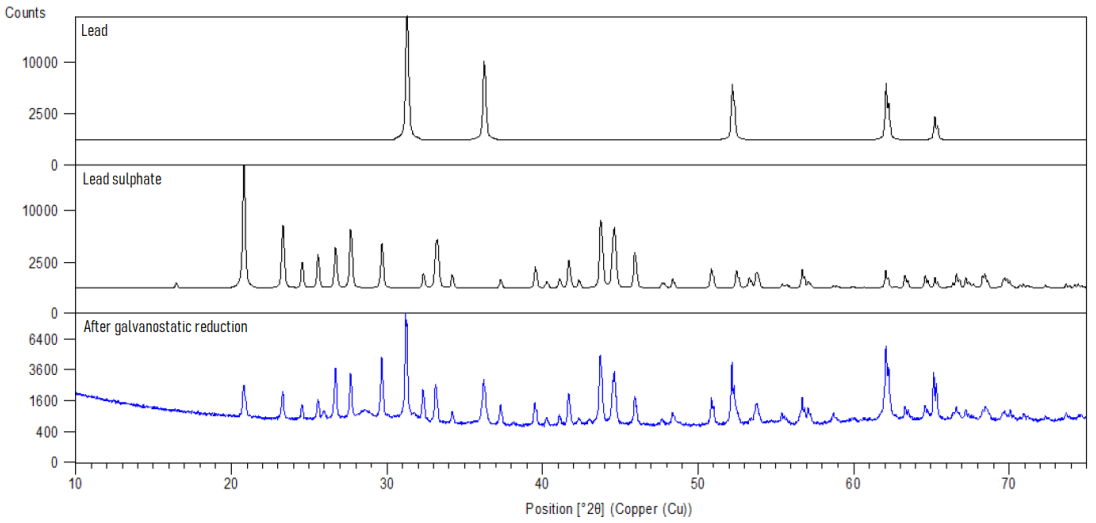

Figure 3-10. Database patterns from International Centre for Diffraction Data® (PDF4+) of lead and lead sulphate (black). Diffractogram obtained after galvanostatic reduction is also presented (blue).

As mentioned in section 3.3.1, the corrosion layer was very complex to identify due to the mixture of different corrosion compounds. These were mainly plumbonacrite and lead acetate hydroxide (Figure 3-6). In contrast, the obtained diffractogram after reduction shown in Figure 3-10, indicated the presence of metallic lead (as observed in the matching angle positions around 32, 37, 53, 62 and 65 degrees) and the formation of lead sulphate ($PbSO_4$) on the metallic surface. The matching peak positions between lead sulphate pattern and the resulting sample after treatment can be observed, particularly around 21, 23, 27, 28, 30, 36, 44, 45 and 46 peak positions. It is worth mentioning that after the electrolytic treatment, the sample remained immersed in the medium (Na_2SO_4) for a few minutes. It should be noted that at this point, the metal surface would be highly reactive [1] and the dissolved oxygen in the medium may promote its oxidation, generating a thin surface layer of lead sulphate.

3.3.2.1.2. Roughness analysis by 3D Optical Measuring System (3D-OMS).

To determine the roughness parameters, a statistical analysis of the resulting profiles was performed through a 3D Optical Measuring System. There is a great variety of parameters that quantify the roughness of a surface or its roughness profiles. As an example, the most relevant parameters are shown in Figure 3-11.

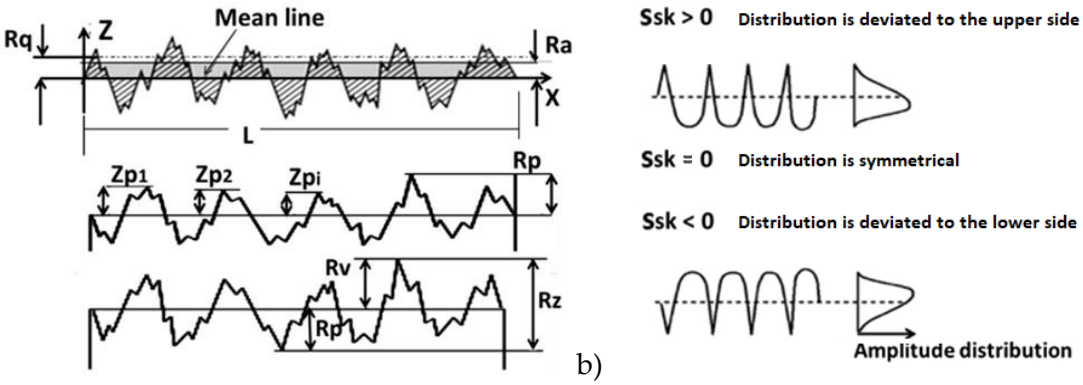

Figure 3-11. *a*; Main roughness parameters of surface evaluation. *Ra (the arithmetic roughness average of the surface), Rq and Rz*), *b*; Symmetry evaluation (*Ssk*) [17].

As shown in Figure 3-11 a, three of the main roughness parameters (*Ra, Rq* and *Rz*) were used to describe the obtained profiles in this chapter [18–21]. *Ra* is represented as the arithmetic roughness average of the surface; *Rq* is the standard deviation of the height distribution; and *Rz* is the sum of the maximum peak height and the maximum valley depth of a profile within the reference length [22]. The bias degree of the roughness shape, related to the asperity, is defined by the *Ssk* value and is represented in figure 3-11 *b* [23].

Therefore, the corroded Pb surface before the treatment and after the electrolytic reduction were analysed by a 3D Optical Measuring System, and the roughness results are presented in Figure 3-12 (both analyses were performed in the same position).

a)

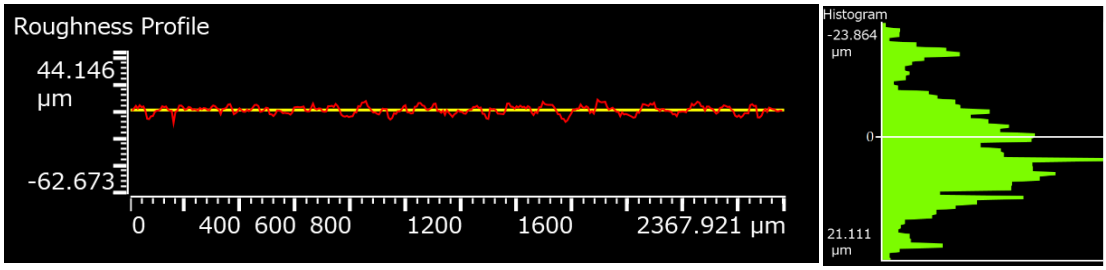

b)

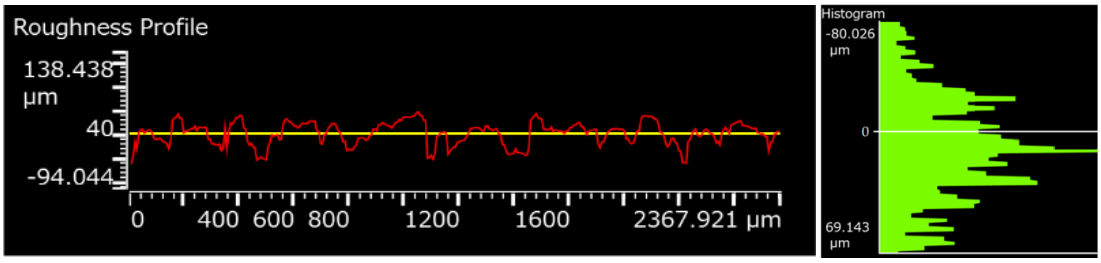

Figure 3-12. Roughness profiles of surfaces and obtained values, *a*; corroded surface in AcOH vapours, *b*; after galvanostatic reduction.

The obtained values for the considered parameters to describe roughness surfaces were:

Table 3-1. Obtained values after roughness analysis

Sample surface	Ra	Rq	Rz	Ssk
Corroded surface in AcOH vapours.	*2.5 µm*	*3 µm*	*13 µm*	*Ssk<0*
After galvanostatic reduction.	*15.8 µm*	*18.7 µm*	*73 µm*	*Ssk<0*

The distribution was shifted to the positive side in both histograms, which means Ssk<0. This is defined as a predominance in valley structures related to abrasion. The galvanostatic reduced surface presented higher roughness values of

Ra, *Rq* and *Rz* respecting the corroded surface, as shown in Figure 3-12. This means that the metallic surface became rougher after the galvanostatic reduction treatment.

The topographic data of both surfaces using micrographs obtained by the 3D Optical Measuring System is shown in Figure 3-13.

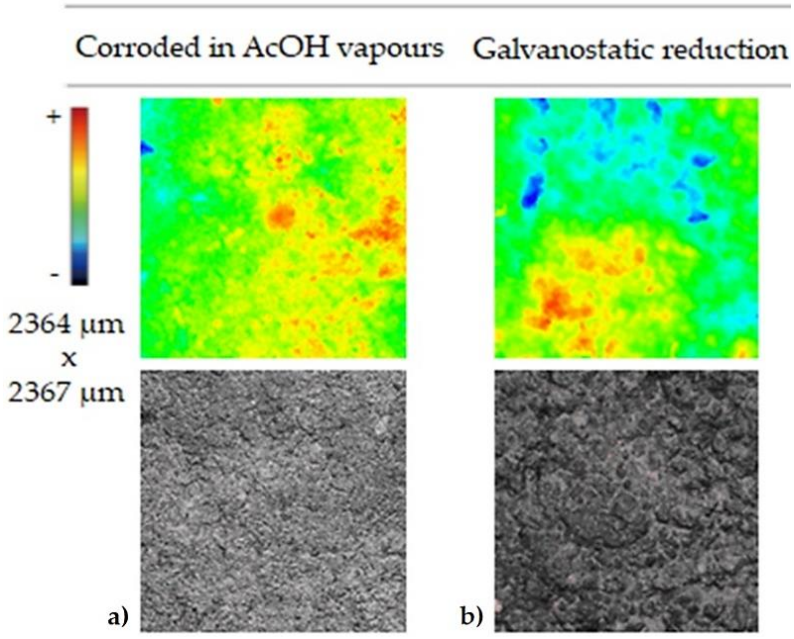

Figure 3-13. Topographic data from optical profilometry showing surface roughness; a corroded surface in AcOH vapours, b after galvanostatic reduction.

As shown in Figure 3-13 *a*, the topographic micrographs corresponded to the corroded sample exposed to AcOH vapours and presented a high peak level with a homogenous distribution. This can be related to the thick corrosion layer with agglomerated lead corrosion compounds on the whole surface. The galvanostatic reduced sample shown in Figure 3-13 *b*, presented a high rough aspect than that for the corroded sample. Without a potential control, an excess of bubble production was generated by the formation of molecular hydrogen. During this process, corrosion products and metallic particles were detached from the sample and the reduction was partial, causing severe irregularities on the metal surface. In addition, the

volume changes of the corrosion products into metallic Pb during the electrolytic treatment resulted in surface cracks.

3.3.3. Potentiostatic reduction measurements

Previously to perform the potentiostatic reduction, the electrochemical behaviour of metallic lead was studied. This allowed us to determine at which potential value the oxidized products can be reduced. To do that, Cyclic Voltammetry was used. The sweep was performed from -2 V to +1.8 V vs Ag/AgCl/KCl at a scan rate of 10 mVs^{-1} in a 0.5 M Na_2SO_4 as an electrolyte, and the voltamperogram is presented in Figure 3-14. From here, in this section all electrochemical potentials were referred to Ag/AgCl/KCl (3 M) reference electrode.

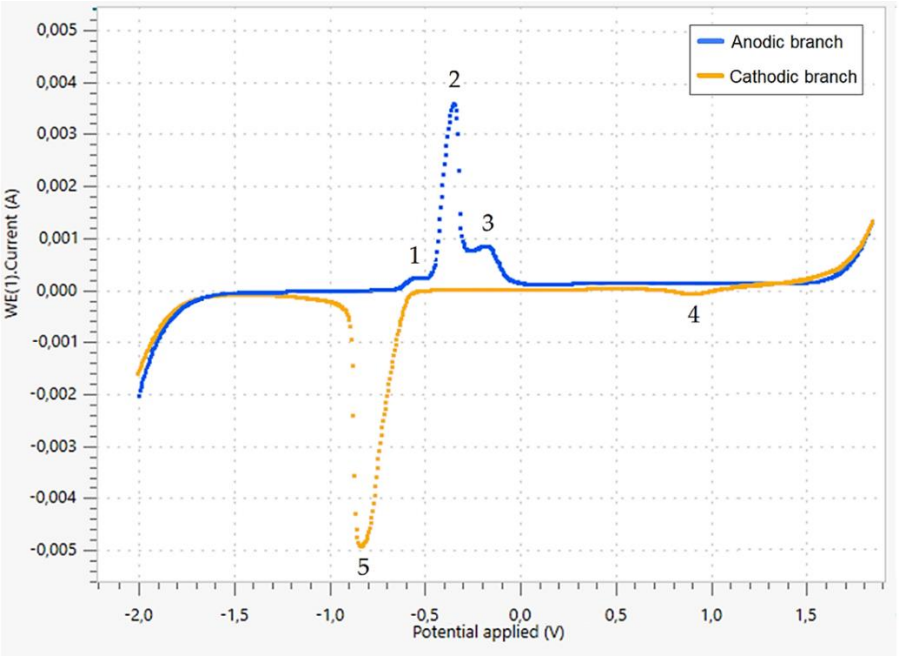

Figure 3-14. Cyclic Voltammetry for a Pb electrode in potential area from -2 V to 1.80 V versus Ag/AgCl/KCl (3 M) as the upper potential in Na_2SO_4 electrolyte. Scan rate at 10 mV/s^{-1} and pre-polarized before at -1.5 V for 10 minutes at a scanning rate of 10 mV/s^{-1}.

The anodic sweep (blue) of the resulting CV curve shown in Figure 3-14, presents a first anodic peak (1), at -0.54 V versus Ag/AgCl/KCl (3 M), and it is related to the formation of a $PbSO_4$ layer on the electrode surface according to the following reaction [24,25]:

Reaction 3-1 $$Pb + SO_4^{2-} \rightarrow PbSO_4 + 2e^-$$

There is a second large anodic peak (2) in the anodic sweep at -0.35 V versus Ag/AgCl/KCl (3 M) assigned to the transformation of lead sulphate to monobasic lead sulphate ($PbO{\cdot}PbSO_4$) and tribasic lead sulphate ($3PbO{\cdot}PbSO_4{\cdot}H_2O$) which are formed along with PbO film formation. The larger particle size of $PbSO_4$ leads to lower water and acid absorption capacity, allowing the PbO formation protected by $PbSO_4$ crystals from the working solution [26,27]. At -0.20 V versus Ag/AgCl/KCl (3 M) a new anodic peak (3) on the descending part of the previous peak, is also obtained. According to different citations [26,28], it is assigned to the electroformation of a PbO film underneath the $PbSO_4$ layer. The formation of PbO occurs via a nucleation and growth mechanism according to the reaction [24,25]:

Reaction 3-2 $$Pb + 2OH^- \rightarrow PbO + H_2O + 2e^-$$

When a $PbSO_4$ layer is formed and becomes thick, the pores formed from inter-crystalline spaces are practically closed. It is only permeable to H^+ which migrates away from the electrode and OH^- which migrate in the opposite direction due to the hindered diffusion of Pb^{2+} and SO_4^{2-} ions. Consequently, the environment underneath the $PbSO_4$ layer becomes more basic and suitable for the formation of PbO and a considerable diffusion potential is generated across the $PbSO_4$ layer [28]. When the interior PbO film grows in the anodic oxidation, the anodic current may be limited by the diffusion of OH^- passing through the outer $PbSO_4$ layer.

The reversed sweep (orange) shown in Figure 3-14, presents two cathodic contributions. The first small peak (4) is observed at 0.9 V versus Ag/AgCl/KCl (3 M) and is related to the reduction of PbO_2 to $PbSO_4$. However, in the anodic scan, the

oxidation of $PbSO_4$ or PbO to PbO_2 is not observed, because PbO_2 is generated in the transpassivation zone, at applied potentials higher than 1.6 V [28]. The last peak (5) is shown as a big cathodic contribution at -0.83 V versus Ag/AgCl/KCl (3 M). This broad appearance of the cathodic peak before reaching its maximum potential is related to the first electroreduction of PbO to Pb. Then, H^+ ions migrate towards the interior oxide layer through the $PbSO_4$ layer where the dissolution of the lead oxide into Pb^{2+} and OH^- ions occurs. Pb^{2+} ions are reduced to Pb while OH^- ions diffuse towards the bulk solution. This result shows that the reduction of interior lead oxide starts before the reduction of the $PbSO_4$ layer, which occurs in the same peak potential of -0.83 V versus Ag/AgCl/KCl (3 M) [28,29]. Finally, hydrogen evolution started at approximately -1.8 V versus Ag/AgCl/KCl (3 M).

In a different set of experiments, the reduction potentials of the corroded sample prepared in the laboratory were determined using a linear sweep voltammetry. For that purpose, a cathodic scan was performed in 0.5 M Na_2SO_4 and a sweep rate of 1 mV/s^{-1}. In addition, the same experiment was performed using a metallic lead electrode to compare its behaviour with the corroded sample. Figure 3-15 shows the obtained voltammograms.

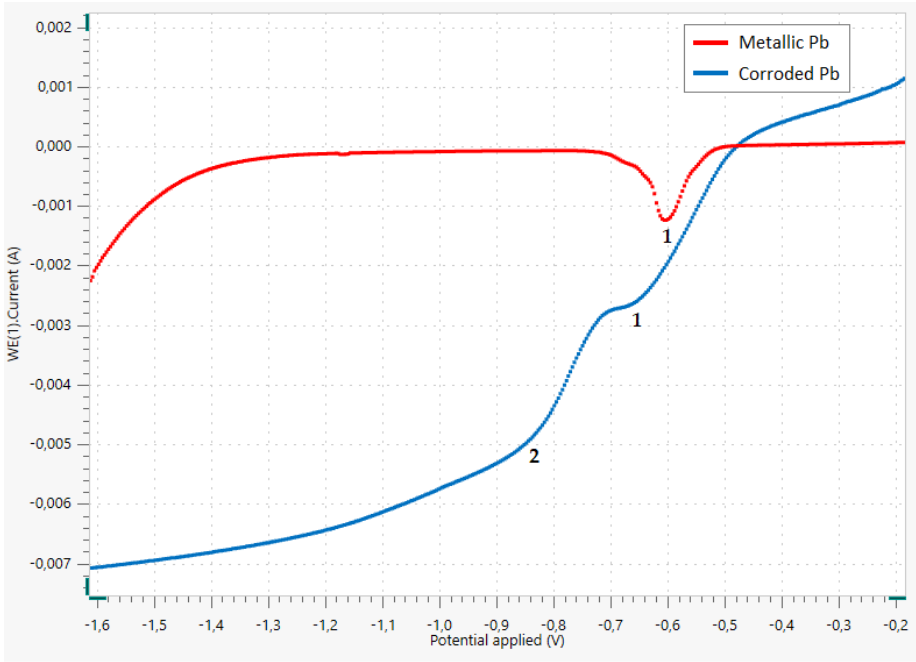

Figure 3-15. Linear Sweep Voltammetry curves for a metallic Pb sample (blue) and the corroded sample by AcOH vapours (red) in a potential area from -1.6 V to -0.2 V versus Ag/AgCl/KCl (3 M) in Na_2SO_4 electrolyte and a scan rate at 1 mV/s^{-1}.

It can be seen in the cathodic voltammogram of metallic lead (red line of Figure 3-15) that when it was initiated (at -0.2 V vs Ag/AgCl/KCl 3 M) a slightly anodic current was flowing. According to Figure 3-14, it was attributed to the oxidation of metallic lead to lead sulphate. In addition, a small reduction peak at -0.6 V was obtained due to the electrochemical reduction of lead sulphate to lead. Note that the peak potential was more anodic than that obtained in Figure 3-14 because of the difference in the sweep rate and the thickness of the sulphate layer in both experiments. In contrast, in the cathodic voltammogram of the corroded lead sample in the laboratory (see the blue line of Figure 3-15), instead of peaks waves were obtained. It was due to the high thickness of the corrosion layer. Note also that current values at potentials more cathodic than -0.5 V corresponded to cathodic processes. The first wave was observed from -0.5 V to -0.7 V and it was attributed to lead sulphate or lead acetate reduction to metallic lead. The second was observed from -0.7 V to -0.9 V and it was attributed to lead carbonate reduction to lead. It is

worth mentioning that Degrigny and Le Gall [10] reported that for artificially carbonated lead coupons, only one reduction peak was visible at around -0.9 V versus SCE and it was attributed to the reduction of the lead carbonate ($PbCO_3$). For naturally carbonated samples the authors reported a small change in the slope of the cathodic linear sweep voltammetry around -0.9 V versus SCE which was attributed to the reduction of lead carbonate. Note that -0.9 V versus SCE (-0.86 V vs Ag/AgCl/KCl 3 M) was in good agreement with our measurements (see Figure 3-15). Then, it was decided that -0.90 V vs Ag/AgCl/KCl (3 M) would be suitable to perform the potentiostatic experiments. Figure 3-16 shows the resulting potentiostatic reduction curve on the corroded Pb sample exposed to AcOH vapours.

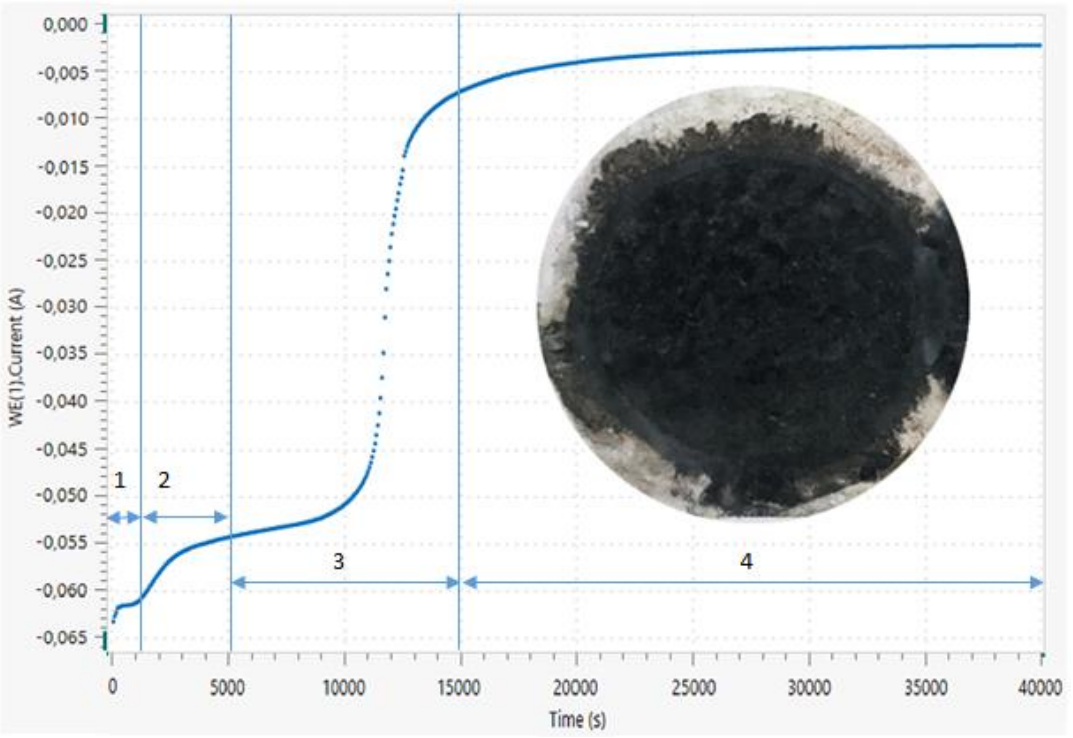

Figure 3-16. Potentiostatic reduction of corroded lead products of plumbonacrite and lead acetate hydroxide.

At the first region (1) shown in Figure 3-16, a small change in the current was observed from the origin to the first ~16 minutes (-0.065 to -0.069 A). At the second

region (2) a current change was observed from ~16 to ~83 minutes (from -0.064 A to -0.054 A). It was related to a first reduction [11]. A second reduction was observed in the next region (3), from ~83 to ~250 minutes, in which a large decrease in the current was obtained (from -0.054 A to -0.007 A). Finally (4), from ~250 minutes until the end of the experiment, the current was progressively stable until reaching a value of -0.002 A, meaning that lead compounds were reduced. Once potentiostatic reduction was finished, the surface was soaked in deionized water and dried using a stream of air.

Note that the potentiostatic approach was selected to avoid hydrogen evolution and it was not observed during the experiments. However, the appearance of the after-reduction surface was very similar to the galvanostatic approach. It seems that no significant improvement was obtained despite the change on the electrolytic mode.

3.3.3.1. Sample characterization after potentiostatic reduction

3.3.3.1.1. Surface characterization

The morphology of the resulting surface after potentiostatic reduction was analysed with SEM-EDS, and the resulting images are shown in Figure 3-17. SEM and XRD conditions were the same as previously described in chapter 2.

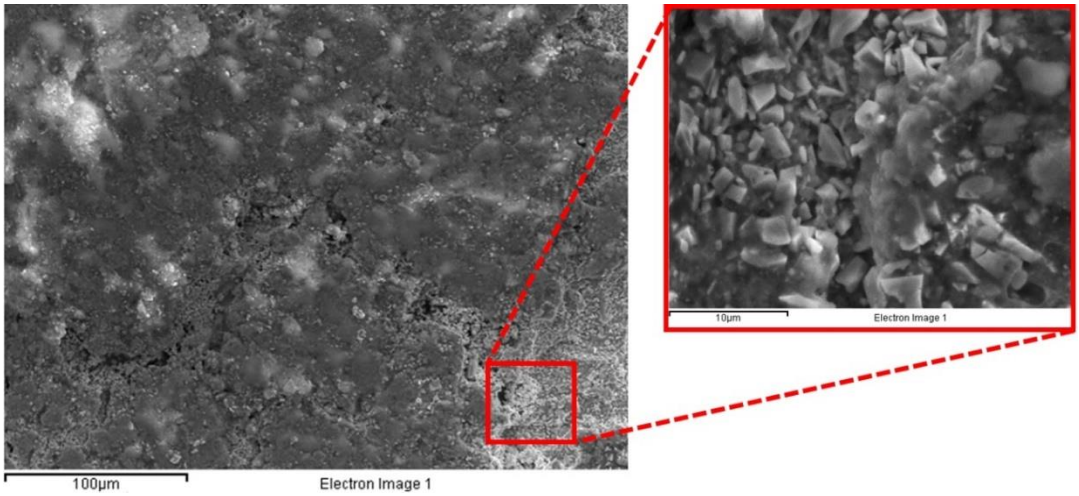

Figure 3-17. *a*; SEM micrograph at 100 µm after potentiostatic reduction and 10 µm amplification of a lead sulphate deposit on the analysed surface, *b*; SEM micrograph at 100 µm after potentiostatic reduction and also amplification at 10 µm of a lead sulphate deposit on the analysed surface.

As shown in Figure 3-17, the potentiostatic reduced sample, presented small cracks and crystals of around 3 µm size, agglomerated in narrow cavities. These heterogeneous distributed crystals were observed in the whole surface and its elementary composition sulphur was identified. To study the crystallographic structure of these superficial compounds after potentiostatic reduction, XRD analyses were performed, and the results are shown in Figure 3-18.

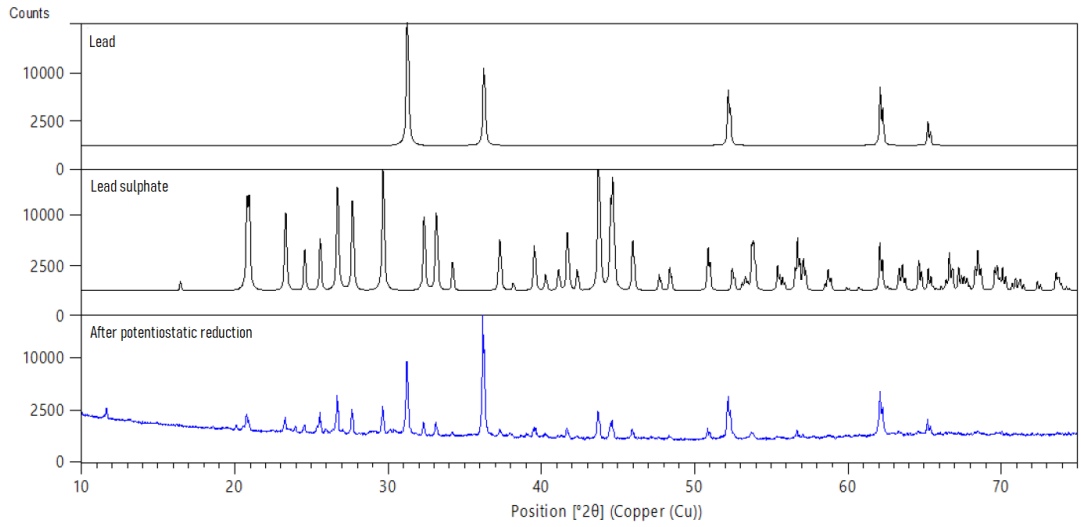

Figure 3-18. Database patterns from International Centre for Diffraction Data® (PDF4+) of lead and lead sulphate (black). Diffractogram obtained after potentiostatic reduction is also presented (blue).

It can be seen in Figure 3-18 that XRD patterns indicated the presence of metallic lead and lead sulphate in the sample after the potentiostatic reduction. Peak positions of metallic lead were observed around 32, 37, 53, 62 and 65 degrees and peak positions of the lead sulphate database pattern corresponded to the resulting sample after treatment (such as peak positions of 21, 23, 27, 28, 30, 36, 44, 45 and 46 degrees). Note that it was also observed in the galvanostatic experiments. It is worth mentioning that after the electrolytic treatment, the sample remained immersed in the medium (Na_2SO_4) for a few minutes. It should be noted that at this point, the metal surface would be highly reactive [1] and the dissolved oxygen in the medium may promote its oxidation, generating a thin surface layer of lead sulphate.

3.3.3.1.2. Roughness analysis by 3D Optical Measuring System (3D-OMS).

The roughness analysis was also performed before and after potentiostatic reduction, and the results are presented in Figure 3-19 (both analyses were performed in the same position).

a)

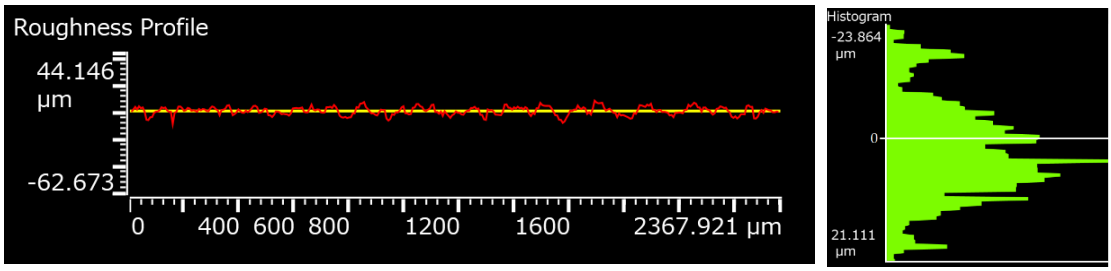

b)

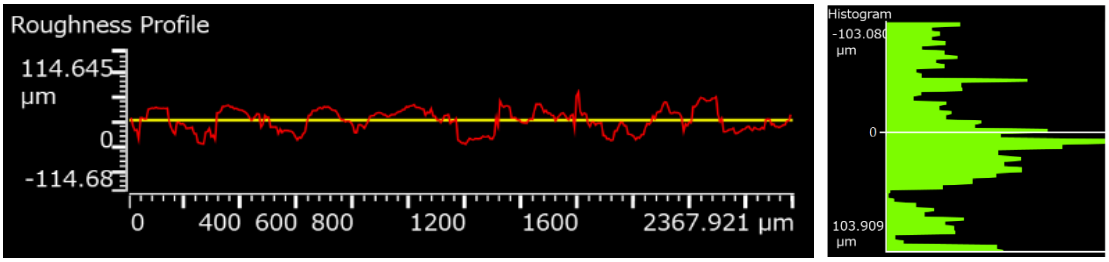

Figure 3-19. Roughness profiles of surfaces and obtained values, *a*; corroded surface in AcOH vapours, *b*; after potentiostatic reduction.

The obtained values for the considered parameters to describe roughness surfaces were:

Table 3-2. Obtained values after roughness analysis

Sample surface	Ra	Rq	Rz	Ssk
Corroded surface in AcOH vapours.	2.5 µm	3 µm	13 µm	Ssk<0
After potentiostatic reduction.	14.9 µm	17.9 µm	72 µm	Ssk~0

The resulting surface also presented higher roughness values respecting the initial corroded surface. The *Ra, Rq* and *Rz* values from potentiostatic reduced surface are similar to the galvanostatic reduced. But in this case, the percentages of maximum height are closer to 0, which means a more uniform roughness distribution in comparison with the corroded surface.

The topographic results obtained by the 3D Optical Measuring System, are shown in Figure 3-20.

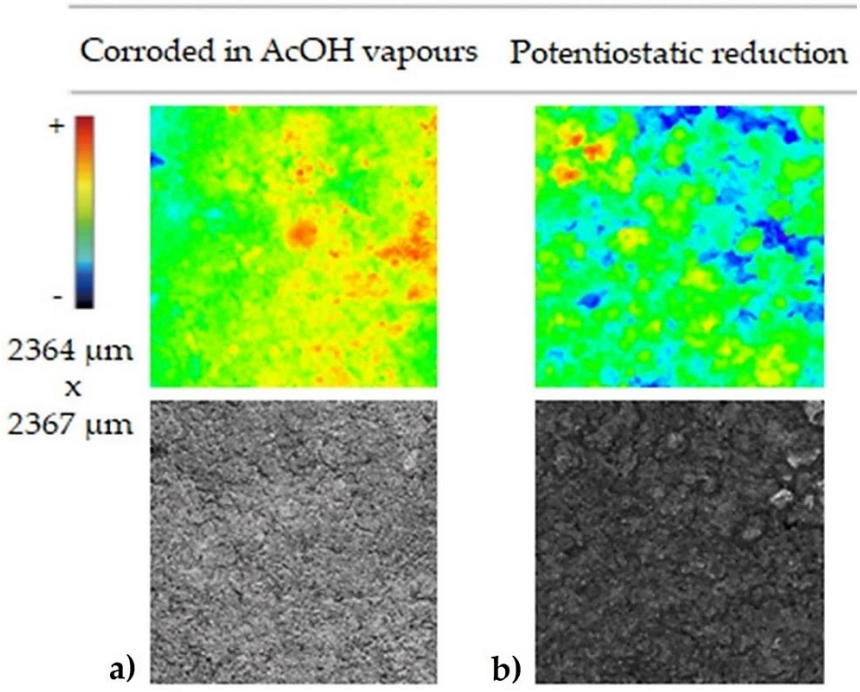

Figure 3-20. Topographic data from optical profilometry showing surface roughness, *a*; corroded surface in AcOH vapours, *b*; after potentiostatic reduction.

Once the surface was treated by potentiostatic reduction, the resulting aspect was rough, and no significant differences were observed in comparison with the galvanostatic reduction. Potentiostatic reduction was used by many authors to achieve a consolidative reduction for the conservation of corroded artefacts [7–10,15,30]. This technique has shown positive results in preventing H_2 evolution, which can cause damage to the surface by stripping off surface products. By using the potentiostatic method, a consolidative/stabilisation reduction of the corroded surface can be achieved on lead artefacts, thereby preventing further corrosion. At that point, it can be said that in the experiments performed the formation of hydrogen was not observed, and thus minimizing the detachment of corrosion products on the

metal surface. However, no improvements in the roughness of the samples were obtained, highlighting that samples with engravings or drawings can suffer from loss of surface detail and definition. This is because the electrochemical reduction occurs preferentially at the protruding parts of the surface, which can lead to a loss of sharpness in the engravings or drawing.

3.4. Concluding remarks

The surface appearance of the metallic Cultural Heritage artefacts is the first impression, providing information about the state of conservation. Colour, brightness and texture are parameters that have a high influence on the aesthetic purposes. In this sense, corrosion is the main problem of metallic artefacts, and the selection of a proper treatment is highly challenging. In the present chapter 3, electrolytic treatments were used to stabilise a previously corroded Pb sample exposed to AcOH. Then, galvanostatic and potentiostatic methods were used in order to be compared.

Since corrosion layers obtained, after a long exposure time, tends to be formed by a mixture of different compounds, the whole process results complex. This is because it can be difficult to know what is happening during the reduction process by using both methods, galvanostatic and potentiostatic. It is worth mentioning that polarization curves such as cyclic voltammetry (CV) and linear sweep voltammetry (LSV) play an important role in identifying which electrochemical transformations can be useful for stabilising the corroded samples. These voltammograms allow determining from which potentials the oxidized forms of lead can be reduced to stabilise its surface. For example, at potentials equal to or more cathodic than -0.9 V vs Ag/AgCl/KCl lead sulphate, acetate, and/or carbonate can be reduced to the metal.

It was observed that after both electrolytic treatments (at a constant current and potential) of the corroded samples new corrosion layers were formed. This was because during the electrolytic reduction process, the corrosion layer is removed, exposing a fresh surface of the underlying metal to the environment. This fresh surface is highly reactive because it has a high surface energy and can easily react with the surrounding environment, including any dissolved oxygen or other

chemicals in the solution. The electrolytic processes were performed in non-deaerated 0.5 M Na_2SO_4, so once the reducing potential/current was discontinued, the metal was exposed to the working solution. The presence of oxygen and sulphate while the sample was still submerged in it caused the formation of a lead sulphate layer covering the metal. Even that, Na_2SO_4 is commonly used for that purpose since it is considered by different authors as an inert electrolyte [10]. However, the obtained lead sulphate layer after cathodic reduction was heterogeneously distributed on the overall surface causing irregularities in the resulted surfaces.

As described in bibliography, potentiostatic methods are used during the electrolytic treatment to prevent hydrogen evolution by controlling the required potential to reduce corrosion products to pure metal [7–10,15,30]. This ensures an effective cleaning of the object's surface without compromising its structural integrity or generating new damage. Without proper control of the reduction potential, galvanostatic treatments can generate excessive hydrogen bubbles that may strip corrosion products from the object's surface, which compromises the object's integrity and transforms the cleaning process into a mechanical one rather than an electrolytic one by cathodic reduction. It should be noted that there was no significant decrease in the surface roughness of the samples before and after applying the two electrolytic processes (potentiostatic and galvanostatic). It is worth mentioning that although the potentiostatic method provides greater control over the electrochemical processes that occur in the corrosion layer (even preventing the generation of hydrogen bubbles), it is not capable of significantly reducing the surface roughness.

For the electrolytic reduction of corroded lead samples, the potentiostatic method is often preferred over the galvanostatic method. This is because the potentiostatic method can control the applied potential of the electrode surface, which allows for better control of the reduction reaction and can help minimize the formation of hydrogen gas. Galvanostatic methods, on the other hand, control the current instead of the potential, which can result in less precise control over the reaction and the release of hydrogen gas. The evolution of hydrogen gas during galvanostatic reduction is dangerous because it can cause bubbles to form on the surface of the sample, which can detach the corroded layer from the metal surface. This can lead to incomplete reduction of corrosion products and potentially damage

the sample. This is especially critical in samples with drawings or engravings, since it can remove or damage the delicate features. To avoid hydrogen evolution while being able to reduce the corrosion layer in the samples prepared in the laboratory, it was demonstrated that -0.9 V vs Ag/AgCl/KCl was sufficient to satisfy both conditions. It is worth mentioning that other authors reported similar values [7,9,10].

In the present experiments, the reduction time of corrosion products for both galvanostatic and potentiostatic methods was approximately between 3 and 4 hours in both cases, although this time may vary depending on the sample. It is important to note that in real objects, the sample may have a greater thickness, which may require a longer reduction time. XRD analyses after galvanostatic and potentiostatic reduction, only lead sulphate was detected, indicating that the other corrosion products were reduced to metallic lead. However, after both electrolytic treatments, the resulting surfaces presented high roughness. This is due to the volume change that corrosion products undergo during reduction. The obtained roughness is not favourable in either of the two methods used in this chapter, indicating that neither method provided entirely satisfactory results for non-uniform corroded surfaces. As an alternative, the use of non-thermal plasma technique for cleaning lead affected by VOCs was discussed in chapter 4.

3.5. References

[1] V. Costa, F. Urban, Lead and its alloys: metallurgy, deterioration and conservation, Studies in Conservation. 50 (2005) 48–62. https://doi.org/10.1179/sic.2005.50.Supplement-1.48.

[2] E.R. CALEY, Coatings and Incrustations on Lead Objects from the Agora and the Method Used for Their Removal, Studies in Conservation. 2 (1955) 49–54. https://doi.org/10.1179/sic.1955.007.

[3] B. Schotte, A. Adriaens, Treatments of Corroded Lead Artefacts AN OVERVIEW, Studies in Conservation. 51 (2006) 297–304. https://doi.org/10.1179/sic.2006.51.4.297.

[4] P.D. R., The Preservation of Antiquities, Nature. 134 (1934) 516–516. https://doi.org/10.1038/134516a0.

[5] R.M. Organ, The consolidation of fragile metallic objects, Studies in Conservation. 6 (1961) 128–134. https://doi.org/10.1179/sic.1961.s031.

[6] A.E.A.W. Harold James Plenderleith, The Conservation of Antiquities and Works of Art: Treatment, Repair and Restoration, (1966) 1–373. https://doi.org/0-7141-0227-X.

[7] A.A.M.G.D.L.V. Bart Schotte, A study of the electrolytic reduction of corroded lead objects and the application, characterization and testing of a protective lead carboxylate coating, Universiteit Gent, Faculty of sciences, 2007.

[8] C. Degrigny, Use of electrochemical techniques for the conservation of metal artefacts: a review, Journal of Solid State Electrochemistry. 14 (2010) 353–361. https://doi.org/10.1007/s10008-009-0896-0.

[9] I.A. Carradice, S.A. Campbell, The Conservation of Lead Communion Tokens by Potentiostatic Reduction, Studies in Conservation. 39 (1994) 100–106. https://doi.org/10.2307/1506559.

[10] C. Degrigny, R. le Gall, Conservation of ancient lead artifacts corroded in organic acid environments: electrolytic stabilisation/consolidation, Studies in Conservation. 44 (1999) 157–169. https://doi.org/10.1179/sic.1999.44.3.157.

[11] B. Schotte, The consolidation of fragile metallic objects, (2007) 1–199. https://biblio.ugent.be/publication/470013.

[12] L.S. Fort González, Rafael ; Álvarez de Buergo, Mónica ; Vázquez Calvo, M. Carmen ; Gómez Villalba, Análisis de la microrugosidad mediante técnicas portátiles: aplicaciones y casos de estudio en patrimonio, in: C. y D. (España) Ministerio de Educación (Ed.), La Ciencia y El Arte, IV: Ciencias Experimentales y Conservación Del Patrimonio., 2013: pp. 198–216.

[13] J. Tétreault, J. Sirois, E. Stamatopoulou, Studies of lead corrosion in acetic acid environments, Studies in Conservation. 43 (1998) 17–32. https://doi.org/10.1179/sic.1998.43.1.17.

[14] A. Doménech-Carbó, Electrochemistry for conservation science, Journal of Solid State Electrochemistry. 14 (2010) 349–351. https://doi.org/10.1007/s10008-009-0934-y.

[15] J. Barrio, J. Chamón, A.I. Pardo, M. Arroyo, Electrochemical techniques applied to the conservation of archaeological metals from Spain: a historical review, Journal of Solid State Electrochemistry. 13 (2009) 1767–1776. https://doi.org/10.1007/s10008-009-0876-4.

[16] D.E. Newbury, Mistakes encountered during automatic peak identification of minor and trace constituents in electron-excited energy dispersive X-ray microanalysis, Scanning. 31 (2009) 91–101. https://doi.org/10.1002/sca.20151.

[17] R.K. Kumar, S. Seetharamu, M. Kamaraj, Quantitative evaluation of 3D surface roughness parameters during cavitation exposure of 16Cr–5Ni hydro turbine steel, Wear. 320 (2014) 16–24. https://doi.org/10.1016/j.wear.2014.07.015.

[18] E.S. Gadelmawla, M.M. Koura, T.M.A. Maksoud, I.M. Elewa, H.H. Soliman, Roughness parameters, J Mater Process Technol. 123 (2002) 133–145. https://doi.org/10.1016/S0924-0136(02)00060-2.

[19] L. Pena-Paras, D. Maldonado-Cortes, C. Martinez, M. Arias, A. Ontiveros, B. Castanos, M. Morales-Martinez, Study of the influence of surface roughness parameters on the frictional characteristics of materials, IOP Conf Ser Mater Sci Eng. 591 (2019) 0120251–0120257. https://doi.org/10.1088/1757-899X/591/1/012025.

[20] D. Draganovská, G. Ižaríková, J. Brezinová, A. Guzanová, The Study of Parameters of Surface Roughness by the Correlation Analysis, Materials Science Forum. 818 (2015) 15–18. https://doi.org/10.4028/www.scientific.net/MSF.818.15.

[21] R. Deltombe, K.J. Kubiak, M. Bigerelle, How to select the most relevant 3D roughness parameters of a surface, Scanning. 36 (2014) 150–160. https://doi.org/10.1002/sca.21113.

[22] L.S.G.V. Rafael Fort, Mónica Álvarez de Buergo Ballester, Carmen Vázquez Calvo, Análisis de la microrugosidad mediante técnicas portátiles: aplicaciones y casos de estudio en patrimonio, in: S.G. de D. y P. Ministerio de Educación Cultura y Deporte (Ed.), La Ciencia y El Arte IV: Ciencias Experimentales y Conservación Del Patrimonio, Instituto del Patrimonio Cultural de España (IPCE), 2013: pp. 198–216.

[23] M. Sedlaček, B. Podgornik, J. Vižintin, Correlation between standard roughness parameters skewness and kurtosis and tribological behaviour of contact surfaces, Tribol Int. 48 (2012) 102–112. https://doi.org/10.1016/j.triboint.2011.11.008.

[24] L.M. Peter, A photoelectrochemical study of the reduction of alpha lead dioxide in aqueous sodium tetraborate, J Electroanal Chem Interfacial Electrochem. 144 (1983) 315–330. https://doi.org/10.1016/S0022-0728(83)80164-8.

[25] Y. Guo, Z. Wei, S. Hua, Effects of H2SO4 concentrations on reduction processes of PbO layer, Electrochim Acta. 42 (1997) 979–984. https://doi.org/10.1016/S0013-4686(96)00275-7.

[26] E.F. El-Sherbini, S.S. Abd El Rehim, Electrochemical behaviour of lead electrode in Na2SO4 solutions, Mater Chem Phys. 88 (2004) 17–22. https://doi.org/10.1016/j.matchemphys.2003.10.020.

[27] J. Wang, M. Li, J. Hu, Y. Ke, W. Yu, Z. Wang, S. Liang, K. Xiao, H. Hou, J. Yang, Effect of particle size on phase transitions of positive active materials made from novel leady oxide during soaking process and its influence on lead-acid battery capacity, J Energy Storage. 28 (2020) 1011751–1011759. https://doi.org/10.1016/j.est.2019.101175.

[28] E.E. Abd El Aal, Cyclic voltammetric behavior of the lead electrode in sodium sulphate solutions, J Power Sources. 102 (2001) 233–241. https://doi.org/10.1016/S0378-7753(01)00804-7.

[29] E.E. Abd El Aal, Studies on the anodic and cathodic polarization of lead in sodium sulphate solution, J Power Sources. 75 (1998) 36–43. https://doi.org/10.1016/S0378-7753(98)00080-9.

[30] C. Degrigny, R. Jeanneret, D. Witschard, C. Baudin, G. Bussy, H. Carrel, A new electrolytic pencil for the local cleaning of silver tarnish, Studies in Conservation. 61 (2016) 162–173. https://doi.org/10.1179/2047058415Y.0000000015.

4. Non-thermal plasma for ductile metals conservation and characterization techniques

Non-thermal plasma techniques are used in the cleaning of corroded artefacts from Cultural Heritage due to their advantages over thermal plasma techniques. These techniques operate at low temperatures, minimizing thermal damage and allowing for precise control over treatment parameters to optimize the cleaning treatment. Christian Degrigny pioneered the use of plasma techniques for corroded lead surfaces in the late 1990s, and since then, non-thermal plasma techniques have become increasingly popular in heritage conservation. This chapter aims to optimize the experimental conditions of the plasma system for lead samples affected by active corrosion, and surface characterization is conducted to evaluate the plasma quality and determine the optimal treatment conditions.

4.1. Introduction

The initial use of plasma treatment is dated to the eighties of the twentieth century when a group of scientists used low-pressure hydrogen plasma for the treatment of Daguerreotypes and tarnished silver objects [1]. The first success for iron artefacts was achieved around the year 1980 using hydrogen plasma. In recent years, scientists from different research fields, have focused on less invasive surface treatments, avoiding the use of unappropriated cleaning methods for metallic artefacts [2–4]. The application of non-thermal plasma was in the front line of these techniques, for example with the use of H_2 plasma on lead corroded artefacts [5,6].

A great advantage of this methodology is that it is a non-invasive technique that does not require physical contact with the artifact, which minimizes the risk of damage. In addition, plasma can generate reactive species, being efficient with fast kinetics. This results in a lower time of cleaning treatment. However, is not

recommended to use this technique on real artefacts without a deep previous study with model samples of corrosion replicates [7]. However, it is reported that the effectiveness of hydrogen plasma treatment depends on several factors, such as the thickness and composition of the corrosion layer, the nature of the metal substrate, and the parameters of the plasma treatment. For example, if the corrosion layer is too thick, the hydrogen plasma may not penetrate deep enough to reach the corroded metal underneath [5].

non-thermal plasma can be also performed through electrons and ions created by a mixture of gases, for example from atomic hydrogen and argon. The temperature of these electrons is high (< 10,000 K) but the density is much lower compared to the atoms. While in a TP (Thermal Plasma) there is an equilibrium between electrons, ions and neutral components, the NTP (Non-Thermal Plasma) is characterized because all energy is carried out by the electrons (so almost all temperature). For this reason, there is a low collision rate in the low-density gas, and ions and neutral components from the plasma remain close to room temperatures (25 °C - 100 °C). Taking into account that metallic lead has a low melting point (327.5 °C) in comparison with other metals, non-thermal plasma (NTP) was used in the present chapter.

In the present study, a non-thermal plasma reactor, designed in our laboratory [8–10], was used to clean corroded lead samples under an argon/hydrogen plasma. In previous studies, we reported that the plasma reactor was a useful tool in order to clean corroded surfaces from Cultural Heritage artefacts. A plasma treatment converts corrosion products in the crust to metallic lead using a hydrogen plasma following the reaction [11]:

Equation 4-1 $$2PbCO_3 \cdot Pb(OH)_2 + 2\,H \rightarrow 3Pb + 2CO_2 + 4H_2O$$

The vacuum chamber was continuously receiving gas and a continuous renewal of the gases was produced inside the chamber. Figure 4-1 presents the behaviour of treatment through this application in corroded lead samples.

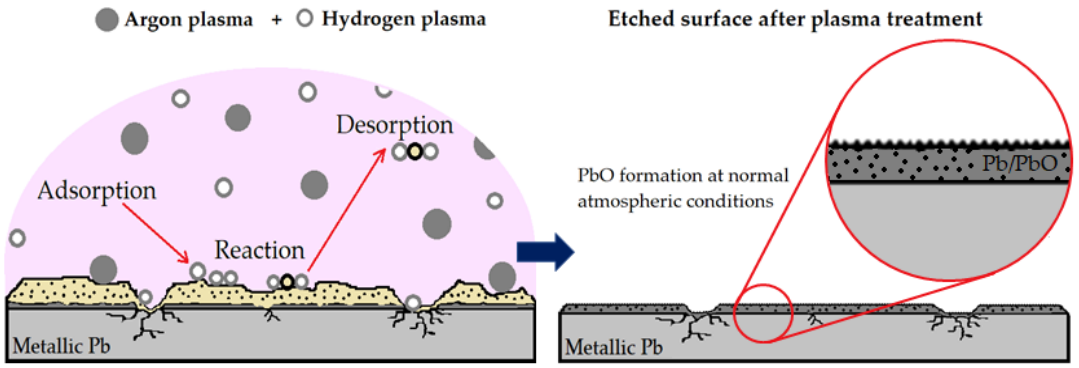

Figure 4-1. Plasma mechanism reactions on a corroded metallic lead (left) and etched surface after plasma treatment (right).

The plasma treatment of the sample, presented in Figure 4-1, leads to a physicochemical alteration on the surface. Under these conditions, a large number of energetic reactive species is generated. The species created on this plasma were composed of charged particles (electrons and ions), photons (in the visible and ultraviolet range), highly reactive neutral species, such as free radicals, and excited atomic and molecular species from the hydrogen and argon gases [7,12,13]. At this point, two general interactions occurred in the system. First, a high number of collisions from the plasma species are created. As the pressure increases, the number of collisions between the particles also increases.

In addition, new reactions are produced between the interaction of plasma species and corrosion products of the metal Pb surface. A high electron movement induces a negative charge into metal (lead), and as a consequence, an interaction is generated between the positive ions and the lead corroded surface. This interaction gives the name of a reductive system through the creation of radicals in the sample.

The result of this effect can vary in its reduction process since it was determined by the established parameters prior to initiating the conservation treatment. Collisions between the reacting particles with enough kinetic energy are crucial to overcoming the activation barrier. The rotational populations of molecular hydrogen in plasma were also measured in previous works involved in this process.

While hydrogen acts as a reduction treatment, the application of argon in the treatment is mainly a physical process. In this process, plasma chemistry is dominantly controlled by Ar^+ and e^- to perform the etching treatment. An etching behaviour may involve a removal of the corrosion layer (see Figure 3-6 from chapter 3) by bombarding the mixture of reactive particles at subsonic velocities. However, the reason for the improvement in the time of treatment is not only an individual implication of the ionized argon. A combination of argon and hydrogen plasma increases the effectiveness of the treatment. Ionized argon induces the creation of new reactive sites since the physical action allows it to achieve a deeper layer level. It means that the reaction efficiency is improved by the hydrogen radicals during the ionized argon activity [7,12–14].

Depending on the applied parameters such as the gas mixture, the pressure and the type of electrical discharge, the treatment's performance changes. Because it is a controlled process of gas composition and flow, intensity, and reaction time, this technique allows for determining specific treatments in different contexts.

The use of hydrogen plasma treatment is limited in its ability to penetrate corrosion layers with a thickness greater than 0.1 to 0.2 mm, which makes it unsuitable for heavily corroded artefacts [5,15]. However, this technique can effectively loosen the compactness of the corrosion layer, allowing for potential post-treatment mechanical cleaning with soft brushes to further reduce its thickness. It should be noted, however, that for objects with active corrosion and thick corrosion layers, electrolytic processes may be more appropriate. Additionally, for objects with inscriptions or decorations on the surface, which are integral to the original appearance of the artefact, plasma treatment may displace these features to the top layers, presenting another potential limitation.

A key question to solve after applying any surface treatment is to assure the integrity of the metallic object. For this reason, is important to develop characterization techniques that give insight into the artefact evolution during the process. In this sense, these techniques were used in this work to analyse how corroded surfaces can variate before and after non-thermal plasma treatment in corroded Pb samples.

4.2. Experimental set-up

4.2.1. Non-thermal plasma reduction

A low-pressure plasma reactor was used to clean metallic lead samples corroded by acidic environments. The experimental set-up was designed by our Group (*Grup d'Enginyeria de Materials* (GEMAT) at the IQS (*Universitat Ramon Llull)* and previously reported in other papers from our group [8–10]. The schematic system of the plasma reactor used is presented in Figure 4-2.

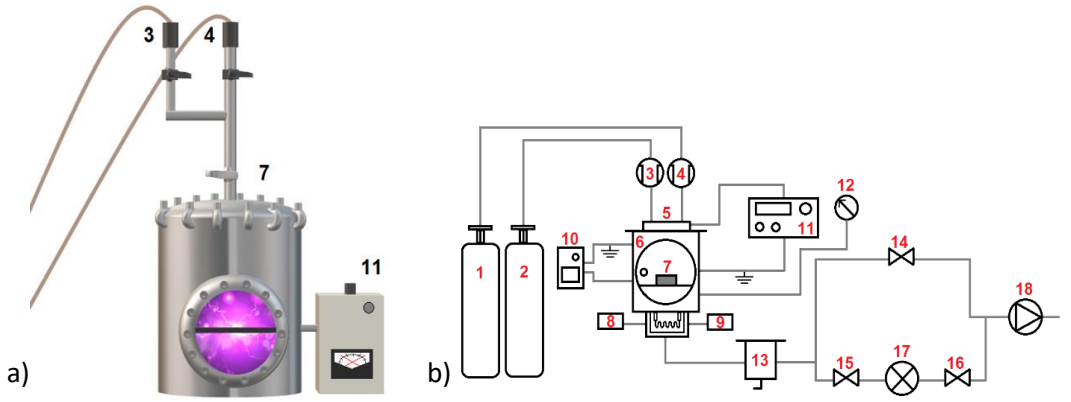

Figure 4-2. *a;* low-pressure plasma reactor, *b*; schematic drawing of the experimental set-up; 1, 2 – hydrogen, argon; 3, 4 – mass flow controllers; 5 – gas inlet and mixing; 6 - reactor chamber; 7 – sample; 8, 9 – thermocouples; 10, 11- RF power supply and matching network; 12 – capacitance pressure gauge; 13 – chemical inlet trap (carbon active); 14, 15, 16 – valves; 17 – refrigerated inlet trap (dry ice); 18 – vacuum pump.

Briefly, the reactor has a Bell Jar design with a stainless-steel chamber (diameter, 25.5 cm; length, 41.6 cm). The ground electrode is the reactor chamber, and the radio frequency (RF) electrode is an aluminium plate, which also is used to hold the samples. Additionally, the RF electrode is connected to an RF pulse generator (13.56 MHz) via a matching box. Gases were injected into the system via a standard manifold. Gas fluxes were adjusted by two mass flow controllers (elements 3 and 4)

and two ball valves were used to cut the gas flux, if needed, in the reactor chamber. The system pressure is monitored using a vacuum gauge controller (MKS PDR900, Andover, MA, USA) connected with a cold cathode/micropirani vacuum transducer (MKS 972 DualMag) positioned at the centre of the reactor. The system used a rotary vane vacuum pump (Trivac D 16BCS/PFPE Leybold, Cologne, Germany). Also, it has a nitrogen cold trap and a chemical trap filled with active carbon to protect the vacuum pump from condensed vapours. The typical base pressure for all experiments is close to 6×10^{-4} mbar, and Ar/H_2 gases were introduced at a constant pressure of ~0.1 mbar.

Before the introduction of the samples placed on an aluminium plate, the chamber was cleaned in continuous wave argon/hydrogen (2:1) plasma for approximately 1800 s at a power of 50 W. To optimize the study, a full factorial design was used. In this study, different conditions (time, power, and argon-hydrogen ratio) were chosen to determine the capacity of reducing corrosion in Pb samples.

To evaluate the effectiveness of plasma treatment on corroded Pb samples (99.99%, Amat Metalplast SA), a set of 8 lead samples was corroded by AcOH vapours following the same conditions described in section 3.2.1 (Chapter 3). In this case, as it was mentioned in section 4.1, a mixture of argon and hydrogen was selected for the non-thermal plasma. The base pressure was 0.06 Pa. Then, argon and hydrogen gases were injected until reaching a working pressure (Pp) of approximately 10 Pa. When the working pressure was reached, the generator was turned on, and the gas in the chamber of the plasma was initiated. The vacuum chamber continuously received gas, so a continuous renewal of the gases was produced inside the chamber.

To optimize the non-thermal plasma treatment a full factorial experimental design for corroded metallic Pb was performed. To classify the results in a normalised scale five features were selected: treatment time (min) (A), plasma power (W) (B and Ar/H_2 ratio (C). Pressure could be a factor to be considered, but it was decided to perform all experiments at 0.06 Pa.

4.2.2. Accelerated corrosion in metallic lead samples

A series of 8 Pb samples of 2,0 x 2,5 cm from a lead sheet of 1.5 mm thickness, were corroded in the laboratory by

AcOH vapours for three months, using acetic acid glacial as described in chapter 3. The sample was suspended using a Teflon thread in a glass reactor at room temperature and exposed to the gas phase of a 3 M AcOH solution. Then, this was exposed to the atmosphere for one week in order to create a lead acetate and carbonate layer on the surface.

4.2.3. Surface characterization after plasma treatment

4.2.3.1. *X-Ray Photoelectron Spectroscopy (XPS) analyses*

Samples treated using the non-thermal plasma were analysed with X-Ray Photoelectron Spectroscopy (XPS) in PHI 5500 Multitechnique System from Physical Electronics, with a monochromatic X-ray source. The selected resolution for the spectra of the different elements in the depth profile spectra was 23.50 eV of Pass Energy and 0.25 eV/step. The high-resolution spectra were obtained through a grade of penetration of 5 nm and the depth profile was of the order of 50 nm. The resulting spectra were analysed and deconvoluted with the Multipak Version 5.0A software. XPS measurements on samples before and after non-thermal plasma treatment were completed with a delay of one day. During this time interval, samples were stored in hermetic polypropylene sample containers (50 ml) purged and filled with argon to remove air.

4.3. Results and discussion

4.3.1. Evaluating non-thermal plasma treatment parameters to improve cleaning of lead surfaces with active corrosion.

In order to evaluate the effectiveness of plasma to clean corroded Pb surfaces, a set of 8 lead samples were chemically corroded by acetic acid for one week, following the procedure explained in section 4.2.2. In this case, as it was mentioned in section 4.2.1, a mixture of argon and hydrogen was selected for the non-thermal plasma. The

point of this section is to optimize the experimental parameters of the non-thermal plasma using prepared samples in the laboratory. Once optimized, these can be used in real samples.

An initial pressure of approximately $6 \cdot 10^{-4}$ mbar was used to generate the vacuum. Then, argon and hydrogen gases were injected until reaching a working pressure (Pp) of approximately 0.1 mbar. When the working pressure was reached, the generator was turned on, and the gas in the chamber begins to ionize.

The behaviour of argon and hydrogen plasma can vary substantially if the experimental parameters are different. In this way, to study the efficiency of the present non-thermal plasma purpose for corroded metallic lead, a first evaluation was made by the variation of three factors (A, B and C) corresponding to the time (min), power (W) and ratio (Ar/H_2) respectively. The pressure was a factor considered to be fixed for all experiments ($6 \cdot 10^{-4}$ mbar) since power and ratio could not achieve a constant value if pressure is changed.

All possible combinations between the established factors were also applied to the following full factorial design (2^3) shown in Table 4-1. This statistical design contemplates the most suitable experiments to know simultaneously what was the effect of each factor on a response and which is the contribution between their interactions.

Table 4-1. Full factorial design of three factors with two possible states (2^3) in the resulting surface (shown as Exp.)

	Factors			Interactions			
Exp.	**A** **Time (min)**	**B** **Power (W)**	**C** **Ar/H_2 Ratio**	**AB**	**AC**	**BC**	**ABC**
1	60 (1)	80 (1)	90:10 (1)	1	1	1	1
2	60 (1)	50 (-1)	70:30 (-1)	-1	-1	1	1
3	15 (-1)	80 (1)	70:30 (-1)	-1	1	-1	1
4	15 (-1)	50 (-1)	90:10 (1)	1	-1	-1	1
5	15 (-1)	50 (-1)	70:30 (-1)	1	1	1	-1
6	15 (-1)	80 (1)	90:10 (1)	-1	-1	1	-1
7	60 (1)	50 (-1)	90:10 (1)	-1	1	-1	-1
8	60 (1)	80 (1)	70:30 (-1)	1	-1	-1	-1

As shown in Table 4-1, for each factor there are two levels, -1 and 1, corresponding to the values of each variable, low and high respectively. The state of the interactions is the product of the state of the factors studied. Based on the values from a qualitative analysis performed on the different surfaces (numbered in the "Exp." column), a statistical study was performed using the Full Factorial design exposed in Table 4-1.

To determine the preliminary assessment, all results were evaluated by qualitative analysis, based on a visual characterization. Each feature represents a variable of the non-desired results on a non-thermal plasma treated sample. To classify the results in a normalised scale, the finished aspect was defined in five features shown in Table 4-2. Each feature was evaluated from 0 to 2 depending on the quantity grade, where 0 is the total absence and 2 is the major quantity resulted. The final response of each experiment was determined by subtracting the sum of the different features to a value of 10, which is a sample with no defects. The higher the response value, the more positive the treatment. Finally, a Pareto Chart and half-normal distribution graph were performed according to the response of each experiment, seen in Figure 4-3.

Table 4-2. Visual evaluation of resulted samples.

Feature	Experiment							
	1	**2**	**3**	**4**	**5**	**6**	**7**	**8**
Heterogeneity	0	2	0	1	2	0	0	1
Carbonate remains	1	2	1	1	2	0	0	2
Colouration	0	0	0	0	1	0	0	1
Decohesion	1	2	2	0	2	1	0	2
Deformation	0	0	0	0	0	0	0	0
Response	8	4	7	8	3	9	10	4

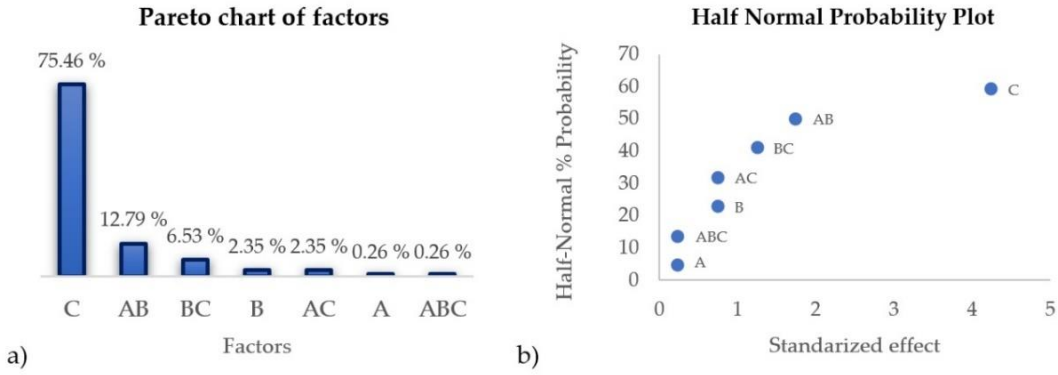

Figure 4-3. *a;* Pareto Chart of Factors graph, *b;* Half-Normal Probability Plot.

The fact that no sample was deformed, confirms that the temperature inside the reactor during each experiment did not reach the melting point of lead (327.5 °C). Thus, due to the visual analysis, it was possible to determine the different contributions of the established factors in the half-normal distribution graph shown in Figure 4-3 *b*.

As mentioned before, three factors mainly influence the results of this method: time, power, and ratio. Based on the values obtained in the qualitative analysis of the eight surfaces resulting from varying treatment conditions (see Table 4-2), the points in the graph of Figure 4-2 *b* will have a specific position. Points that approach zero on both axes indicate that the data follows a normal distribution and that there are no outliers, which means that in this case, the factors, either together or separately,

will have less impact on surface changes. On the other hand, points that move away from zero on both axes suggest that the data may not follow a normal distribution and that there may be outliers. In this case, the outliers are the ones that have the most positive effect on surface cleaning.

As can be seen, point (A) corresponded to the isolated factor of time and is near 0 on both axes. This means that in the process of cleaning surfaces with plasma, it is more relevant to control and adjust the power and ratio of gases applied in the treatment than time, as these parameters mainly determine the changes that occur in the treated surface. However, its contribution increases a bit more with the combination of ratio (AC) and the three factors together (ABC), as observed in the points that contain (A) and are above 10%. This last interaction decreases in the contribution range compared with the other couples of factors, because superficial damage occurred. It was due to the long exposition time to the high power (80 W) and high argon addition (90:10 Ar/H_2), resulting in a too-aggressive treatment. This explains the low difference between the response value of Exp. 1 and 6, (Exp. 8 and 9 values respectively) fixing the power and ratio for both experiments and varying the factor of time.

The element B corresponds to power, and as seen in the graph in Figure 4-3, the point moves away from 0 on both axes when power is combined with time (AB). This means that the effect of varying this parameter is more influential on surface cleaning when combined with time, as observed in Exp. 8. It was also seen in Exp. 6, where with a higher potential, the surface cleaning was accelerated in less time. If the time factor was high (60') in combination with high potential (80 W), the resulting surface also presented decohesion due to the excessive treatment to which the sample was subjected. However, the contribution between the interaction of power with ratio (BC) is a bit lower. High changes were observed between Exp. 4 and 5 (response values of Exp. 8 and 3 respectively), as also minor changes between Exp. 3 and 6 (7 and 9 respectively) by fixing the power.

As it was shown, element C corresponded to the ratio and had a higher contribution. The effect was observed in Exp. 1 and 8, in which the contribution of the ratio is demonstrated between the difference of responses (response value of 8 and 4 respectively). Fixing the time and power factors and varying the ratio, the

response value decreases to half when argon also decreases. With that, it was demonstrated that the etching effect of argon is especially advantageous in terms of extracting corrosion products from the surface. A ratio of 90:10 (Ar/H_2), in combination with a power value of 50 W during 3600 seconds, ensures that the sample is not overheated, and the treatment can be prolonged, if necessary, without risk of surface damage.

The study allowed for a quantitative evaluation of the results from a qualitative analysis. It was observed that variable C (referring to the ratio) had the most influence on the non-thermal plasma cleaning of the surface. The results suggest that the use of certain amounts of argon and hydrogen can have a greater effect on the sample than varying the power or time. Additionally, it was suggested that argon, as an etching agent, helps the H_2 plasma reach deeper surface levels to reduce corrosion products to metallic lead.

4.3.2. Surface characterization after non-thermal plasma treatment

4.3.2.1. Scanning Electron Microscopy- Energy Dispersive X-ray spectroscopy (SEM-EDS) and X-Ray Photoelectron Spectroscopy analyses.

In this way, the selected parameters of Exp. 7, demonstrated that the metallic surface was visually cleaned. A first analysis by SEM was performed and the result is shown in the following Figure 4-4.

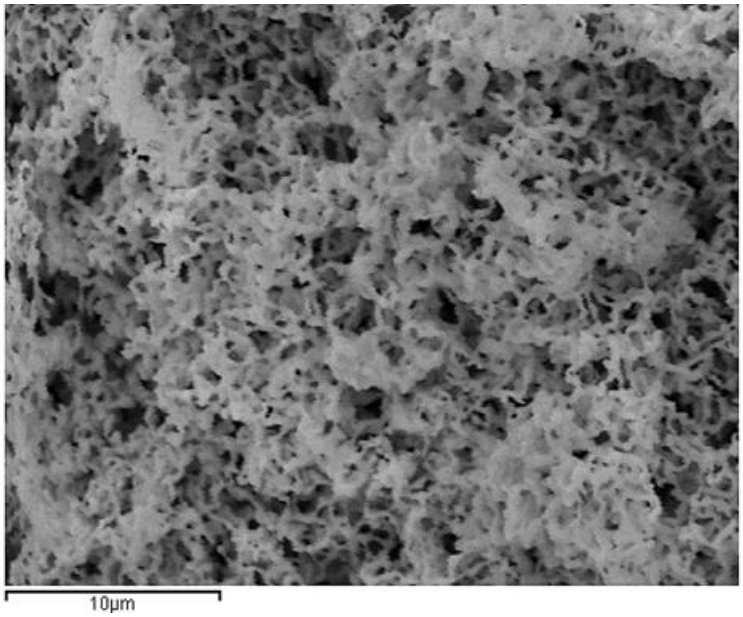

Figure 4-4. SEM micrography of the selected sample (Exp. 7 on Table 4-1) after being treated with non-thermal plasma, scaled at 10 μm.

As it was observed, the treated Pb surface presented small pores in the surface (<2 μm approximately). These were homogeneously distributed on the surface, resulting in a spongy aspect. After treating the corroded Pb sample with the non-thermal plasma, small pores of around one micron in size were created on the surface due to the etching process. However, this cleaning process also helped to reduce the surface roughness, resulting in a more uniform appearance compared to the electrolytically treated sample. As observed later (Table 4-3), the roughness values are lower for the plasma-cleaned sample compared to the electrolytically treated sample (see also Figure 4-9).

To complete the surface analysis, X-ray Photoelectron Spectroscopy was used to identify the chemical state and to estimate electronic structures. XPS can be a good tool to characterize the resulting surfaces and to compare the different superficial compositions, and for this reason, the technique was selected following the reference bibliography found in different data-base [16,17]. To perform this analysis, three samples (Exp. 5, Exp. 7 and Exp. 8) were selected to be characterized by XPS in order

to compare their superficial products. Results are shown in Figure 4-5 for general measurement and Figure 4-6 for high-resolution measurements.

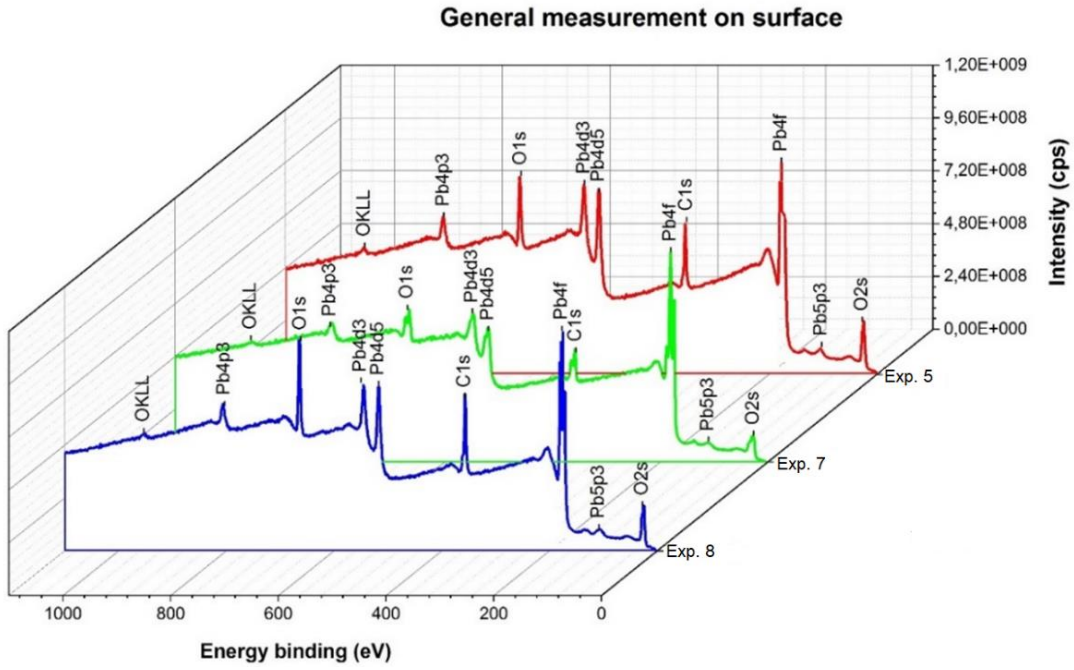

Figure 4-5. General XPS analysis of the selected samples (Exp. 5, Exp. 7 and Exp. 8) for Pbf4 (lead), O1s (oxygen) and C1s (carbon).

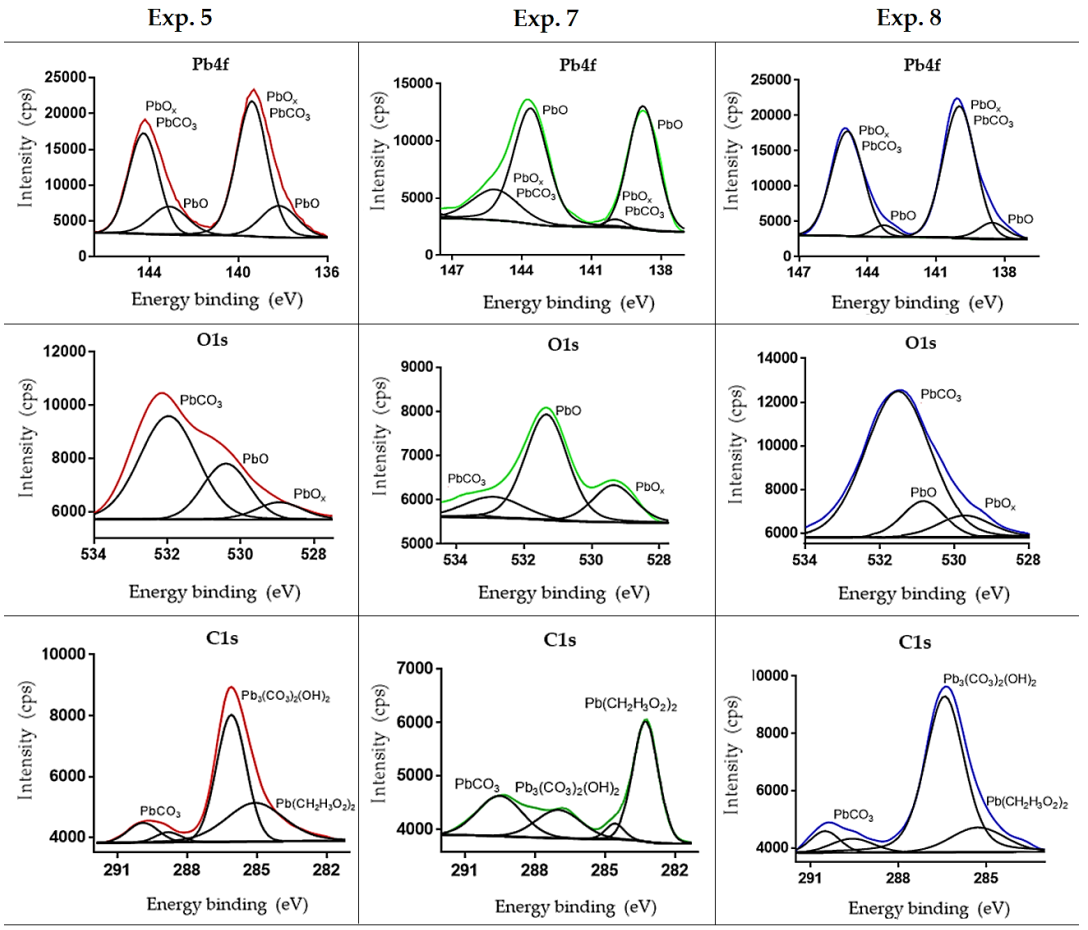

Figure 4-6. High-resolution XPS analysis of the selected samples (Exp. 5, Exp. 7 and Exp. 8) for Pbf4 (lead), O1s (oxygen) and C1s (carbon).

As it was expected, the deconvolutions obtained on the high-resolution results (depth of 5 nm) showed variations, especially in the spectra of exp. 7 compared with exp. 5 and 8. The Pb4f signal of XPS graphs presented in Figure 4-6, shows clear differences between experiments. The Pb4f of XPS graphs shown in Figure 4-6, a great difference between the Exp. 7 from Exp. 5 and Exp. 8.

In all spectra, the PbO corresponded to the signal in the 138-eV region was presented. Species of lead oxide and $PbCO_3$ were associated with the 139.5 eV region. The main difference is represented in Exp. 7, where the PbO signal is greater than in Exp. 5 and 8. Comparing both samples, in Exp. 7 a lower signal of $PbCO_3$ and PbO_x was shown. For Exp. 5 and 8, peaks belonging to some carbonate species (138.5 eV

region) suggest a certain lack of reduction of the corrosion products. In both experiments was suggested also the presence of PbO_2 equivalent to the 137.8 eV region and $Pb(OH)_2$ in the 138.2 eV region.

For the O1s spectra in Exp. 5 and 8, a bigger amount of lead carbonate was associated with the 531 eV and 532 eV regions. The intensity of the signal reaches ~12500 cps for the Exp. 8 sample, ~9600 cps for the Exp. 5 sample and ~6000 cps for the Exp. 7. This fact demonstrated that for Exp. 7 the residual compounds of lead carbonate were much lower than the other two samples. PbO signals in the region of the 531 eV were also seen in the three experiments, being much higher for Exp. 7.

To study the lead carbonate compounds, some signals were found in the literature [18], associated to the formation of cerussite and hydrocerussite. The 285 eV signals corresponded to aliphatic carbon and/or defects, associated in this study to the residual lead acetate $Pb(C_2H_3O_2)_2$. This was related to the formation of hydrocarbons in the metallic lead surface during the acetic acid gas phase corrosion.

Signals in the 286 eV and 287 eV region corresponded to C=O and C–OR formation (R including H) corroborating the presence of hydrocerussite compound. This product is present in all experiments with an intensity signal of ~8900 cps for Exp. 5, and ~4400 cps for Exp. 7 and ~9500 cps for Exp. 8. It means that although there is a real percentage corresponded to a lack of reduction in a small area, the amount of carbonate decreased considerably for Exp. 7.

The 289-eV signal is associated with O=C=O–R (R including also H) and carbonate. The presence of $PbCO_3$ related to cerussite formation was shown in all experiments, but with much lower intensity than the other products (~4500 cps for all). The presence of residual lead oxide and carbonate in all experiments, demonstrated that the non-thermal plasma treatment did not reach the total effectiveness as expected, but corrosion products decreased considerably for Exp.7. For this sample, signals of lead carbonate and lead oxide were much lower compared with Exp. 5 and 8, indicating that the selected parameters for Exp. 7 were positive.

In order to study the internal layers, a depth profile (depth of 2 nm/sputtering) of Exp. 5, Exp. 7 and Exp. 8 was performed. The objective was to analyse possible

changes between the lead oxide from the internal layers and the form of passivation of each sample. The association of the resulting peaks was done following the previous XPS studies in the Pb4f and O1s region [18,19]. Results were simulated in different graphs shown in Figure 4-7.

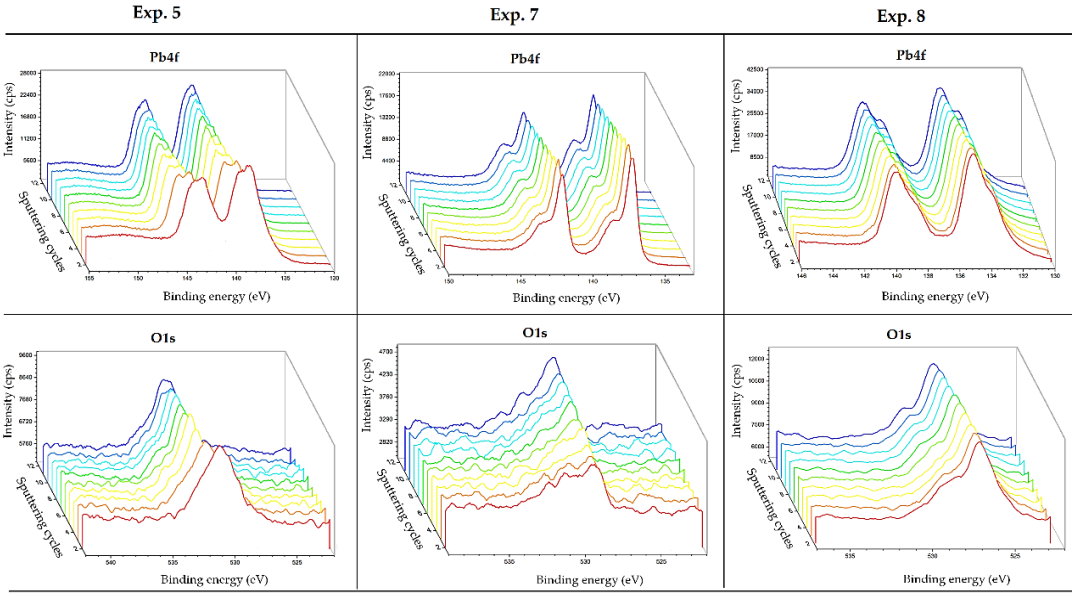

Figure 4-7. Depth profile XPS analysis of Exp. 5, Exp. 7 and Exp. 8 samples for Pbf4 and O1s.

As it is shown in Figure 4-7, different signals for Pbf4 and O1s were shown in an accurate analysis from the inner layer. In Exp. 5, the amount of PbO and PbO_x are similar, especially in the external layers. However, in Exp. 5 the intensity of the PbO_x species associated also to $PbCO_3$ increases as the sputtering cycle becomes more internal. For Exp. 8, a similar behaviour was observed.

However, in this sample, the first sputtering cycles corresponded to the adjacent layers and presented a higher peak of PbO_x. It demonstrates that for Exp. 5 and 8, the residual corrosion compounds were present in much quantity than in Exp. 7 included in the internal layers. The intensity peaks in the deep-profile spectra from Figure 8,

determine a bigger amount of corrosion products for Exp. 8, being also present in the subjacent layers.

The PbO_x signal suggests the presence of Pb (II) and Pb (IV) such as PbO_2 or Pb_3O_4 compounds as can be seen in the 528.9 eV region. Species of this region can be related to lead oxide minerals as massicot or minimum [20,21]. This fact could explain why especially in Exp. 8 was still present a yellowness/reddish localized colouration before and after treatment on the sample (see 4.2).

For the O1s spectra, Exp. 5 presented the same products in the subjacent layers associated with PbO_x products and lead carbonate as for Exp. 8, reaching intensities of almost ~8600 cps and ~12000 cps respectively. The oxide and carbonate compounds were also present in the internal layers in the Exp. 8, although power and time were higher during the non-thermal plasma treatment applied to this sample (see Table 4-1). It corroborated the effectiveness of argon in a large time by lowering the power parameter. For Exp. 7, a PbO layer keeps present in the subjacent layers but in smaller intensity (~4700) together with a lower signal in the 532-eV region corresponding to residual carbonate products.

4.3.3. Comparison between electrolytic reduction and non-thermal plasma treatment

4.3.3.1. X-ray Diffraction (XRD) analyses

In order to analyse the composition of the resulting surface after non-thermal plasma treatment, an XRD analysis was performed. Results were also compared with a treated lead sample by and electrolytic reduced sample (using a potentiostatic system). Figure 4-8 *a,* show the obtained results of XRD analysis for the non-thermal plasma treated sample with the parameters used for Exp. 7 (see Table 4-1). In order to compare it with the electrolytic treatments shown in chapter 3, Figure 4-8 *b* shows the obtained results of XRD analysis for the resulted sample treated by potentiostatic reduction at -0.9 V in 0.5 M $NaSO_4$ after being exposed for three months to acetic acid vapours (see section 3.3.3.1.1.).

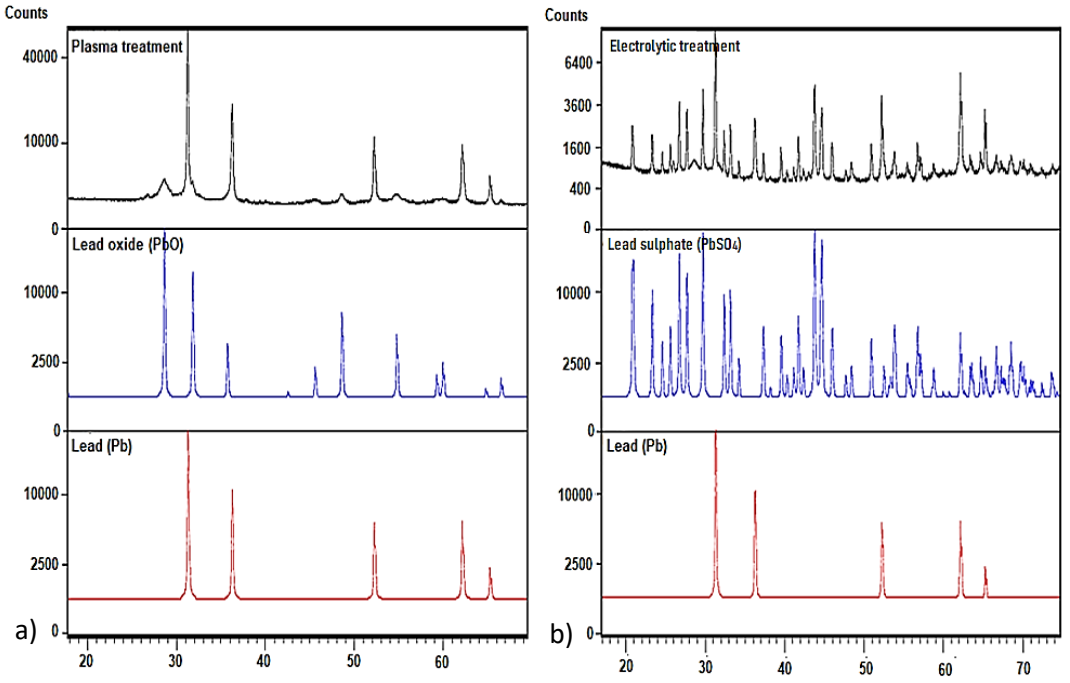

Figure 4-8. Database patterns from International Centre for Diffraction Data® (PDF4+); *a;* after non-thermal plasma tretment and database patterns of lead and lead oxide, *b;* after electrolytic treatment and database patterns of lead and lead sulphate.

As shown in Figure 4-8 *a*, after the non-thermal plasma treated sample, the presence of metallic lead was detected (peaks around 32, 37, 53, 62, and 65) and some very small peaks that may correspond to lead oxide (as observed in positions that fit around 29, 32, 49, 55, 60, and 67). After cleaning, the metallic surface exhibits significant reactivity and upon exposure to ambient air, the surface is prone to oxidation by atmospheric oxygen. In the case of the electrochemical treated sample from Figure 4-8 *b*, the resulting surface also showed the presence of metallic lead peaks (positions previously mentioned) and $PbSO_4$ as observed in peak positions of 21, 23, 27, 28, 30, 36, 44, 45 and 46 degrees (see Figure 3-18 from chapter 3). It is worth mentioning that after the electrolytic treatment, the sample remained immersed in the medium (Na_2SO_4) for a few minutes. It should be noted that at this point, the metal surface would be highly reactive and the dissolved oxygen in the medium may promote its oxidation, generating a thin surface layer of lead sulphate.

4.3.3.2. Confocal Image Profiling analyses

In addition, further investigations regarding the surface morphology were performed. To obtain the roughness parameters, the corroded sample by acetic acid vapours, the potentiostatically reduced sample (conditions described in section 3.3.3) and the plasma treated surface (conditions of Exp. 7), were analysed through the use of a confocal microscope. Roughness parameters and 3D images of the respective surface topographies are presented in Table 4-3 and Figure 4-9.

Table 4-3. Obtained results of the roughness parameters with the Confocal Microscopy for the different samples.

Corroded sample			**Mean**	**Std dev**	**Min**	**Max**
Amplitude parameters – Roughness profile						
Ra	um	*Gaussian filter, 0,8 mm*	27.31	3.09	19.05	36.42
Rq	um	*Gaussian filter, 0,8 mm*	34.92	4.30	25.03	49.32
Amplitude parameters – Primary profile						
Pp	um		89.90	16.85	65.30	222.05
Pv	um		179.03	35.83	78.70	289.12
Pz	um		268.92	43.53	158.30	467.30
Plasma treatment			**Mean**	**Std dev**	**Min**	**Max**
Amplitude parameters – Roughness profile						
Ra	um	*Gaussian filter, 0,8 mm*	25.30	2.11	19.66	32.35
Rq	um	*Gaussian filter, 0,8 mm*	31.80	3.35	24.60	44.83
Amplitude parameters – Primary profile						
Pp	um		161.40	29.40	62.25	204.40
Pv	um		143.30	17.95	68.33	181.80
Pz	um		304.70	34.75	191.72	349.40
Electrochemical treatment			**Mean**	**Std dev**	**Min**	**Max**
Amplitude parameters – Roughness profile						
Ra	um	*Gaussian filter, 0.8 mm*	29.70	2.96	21.63	38.30
Rq	um	*Gaussian filter, 0.8 mm*	37.80	3.90	27.08	48.63
Amplitude parameters – Primary profile						
Pp	um		152.13	34.81	88.95	357.82
Pv	um		212.90	36.50	127.82	290.70
Pz	um		365.03	54.97	251.32	626.97

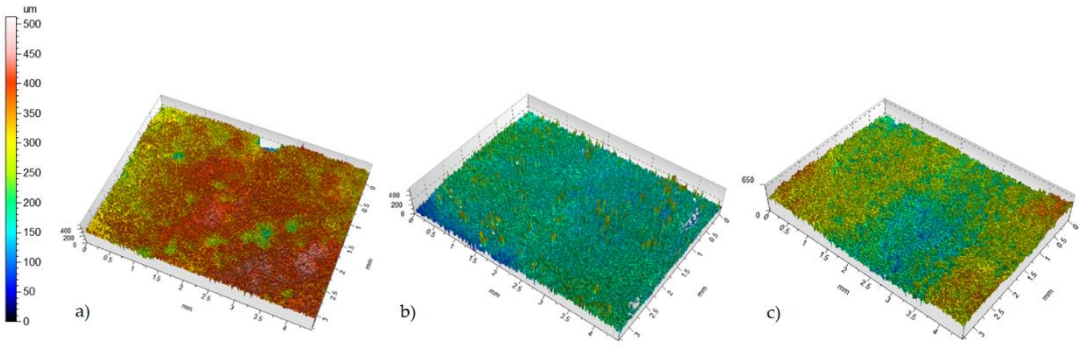

Figure 4-9. 3D roughness topography: *a*; corroded sample, *b*; non-thermal plasma, *c;* electrolytic reduction in a potentiostatic system.

Since hydrogen/argon non-thermal plasma acts as an "etchant", the surface becomes homogeneous and reaches lower values, therefore reducing surface roughness. In contrast, the value of Ra (roughness average) increases for the corroded sample and the reduced by the electrolytic treatment. This phenomenon describes the main problems of the technique, such as the heterogeneity, the high porosity, the creation of small cracks after being immersed in an aqueous medium and the introduction of new chemical species. It means that the average of surface peaks and valleys is accentuated after the electrochemical treatment respecting the plasma treatment, even exceeding the corroded sample. When the surface is uniform and smooth, it is less susceptible to corrosion compared to the substrate material. This is because a smooth surface with few defects and pores is less likely to provide sites for corrosion initiation [22]. Therefore, the more heterogeneous the resulting surface, the higher the risk of damage in the future. This fact demonstrates that plasma treatment can significantly reduce the roughness effect that may appear in other treatments such as electrolytic reduction.

4.4. Concluding remarks

In this chapter was demonstrated that non-thermal plasma is capable to clean corroded surfaces of metals with malleable characteristics and a low melting point. This was described as a less invasive treatment than other techniques such as some electrolytic reduction. In particular, the effectiveness was proven under the use of lead samples affected by corrosion using acetic acid vapours. Due to the low temperature of the non-thermal plasma (25 °C - 100 °C) used to clean corroded lead samples, no damage to the structure was observed. After the plasma treatment, the resulting surfaces were analysed with different characterization techniques. Conditions of XRD and SEM analyses were described in chapter 2, and Confocal Image Profiling analyses were described in the previous chapter 3.

The plasma treatment was performed using hydrogen and argon to clean the corroded surface. The hydrogen acts as a reductive specie causing the reduction of the oxidised surface. Additionally, argon acts not only as a reductant, but also as an etchant element. By bombarding argon ions, the surface is reduced in microns, releasing it from corrosion products [23,24]. A postulated etching behaviour is involved on the removal of lead carbonates and oxides by bombarding the mixture of reactive particles at subsonic velocities. The reason for optimising the time of the cleaning process is the combination of both gases to create a mixed plasma that improves the effectiveness of the treatment. Since plasma generates reactive species, the interaction between the particles and the surface is very efficient thanks to the fast kinetic. It allows to clean the corroded surface in less time than electrolytic reductions, optimizing the time of treatment.

An issue to consider is that the non-thermal plasma of H_2 has a limited depth of penetration, meaning that only the surface layer can be treated [5,15]. The use of argon as in the present chapter, promotes the penetration of hydrogen plasma into deeper cavities by producing a surface etching. However, non-thermal plasma technique is not recommended to apply for very thick layers and a mechanical cleaning may be required prior to the treatment to reduce its thickness. This is because after treatment, these are in low compactness allowing to be removed with soft brushes [4,25]. After that, a second non-thermal plasma treatment with the same parameters may be needed.

In this study, a Pb sheet was corroded by acetic acid vapours in the laboratory, and the result was an irregular corrosion layer spread over the entire surface. The sample sheet was divided into several parts to perform a set of experiments with different conditions. Taking advantage of the fact that with this methodology is possible to control parameters, a full factorial design with 8 experiments was performed by varying time (min), power (W) and Ar/H_2 ratio. The samples were visually evaluated by different features (heterogeneity, carbonate remains, coloration, decohesion and deformation). No sample resulted in deformation, which confirms the feasibility of non-thermal plasma on malleable metallic samples. Through a half-normal distribution graph, was observed that at a ratio of 90:10 (Ar/H_2), in combination with a power value of 50 W during 1 hour, the sample is not overheated, and the treatment can be prolonged if is necessary without visual damage.

This last corresponded to Experiment 7, and was compared with Experiment 5 (ratio 70:30 Ar/H2, 50 W during 15 minutes) and Experiment 8 (ratio 70:30 Ar/H_2, 80 W during 60 minutes), which showed different results. These were analysed by different characterisation techniques to study the residual surface products after treatment. By using XPS, was demonstrated that the resulted surfaces presented very small lead oxide phases and some traces of carbonates. Carbonate remains were predominant in the samples of Exp. 5 and Exp. 8. To analyse possible changes between the oxides from the internal layers and the form of passivation of each sample, a depth profile (depth of 2 nm/sputtering) was also performed for Exp. 5, Exp. 7 and Exp. 8. On these analyses, was observed that for Exp. 5 and 8, the residual corrosion compounds were present in much quantity than in Exp. 7 including in the internal layers. PbO_x signals were observed in all samples into the internal layers.

After analysing the non-thermal plasma treated sample (parameters of Exp. 7), the obtained surface presented small pores distributed homogeneously and resulting in a spongy surface aspect. If the surface is too porous and reactive after the treatment, it can be contaminated by the adsorption of chemical elements present in the atmosphere. For this reason, it is important to maintain the metallic lead object in an innocuous medium after being cleaned to create a good natural passivation layer in order to stabilise the surface. Additionally, roughness analyses were performed in a plasma treated surface (parameters of Exp. 7), an electrochemical reduced surface (potentiostatic system) and a corroded Pb sample by AcOH vapours. Lower roughness parameters and a more homogeneous distribution for the plasma treated

were obtained. This demonstrated that plasma treatment can lessen the heterogeneity obtained after applying the electrolytic method. Although these conditions were concluded in good results on the use of non-thermal plasma, a deep study with of surface characterization was needed.

Until this point, corroded surfaces by different vapour tests and two treatments of cleaning Pb metals degraded by AcOH vapours (electrolytic and plasma treatments), were presented. As observed, characterization techniques are useful to study the resulting surfaces; their morphology and composition. However, in the following chapter 5, Electrochemical Impedance Spectroscopy (EIS) was proposed to obtain more complete and detailed information about the different surfaces. With this, the evaluation of the effectiveness of these treatments used in the previous chapters (electrolytic reduction and non-thermal plasma treatment) was performed.

4.5. References

[1] E.G. Ioanid, A. Ioanid, D.E. Rusu, F. Doroftei, Surface investigation of some medieval silver coins cleaned in high-frequency cold plasma, J Cult Herit. 12 (2011) 220–226. https://doi.org/10.1016/j.culher.2010.09.004.

[2] O. Schalm, P. Storme, A. Gambirasi, M. Favaro, A. Patelli, How effective are reducing plasma afterglows at atmospheric pressure in removing sulphide layers: Application on tarnished silver, sterling silver and copper, Surface and Interface Analysis. 50 (2018) 32–42. https://doi.org/10.1002/sia.6329.

[3] A. Patelli, E. Verga, L. Nodari, S.M. Petrillo, A. Delva, P. Ugo, P. Scopece, A customised atmospheric pressure plasma jet for conservation requirements, IOP Conf Ser Mater Sci Eng. 364 (2018) 012079–012088. https://doi.org/10.1088/1757-899X/364/1/012079.

[4] R. Tiňo, K. Vizárová, F. Krčma, Plasma Surface Cleaning of Cultural Heritage Objects, in: Nanotechnologies and Nanomaterials for Diagnostic, Conservation and Restoration of Cultural Heritage, Elsevier, 2019: pp. 239–275. https://doi.org/10.1016/B978-0-12-813910-3.00011-2.

[5] R.L.G. C. Degrigny, Conservation of ancientlead artifacts corroded in organic acid environments: electrolytic stabilisation/consolidation, Studies in Conservation. 44 (1999) 157–169.

[6] A.S.T.J. Claus Gottlieb, A new method for cleaning and conservation of lead objects using hydrogen and oxygen plasma, Materials Science. 2 (1993) 767–771.

[7] P. Fojtíková, V. Sázavská, F. Mika, F. Krčma, Effect of Hydrogen Plasma on Model Corrosion Layers of Bronze, J Phys Conf Ser. 715 (2016) 012006. https://doi.org/10.1088/1742-6596/715/1/012006.

[8] S.B.G. Joan Esteve, Mercedes Alonso, Método para la restauración de planchas calcográficas de cinc mediante la técnica de plasma frío, Goya: Revista de Arte. (2001) 308–312.

[9] M.J.A. Salvador Borrós Gómez, L. Robbiola, J. Esteve, M. Pugès, Reducción mediante plasma frio de hidrogeno en un protocolo de restauración-conservación de objetos metalicos de interes arqueológico, Revista de Química Teórica y Aplicada. 62 (2005) 513–519.

[10] N.A. Salvador Borrós Gómez, La técnica de plasma de frío como herramienta en restauración y conservación de Material Arqueológico, in: J.B. Martín (Ed.), Innovación Tecnológica En Conservación y Restauración Del Patrimonio, 2006: pp. 64–73.

[11] B. Ramírez Barat, E. Cano, In Situ Electrochemical Impedance Spectroscopy Measurements and their Interpretation for the Diagnostic of Metallic Cultural Heritage: A Review, ChemElectroChem. 5 (2018) 2698–2716. https://doi.org/10.1002/celc.201800844.

[12] K. Schmidt-Ott, V. Boissonnas, Low-Pressure Hydrogen Plasma: an Assessment of its Application On Archaeological Iron, Studies in Conservation. 47 (2002) 81–87. https://doi.org/10.1179/sic.2002.47.2.81.

[13] K.C. Sabat, P. Rajput, R.K. Paramguru, B. Bhoi, B.K. Mishra, Reduction of Oxide Minerals by Hydrogen Plasma: An Overview, Plasma Chemistry and Plasma Processing. 34 (2014) 1–23. https://doi.org/10.1007/s11090-013-9484-2.

[14] P. Vankan, D.C. Schram, R. Engeln, High rotational excitation of molecular hydrogen in plasmas, Chem Phys Lett. 400 (2004) 196–200. https://doi.org/10.1016/j.cplett.2004.10.107.

[15] V. Costa, F. Urban, Lead and its alloys: metallurgy, deterioration and conservation, Studies in Conservation. 50 (2005) 48–62. https://doi.org/10.1179/sic.2005.50.Supplement-1.48.

[16] N.I. of S. and Technology, NIST X-ray Photoelectron Spectroscopy Database. NIST Standard Reference Database 20, Version 4.1, Alexander V. Naumkin, Anna Kraut-Vass, Stephen W. Gaarenstroom, and Cedric J. Powell. (2000). https://doi.org/http://dx.doi.org/10.18434/T4T88K.

[17] D. Briggs, Handbook of X-ray Photoelectron Spectroscopy C. D. Wanger, W. M. Riggs, L. E. Davis, J. F. Moulder and G. E.Muilenberg Perkin-Elmer Corp., Physical Electronics Division, Eden Prairie, Minnesota, USA, 1979, 190 pp, Surface and Interface Analysis. 3 (1981). https://doi.org/10.1002/sia.740030412.

[18] Y.-Y. Wang, K. Kusumoto, C.-J. Li, XPS Analysis of SiC Films Prepared by Radio Frequency Plasma Sputtering, Physics Procedia. 32 (2012) 95–102. https://doi.org/10.1016/j.phpro.2012.03.524.

[19] B. Strohmeier, R. White, T. Nunney, P. Mack, A. Wright, Chemical Characterization of Material Surfaces Using X-ray Photoelectron Spectroscopy (XPS): The Perfect Complement to Electron Microscopy Techniques, Microscopy and Microanalysis. 20 (2014) 2062–2063. https://doi.org/10.1017/S1431927614012045.

[20] P. Mattesco, N. Bui, P. Simon, L. Albert, Effect of polarisation mode, time and potential on the properties of the passive layer on lead-tin alloys, Journal of Power Sources. 64 (1997) 21–27. https://doi.org/10.1016/S0378-7753(96)02495-0.

[21] A. Coccato, L. Moens, P. Vandenabeele, On the stability of mediaeval inorganic pigments: a literature review of the effect of climate, material selection, biological activity, analysis and conservation treatments, Heritage Science. 5 (2017) 1–25. https://doi.org/10.1186/s40494-017-0125-6.

[22] M. Isakhani-Zakaria, S.R. Allahkaram, H.A. Ramezani-Varzaneh, Evaluation of corrosion behaviour of Pb-Co3O4 electrodeposited coating using EIS method, Corros Sci. 157 (2019) 472–480. https://doi.org/10.1016/j.corsci.2019.06.023.

[23] R. Groenen, M. Creatore, M.C.M. van de Sanden, Dry etching of surface textured zinc oxide using a remote argon–hydrogen plasma, Appl Surf Sci. 241 (2005) 321–325. https://doi.org/10.1016/j.apsusc.2004.07.034.

[24] V. Krishnamurthy, I.L. Kamel, Argon plasma treatment of glass surfaces, J Mater Sci. 24 (1989) 3345–3352. https://doi.org/10.1007/BF01139063.

[25] V.M. Donnelly, A. Kornblit, Plasma etching: Yesterday, today, and tomorrow, Journal of Vacuum Science & Technology A: Vacuum, Surfaces, and Films. 31 (2013) 0508251–05082548. https://doi.org/10.1116/1.4819316.

5. Lead corrosion layers study and evaluation after surface treatments using Electrochemical Impedance Spectroscopy technique

A key question to solve after applying any surface treatment, is to assure the integrity of the treated surface. For this reason, it is important to perform different analysis to obtain a complete diagnostic of the surface. The aim of this chapter is to provide a working background for conservator scientists about the use of Electrochemical Impedance Spectroscopy (EIS) to analyse different surfaces. The emphasis will be on practical and empirical interpretations of corroded samples through the obtained results. In this context, the use of EIS is proposed in the present work to characterize corroded Pb surfaces prior and after surface treatments through electrochemical and non-thermal plasma treatments.

5.1. Introduction

As described in previous chapters, different compounds can be formed when lead artefacts are exposed to oxidative environments. As a result, many surface species can be formed, and different characterization techniques are required to analyse the corroded surface. This involves obtaining not only chemical information, but also other characteristics such as porosity and roughness. For this reason, Electrochemical Impedance Spectroscopy (EIS) is proposed in the present chapter 5, to provide better diagnosis and also to consider the effectiveness of the proposed surface treatments for cleaning and stabilisation corroded surfaces.

Electrochemical Impedance Spectroscopy (EIS) allows to obtain a great deal of information about the surface properties by modelling the physical system to an electrical equivalent circuit (EC). In this context, the different surface structures

correspond to an element or a set of elements in the EC. The interpretation of the obtained response by EIS, must have coherence with the purposed elements of the EC. Therefore, monitoring these elements is possible to obtain information about the corrosion phenomena on the metal surface.

EIS working principle is based on the application of a small sinusoidal (AC) current. It displaces the system from its equilibrium producing a sinusoidal current of the same frequency, but different in amplitude and phase angle, as shown in Figure 5-1.

Figure 5-1. Basic fundaments of EIS application in metallic surfaces.

Performing a frequency sweep, usually between 100 kHz - 10 mHz, the system impedance as a function of frequency is obtained. Impedance *(Z)* can be defined as the opposition that a circuit presents to the flow of current *(AC)*, expressed in *Ω*. Thus, the instrument used processes the measurements of potential – time and current – time, resulting in a series of impedance values corresponding to each frequency studied [1].

The relationship of the impedance and frequency values is called the impedance spectrum. This process can be described by the following expression:

Equation 5-1
$$Z = \frac{E}{I} = \frac{E_0 \cdot sin(\omega \cdot t)}{I_0 \cdot sin(\omega \cdot t + \varphi)} = Z_0 \cdot \frac{sin(\omega \cdot t)}{sin(\omega \cdot t + \varphi)}$$

where E_0 is the maximum amplitude (expressed in voltage), ω the angular frequency of the sine wave (expressed in radians/second), t is the time (expressed in seconds), I_0 is the maximum current (expressed in amperes) and φ the phase shift (which is the distance response current when is shifted ahead of the voltage and is expressed in radians).

An analysis of the charge transport processes will often suggest an EC of ideal resistors and capacitors (even inductors or negative capacitors in some instances). Into the obtained spectra, these are generally used to represent different phenomena, which defines the behaviour of an electrochemical system. For example, if it is a single homogeneous layer, is represented by a specific EC, but in the case of more than one structure, more elements must be introduced in the EC. In this context, the selected EC model must allow a physical interpretation of what is happening on the surface. In Figure 5-2, possible EC models that can be used and their Nyquist plots are presented.

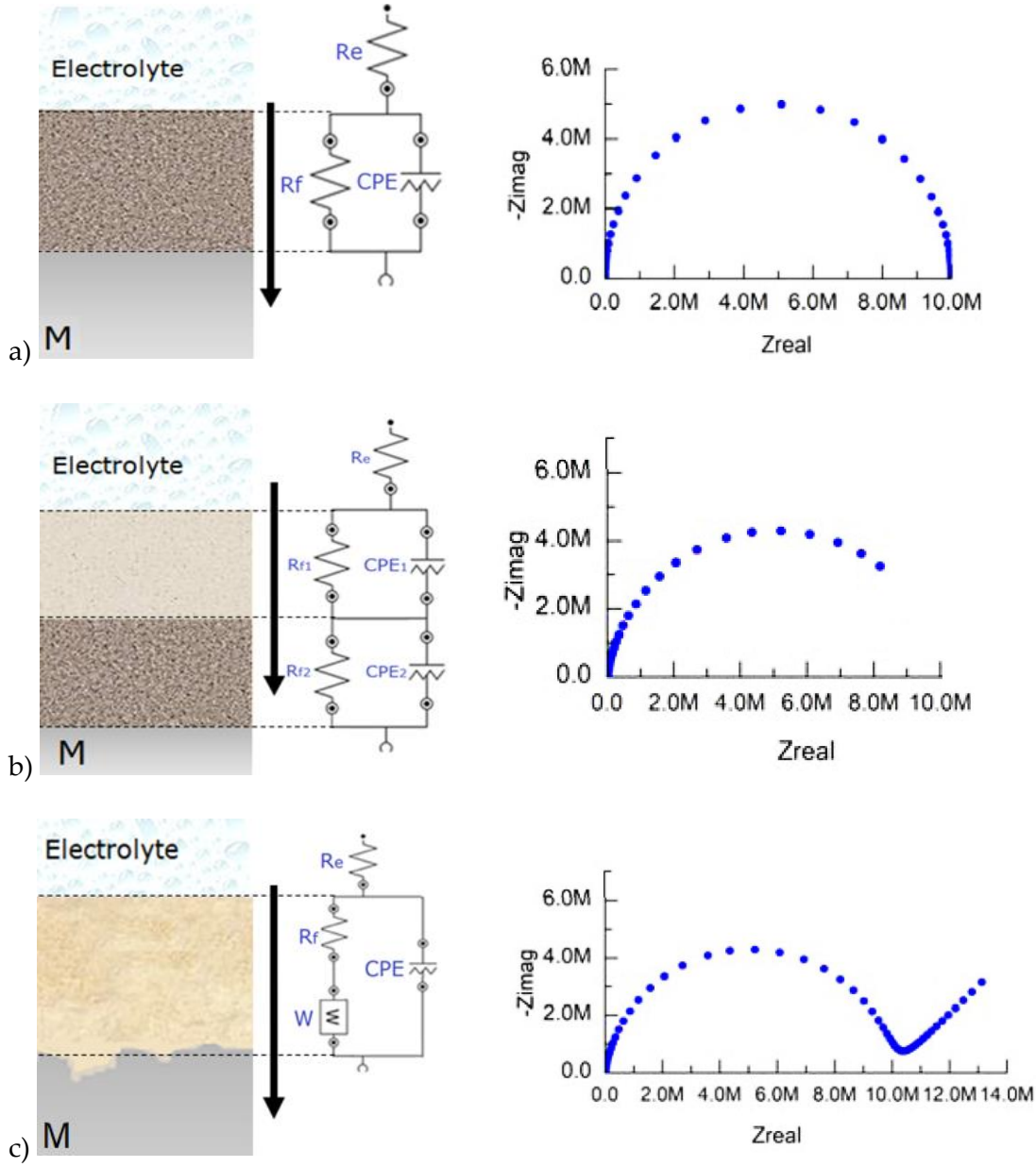

Figure 5-2. ECs applied in different corrosion systems, *a;* corresponded to the non-corroded sample, or with a very smooth and intact thin coating in which the signal must be low, *b;* corresponded to a $PbO/PbSO_4$ corroded sample, *c;* corresponded to the corroded Pb sample under AcOH vapours.

In Figure 5-2, different cases of surface structures are presented with a related EC, which determines the electrical properties of a system. Next, the corresponding Nyquist plots to the ECs, are also shown as the typical graphical representations. In this plot, the real part of the measured impedance is represented as a function of the imaginary part. The interpretation of the obtained spectra is often challenging and difficult to understand without a previous exploration in bibliographic resources.

The EC shown in Figure 5-2 *a*, is composed by a by a Constant Phase Element (CPE). The surface irregularity or the low conductivity of the electrolyte, produces deviations on the experimental results from the ideal behaviour. However, as described in bibliography [2], this is also related to non-uniform potential or current distributions. Thus, to fit the experimental results with an EC, the CPE element is commonly used, instead of a pure capacitor. The CPE element is in parallel with Rf. It corresponds to the resistance of the coating, in series with Re, which corresponds to the resistance of the electrolyte [3]. The combination of a CPE with a Rf and a Re, can be used to model a compact layer but with some low roughness or a metallic surface with small irregularities [1,4–6]. For example, this simple EC is used to model EIS measurements on a metallic steel surface with some inhomogeneities, based on artefacts from World War I [6].

In the case of Figure 5-2 *b*, an EC composed of a parallel combination of Rf_1 and CPE_1 in series with another parallel Rf_2 and CPE_2 combination is shown. This EC, is purposed to explain a double layer structure consisted of two adjacent layers on a metallic surface. This model is also valid for rough but adherent superposed corrosion layers with different morphology [7]. A very similar EC using CPE for accounting non-ideality of two interfaces with different properties was described in bibliography [8]. For example, it was used to model EIS measurements on archaeological copper/bronze coins in which the metal nucleus was covered by a thin layer of cuprite eventually covered by a secondary corrosion layer [8].

Finally, in Figure 5-2 *c* EC describes a very porous and irregular layer in which a Warburg element (W) is used for modelling a diffusion behaviour [9]. Warburg impedance is a specific element used to model semi-infinite linear diffusion processes, and is mathematically equivalent to a CPE with n=0.5 [7]. This element is commonly used when there is a diffusion phenomenon of the species through the

pores from the layer, acting as a diffusion barrier. An example of the use of Warburg element in ECs, was described in bibliography to model a heterogeneous layer of corrosion products (mainly composed by green crystals of copper salts and white, amorphous precipitates of zinc) on a bronze metal used for artistic castings [10].

As discussed in chapter 2, layers formed by compact structures and adherent to the metal surface, provide greater corrosion resistance than porous and poorly adherent layers. For example, layers formed by PbO and/or $PbSO_4$ are very compact, conferring a great electrical protection (high impedance) to the bare conductive metal. In other cases, the resulted layers can be thicker but with little compactness, allowing the current to flow through the pores of the corroded structure. This is the case of the layers formed by lead acetate. These layers were irregular with heterogeneous crystal size. As described in chapter 2, their morphological structure does not act as a good insulator and are not capable to avoid further corrosion processes. Electrochemical Impedance Spectroscopy (EIS) is typically used for fine-tuning mechanisms and determining the kinetics of processes, resistances, and capacitances. However, in the present work it will be used to evaluate the surface characteristics on corroded lead samples [11–21]. In addition, final surface of treated Pb samples (using electrolytic methods and non-thermal plasma) were evaluated using EIS.

5.2. Experimental set-up

5.2.1. Preparation of working electrodes for electrochemical experiments

The working electrode consisted of a 6 mm diameter Pb disk. It was prepared by inserting a Pb rod (6 mm diameter and 15 mm length, 99.999% Sigma-Aldrich) into a PTFE holder. Electrical contact with the lead working electrode was provided using an internal spring-loaded probe. Then, the surface of the working electrode was initially prepared by mechanical wet polishing with SiC polishing paper (supplied by Struers) with successive decreasing the grain size; 800 μm - 1200 μm - 2000 μm - 4000 μm.

5.2.2. Fast preparation of corrosion Pb samples

5.2.2.1. *Anodized Pb samples*

Anodic polarization was performed in 5 M H_2SO_4 at different potentials (0 V, 0.4 V and 0.8 V vs reference electrode) during 1800 seconds to create different corrosion thickness. The working solution was stirred during the anodic polarization. All experiments were performed using a three-electrode set-up and a potentiostat/galvanostat Autolab PGSTAT 302N.

5.2.2.2. Liquid phase induced corrosion on the working electrodes

A different set of samples was chemically corroded using acetic acid. Specimens were corroded with the addition of a thin surface layer of acetic acid that covered the entire metal surface. After 1 hour, surface was dried using a stream of hot air. In a first set of samples, the procedure was repeated 3 times (identification code 3 hours). A second set of samples was prepared by repeating the procedure 3 times a day for 3 days (identification code 3 days). A final set of samples was prepared by repeating the procedure 3 times a day for 7 days (identification code 1 week).

5.2.3. Electrochemical Impedance Spectroscopy

EIS measurements were performed using a Metrohm Autolab PGSTAT 302N equipped with a FRA2 module. The experimental set-up consisted of a three-electrode cell. Impedance measurements were performed using a signal amplitude of 10 mV respect to the open circuit potential. The frequency range was from 100 kHz to 1 Hz, and it was performed at 10 points per decade [7,8]. For these experiments, 5 M H_2SO_4 electrolyte was used. Oxygen in the electrolyte was displaced by sparing nitrogen during one-hour prior the measurements. Data modeling was performed using Nova 2.1 Software.

5.3. Results and discussion

5.3.1. Electrochemical Impedance Spectroscopy on fast corroded Pb samples

In a first set of experiments, impedance measurements on a metallic lead surface were performed. The point of this experimental campaign was to stablish an impedance reference value for a non-corroded lead surface. In order to perform the measurements, Pb samples were polished and polarized at -0.9 V in a 5 M H_2SO_4 solution for 30 minutes. During polarization, the working solution was stirred to force the removal of hydrogen bubbles formed in the electrode surface during polarization. Figure 5-3 shows the obtained Nyquist diagram.

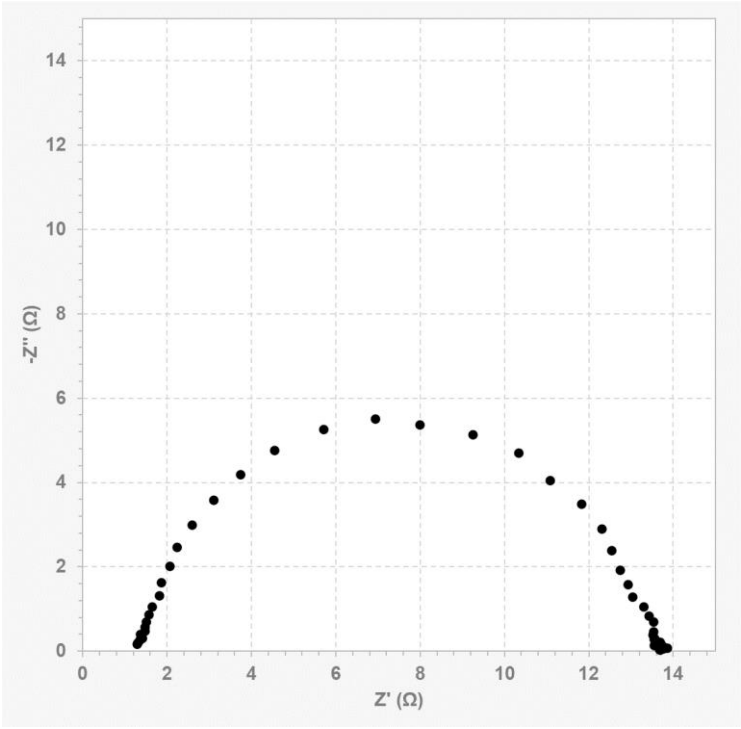

Figure 5-3. Nyquist plot for the polished polished Pb

The shape of the impedance spectrum obtained for the non-corroded Pb sample, exhibited a small capacitive semicircle. In addition, the obtained impedance

spectrum was slightly depressed. Deviations of this kind are often referred to a frequency dispersion that are attributed to inhomogeneities on solid surfaces [22].

To interpret the resulted values, ECs with different elements can be used. A practical way to represent distributed processes like this is using an element that follows its distribution, such a constant phase element (CPE). The CPE is defined as:

Equation 5-2 $Z_{CPE} = 1/c(j.\omega.)^n$

where c is the ideal capacitance and n $(0 \leq n \leq 1)$ is an empirical constant. When $n = 1$ the electrode behaves like a real capacitor and when $n = 0$ it reflects a complete resistor-type electrode, whereas $n = 0.5$ indicates diffusive characteristics of the electrode [23,24]. The capacitive loop can be discussed in terms of an Rf-CPE parallel combination in series with an ohmic resistance Re. The high frequency limit Re corresponds to the ohmic resistance of the electrolyte, whereas Rf and CPE represent the charge transfer resistance and the double layer capacitance. The fitting of the Nyquist plot for the non-corroded Pb sample and the used EC, are shown in Figure 5-4.

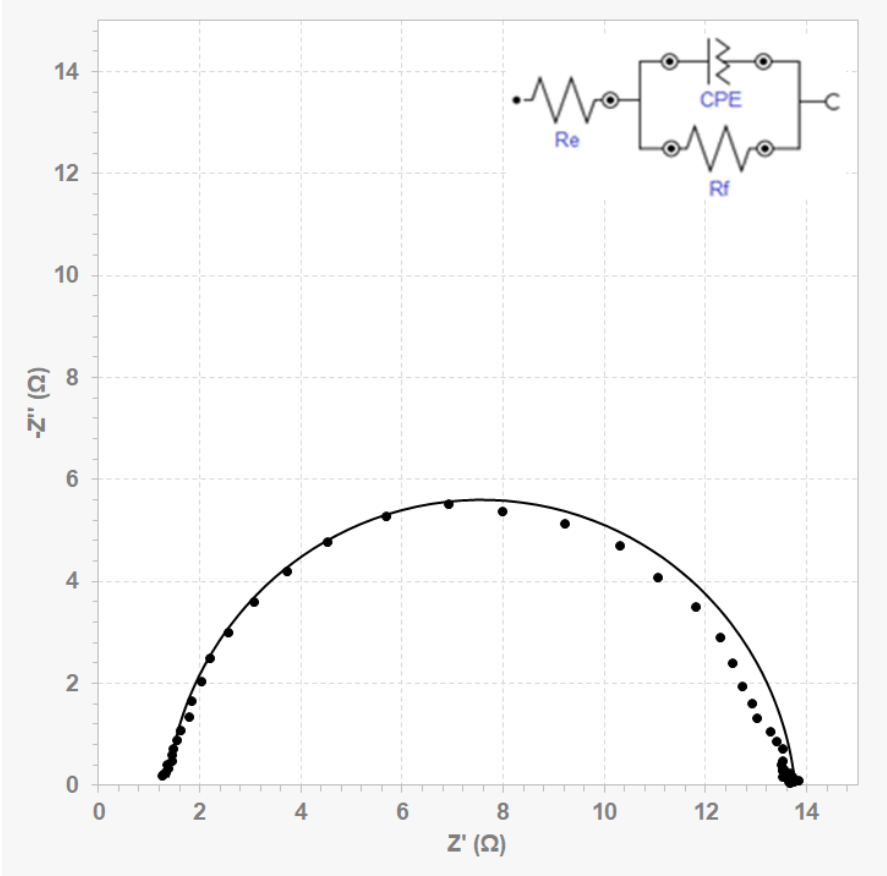

Figure 5-4. Nyquist plot for the polished polished Pb

A very small resistance should be expected in a non-corroded metallic surface. In that case, as seen Figure 5-4, the total impedance modulus had a value around 14 Ωcm^2, estimated as the cut of the semicircle with the real part of the impedance spectrum. The obtained value is of the same order of magnitude as those described in bibliography [25]. This semicircle is related to the charge transfer resistance of the faradaic process. The electrolyte resistance (Re) was estimated at 1.35 Ωcm^2, which is in good agreement to different authors [25–27]. The CPE values represented the double layer capacitance, resulting in 22 $\mu\Omega^{-1}cm^{-2}s^n$ and n= 0.934, which means that the behaviour of the signal describes almost a perfect capacitor.

A new experimental campaign was performed in order to generate lead sulphate layers by anodization. As described in the CV analysis in chapter 3, $PbSO_4$ formation in H_2SO_4 occurs within the potential range of -0.5 V to 0 V. Then, it is expected to obtain a lead sulphate layer on the metal surface when polarized in this range. However, when a $PbSO_4$ layer is formed and becomes thick, it turns out to be impermeable to HSO_4^- and SO_4^{2-} but is permeable to H^+. Consequently, the environment underneath the $PbSO_4$ layer becomes more basic and suitable for the formation of PbO [28]. Thus, a mixed layer of $PbSO_4$/PbO by anodizing at 0.4 V can be obtained. At higher anodization potentials such as 0.8 V, it is expected that PbO will increase becoming more resistive than $PbSO_4$. Therefore, it can contribute to an increase of the total impedance modulus [29]. Then, samples were anodized at 0 V, 0.4 V and 0.8 V during 1800 seconds in 5 M H_2SO_4.

In this situation, the modelling of the experimental results can be performed by an EC composed of a parallel combination of Rf_1 and CPE_1 representing the charge transfer resistance and the double layer capacitance, in series with another parallel Rf_2 and CPE_2 combination due to the presence of PbO. The EC was chosen as suggested by different authors [30–32]. Figure 5-5 shows the impedance measurements obtained and also the fitting spectra using the proposed EC. In addition, the EC is also shown in the right insert.

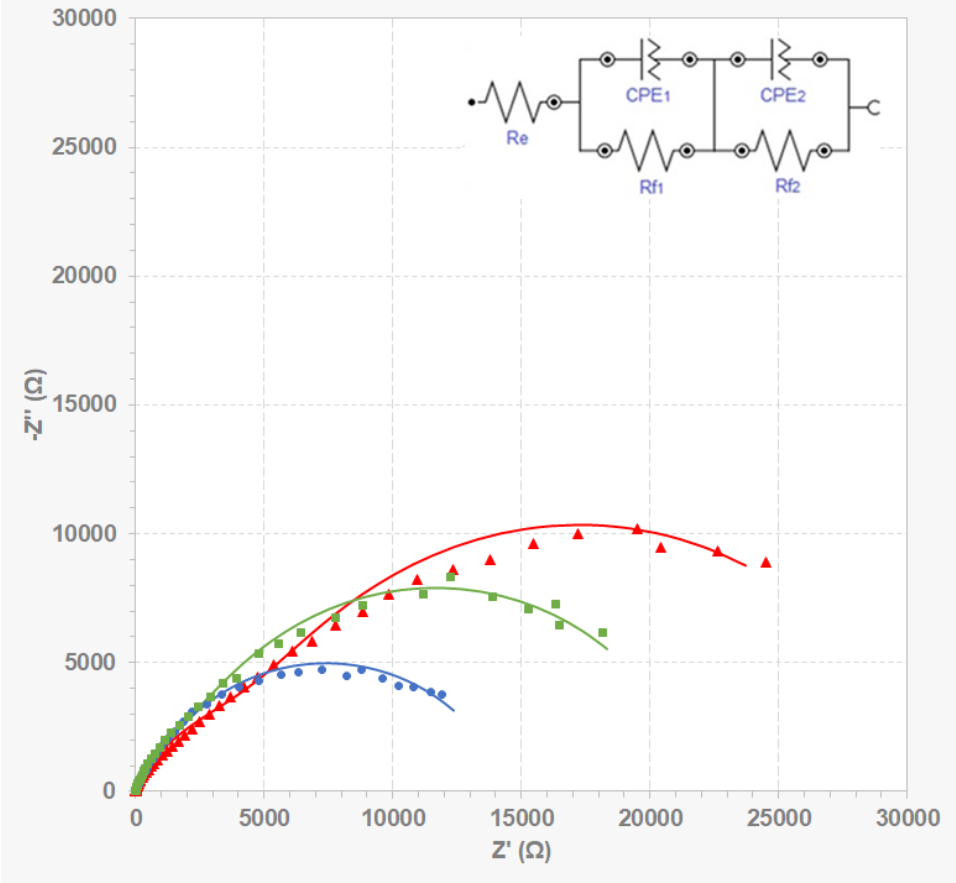

Figure 5-5. Nyquist plots for the anodized samples in 5 M H_2SO_4 at different potentials (●; 0 V, ■; 0.4 V and ▲; 0.8 V) during 1800 seconds, and the EC Re(Rf_1-CPE1)(Rf_2-CPE_2) used for the fitting curves.

It can be seen in Figure 5-5 that the total impedance modulus obtained when the electrode was polarized at 0 V was around 14 kΩcm². When the anodization potential was increased to 0.4 V and 0.8 V the total modulus also increased to 22 kΩcm² and 31 **k**Ωcm² respectively. The increase in the total modulus can be explained on the one hand with the increase of the compactness and thickness of the surface layer when more anodic potentials were applied. On the second hand, it should also be considered that PbO formation becomes more dominant at more anodic potentials. Then, as PbO is more resistive than $PbSO_4$, it also contributes to the increase of the

total modulus impedance. This fact is discussed with the data fitting values shown in Table 5-1.

Table 5-1. EC parameters for anodized samples in 5 M H_2SO_4 at different potentials; 0 V, 0.4 V and 0.8 V during 1800 seconds.

	Anodized at 0V	**Anodized at 0.4V**	**Anodized at 0.8V**
Element	**Value**	**Value**	**Value**
Re (Ωcm^2)	1.90	1.36	1.70
Rf ($k\Omega cm^2$)	14.3	19.1	25.8
CPE ($\mu\Omega^{-1}cm^{-2}s^n$)	10.4	6	9.50
n	0.777	0.878	0.841
Rf_2 ($k\Omega cm^2$)	275	2.77	4.86
CPE_2 ($\mu\Omega^{-1}cm^{-2}s^n$)	12.4	4.46	4.37
n	0.95	0.84	0.76

As shown in Table 5-1, obtained values for Re were as expected (average value of 1.65 Ωcm^2) and no significant changes between experiments were observed. Regarding to the Rf values, the more anodic the applied potential the higher Rf_1 and Rf_2 were. This fact is attributed to the increased compactness of the $PbSO_4$ layer at more anodic potentials. When the applied voltage was increased to 0.4 V and 0.8 V, Rf_2 increased to 2.77 $k\Omega cm^2$ and 4.86 $k\Omega cm^2$ respectively. This fact points to the formation of a mixture of $PbSO_4$/PbO at more anodic potentials than approximately 0.4 V. In addition, CPE_1 (10.4 $\mu\Omega^{-1}cm^{-2}s^n$) and CPE_2 (12.4 $\mu\Omega^{-1}cm^{-2}s^n$) values at 0 V were higher than those obtained at 0.4 V an 0,8 V (4.46 $\mu\Omega^{-1}cm^{-2}s^n$ and 4.37 $\mu\Omega^{-1}cm^{-2}s^n$ respectively). It is attributed to the fact that the $PbSO_4$ layer is less compact at 0 V, allowing faster charge transfer processes from the electrolyte to the electrode than at 0.4 and 0.8 V.

In order to evaluate the effectiveness of EIS on the study of corroded Pb surfaces exposed to VOCs, a new set of experiments was carried out. As described in previous chapters, metallic lead surface become covered by voluminous and porous corrosion layers when exposed to VOCs. In this context, polished lead samples were corroded

with acetic acid. In order to obtain different layer thickness, samples were induced to corrosion at different exposure times to AcOH (during 3 hours, 3 days and one week) and impedances were measured in 5 M H_2SO_4.

In this case, due to the differences on the layer morphology compared to those formed by anodization, a different EC was needed. Although there was some noise on the obtained signals due to the complexity of the surface layer, a diffusional behaviour of electroactive species was observed at low frequencies [33]. The Warburg element was used on the EC to represent this phenomenon. The obtained data and fitting curves are shown in Figure 5-6. In addition, the EC is also shown in the right insert.

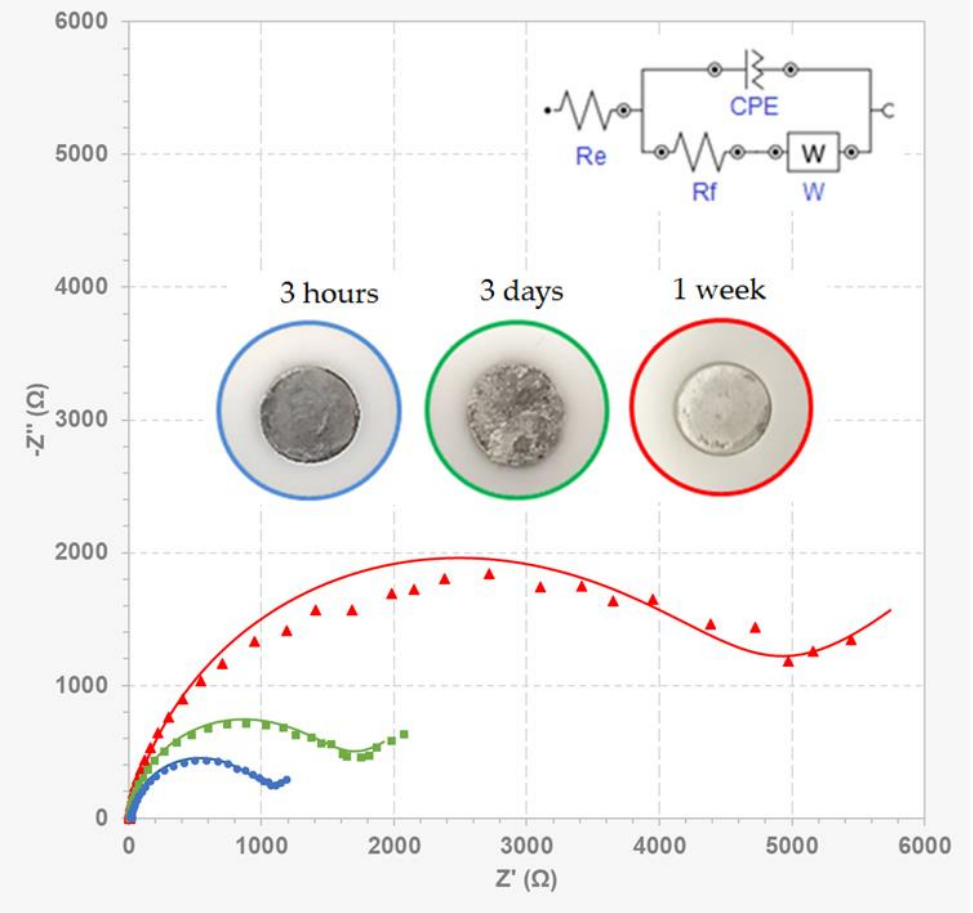

Figure 5-6. EIS of the corroded samples in AcOH at three times of exposition (●; 3 hours, ■; 3 days and ▲; one week) in acetic acid environment, using 5M H_2SO_4 electrolyte and the EC Re(Q[RW]) used for the fitting curves.

Although a diffusional control was observed in the results shown in Figure 5-6, it can be seen that the impedance modulus increased with the exposure time to AcOH. It is worth mentioning that these values were lower than those obtained with the anodized samples in H_2SO_4. The highest impedance value was obtained for the exposed surface during one week to AcOH, which showed a total impedance modulus of 6 kΩcm^2 approximately. Note that this value was much smaller than that obtained with the anodized sample in H_2SO_4 at 0 V, with a total impedance modulus of 14 kΩcm^2. This fact was attributed to the porosity of the surface layer produced

when metallic lead was exposed to acetic acid. As described in chapter 2, the sample exposed to AcOH resulted in a high porosity with agglomerated crystals of lead acetate.-The EC fitting data of the corroded samples with AcOH is presented in Table 5-2.

Table 5-2. Obtained results of the corroded samples in AcOH vapours.

	3 hours in acetic acid	**3 days in acetic acid**	**1 week in acetic acid**
Element	**Value**	**Value**	**Value**
Re (Ωcm^2)	1.80	1.90	1.50
Rf ($k\Omega cm^2$)	1.46	1.95	4.54
CPE ($\mu\Omega^{-1}cm^{-2}s^n$)	54.3	12.6	10.9
n	0.698	0.836	0.873
W	18.2	1.06	0.652

For samples exposed 3 hours and 3 days to acetic acid, simmilar values of R_f were obtained (1.46 $k\Omega cm^2$ and 1.95 $k\Omega cm^2$ respectively). However, when the surface was exposed during one week to AcOH, a higher R_f value was obtained (4.54 $k\Omega cm^2$), pointing to the formation of a thicker lead acetate layer.

When a thin surface layer is formed on the electrode, surface ions can easly reach inner layers. That implies that charges can be easily reorganized yielding higher CPE values. This tendency was observed in CPE values (shown in Table 5-2), where the higher the exposure time the smaller the CPE value was obtained. Finally, samples exposed 3 hours and 3 days showed W values of 18.2 $\mu\Omega^{-1}cm^{-2}s^n$ and 1.06 $\mu\Omega^{-1}cm^{-2}s^n$, while the sample exposed one week had a W value of 0.652 $\mu\Omega^{-1}cm^{-2}s^n$. The decrease on the W value indicates a lower conductivity during the measurement due to the small number of ions that can penetrate inside the surface layer.

5.3.2. Analysis of morphological differences between the obtained surface layers

The objective of this section was to determine the effectiveness of EIS to characterize surface layers with different morphology. For this reason, the compact lead sulphate layer obtained at 0.8 V, was compared with the porous lead acetate layer obtained after one week of exposure to AcOH. Both are shown together in Figure 5-7.

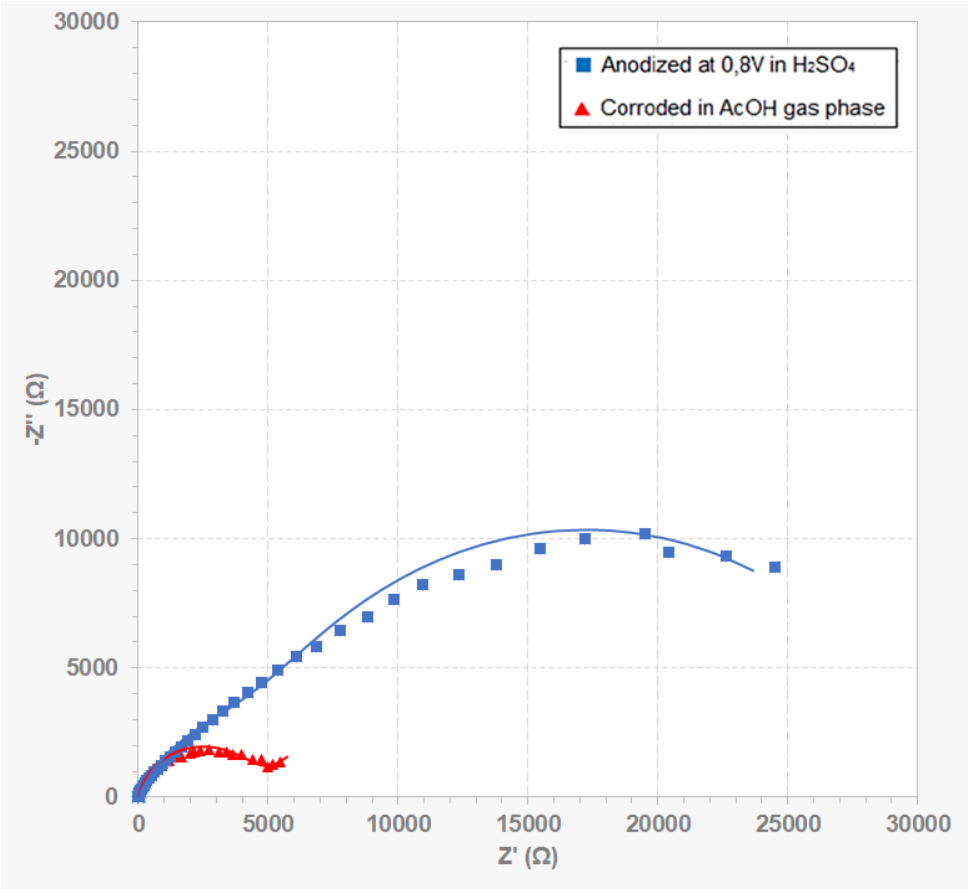

Figure 5-7. EIS spectra of corroded samples, ▲ anodized at 0.8 V vs ref during 1800 s in 5 M H_2SO_4 and ■ exposed at AcOH (g) for one week.

It can be seen in Figure 5-7 that the total impedance modulus obtained when the electrode was polarized at 0.8 V vs ref. in sulphuric acid was around 30 $k\Omega cm^2$. Different authors reported that anodized led yields a value between 15 – 60 $k\Omega cm^2$. In any case, that value is highly dependent on the applied potential and polarization time. In general, the more anodizing the applied potential and polarization time the higher the total impedance modulus will be [32,34]. This large total modulus describes the compactness and thickness of the surface layer. Furthermore, as discussed previously, when a $PbSO_4$ layer grows thicker and compact at anodic potentials, the environment underneath the $PbSO_4$ layer becomes more suitable for the formation of PbO. This last is more resistive than $PbSO_4$ [29], resulting in a large increase of the total modulus impedance.

A very different situation was obtained when the lead sample was exposed to vapours of acetic acid. In that case, the obtained impedance modulus was around 6 $k\Omega cm^2$, which is much smaller than the value obtained in sulphuric acid (30 $k\Omega cm^2$). It is worth mentioning that similar total impedance modulus is reported in copper when porous corrosion layers are formed in the metal surface [35,36]. This value is much smaller than the resistive values obtained with the sample anodized in sulphuric acid due to the high porosity of the corrosion layer and its lack of passivation.

These differences on the morphology between both layers, is presented in the micrographs of Figure 5-8.

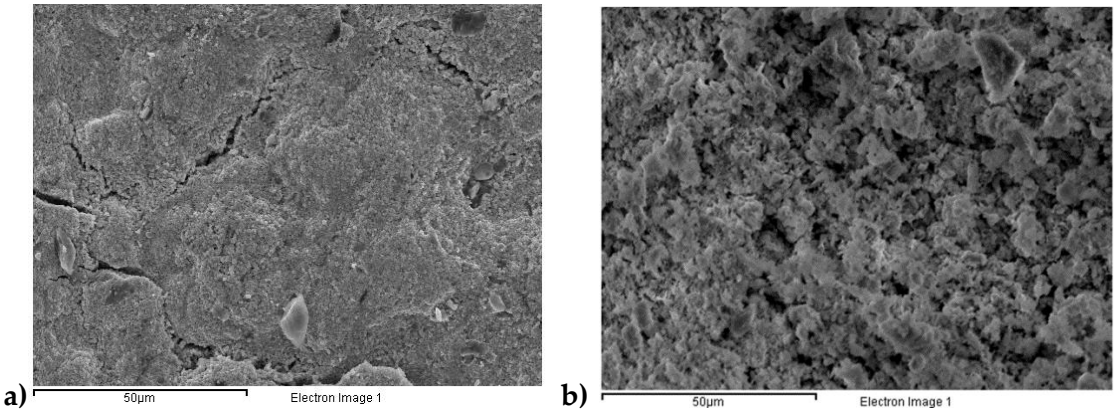

Figure 5-8. *a;* Surface micrograph of the lead sulphate layer, *b;* surface micrograph of the lead acetate layer. Both scaled at 50 µm.

As shown in Figure 5-8, lead sulphate and lead acetate layers showed clear differences in porosity. As shown in Figure 5-8 *a*, the surface layer formed by $PbSO_4$ has a compact and adherent structure, despite the small cracks formed on the surface layer. As previously described, it is common to find that ideal capacitors are not able to model experimental data in cases such as non-uniform layers, surface roughness or inhomogeneous current distribution [5,10,37]. Furthermore, on these practical cases, the transfer functions obtained in EIS measurements do not follow the theoretically expected patterns, showing distortions generally in form of "depressed semicircles" [5], as observed in Figure 5-5. In such cases, CPEs are used on ECs to model EIS measurements on surface layers that are compact but present heterogeneities on the surface such are observed in Figure 5-8 *a*.

However, as observed in Figure 5-8 *b*, the lead acetate layer was formed by a very porous structure, with large irregularities on the surface. In this case, the Warburg element was used to model the obtained EIS measurements. As also mentioned before, Warburg is used when the impedance is associated to diffusion processes and is commonly used when the diffusion of species through the pores of the layer controls the corrosion rate, producing a distinctive 45° tail in the low-frequency region of the Nyquist plot [3,33]. This last was related to the high frequency signals observed on the resulted impedances shown in Figure 5-6, that

suggest a diffusional behaviour. This comparison between both surfaces shows the feasibility of EIS for analysing layers with different morphology.

5.3.3. EIS Surface analysis of lead samples after potentiostatic reduction.

At that point, EIS was used to evaluate the obtained surfaces after potentiostatic reduction. In a first set of experiments, the anodized samples in 5 M H_2SO_4 at 0 V, 0.4 V and 0.8 V during 1800 seconds, were electrochemically reduced. For that purpose, the corroded samples were polarized, under stirring, at a constant potential of -0.9 V during 1800 seconds in 5 M H_2SO_4. Figure 5-9 shows the Nyquist plot corresponding to the impedance spectra of the three samples. An EC with two resistor elements was used to characterize the obtained surface.

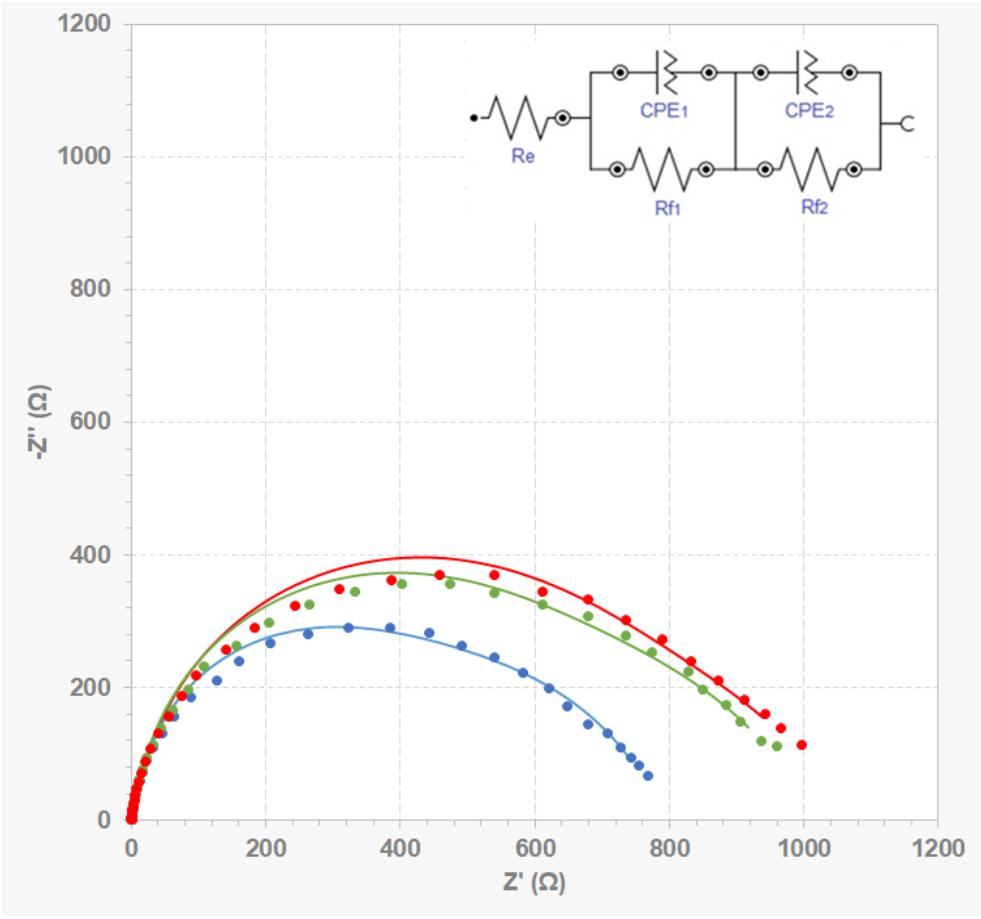

Figure 5-9. Nyquist plots after potentiostatic reduction on Pb samples previously anodized at (●; 0 V, ■; 0.4 V and ▲; 0.8 V) and the EC used for the fitting curves. Samples were polarized at -0.9 V during 1800 seconds in 5 M H_2SO_4 previous EIS measurenments.

The spectra of the three impedances indicated the presence of a residual surface layer with a certain degree of porosity. The total impedance modulus obtained in the sample anodized at 0 V is slightly smaller than those obtained at 0.4 V and 0.8 V. It is worth mentioning that the resulted values after electrolytic reduction are much smaller than those obtained after the anodization. This fact is attributed to the thinning of the surface oxidation layer when reducing $PbSO_4$/PbO to metallic lead.

As it was observed, the electrochemical treatment was efficient to reduce the $PbSO_4$/PbO layers, but these do not totally disappear. For this reason, the EC was composed of a parallel combination of Rf_1 and CPE_1 representing the charge transfer resistance and the double layer capacitance, in series with another parallel Rf_2 and CPE_2 combination due to the presence of a residual layer of $PbSO_4$. It is worth mentioning that after the electrolytic treatment, the sample remained immersed in the medium (H_2SO_4) for a few minutes before starting the EIS measurement. It should be noted that at this point, the metal surface would be highly reactive and the dissolved oxygen in the medium may promote its oxidation, generating a thin surface layer of lead sulphate (see section 3.3.3.1.1.). The parameters of the EC after fitting, are shown in Table 5-3.

Table 5-3. Obtained results of the impedances after reduced $PbSO_4$ layers.

	After reduction (0 V)	**After reduction (0.4 V)**	**After reduction (0.8 V)**
Element	**Value**	**Value**	**Value**
Re (Ωcm^2)	1.12	1.14	0.936
Rf (Ωcm^2)	522	528	610
CPE ($\mu\Omega^{-1}cm^{-2}s^n$)	13.4	13.2	16.3
n	1	1	1
Rf_2 (Ωcm^2)	265	479	450
CPE_2 ($\mu\Omega^{-1}cm^{-2}s^n$)	534	159	289
n	0.665	0.705	0.708

The Re had an average value of 1.0 Ωcm^2, corresponding to the normal range of the electrolyte resistance. As can be shown by comparing Table 5-1 and Table 5-3, after electrolytic reduction, resistance values of Rf_1 and Rf_2 were very small in comparison with those obtained with the anodized samples. The *n* values for the CPE_1 element are 1 indicating a pure capacitive behaviour. In contrast, *n* value CPE_2 are closer to 0.5. This fact can be explained as a consequence of the resulted irregular

surface after electrolytic reduction. The elongated semicircles also defines that the resulting surface is somewhat porous.

At this point, EIS was used to evaluate the quality of the obtained surfaces after being treated with non-thermal plasma (90:10 argon/hydrogen, 50 W, 60') and electrolytic reduction (at -0.9 V in a 0.5 M Na_2SO_4 solution as described in section 3.3.3 from chapter 3). The electrodes were exposed to acetic acid vapours during one-week prior surface conservation treatments. In order to compare both treatments, the resulted spectra using a Randless EC using a CPE, are presented in Figure 5-10. The impedance spectrum of the non-corroded Pb electrode (see Figure 5-4) was also included.

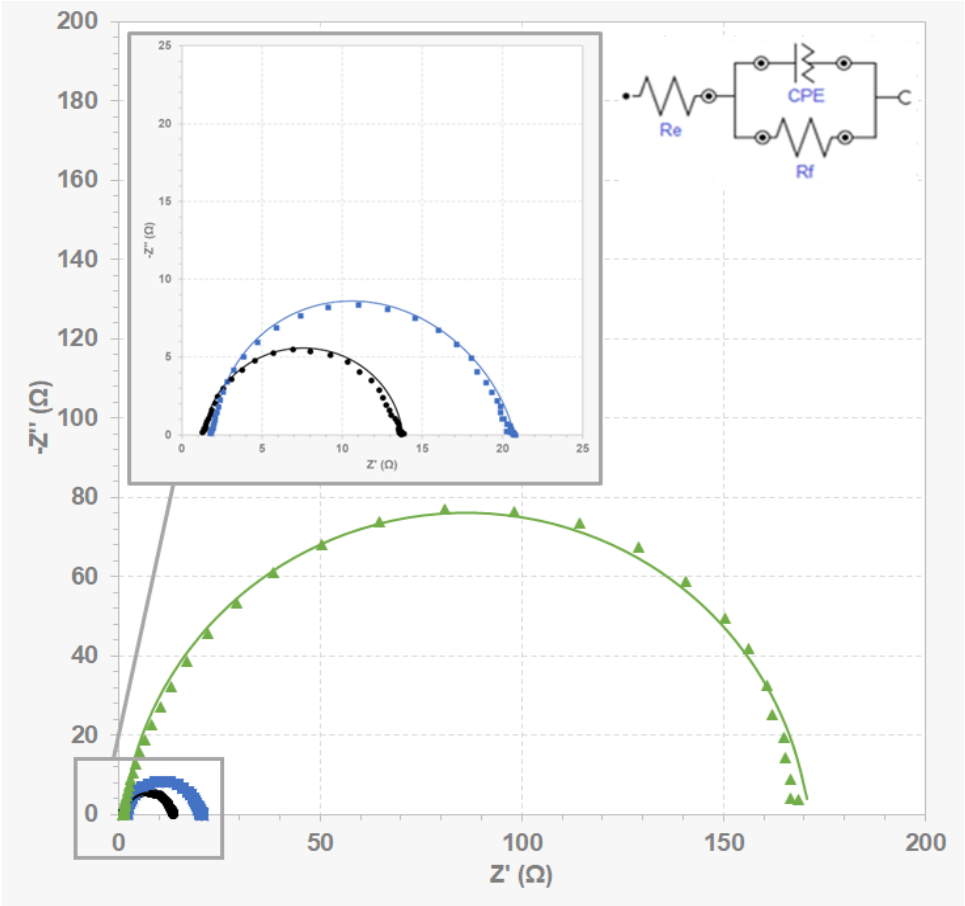

Figure 5-10. EIS plot form a cleaned Pb surface previously corroded one week to acetic acid using and argon/hydrogen (90:10) plasma at a potential of 50 W during 3600 seconds; ■, EIS

plot from a Pb surface cleaned by potentiostatic reduction at -0.9 V in a 0.5 M Na_2SO_4 solution for 1800 seconds after being exposed one week to acetic acid; ▲, and metallic Pb sample; ●.

As shown in Figure 5-10, the electrochemically reduced sample presented a more resistive surface (around 162 Ωcm^2) than the non-thermal plasma cleaned surface (around 22 Ωcm^2). This was related to the $PbSO_4$ surface layer formed by the electrolyte used to perform the cathodic reduction. The case of the non-thermal plasma cleaned surface was compared with the metallic Pb, this last presenting a very similar total modulus (around 14 Ωcm^2). Differences were nearly imperceptible in the obtained values, which means that the plasma treatment was much more effective than the electrochemical treatment. The resulting surface presented very low inhomogeneities, due to the non-invasive technique in which no corrosion compounds were formed. Furthermore, the surface was slightly smoothed due to the etchant processes during the application of non-thermal plasma.

The fitting data obtained for the Pb electrode (see Figure 5-4), the non-thermal plasma treated and the electrochemical reduced, is presented in Table 5-4.

Table 5-4. Obtained results of the Electron Impedance Spectroscopy resistances after reduced samples.

	Metallic Pb	**Plasma treatment**	**Electrolytic reduction**
Element	**Value**	**Value**	**Value**
Re (Ωcm^2)	1.35	1.85	1.17
Rf (Ωcm^2)	12.4	18.7	124
CPE ($\mu\Omega^{-1}cm^{-2}s^n$)	22	34.5	71.9
n	0.934	0.948	1

In accordance to the presented values in Table 5-4, the resistance values between the metallic Pb and the plasma treated sample were very similar (12.4 Ωcm^2 and 18.7 Ωcm^2) in contrast to the electrochemically reduced surface (124 Ωcm^2). Note that Karbasi et al. reported that metallic Pb yields a resistance value of around 12 Ωcm^2

[38]. In addition, Khatbi et al. reported similar values for lead-aluminium casting alloys for lead-acid batteries [39]. Furthermore, after electrolytic reduction, the CPE value was higher (71.9 $\mu\Omega^{-1}cm^{-2}s^{n}$) than those obtained on the metallic Pb (22 $\mu\Omega^{-1}cm^{-2}s^{n}$) and after non-thermal plasma treatment (34.5 $\mu\Omega^{-1}cm^{-2}s^{n}$). This fact describes the dielectric properties of a rougher surface on the reduced sample. Since the aim of modern conservation is to preserve and stabilise historical artifacts while respecting their cultural and historical significance, non-thermal plasma resulted in a good alternative for this purpose. Due to the adverse effects that electrochemical treatment produces, the non-thermal plasma technique is less invasive even for corroded objects in a poor state of conservation.

In addition, in Figure 5-11 in shown the spectrum of the corroded surface during one week by AcOH liquid phase, together with the resulting surface after applying non-thermal plasma. The impedance spectrum of the non-corroded Pb electrode (see Figure 5-4) was also included.

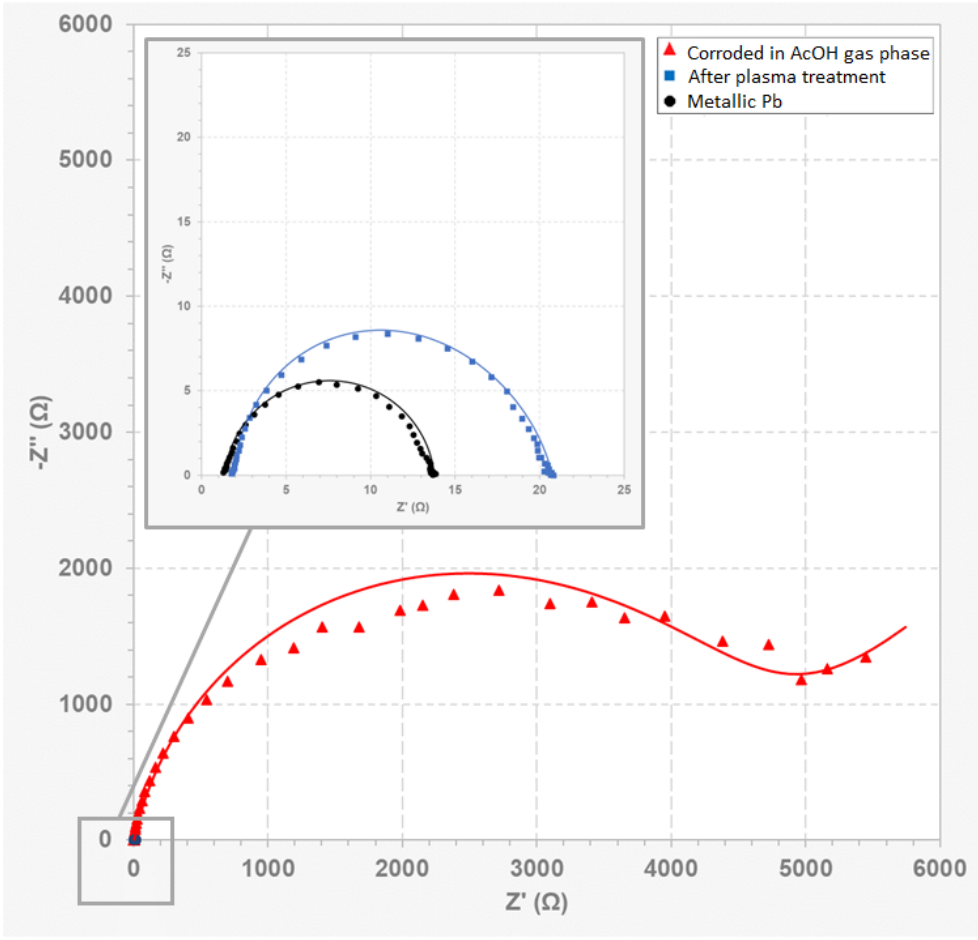

Figure 5-11. EIS spectra of the sample exposed one week to acetic acid (▲) and after being treated using an hydrogen/argon (90:10) plasma at a potential of 50 W during 3600 seconds (■). EIS spectrum of metallic Pb sample is also included (●).

As shown in Figure 5-11, the total modulus of the corrode sample (around 6 kΩcm^2) was indeed much higher than the one obtained once the surface was treated by non-thermal plasma (around 22 Ωcm^2). The spectrum shape obtained from the corroded sample resulted in a depressed semicircle ending in a poorly defined signal, which is outlined upwards due to diffusion effects, causing the semicircle does not close. On the contrary, the non-thermal plasma cleaned surface presents a compact surface with very few imperfections, which is reflected on the more rounded and

closed semicircle. This was very similar to that small semicircle obtained on the metallic Pb EIS measurements. In general terms, EIS technique was capable to read surfaces of totally different morphology. It means that it can be a powerful tool to characterize surfaces in order to evaluate the effectiveness and harmlessness of cleaning techniques on corroded surfaces.

5.4. Concluding remarks

Surface characterization is the first approach to know the state of artefacts conservation and the effectiveness of any treatment. Techniques such as XRD, XPS and SEM-EDS are frequently used in the field of Cultural Heritages conservation to characterize corroded surfaces. It should be noted that, in this context, the use of Electrochemical Impedance Spectroscopy is very infrequent. The present work demonstrated the potential of this technique to provide a fairly accurate analysis of different surfaces and it was presented as a useful complementary tool in front of the traditional characterization techniques.

At this point, it is worth mentioning that EIS is commonly used for studies on understanding the fundamental processes of diffusion and faradaic reaction at electrodes. Very little information can be found in literature about the use of EIS applied to the surface study of cultural Heritage artefacts. In this chapter, EIS was used to evaluate the surface characteristics of corroded lead samples and also its potential to evaluate the effectiveness of a cleaning treatment on corroded surfaces.

In this work, it was demonstrated that EIS is capable to describe surface layers with different morphology. For example, when metallic Pb is corroded forming a stable, compact and homogeneous layer after sulphuric exposure to the gas phase of solutions containing sulfuric acid, the obtained impedance spectra had a large impedance modulus. This means that the metal was protected against further corrosion processes. In addition, the surface layer was more compact when increasing the anodization potential, and as a result, the impedance modulus was higher.

In contrast, when porous and partially soluble corrosion products were formed after exposure in the gas phase of solutions containing acetic acid, a small impedance

modulus was obtained. In this case, lead acetate layers were formed by the AcOH gas phase exposure during different periods of time (3 hours, 3 days and one week). These resulted corrosion layers were porous and irregular, allowing the metal exposition. Due to the high heterogeneity of the corroded surface, diffusion effects were descried in the impedance spectra. The surface layer was thicker when increasing the time of exposition, and as a result, the impedance modulus was higher.

EIS was also useful to analyse and evaluate the effectiveness of different surface treatments. EIS was capable to measure the intrinsic characteristics of the obtained surfaces before and after treatment and also to detect the different electrical properties of the surfaces as a function of the selected cleaning method. In the case of electrolytic reduced surfaces, the resistance values decreased considerably in comparison with the anodized samples. However, a residual layer of $PbSO_4$, formed by the surface contact with the electrolyte in the presence of dissolved oxygen, was detected. This last, was compared with a non-thermal plasma treated surface (selected conditions described in Exp. 7 from chapter 4). The impedance modulus was very similar to the non-corroded sample with non-relevant differences in the EC element values. This describes the effectiveness of the non-thermal plasma treatment in returning the corroded surface to a near initial state of metallic Pb.

As described in this chapter, EIS was effective to compare different surfaces after cleaning treatments. Plasma treatment proved to be more effective in restoring the surface without leaving a significant amount of corrosion products formed during the treatment, as in electrochemical treatments. Additionally, as mentioned in the previous chapters, some problems in electrolytic reduction for metallic artefacts were described. For this reason, plasma treatment was selected to clean a corroded lead artefact from Cultural Heritage, which will be described in next chapter 6.

References

[1] C. Degrigny, Use of electrochemical techniques for the conservation of metal artefacts: a review, Journal of Solid State Electrochemistry. 14 (2010) 353–361. https://doi.org/10.1007/s10008-009-0896-0.

[2] X. Zhang, W. He, I. Odnevall Wallinder, J. Pan, C. Leygraf, Determination of instantaneous corrosion rates and runoff rates of copper from naturally patinated copper during continuous rain events, Corros Sci. 44 (2002) 2131–2151. https://doi.org/10.1016/S0010-938X(02)00015-X.

[3] E. Cano, D. Lafuente, D.M. Bastidas, Use of EIS for the evaluation of the protective properties of coatings for metallic cultural heritage: a review, Journal of Solid State Electrochemistry. 14 (2010) 381–391. https://doi.org/10.1007/s10008-009-0902-6.

[4] S. Grassini, Electrochemical impedance spectroscopy (EIS) for the in-situ analysis of metallic heritage artefacts, in: Corrosion and Conservation of Cultural Heritage Metallic Artefacts, Elsevier, 2013: pp. 347–367. https://doi.org/10.1533/9781782421573.4.347.

[5] Z. Lukács, T. Kristóf, A generalized model of the equivalent circuits in the electrochemical impedance spectroscopy, Electrochim Acta. 363 (2020) 137199. https://doi.org/10.1016/j.electacta.2020.137199.

[6] E. Pons, C. Lemaitre, D. David, D. Crusset, Electrochemical study of steel artefacts from World War I: Contribution of A.C. impedance spectroscopy and chronoamperometry to describe the behaviour of the corrosion layers, in: Corrosion of Metallic Heritage Artefacts, Elsevier, 2007: pp. 77–91. https://doi.org/10.1533/9781845693015.77.

[7] B. Ramírez Barat, E. Cano, In Situ Electrochemical Impedance Spectroscopy Measurements and their Interpretation for the Diagnostic of Metallic Cultural Heritage: A Review, ChemElectroChem. 5 (2018) 2698–2716. https://doi.org/10.1002/celc.201800844.

[8] F. Di Turo, N. Montoya, J. Piquero-Cilla, C. De Vito, F. Coletti, G. Favero, A. Doménech-Carbó, Archaeometric analysis of Roman bronze coins from the Magna Mater temple using solid-state voltammetry and electrochemical impedance

spectroscopy, Anal Chim Acta. 955 (2017) 36–47. https://doi.org/10.1016/j.aca.2016.12.007.

[9] D.M. Tartakovsky, M. Dentz, Diffusion in Porous Media: Phenomena and Mechanisms, Transp Porous Media. 130 (2019) 105–127. https://doi.org/10.1007/s11242-019-01262-6.

[10] C. Chiavari, A. Colledan, A. Frignani, G. Brunoro, Corrosion evaluation of traditional and new bronzes for artistic castings, Mater Chem Phys. 95 (2006) 252–259. https://doi.org/10.1016/j.matchemphys.2005.06.034.

[11] L. La-Torre-Riveros, A. Doménech-Carbó, C.R. Cabrera, M.T. Doménech-Carbó, W. Huahuasoncco-Condori, D. Quispe Guzmán, M. del C. Gutiérrez-Castillo, K. Carmona-Ochoa, A. Pérez-Trujillo, Solid-state electrochemical analysis of Inka pottery from Qotakalli archeological site in the Cusco (Perú) area, Journal of Solid State Electrochemistry. 23 (2019) 1541–1552. https://doi.org/10.1007/s10008-019-04243-3.

[12] E. Apchain, D. Neff, J.-P. Gallien, N. Nuns, P. Berger, A. Noumowé, P. Dillmann, Efficiency and durability of protective treatments on cultural heritage copper corrosion layers, Corrosion Science. 183 (2021) 109319–109331. https://doi.org/10.1016/j.corsci.2021.109319.

[13] Valentini, Smart Electrochemical Portable Tools for Cultural Heritage Analysis: A Review, Sensors. 19 (2019) 4303–4336. https://doi.org/10.3390/s19194303.

[14] D. Mikić, H. Otmačić Ćurković, T. Kosec, N. Peko, An Electrochemical and Spectroscopic Study of Surfaces on Bronze Sculptures Exposed to Urban Environment, Materials. 14 (2021) 2063–2080. https://doi.org/10.3390/ma14082063.

[15] F. di Turo, P. Matricardi, C. di Meo, F. Mazzei, G. Favero, D. Zane, PVA hydrogel as polymer electrolyte for electrochemical impedance analysis on archaeological metals, Journal of Cultural Heritage. 37 (2019) 113–120. https://doi.org/10.1016/j.culher.2018.09.017.

[16] J.C. Aguilar, D.E. Arceo-Gómez, M.A. Hernandez-Perez, R. Galvan-Martinez, R. Orozco-Cruz, Electrochemical Analysis of a Rust Converter Applied on Materials of Historical Interest, ECS Trans. 94 (2019) 345–353. https://doi.org/10.1149/09401.0345ecst.

[17] L. Iannucci, J.F. Ríos-Rojas, E. Angelini, M. Parvis, S. Grassini, Electrochemical characterization of innovative hybrid coatings for metallic artefacts, The European Physical Journal Plus. 133 (2018) 522–529. https://doi.org/10.1140/epjp/i2018-12368-3.

[18] L.E. Sebar, E. Angelini, S. Grassini, L. Iannucci, M. Parvis, An op amp-less Electrochemical Impedance Spectroscopy System, in: 2020 IEEE International Instrumentation and Measurement Technology Conference (I2MTC), IEEE, 2020: pp. 1–6. https://doi.org/10.1109/I2MTC43012.2020.9129355.

[19] D. Arguelles, C. Campechano, R. Galván-Martínez, T. Jimenez, R. Orozco-Cruz, Corrosion Protection Behavior of Patinas on Copper Alloys in Historical Metal Heritage: Electrochemical Study, ECS Meeting Abstracts. MA2018-02 (2018) 2072–2072. https://doi.org/10.1149/MA2018-02/58/2072.

[20] C. Petiti, L. Toniolo, D. Gulotta, B. Mariani, S. Goidanich, Effects of cleaning procedures on the long-term corrosion behavior of bronze artifacts of the cultural heritage in outdoor environment, Environmental Science and Pollution Research. 27 (2020) 13081–13094. https://doi.org/10.1007/s11356-020-07814-4.

[21] L.E. Sebar, L. Iannucci, E. Angelini, S. Grassini, M. Parvis, Electrochemical Impedance Spectroscopy System Based on a Teensy Board, IEEE Trans Instrum Meas. 70 (2021) 1–9. https://doi.org/10.1109/TIM.2020.3038005.

[22] K. Jüttner, Electrochemical impedance spectroscopy (EIS) of corrosion processes on inhomogeneous surfaces, Electrochim Acta. 35 (1990) 1501–1508. https://doi.org/10.1016/0013-4686(90)80004-8.

[23] S.P. Jung, S. Pandit, Important Factors Influencing Microbial Fuel Cell Performance, in: Microbial Electrochemical Technology, Elsevier, 2019: pp. 377–406. https://doi.org/10.1016/B978-0-444-64052-9.00015-7.

[24] P.-Y. Zhang, Z.-L. Liu, Experimental study of the microbial fuel cell internal resistance, J Power Sources. 195 (2010) 8013–8018. https://doi.org/10.1016/j.jpowsour.2010.06.062.

[25] J. Yu, Z. Qian, M. Zhao, Y. Wang, L. Niu, Effects of sodium sulphate as electrolyte additive on electrochemical performance of lead electrode, Chem Res Chin Univ. 29 (2013) 374–378. https://doi.org/10.1007/s40242-013-2261-1.

[26] M.M. Burashnikova, I.A. Kazarinov, I.V. Zotova, Nature of contact corrosion layers on lead alloys: A study by impedance spectroscopy, J Power Sources. 207 (2012) 19–29. https://doi.org/10.1016/j.jpowsour.2011.12.042.

[27] P. Mattesco, N. Bui, P. Simon, L. Albert, Effect of polarisation mode, time and potential on the properties of the passive layer on lead-tin alloys, J Power Sources. 64 (1997) 21–27. https://doi.org/10.1016/S0378-7753(96)02495-0.

[28] E.E. Abd El Aal, Cyclic voltammetric behavior of the lead electrode in sodium sulphate solutions, J Power Sources. 102 (2001) 233–241. https://doi.org/10.1016/S0378-7753(01)00804-7.

[29] R. Brinic, S., Metkos-Hukovic, M., & Babic, Impedance spectroscopy as a tool for characterization of surface films on lead and lead alloys., Journal of New Materials for Electrochemical Systems. 8(4) (2005) 273.

[30] S. Grassini, Electrochemical impedance spectroscopy (EIS) for the in-situ analysis of metallic heritage artefacts, in: Corrosion and Conservation of Cultural Heritage Metallic Artefacts, Elsevier, 2013: pp. 347–367. https://doi.org/10.1533/9781782421573.4.347.

[31] F. Mansfeld, Electrochemical impedance spectroscopy (EIS) as a new tool for investigating methods of corrosion protection, Electrochim Acta. 35 (1990) 1533–1544. https://doi.org/10.1016/0013-4686(90)80007-B.

[32] F.E. Varela, L.M. Gassa, J.R. Vilche, Characterization of passive layers formed on lead by electrochemical impedance spectroscopy, Journal of Electroanalytical Chemistry. 353 (1993) 147–160. https://doi.org/10.1016/0022-0728(93)80293-Q.

[33] J. Huang, Diffusion impedance of electroactive materials, electrolytic solutions and porous electrodes: Warburg impedance and beyond, Electrochim Acta. 281 (2018) 170–188. https://doi.org/10.1016/j.electacta.2018.05.136.

[34] M.M. Burashnikova, I.A. Kazarinov, I.V. Zotova, Nature of contact corrosion layers on lead alloys: A study by impedance spectroscopy, Journal of Power Sources. 207 (2012) 19–29. https://doi.org/10.1016/j.jpowsour.2011.12.042.

[35] I. Martinović, Z. Pilić, Corrosion behavior of copper, tin, and bronze CuSn14 in acid rain solution, Materials and Corrosion. 72 (2021) 1635–1642. https://doi.org/10.1002/maco.202112470.

[36] F. Deflorian, M. Fedel, Electrochemical analysis of the degradation of lead alloy organ-pipes due to acetic acid, J Cult Herit. 14 (2013) 254–260. https://doi.org/10.1016/j.culher.2012.06.002.

[37] E. PONS, C. LEMAITRE, D. DAVID, D. CRUSSET, Electrochemical study of steel artefacts from World War I: Contribution of A.C. impedance spectroscopy and chronoamperometry to describe the behaviour of the corrosion layers, in: Corrosion of Metallic Heritage Artefacts, Elsevier, 2007: pp. 77–91. https://doi.org/10.1533/9781845693015.77.

[38] M. Karbasi, E. Keshavarz Alamdari, E. Amirkhani Dehkordi, F. Tavangarian, Electrochemical and anodic behaviors of MnO2/Pb nanocomposite in zinc electrowinning, J Appl Electrochem. 48 (2018) 379–390. https://doi.org/10.1007/s10800-018-1163-9.

[39] S. Khatbi, Y. Gouale, S. Mansour, A. Lamiri, M. Essahli, Electrochemical and Metallurgical Behavior of Lead-Aluminum Casting Alloys as Grids for Lead-Acid Batteries, Portugaliae Electrochimica Acta. 36 (2018) 133–146. https://doi.org/10.4152/pea.201802133.

6. The Violinist sculpture by Pau Gargallo (1920); non-thermal plasma treatment

6.1. Introduction

Under the concept of irreversibility, the aim of restoring Cultural Heritage artefacts is to return them to their original state as far as possible, when were degraded over time. After being analysed and compared different methodologies to clean corroded lead metals by VOCs, the present chapter is based on *The Violinist* (1920) sculpture made by Pau Gargallo as a real case study. The incompatibility of its materials composition based on an internal pine wood structure covered by lead sheets, produced severe corrosion problems. Non-thermal plasma technique was proved to be an effective treatment to recover corroded Pb surfaces affected by AcOH, and it was used to cleaning purposes.

The state of conservation of Cultural Heritage artefacts helps to explain circumstances in which the objects were subjected at different historical contexts. In this sense, a previous analysis can be useful to understand how the artefact was created and its aging processes during long periods of time. As demonstrated in the previous chapters, the surface analysis is the first step to study the degradation of materials before determining a cleaning and stabilisation method. Characterization techniques also helps to analyse the effectiveness of surface treatments by testing corrosion models manufactured in the laboratory, which are made to recreate degraded surfaces. In this context, the conservator must also be aware when selecting the appropriate treatment.

Basing on the incompatibility of materials and the corrosion problems of metallic lead artefacts, the case study of the present chapter is *The Violinist* (1920) sculpture made by Pau Gargallo [1]. This sculpture was a portrait of the musician Francesc

Costa (1891-1959) [2] and actually is located in the *Museu d'Art de Catalunya (MNAC)* in Barcelona, Spain. *The Violinist* is the first in a series of lead sculptures that Gargallo made between 1920 and 1923, in which the artist worked with this metal thanks to its malleability and softness.

The size of the sculpture is 55.3 x 31.8 x 21.6 cm (11.9 kg) and is composed by lead sheets of 2.5 mm to 1.5 mm thickness, depending on the intensity and impact of hammering. Lead sheets were soldered each other and superposed on a wood structure [1]. This sculpture was the only one made by this way in comparison with the other sculptures from by Pau Gargallo, which were manufactured by using much thicker lead sheets and with no wood structures. Before applying the conservation treatments, the sculpture presented a poor state of conservation. In Figure 6-1, is presented a photograph of *The Violinist* sculpture taken in 1920-1924, in comparison with the right picture taken in 2014.

Figure 6-1. Frontal views of The Violinist [1], by Pablo Gargallo, *a;* picture taken between 1920-1924, *b;* present state.

The initial structural properties and state of conservation were described in bibliography [1]. This resulted from inappropriate handling of the sculpture, producing fatigue, cracking or breakage on the metal sheets. Additionally, in the last years, different swollen areas on both legs were noticed for the first time, as observed in the right picture from Figure 6-1. These areas grew up and began to open, exposing the internal corrosion compounds mainly identified as hydrocerussite. The degradation process was mainly originated by the VOCs emission from the wood core to the lead sheets, in combination with air and humidity during more than a hundred years.

Its fragility and delicate state of conservation was the cause of the need for intervention by using a particular treatment. In this context, the sculpture was first preserved in the laboratory of the *Museu d'Art de Catalunya,* in a methacrylate case with silica gel at a controlled atmosphere of low relative humidity (below 39 %). As described in the bibliographic report [1], the sculpture was analysed by neutron radiography imaging, with tomography and 3D volume reconstruction. These analyses were done at NEUTRA of the Paul Scherrer Institute (PSI), which is situated at the spallation neutron source SINQ [3]. An example of tomography and 3D reconstruction with the inner wood is shown in Figure 6-2.

a) 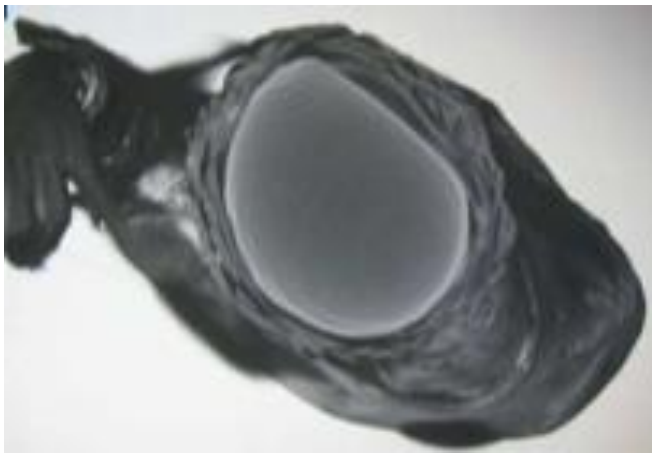 b) 

Figure 6-2. *a;* detail of the head and upper part of body cross sectioned in the 3D reconstruction, *b;* 3D reconstruction of the sculpture with the inner wood [1]. Images supplied by the art curator Àlex Masalles from the *Museu d'Art de Catalunya.*

Neutron imaging was used as a suitable non-invasive technique for the examination of the lead sculpture. The radiographic sequence produced good quality of tomograms as also 3D reconstruction details. The results allowed to obtain information specially about the manufacturing technique and its internal state of conservation. Thanks to the different contrast of metallic lead and lead carbonate was possible to analyse the degree of corrosion compounds growing up in the internal structure. Previous measurements of the lead carbonate layers were obtained in the range from $4x10^{-1}$ mm to nearly 2 cm in the blister of the right leg where no metallic lead is preserved [1].

The dismantling of the metallic lead sheets allowed to analyse for the first time the real situation inside the sculpture. Localised areas with active corrosion were observed, which generated severe lead carbonate crusts of greater or lesser magnitude. In addition, these crusts were not homogeneous in the whole surface, finding basically two types. One of very compact aspect with little thickness that did not seem to attack the underlying lead, and another one with a more granular and discontinuous aspect that was penetrated within the metallic lead sheets.

It is worth mentioning that the restoration of "*The Violinist*" lead sculpture by Pau Gargallo was performed in cooperation with the *Museu d'Art de Catalunya* together with the *Institut Químic de Sarrià* (IQS).

As described throughout the previous chapters, the obtention of corrosion models on the laboratory for testing, is very important prior to perform conservation methods. Taking into account that Cultural Heritage artefacts are unique objects with particular properties, these need to be analysed and treated under an accurate selection of characterization techniques and surface treatments. A deep analysis of the surface provides information of the effects of deterioration and palliative treatments for its proper conservation. The sculpture subjected to treatment belongs to the *Museu d'Art de Catalunya* and is responsibility of its curator, Àlex Masalles. Based on the results shown in the previous chapters, non-thermal plasma was selected as the best possible treatment (90:10 argon/hydrogen, 50 W during 60'). It is worth mentioning that *Museu d'Art de Catalunya* and its curator decided to perform a mechanical cleaning by micro-sandblasting before using the non-thermal plasma. The point here was to reduce the thickness of the corrosion layer in those zones with a large accumulation of corrosion products.

6.2. Experimental set-up

6.2.1. Micro-sandblasting technique

Micro-blasting tests were performed in the *Museu d'Art de Catalunya*, by the art curator Àlex Masalles. These allowed to minimize the big parts of carbonate crust using abrasive pumice (powdered pumice stone) and abrasive alumminum silicat*e.* Nederman Blasting Gun for the SB-750 extracted sandblaster was used to remove the remained particles. This mechanical cleaning was performed in a vacuum cleaner and an extractor hood, closed by a hinged methacrylate screen with a suction collection system, both with high-efficiency HEPA filters.

6.2.2. Argon/hydrogen non-thermal plasma application

The low-pressure plasma reactor was used for restoring corroded lead samples by VOCs. The experimental set-up was designed by the *Grup d'Enginyeria de Materials* (GEMAT) at the Institut Químic de Sarrià (*Universitat Ramon Llull)*.

The plasma reactor was described in chapter 4. Before introduction of the samples placed on an aluminium sheet, the chamber was cleaned in continuous wave argon/hydrogen (2:1) plasma for approximately 1800 seconds at a power of 50 W. The selected conditions for the cleaning of the corroded lead sculpture, were performed at 90:10 argon/hydrogen and 50 W during 1800 seconds as also described in the experimental set-up section of chapter 4. In some cases, the surface treatment was repeated 30 minutes after the first treatment. After this, surfaces were mechanically cleaned with a soft bristle brush.

6.3. Results and discussion

6.3.1. Corrosion characterization

The formation of lead corrosion from *The Violinist* sculpture was very heterogeneous, presenting differences in the surface layer morphology. As shown in the following Figure 6-3, the inner face of the lead sheets from the sculpture were very damaged due to corrosion processes produced by VOCs from the pine wood core.

Figure 6-3. Severe corrosion on the inner face of lead sheet from the sculpture The Violinist by Pau Gargallo.

The internal part of these lead sheets resulted in severe corrosion produced by the organic vapours from the pine wood. The surface corrosion was very heterogeneous, meaning that the corrosion is not evenly distributed across the entire surface of the lead sheets. It is worth mentioning that the corrosion products formed on the surface presented different morphologies, as can be observed in Figure 6-4.

a)  b) 

Figure 6-4. Details of the two types of crust found inside the lead sheets, *a;* uniform thin corrosion layer, *b;* localised corrosion compounds.

Two types of corrosion were observed in the lead sheets as shown in Figure 6-4. This difference gives information about the internal corrosion processes produced in different areas between the pine wood and the lead sheets. In Figure 6-4 *a*, the corrosion layer appearance was very compact. This type of homogeneous and thin layer describes a uniform corrosion, in which a passivation process occurred. The metallic lead sheet is not highly degraded due to the compact film created in the surface [4]. However, in Figure 6-4 *b*, a more severe degradation process is shown. The corrosion layer was formed by a thick corrosion crust with localised patches. In these areas, some deformations were clearly observed on the structure metallic lead. These differences on the corrosion morphology may be related to the concentration of VOCs and the air conditions between the lead sheets and the wood core as described in chapter 2. On these areas, the Pb matrix structure was very degraded. In this context, two different kinds of corrosion were observed: a thin compact corrosion layer (approximately 20 μm of thickness) and thick porous patches (approximately 200 μm of thickness).

6.3.1.1. Optical microscope

As described in chapter 2, the conversion of corrosion compounds formed by VOCs such as lead acetate into carbonate, is influenced by the contact with CO_2 and O_2 from the atmosphere. Lead carbonate are mainly formed by cerussite, hydrocerussite or plumbonacrite compounds. These usually are present in form of thick and very porous layers. In order to characterize these products from a real case study, different small samples were collected from the thick corrosion crust of *The Violinist* lead sculpture and were analysed by optical microscope. The results are presented in Figure 6-5.

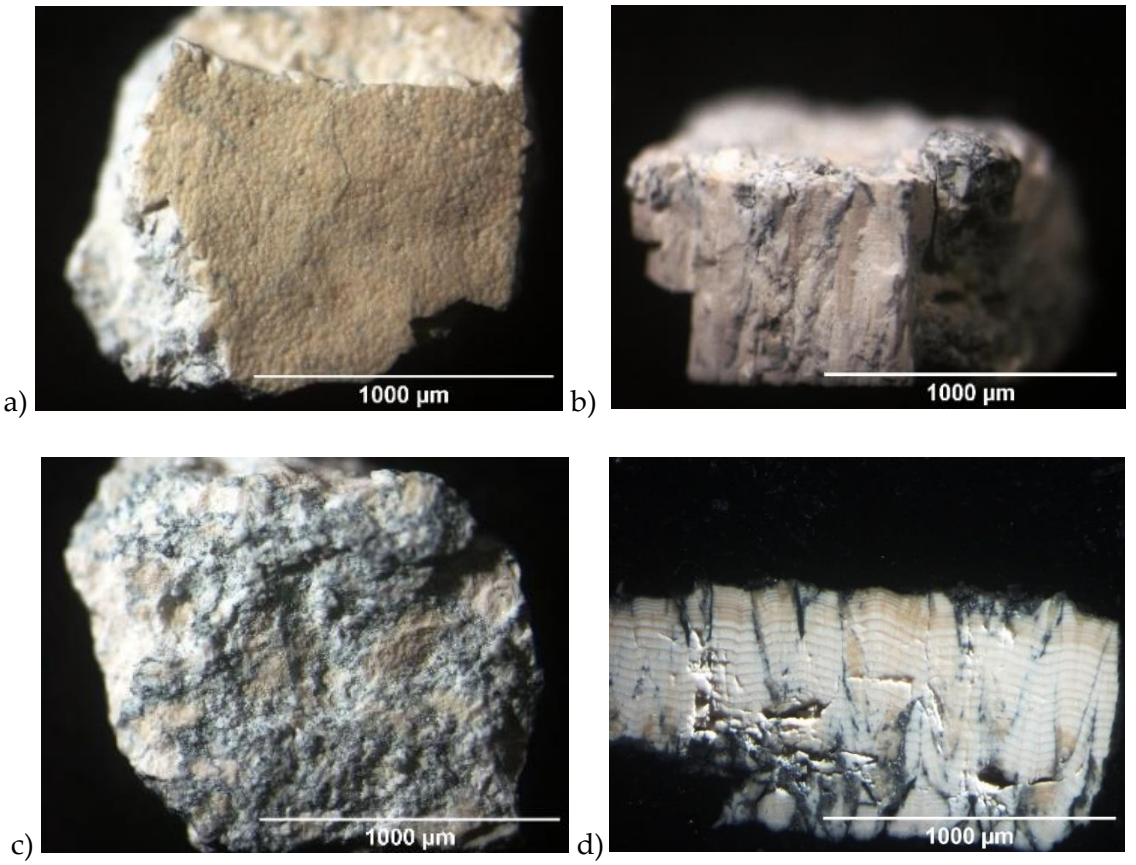

Figure 6-5. Detail of a lead carbonate particle from *The Violinist* sculpture, *a;* frontal side of the corrosion particle which is in contact with the environment, *b;* lateral side of the thick

corrosion particle, *c;* reverse side which was in contact with the metallic surface, *d;* transversal stratigraphy of the corrosion lead carbonate.

As observed in Figure 6-5 *a*, the lead carbonate particle has a yellowish face. This face corresponds to the corrosion layer in contact with the O_2 from the environment which tends to oxidate. As can be seen in the micrograph, the surface was more homogeneous than the subjacent appearance, given the passivation process when in contact with the environment.

In the case of Figure 6-5 *b*, corresponded to the lateral side of the corrosion particle, in which the remaining metal veins can be observed. This describes the great dissolution of the metallic Pb and the formation of the thick corrosion crust into the surface. Figure 6-5 *c*, showed the reverse face in which the lead carbonate was in contact with the metallic surface which was hardly degraded. Finally, in Figure 6-3 *d*, small metallic veins are observed from the metallic structure to the surface corrosion layer were also observed among the carbonate crust.

6.3.1.2. X-Ray Diffraction analysis

In order to analyse how long the formation of the corrosion compounds from *The Violinist* sculpture can take, XRD analyses were performed on three Pb samples exposed to AcOH vapours at different periods of time. In this context, a small sample of corrosion from the Pb sculpture exposed to pine wood during more than 100 years, was compared with two corrosion simulations obtained by AcOH vapours. As described in chapter 2, the first sample was exposed to vapour test using 8 M AcOH during one month, and the second sample was obtained by VOCs from pine wood during 3 years. The XRD patterns are presented in Figure 6-6.

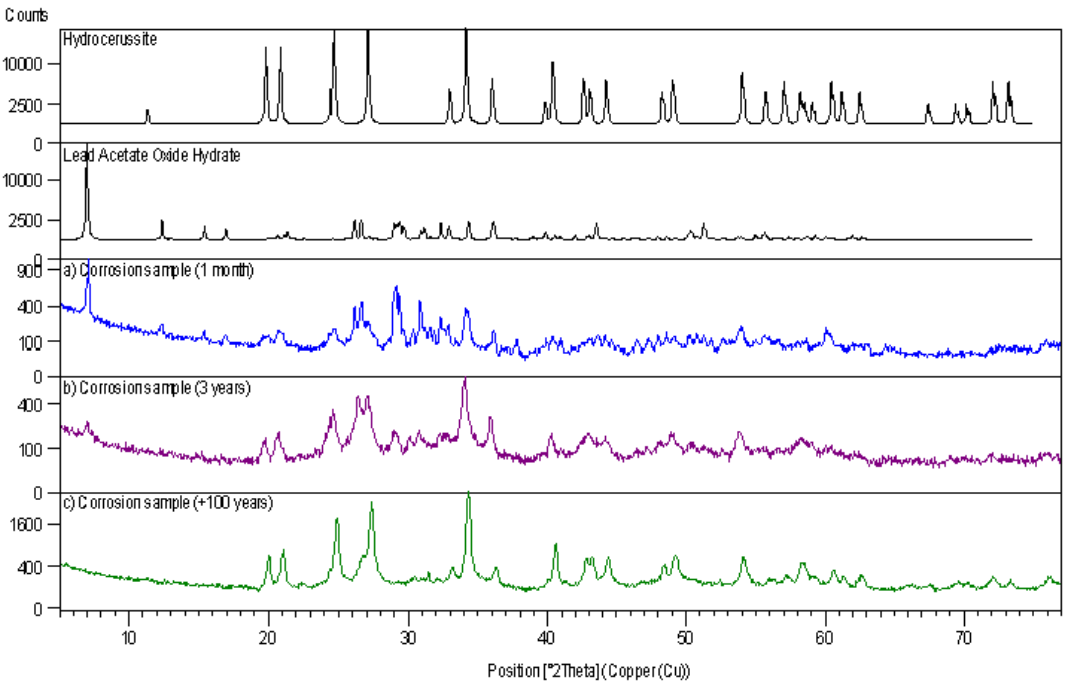

Figure 6-6 Database patterns from International Centre for Diffraction Data® (PDF4+) of hydrocerussite and lead (II) acetate hydroxide (black), *a;* AcOH 8M gas phase during 28 days and *b*; AcOH (from pine wood) during 3 years, *c;* AcOH (from pine wood) during more than 100 years, corroded sample extracted from a lead sculpture *El Violinista*, made by Pau Gargallo in 1920.

The corrosion compounds obtained by the first simulation (Pb exposition to AcOH vapours during one moth) was studied and described in chapter 2. The second simulation of the Pb exposed to VOCs during approximately 3 years, presented a mixture of lead acetate, lead oxide and lead carbonate. However, in comparison with the corroded sample from the Pb sculpture, it was observed that the process to obtain the Pb corrosion compounds of the real sample is very slow and takes many years.

According to the morphological analysis of the corrosion products, it seemed that non-thermal plasma was the most adequate method. The difference between non-thermal plasma and electrolytic methods lies in the way they remove the corrosion products. non-thermal plasma uses reactive species generated by a high-energy electrical discharge to break down the corrosion products into volatile

compounds, which are then removed by a vacuum system. On the other hand, electrolytic methods involve the immersion of the object in a chemical solution and the application of an electrical current. As explained in chapter 3, this process can result in uneven reduction due to the non-compact nature of the corrosion layer, which can detach during the treatment process, causing partial reduction. This may lead to a surface with a very rough and heterogeneous appearance. Additionally, there is an increased risk of new corrosion compounds forming on the surface due to the contact with the electrolyte if it is not properly removed after treatment.

Given the heterogeneity and different thickness of the corrosion layers in the sculpture, it may be challenging to find an electrolytic method by immersing the sculpture that can reduce the corrosion products evenly without producing several changes on the surface. Non-thermal plasma may be a better option as it is a gentler process that, as described in chapter 4, can be fine-tuned to selectively remove specific corrosion products without affecting the underlying metal. However, one of the limitations on the use of non-thermal plasma is its effectiveness on thick corrosion layers, such as the ones present on the lead sculpture. Then, it was decided by the property of the sculpture (*Museu d'Art de Catalunya)*, to apply a mechanical cleaning by micro-sandblasting before the use of the non-thermal plasma.

6.3.2. Mechanical cleaning by micro-sandblasting technique

As previously mentioned, electrolytic reduction presented some limitations when restoring very damaged ancient artefacts such as Pb affected by VOCs. These techniques can be dangerous as they are difficult to control during treatment, as well as the use of new chemical compounds in an aqueous medium for long hours. In fact, localised reduction using an electrolytic pencil was developed, avoiding the immersion of the entire artefact with non-uniform corroded surface. This last has been documented for different metals such as on heterogeneous tarnished silver artefacts or lead metals which suffered active corrosion due to VOCs exposure, with good results [5,6]. However, once the composition, structure and state of conservation were known, a particular conservation protocol was established for the artefact in question. In the present study case, the Pb sheets from the sculpture affected by VOCs presented a heavily deterioration, with a highly reactive surface

due to the instability of products and the metal loss in some parts. Therefore, given its low state of conservation, it was decided to perform a non-thermal plasma treatment in which no new chemical compounds were introduced on the surface while optimising the treatment time.

However, given that plasma is not capable of reaching the depth in such thick layers [7] as those present in *The Violinist* sculpture, it was decided by the art curator Àlex Masalles from the *Museu d'Art de Catalunya* to apply a mechanical cleaning by micro-sandblasting. Micro-sandblasting is based on the projection of sand particles with a pressure gun in a closed chamber. The idea was to reduce the thickness of the carbonate layer formed on the surface without subjecting the metal to severe abrasion. After that, it was proposed that the residual surface layer would be cleaned with non-thermal plasma under the conditions described in chapter 4.

When separating the lead sheets of *The Violinist* from the wooden core, it was observed that the surface was still wet due to the long exposure to VOCs and to a humid environment. This causes the layer of carbonate and other corrosion products to be more compact and more difficult to remove with the micro-sandblasting. Therefore, in order to release the moisture from these layers, the Pb sheets were first of all placed in a vacuum chamber with controlled temperature, as they did not fit in the plasma reactor due to their bigger size.

In this context, the first step before the mechanical cleaning, was to introduce the corroded Pb sheets into the vacuum pump as observed in Figure 6-7, during 3 days at a temperature of 55 to 70 °C progressively.

a)  b) 

Figure 6-7. Lead sheets of *The Violinist* sculpture introduced in the vacuum chamber prior to the mechanical cleaning.

As shown in Figure 6-7, the pieces were carefully introduced into the vacuum chamber by means of a Teflon-coated foam system, which was designed by the art curator Àlex Masalles from the *Museu d'Art de Catalunya*.

Once this pre-treatment was performed, it was observed that the corrosion crust on the Pb sheets was more decohesioned as practically all the humidity was reduced, facilitating its mechanical clean. After that, the surface was then cleaned with micro-sandblasting. To determine the needed conditions, the art curator Alex Masalles first tested on lead sheets corroded by AcOH vapours during approximately three years in the conservation-restoration laboratory at the *Museu d'Art de Catalunya*. These tests were performed in a distance of 6 cm at 1 bar, using different times; 1, 3, 5, 7 and 10 seconds. With this, pulsed cleanings were also performed to avoid excessive incrustation of small particles into the metallic surface.

The micro-sandblasting tests in a corroded sample by AcOH vapours in the laboratory are shown in Figure 6-8.

a)  b) 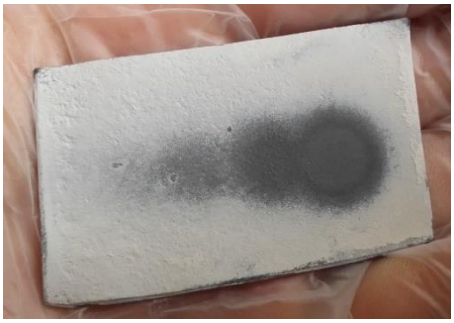

Figure 6-8. *a;* micro-sandblasting test performed on artificially carbonated lead samples, *b;* micro-sandblasting test with pumice (pumice stone) on artificially carbonated test tube. Each spot corresponds to the area affected by the abrasive for 1, 3, 5, 7 and 10 seconds respectively.

Micro-sandblasting tests were performed with two types of abrasives: aluminium silicate and pumice. In order to select the most suitable abrasive for such a malleable metal as lead, SEM-EDS analyses were performed in order to observe the metallic surface after blasting tests.

6.3.2.1. SEM-EDS analyses

SEM-EDS analyses were performed on the two resulting surfaces micro-blasted with aluminium silicate and pumice abrasive in order to minimize the corrosion crust. In Figure 6-9, the obtained SEM-EDS results for the micro-sandblasting with aluminium silicate abrasive are presented.

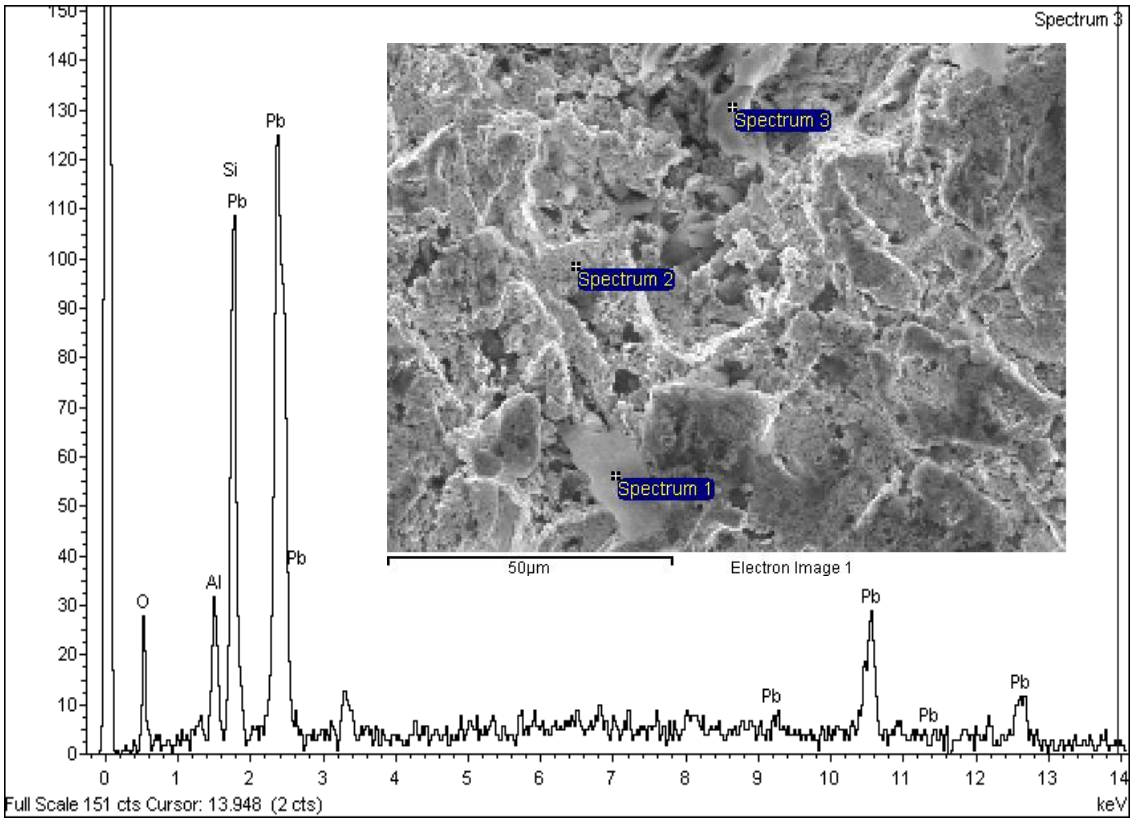

Figure 6-9. SEM-EDS analyses of the Pb micro-blasted with aluminium silicate abrasive.

As seen in the micrograph of Figure 6-9, there was an excessively rough surface with embedded Si and Al residues. These clustered particles into the metallic matrix can cause reactivity or physical instability on the surface at large time. For this reason, this technique was discarded in order to minimize the risk of damaging the metallic lead sheet.

Micro- sandblasting tests were also performed with pumice and results are shown in Figure 6-10.

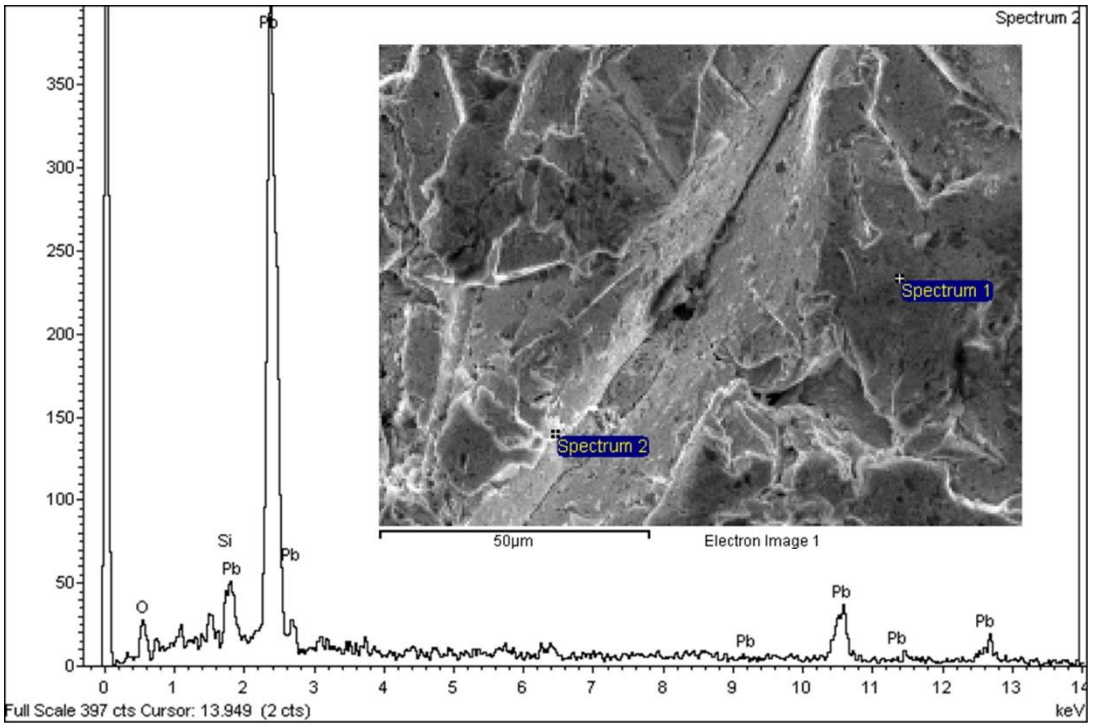

Figure 6-10. Micrographs obtained with SEM analyses of the Pb sample test, micro-blasted with pumice abrasive.

The surface obtained after being micro-blasted with pumice, presented a more favourable result due to the uniformity and the smaller quantity of particles. As seen in Figure 6-10, very small amounts of Si were observed in the EDS obtained. Note that using pumice abrasive the surface is less rough than using aluminum silicate. A small contamination of the abrasive on the metal surface was detected, although much lower than when using aluminum silicate. It was decided by the property of the sculpture (*Museu d'Art de Catalunya)*, to apply a mechanical cleaning by micro-sandblasting using pumice abrasive.

Therefore, it was decided to use pumice abrasive in order to reduce the lead carbonate thickness of *The Violinist* by using the spray gun at a distance of 6 cm and 1 bar of power. An example of a result after this mechanical cleaning is shown in Figure 6-11.

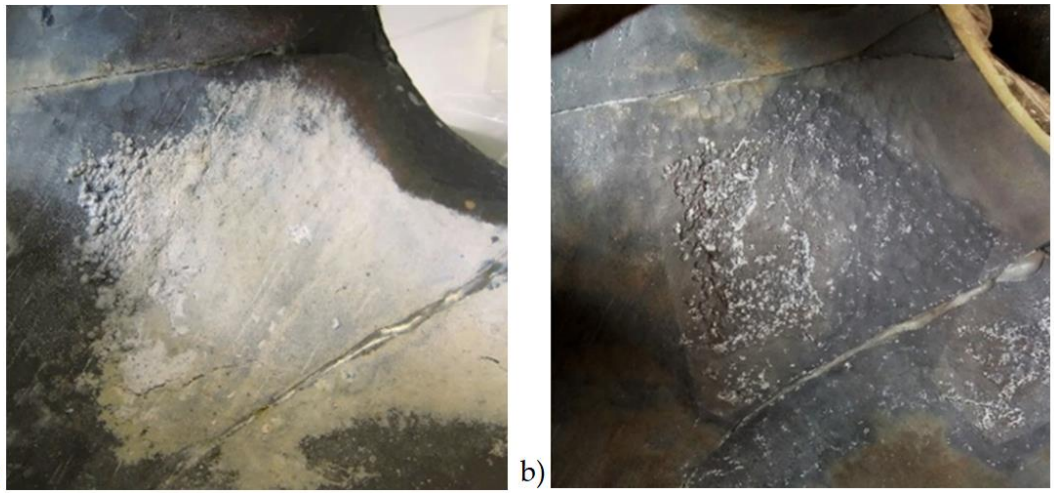

Figure 6-11. *A;* before to the micro-sandblasting with pumice abrasive, *b;* and after the micro-sand-blasting. Lead carbonate remains are still visible in the surface.

As seen in Figure 6-11, the resulting surface presented severe degradation on the metallic matrix produced by the corrosion processes. As a result of the deterioration of the metal, there were many holes in localized areas all over the surface with corrosion products. After mechanical cleaning, a combination of reduction and etching processes was carried out using a mixture of hydrogen and argon plasma.

6.3.3. Non-thermal plasma technique

A plasma design was applied to the corroded lead sculpture, following the optimal conditions selected in chapter 4. An etchant treatment was performed through the 90:10 argon/hydrogen non-thermal plasma at 50W during 60 minutes. In Figure 6-12, the mechanism of corrosion cleaning by non-thermal plasma is presented.

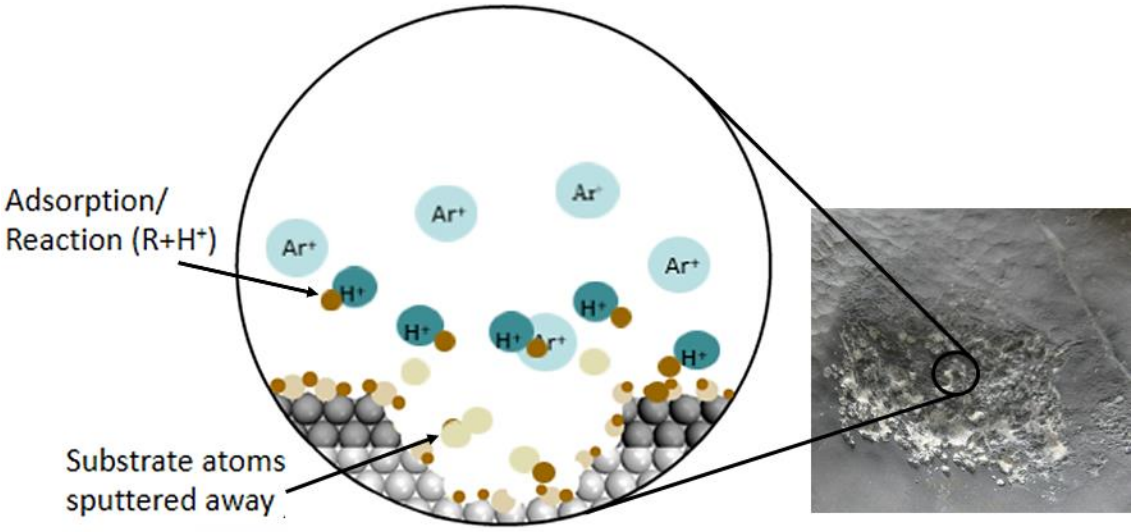

Figure 6-12. Etching process by the argon/hydrogen non-thermal plasma treatment in the corroded Pb sheet.

The corroded surface was treated by introducing the metallic lead sheets in the reactive gas (etchant species) generated from the plasma. When spreading them onto the metal surface, adsorption (and migration) occurs causing different reactions resulted in the desorption of by-products that spread through the gas stream. This treatment was described in chapter 4 using corroded Pb by AcOH vapours and subsequently aerated to form lead carbonate (as shown in Figure 3-6 from chapter 3) and micrographs of the resulting surfaces before and after treatment are presented in Figure 6-13.

a) 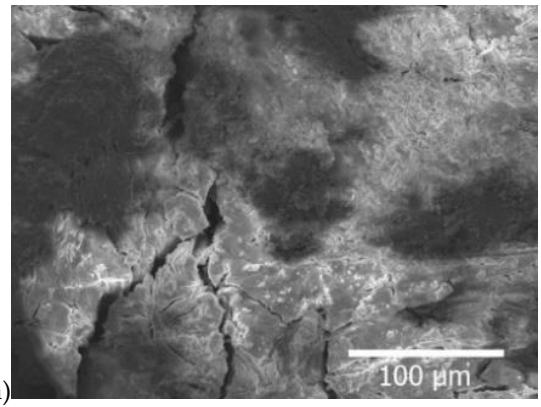

b) 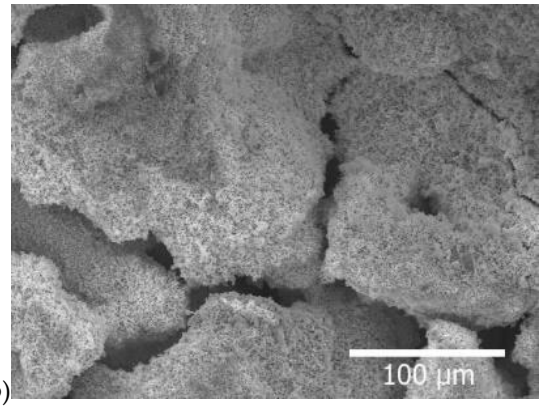

Figure 6-13. *a;* corroded surface by VOCs before treatment, *b;* after treatment with plasma of Argon and Hydrogen 2:1, at a potential of 80 W during 30 minutes.

As seen in the SEM micrographs shown in Figure 6-13 and described in chapter 4, the treated Pb surfaces with non-thermal plasma presented a higher porosity. This fact shows the reduction of lead through the introduction of hydrogen plasma while an etching process is produced by the bombardment of argon ions. Once the treatment was ended, the metallic sheets were left during 30 minutes approximately into the vacuum pump. This was done to avoid the rapid interaction of environmental species on the reactive surface. As an example, Figure 6-14 shows the disassembly of what the hair represents and the exposed internal wood.

Figure 6-14. Example of disassembly of the upper lead sheet which represents the hair of *The Violinist*. The wooden core can be seen exposed.

The different parts of the entire sculpture were disassembled and treated separately using non-thermal plasma. Some of these parts are shown in the following Figure 6-15 before and after treatment.

a)  b) 

Figure 6-15. Before and after non-thermal plasma cleaning of corroded specimens, *a* and *b*; violin handle, *c* and *d;* hair piece, *e* and *f;* left hand of the violinist; *g* and *h;* hair piece.

The restoration treatment for corroded lead samples by VOCs was effective. The lead carbonate remains after mechanical cleaning disappeared once the metallic sheets were treated with non-thermal plasma.

After the non-thermal plasma restoration, the lead sheets were returned to the conservation-restoration laboratory of the *Museu d'Art de Catalunya* to proceed with

the assembly of these parts on a polymeric core which will replace the original pinewood structure. Thus, with the substitution of the wooden core, the emission of organic acids is avoided and therefore an adequate conservation is obtained.

6.4. Concluding remarks

This chapter is based on the application of a non-thermal plasma design for the corrosion cleaning of a lead artefact from Cultural Heritage. Chapter 2 provides a detailed explanation of the conditions required for characterization analyses using an optical microscope, as well as XRD and SEM analyses. As mentioned, *The Violinist* sculpture made by Pau Gargallo, consisted on lead sheets placed on a wooden core. These showed great deterioration due to the exposure of the Pb sheets to VOCs from the wooden core during more than 100 years. The XRD pattern obtained from the corrosion sample of the sculpture was compared with two other corrosion samples simulated in the laboratory by acetic acid and VOCs from pine wood (the first one during one month, and the second one during three years). The results obtained showed that it takes many years to obtain the carbonate layer presented in *The Violinist*, mainly formed by hydrocerussite, since the conversion of lead acetate and lead oxide to lead carbonate is very slow.

Before the use of non-thermal plasma, a mechanical cleaning was performed to reduce the thickness of the corrosion layers by micro-sandblasting. For this purpose, the lead sheets were first introduced into a vacuum chamber in order to extract the moisture from the corrosion layers and facilitate their removal. It was decided to use abrasive pumice instead of aluminium silicate because of the lower quantity of embedded particles under the same conditions and the more uniform appearance. Afterwards, the lead sheets were stabilised with non-thermal plasma based on the most suitable results obtained in chapter 4 for corroded Pb by AcOH vapours (90:10 Ar/H_2, 50 W during 60'). Once the treatment was finished, the metallic sheets were left for 30 minutes approximately into the vacuum pump in order to avoid the interaction of environmental species into the reactive surface after treatment. It was favourable to obtain a natural passivation layer on the surface after the treatment in order to keep the surface protected.

After 30 minutes of resting in the vacuum chamber, a second non-thermal plasma application under the same conditions was performed on the lead sheets with more predominant areas of rust. Then, the surfaces were mechanically cleaned with a soft bristle brush. Once the metal pieces were treated, there was a significant improvement over the appearance before the cleaning procedure. After treatment, the exposed surface is very reactive. Additionally, the obtained surface presented small pores distributed homogeneously and resulting in a spongy surface aspect (as observed in the present chapter) which also can increase the risk of corrosion. For this reason, it is important to maintain the metallic lead object in an innocuous medium after being cleaned to create a good natural passivation layer in order to stabilise the surface. Sometimes, this passivation is induced in the same reactor after cleaning, with O_2 plasma to create a passive layer of lead oxide [8,9].

Before restoring Cultural Heritage artefacts, it's crucial to conduct laboratory tests on simulated samples. In this scenario, chapter 3 and chapter 4 studies led to the discovery that plasma cleaning was an appropriate solution for Pb sheets in a poor state of preservation, as well as the necessary VOC corrosion conditions.

Mechanical cleaning was previously carried out by the MNAC. After this, and under their supervision, the sculpture was provided to our research group to undergo non-thermal plasma cleaning using a mixture of argon and hydrogen. It should be noted that all conservation techniques are invasive to some degree, as they produce changes on the surface, some more significant than others. The plasma cleaning process is relatively harmless, allowing the surface to stabilise and become as homogeneous as possible, without the risk of causing the reappearance of new corrosion products through contact with reactive metal surfaces. As mentioned in previous chapters, before any treatment in real Cultural Heritage artefacts, it is important to perform tests on simulated samples in the laboratory. In this case, thanks to the different studies obtained in chapter 3 and chapter 4, it was possible to determine that plasma was ideal for these Pb sheets in a poor state of conservation, as well as the necessary conditions for this type of corrosion obtained by VOCs. The final result was favourable and therefore, the lead sheets were returned to the *Museu d'Art de Catalunya* to be welded again on an inert polymer core as a substitute for pine wood.

6.5. References

[1] A. Masalles, E. Lehmann, D. Mannes, Non-destructive Investigation of "The Violinist" a Lead Sculpture by Pablo Gargallo, Using the Neutron Imaging Facility NEUTRA in the Paul Scherrer Institute, Phys Procedia. 69 (2015) 636–645. https://doi.org/10.1016/j.phpro.2015.07.090.

[2] M.P. i Santacana, Francesc Costa, retrats d'un violinista, Revista de Catalunya. 231 (2007) 45–65.

[3] E.H. Lehmann, P. Vontobel, L. Wiezel, Properties of the radiography facility neutra at sinq and its potential for use as European reference facility, Nondestructive Testing and Evaluation. 16 (2001) 191–202. https://doi.org/10.1080/10589750108953075.

[4] D. Mérillou, S., Dischler, J., & Ghazanfarpour, Corrosion: Simulating and Rendering., in: Graphics Interface., 2001.

[5] C. Degrigny, R. Jeanneret, D. Witschard, C. Baudin, G. Bussy, H. Carrel, A new electrolytic pencil for the local cleaning of silver tarnish, Studies in Conservation. 61 (2016) 162–173. https://doi.org/10.1179/2047058415Y.0000000015.

[6] R.D.C.F.C.W.D.T.A. JEANNERET, Using the Pleco for electrolytic treatments of inseparable metal components on artefacts comprising organics, in: C.C. and A.P. R. Menon (Ed.), Proceedings of the ICOM-CC Metal WG Interim Meeting, METAL 2016, New Dehli, India, 2016: pp. 228–234.

[7] C. Degrigny, R. le Gall, Conservation of ancient lead artifacts corroded in organic acid environments: electrolytic stabilisation/consolidation, Studies in Conservation. 44 (1999) 157–169. https://doi.org/10.1179/sic.1999.44.3.157.

[8] V. Costa, F. Urban, Lead and its alloys: metallurgy, deterioration and conservation, Studies in Conservation. 50 (2005) 48–62. https://doi.org/10.1179/sic.2005.50.Supplement-1.48.

[9] A.S.T.J. Claus Gottlieb, A new method for cleaning and conservation of lead objects using hydrogen and oxygen plasma, Materials Science. 2 (1993) 767–771.

7. Conclusions

In the present thesis, the use of Non-thermal plasma to clean and stabilize ductile metals was proposed as an alternative of electrochemical techniques. It was focused on lead as an example of a metal with malleable properties that limit the use of traditional techniques. Based on all the objectives presented in the first chapter, it can be concluded the following points:

1. Several tests were performed exposing metallic Pb samples to the gas phase of solutions containing NaCl, H_2SO_4, HCOOH and AcOH at different concentrations for one month. In general, the resulted corrosion layers presented different morphologies depending on physicochemical properties of the formed compounds. Note that the Pb exposition to AcOH produced the most severe corrosion process because a protective layer cannot be formed. With the obtained results, it was proven that corrosion on lead is not mainly controlled by electrochemical processes, but also by the morphology of corrosion layers obtained in different atmospheres.

2. Electrolytic reduction was evaluated using galvanostatic and potentiostatic systems. These techniques are described to be useful for cleaning and stabilizing corrosion surfaces of different metals with different results. The potentiostatic mode is used in conservation field because it allows for better control of the reduction reaction and can minimize the formation of hydrogen gas by controlling the applied potential of the electrode surface. Before proceeding, it is important to know the reduction potential by creating models that mimic these corrosion products. Moreover, there are some limitations in electrolytic treatments, such as non-uniform corrosion, inseparable non-metallic parts, or the size of the object. For objects that can be fully immersed in the electrolyte, the counter electrode should not be smaller to avoid limiting the charge flow. The resulting surface was rough after treatment, and furthermore, there is a risk of forming new crystals on the surface (in this case of $PbSO_4$) if the reactive metallic surface after cathodic reduction remains in the electrolyte, or if it is not properly washed afterwards.

3. Non-thermal plasma was evaluated to clean and stabilize corroded Pb surfaces by AcOH vapors. A combination of etching and reduction processes was performed. To do that, a plasma of 90:10 argon/hydrogen, at a power of 50 W during 60 minutes was proven to be effective without corrosion remains and/or surface alteration. Since plasma generates reactive species, its interaction with the surface was very efficient thanks to the fast kinetic, optimizing the treatment time. Parameters such as time, power or Ar/H_2 ratio were optimized using a full factorial analysis. With the optimized parameters (60 minutes, 50W and 90:10 Ar/H_2) samples were not overheated or deformed and the treatment can be prolonged, if necessary, without visual damage. In addition, the size of the reactor can be a limiting factor when introducing the whole artefact, and it has to be disassembled to treat each part individually. Moreover, non-thermal plasma of H_2 has limited penetration depth. Argon was used in this chapter to enhance hydrogen plasma penetration by etching the surface, but the technique is not recommended for very thick layers and may require prior mechanical cleaning to reduce thickness.

4. As a useful and complementary tool to the usual characterization techniques, Electrochemical Impedance Spectroscopy (EIS) was evaluated to characterize surfaces before and after surface treatments (electrolytic reduction and non-thermal plasma techniques). Although the obtained results using EIS have complex interpretations, the present work demonstrated the potential of this technique to provide a fairly accurate analysis of its surface. In the present work, EIS was successful to compare surfaces after and before different cleaning treatments. Moreover, non-thermal plasma treatment proved to be the most effective method in restoring corroded surfaces.

Thanks to the previous simulations of corroded lead in the laboratory, it was possible to apply the optimal cleaning treatments for a real study case of metallic Cultural Heritage. In this context, the corrosion cleaning from *The Violinist* sculpture with non-thermal plasma was performed based on the conditions previously described for affected by VOCs. It should be mentioned that the conservation protocols of Cultural Heritage artefacts must be specific to their condition, given the uniqueness that presents each object with single value.